Geometrical Modelling and Numerical Analysis of Thermal Behaviour of Textile Structures

Muhammad Owais Raza Siddiqui

Submitted for the degree of Doctor of Philosophy

Heriot-Watt University

School of Textiles and Design

August 2015

ABSTRACT

The thermal properties of fabric are an important factor in the understanding of the thermo-physiological comfort of clothing. The principal aim of this research was to develop novel numerical methods, Graphical User Interface (GUI) plug-ins and experimental setup to evaluate the effective thermal conductivity and thermal resistance of different textile structures which has significant impact on the thermal comfort of clothing. The numerical methods also include the analysis of the effect of fibre orientation, thermal anisotropy of fibre, temperature dependent thermal conductivity and fibre volume fraction on the effective thermal conductivity and thermal resistance of textile fabrics.

The research covers the development of geometrical models of woven, knitted, nonwoven and the composites fabric structures, evaluation of their thermal properties by using finite element method, creation of user friendly plug-ins and the extended application tools. Micro and mesoscopic scale modelling approaches were used to investigate the effective thermal conductivity and thermal resistance of textile structures. Various techniques, including scanning electron microscopy, x-ray microtomography and experimental method have been adopted to obtain the actual 3D dimensional parameters of the fabrics for finite element analysis.

Research revealed that, the thermal anisotropy of fibres, fibres material orientation and temperature dependent thermal conductivity of fibre have significant impact on the effective thermal conductivity of fabrics because experimental and simulated results were highly correlated with the consideration of above mentioned factors. In addition a unique technique has been developed in modelling fabric coated by microencapsulated phase change material for temperature stable textile and clothing system.

User friendly GUI plug-ins have been developed to generate both microscopic and mesoscopic scale models for finite element analysis. The plug-ins were developed by using Abaqus/CAE as a platform. The GUI Plug-ins enable automatic model generation and property analysis of knitted fabrics and composites.

Apart from finite element analysis of various fabric structures, an experimental device has been developed for testing thermal conductivity of fabrics which is capable of testing small sample size within very short period of time. The device was validated by commercial available apparatus for testing of fabric thermal conductivity.

ACKNOWLEDGMENT

First and foremost, praises and thanks to Almighty Allah who given upon us all the blessings.

I would like to give my deepest gratitude to my supervisor Dr Danmei Sun, whose guidance, continuous support and encouragement, were the invaluable contribution to this thesis. Her supervision was admirable to manage and timely complete the PhD project.

Very special thanks to Mrs Ann Hardie and Mr George McGill for their support. I am thankful to Dr Ian B. Butler from the University of Edinburgh for his technical support for X-ray tomography.

I am extremely thankful to my parents, wife and kids for their love, continuous moral support and encouragement.

I would like to thank NED University of Engineering and Technology for the scholarship to pursue my PhD studies.

ACADEMIC REGISTRY
Research Thesis Submission

Name*:*	Muhammad Owais Raza Siddiqui		
School/PGI:	School of Textiles and Design		
Version: *(i.e. First, Resubmission, Final)*	Final	Degree Sought (Award **and** Subject area)	PhD (Textiles)

Declaration

In accordance with the appropriate regulations I hereby submit my thesis and I declare that:

1) the thesis embodies the results of my own work and has been composed by myself
2) where appropriate, I have made acknowledgement of the work of others and have made reference to work carried out in collaboration with other persons
3) the thesis is the correct version of the thesis for submission and is the same version as any electronic versions submitted*.
4) my thesis for the award referred to, deposited in the Heriot-Watt University Library, should be made available for loan or photocopying and be available via the Institutional Repository, subject to such conditions as the Librarian may require
5) I understand that as a student of the University I am required to abide by the Regulations of the University and to conform to its discipline.

* *Please note that it is the responsibility of the candidate to ensure that the correct version of the thesis is submitted.*

Signature of Candidate*:*		Date:	

Submission

Submitted By *(name in capitals):*	
Signature of Individual Submitting:	
Date Submitted:	

For Completion in the Student Service Centre (SSC)

Received in the SSC by *(name in capitals):*			
1.1 Method of Submission *(Handed in to SSC; posted through internal/external mail):*			
1.1 E-thesis Submitted (mandatory for final theses)			
Signature:		Date:	

TABLE OF CONTENTS

LIST OF TABLES

LIST OF FIGURES

GLOSSARY

Anisotropic material: A material that has different physical properties in various directions.

Cloth: A basic term used for all textile fabrics.

Coated fabric: A fabric with one or more polymeric layers on one or both of its faces.

Coating: The application of a polymeric material to one or both faces of a textile fabric.

Core-spun yarn: A yarn made by twisting staple fibres around a filament.

Count: A numerical term which defines the mass per unit length or length per unit mass of yarn.

Course: A row of loops running across a knitted fabric.

Fabric: A flexible textile structure produced by weaving, knitting or by any nonwoven technique.

Fibre: A fibre can be spun into yarn or it can be converted into textile structures by different manufacturing process such as weaving, knitting and nonwoven. A fibre is considered by having a length at least 100 times its diameter.

Fibre volume fraction: Fibre volume fraction is defined as the ratio of fibre volume within the boundaries of a material to the total volume.

Filament yarn: A yarn made of extreme long fibres which run along the whole length of the yarn. Filament yarn can be flat and texturized and it can be made with or without twist.

Isotropic material: A material that has the same physical properties in various directions.

Knitting: A method of constructing fabrics by the inter-looping of yarn.

Point bonding: The process is used to create a nonwoven fabric by the application of heat and pressure to bind thermoplastic fibres into a nonwoven fabric in order to achieve the distinct pattern of fibre bonds.

Porosity: The ratio of the volume of air or void space within a material to the total volume (which includes solid substance and air) expressed in terms of percentage.

Spun yarn: A yarn made of staple fibres generally bound together by twist.

Tex: A unit for measuring linear density defined as the weight in grams of 1 kilometre of fibre.

Thermal conductivity: A measure of heat flow through a material.

Transverse thermal conductivity: Thermal conductivity perpendicular to the longitudinal axis of yarn.

Weft knitting: A method of constructing fabric by the inter-looping of yarn is called knitting. There are two common types of knitting such as warp and weft knitting. In weft knitting, yarns run in a crosswise or circular direction. Types of weft knitting are: circular and flat knitting.

Wale: A column of loops lying lengthwise in a knitted fabric.

Warp: In a woven fabric, the yarn running along the length wise direction of fabric or parallel to the selvedge.

Weaving: A method used to produce woven fabrics which are composed of two sets of yarns which interlace with each other at 90 degrees.

Weft: In a woven fabric, the yarn running along the width wise direction of fabric or at right angles to the warp yarn.

Yarn: A general term used to define the assembly of textile fibres which can be used for making textile fabrics.

LIST OF PUBLICATIONS

Journal Articles

1. Siddiqui MOR, Sun D, Porosity prediction of plain weft knitted fabrics, fibers, 3: 1-11, 2015. DOI: 10.3390/fib3010001.
2. Siddiqui MOR, Sun D, Automated model generation of knitted fabric for thermal conductivity prediction using finite element analysis and its applications in composites, Journal of industrial textiles, 2014.DOI: 10.1177/1528083714551440.
3. Siddiqui MOR, Sun D, Computational analysis of effective thermal conductivity of microencapsulated phase change material coated composite fabrics, Journal of Composite Materials, 2014. DOI: 10.1177/0021998314545193
4. Siddiqui MOR, Sun D, Finite element analysis of thermal conductivity and thermal resistance behaviour of woven fabric, Computational Materials Science, 75, p. 45-51, 2013. DOI:10.1016/j.commatsci.2013.04.003

Conference Papers

1. Siddiqui MOR, Sun D, Prediction of effective thermal conductivity of micro-encapsulated phase change composites, 15th Autex world textile conference, Bucharest, Romania, 10-12 June 2015.

2. Siddiqui MOR, Sun D, Prediction of thermal conductivity of woven fabric using finite element method, proceedings of 14th Autex world textile conference, Bursa Turkey, 26-28 May 2014.

Poster

Siddiqui MOR, Sun D**,** Heat transfer analysis of textile fabric by finite element method, Simulia Community Conference, 20-22 May 2014.

Chapter 1 Introduction

1.1 Background Information

The thermal properties of fabric have significant impact on thermal comfort of the wearers. Clothing comfort can be categorised into three groups: psychological which is related to fashion, tactile which includes the mechanical interaction of the fabric with skin and has strong relationship with fabric surface and mechanical properties, and thermal comfort related to the ability of a fabric to regulate the temperature of the skin through heat and moisture transfer [1].

The main function of clothing is to maintain the body temperature under the different conditions of environment [2]. In an extreme high temperature working condition body releases a lot of heat and sweats. In order to keep the body dry these heat and sweat should be released in the environment. The thermal comfort of the fabrics mainly depends on how well they transmit heat and moisture from body to the environment [3, 4] and it is achieved by obtaining the thermal balance between the inner surface of cloth and skin [5]. Fibre and yarn type, fabric construction methods and parameters, and finishing process influence the thermal comfort performance of a fabric.

Thermal-insulation properties of textile materials play a significant role in material engineering of protective clothing. Thermal-insulation properties are very important from the point of view of thermal comfort of a wearer as well as clothing protective efficiency against low or high temperature, it depends on the thermal conductivity and thermal resistance of the fabric [6]. The thermal resistance indicates the ability of fabric provide thermal barrier to the wearer [7].

Heat flow mechanism of clothing assembly can be improved by special finishes [8]. Microencapsulated Phase Change Materials (MicroPCMs) have been widely used to develop thermo-regulating textile fabrics; it can be applied on to fabric by various techniques including coating process [8] . Phase Change Material (PCM) has unique property of latent heat that can absorb and release energy over constant temperature range which enhances the thermal comfort of the clothing microenvironment [9-13].

PCMs have been widely used in thermo-regulating textile fabrics by different application techniques [8]. Such fabrics can be used for making smart textiles and garments [14].

The microencapsulation of PCM involves enclosing PCM in thin and resilient polymer shell so that the PCMs can be changed from solid to liquid and back again within the shells [15]. Thermo-regulating textile clothing was developed in the early 1980s under National Aeronautics and Space Administration (NASA) research programme by using PCM [16]. Microencapsulated PCM thermo-regulating fabrics have been widely used in many application areas: protective clothing, sportswear, electronic textiles and many others.

Paula Sánchez reported that the use of microencapsulated PCM for fabric coating offers successful production of thermo-regulating textiles resulting in a substantial improvement of the thermal comfort [17].

1.1.1 Thermal Property of Textile Structures

In case of extreme cold condition it is necessary to restrict the heat flow from body to the external environment therefore the purpose of a fabric is to act as an insulator [18]. It means that the fabric has low thermal conductivity or higher thermal resistance. The thermal conductivity is an important material property because it affects the heat flow in the material. Heat can be transferred from clothing to the environment to maintain its thermal balance through conduction, convection and radiation.

Conduction: Thermal conduction is the mode of heat transfer in which energy transfers from the higher temperature part of body to the lower temperature part by kinetic movement of molecules. In textile clothing system the conduction heat transfer is through fibres with still air inside the fibrous assembly.

Conduction heat transfer (Q_{cond}) along the thickness of textile fabric is directly proportional to the temperature difference (ΔT) across the fabric and surface area of fabric (A), but inversely proportional to the thickness of fabric (t) and it can be determined by Fourier's law of conduction:

$$Q_{cond} = -K_{eff} A \frac{\Delta T}{t} \qquad 1.1$$

where K_{eff} is the effective thermal conductivity of textile fabric.

Convection: In convection, heat transfers from the solid surface by the interaction of moving fluid and it may occur within the fluid. Convection heat transfer depends on the nature of fluid flow; by means of either buoyancy forces that arise due to the density difference caused by the temperature difference in natural convection or an external force in case of forced convection. Convective heat transfer flow in a fabric can be negligible even at low fibre volume fraction [19, 20]. The convective heat transfer (Q_{conv}) occurs at the surface of the fabric and it can be expressed as:

$$Q_{conv} = h\,A(T_s - T_\infty) \tag{1.2}$$

where h is the convective heat transfer coefficient, A is the surface area of fabric through convective heat transfer occur, T_s is the surface temperature (K) and T_∞ is the ambient air temperature (K).

Radiation: In radiation, heat transfer is due to electromagnetic radiation emitted by the body which arises in temperature [21]. Radiative heat flow through fabrics can be predicted if the temperature profile is known. The simplest approach is to consider the linear profile of temperature with respect to the distance through the fabric as in conduction heat flow [22]. At the centre of a fabric the radiative conductivity can be calculated by [20]:

$$K_{Rad} = 8\sigma T^3 R / f\varepsilon \tag{1.3}$$

where σ is the Stephen Boltzmann constant, T is the mean temperature between heat source and sink (K), R is the radius of fibre, f is the fibre volume fraction and ε is the thermal emissivity of surface.

In place of natural fibres high performance fibres such as Nomex® and Twaron® are widely used in fire protection and body armour clothing respectively [23-29]. The heat transfer behaviour of these materials is necessary to be analysed when they are subjected to intense environment.

Heat flow through the clothing assembly mainly depends on the thermal conductivity of fibrous material, fibre volume content, construction of fabric, and orientation of fibre with respect to the heat flow direction [30, 31].

The thermal conductivity and thermal resistance are the key parameters for heat flow in the fabric for conduction and it can be evaluated by different ways: experimental method, analytical solution method and numerical method [32, 33].

There are numerous ways of obtaining the numerical formulation of a heat conduction problem, such as finite difference method, finite element method, boundary element method, and energy balance (or control volume) method [21]. In this research work finite element method (FEM) is used to evaluate the thermal property of fabric. It is a powerful computational process for imprecise solutions to a variety of applied engineering problems having complex domains subjected to general boundary conditions.

1.2 Research Gap and Motivation

Significant research work has been carried out to determine the effective thermal conductivity and thermal resistance of fabric by using mathematical modelling and numerical analysis. The detailed literature review in Chapter 2 demonstrates the research work has been done in the area of thermal conductivity and thermal resistance of fabrics [4, 20, 24, 33-59]. However the combined effect of fibre orientation, thermal anisotropy nature of fibre, temperature dependent thermal conductivity of fibre and the accurate geometrical construction of the fabric which are important factors and have significant impact on the heat transfer phenomena of textiles have not been considered to most of the publications. In this research work all the aforementioned factors will be taken into consideration to evaluate the effective thermal conductivity and thermal resistance of textile structures by using finite element method.

1.3 Aim and Objectives

The overall aim of this research work is to develop a finite element models to simulate and predict the effective thermal conductivity and thermal resistance of textile structures, an experimental setup, and plug-ins for the generation of the geometrical models of different textile structures. The thesis is divided into three main parts.

(1) Analysis of the heat transfer behaviour of textile structures. The subsidiary objectives have been set up accordingly:

(a) to develop finite element models of textile structures by using the actual geometrical parameters and material thermal properties.
(b) to analyse and investigate the effect of thermal anisotropy, temperature dependent thermal conductivity and fibre orientation on the effective thermal conductivity of textile structures based on the validated finite element models.
(c) to validate the finite element models results by comparing results from model calculations and obtained from experimental setup.

(2) The development of plug-ins. The objectives in this part are listed below:

(a) to develop a user friendly Graphical interface (GUI) plug-ins in Abaqus/CAE environment by using python scripting, to enable automatically generate geometrical models of textile structures.
(b) to develop plug-ins which are capable of generating 3D finite element model of Microencapsulated PCM composite and plain weave composite, and to predict their effective thermal conductivity.

(3) The experimental measurement of thermal conductivity and thermal resistance of textile fabrics. The objectives in this part are:

(a) to develop an in-house experimental setup for evaluation of the thermal conductivity and thermal resistance of textile fabrics.
(b) to design an experimental setup in a way that the tests can be carried out using small sized samples and within short period of time.

1.4 Thesis Layout

The thesis contains seven other chapters following the Introduction Chapter. Chapter 2 presents a review of the literature in heat transfer analysis of woven, knitted and nonwoven fabrics, effect of phase change material on heat transfer of textile polymers and fabrics and current experimental setup for thermal conductivity and thermal resistance of fabrics. It also includes a brief methodology of the research in the end of the chapter.

Chapter 3 focuses on the design and development of experimental setup. Furthermore, a procedure for conducting thermal conductivity test and data analysis from the developed experimental setup is explained.

In Chapter 4 following the initial study about the geometrical modelling of woven, knitted, nonwoven and MicroPCMs coated woven fabric, the technical approaches of finite element model generation are described

Chapter 5 explores a method which can be used to predict the effective thermal conductivity and thermal resistance of woven, knitted, nonwoven and MicroPCMs coated woven fabrics by using finite element method.

Chapter 6 includes the development of Graphical User Interface (GUI) plug-ins which automatically generates the geometrical model of fabrics and predicts the effective thermal conductivity of MicroPCMs coated textile composite and plain weave composite.

Chapter 7 of the thesis focuses on the model validation and the heat transfer behaviour of textile fabrics which is affected by material orientation, temperature dependent thermal conductivity and thermal anisotropy of fibres.

Finally the conclusions of this project are presented in Chapter 8. This chapter also contains the suggestions for future work.

Chapter 2 Literature Review and Methodology

2.1 Introduction

This chapter presents a comprehensive literature review in the proposed research area, including: (1) prediction of thermal conductivity by analytical method along with the identification of research gap, (2) measurement of thermal conductivity by experimental methods, and (3) the effect of PCM on heat transfer behaviour of textiles. Furthermore the research methodology will be described in this Chapter.

In this research work different fabrics for different applications such as protective clothing, normal wear clothing, insulation etc. will be studied. Thermal, moisture transfer through fibres, yarns and fabrics has major influence on the field of thermal comfort of fabric and the clothing [20, 24, 42, 52, 56]. Thermal conductivity and thermal resistance are the main parameter which have influence on the thermal comfort of the clothing [32, 33].

2.2 Prediction of Thermal Conductivity by Analytical Models

A textile fabric as non-homogeneous material contains heterogeneous mixture of fibre substance and air. Heat can be transferred through textile fabrics by means of conduction, convection and radiation. Convection heat transfer is subjected to the movement of substances and, if occurring, it occurs only at the surface of a normal solid material. Heat transfer through conduction mainly depends on the temperature gradient and when that temperature gradient is small, heat transfer via radiation can be ignored [44]. The term thermal conductivity should be replaced by overall thermal conductivity which defined as the rate of heat flow through fabric by all means of mode of heat transfer per unit area of fabric at unit temperature difference [19]. The overall or effective thermal conductivity (K_{eff}) of fabric can be calculated by Fourier's law of conduction:

$$K_{eff} = \frac{Q \cdot t}{A \Delta T} \qquad 2.1$$

where Q is the heat flow, A is the surface area, t is the thickness of fabric and ΔT is the temperature difference.

The most important thermal property of fabric is insulation against the heat flow in cold environment to keep the normal body temperature. The insulation property of fabric is measured by thermal resistance. Thermal resistance (R) of fabric is defined as the ratio of temperature difference to the rate of heat flow per unit area.

Thermal resistance of fabric can be expressed by electrical analogy according to the Ohm's Law:

$$R = \frac{\Delta T}{Q/A} \tag{2.2}$$

where Q is the heat flow, A is the surface area and ΔT is the temperature difference

Thermal resistance can also be calculated by effective thermal conductivity of fabric:

$$R = \frac{t}{K_{eff}} \tag{2.3}$$

where t is the thickness of fabric.

Many researchers tried different techniques to predict the effective thermal conductivity of fibrous material. Schuhmeister in 1987 [37] used a method which developed by Stefan [60] to calculate the thermal conductivity of gases. In those research bulk fibres were placed between the two side-by-side cylinders and the cylinder which was in the middle for the measurement of the temperature to be used as air thermometer. Schuhmeister concluded that the result obtained from this method can be expressed by the following equation:

$$K_m = K_g + f\,C \tag{2.4}$$

where K_m is the conducting power or effective thermal conductivity of mixture of gas and fibre, K_g is the conducting power of gas, f is the weight of textile fibre present in mixture and C is constant.

The above equation can be modified by using the volume occupied by fibre:

$$K_m = K_g + a\rho_f \tag{2.5}$$

where ρ_f is the bulk density of fibre and a is constant.

Schuhmeister [37] also developed a relationship to calculate the thermal conductivity of mixture of air and fibre, the following assumption has been taken:

a) in all directions solid fibres were uniformly distributed;
b) one third of the bulk solid fibres were placed parallel to the heat flow; and
c) two third of the bulk solid fibres were placed series or perpendicular to the heat flow.

The developed relationship on the basis of above assumptions is:

$$K_m = \frac{1}{3}\left(K_a V_a + K_f V_f\right) + \frac{2}{3}\left(\frac{K_a K_f}{K_a V_f + K_f V_a}\right) \qquad 2.6$$

where K_a is the thermal conductivity of air, K_f is the thermal conductivity of fibre, V_a is the fractional volume of air, V_f is the fractional volume of fibre and $V_a + V_f = 1$.

The first part of the above equation described that the fibres are parallel to the direction of heat flow and second part presented that fibres are oriented perpendicular to the direction of heat flow, which is demonstrated in Figure 2.1.

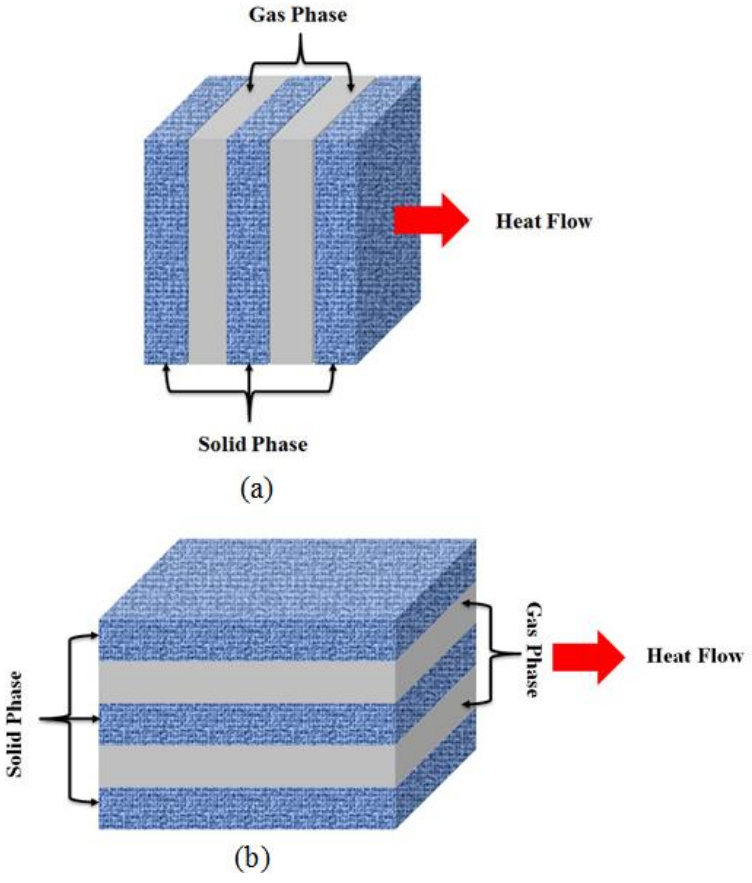

Figure 2.1: Heat flow mechanism in solid and gas are in : (a) Series ; and (b) Parallel

Farnworth [20] utlized the first part of the equation $\left(K_a V_a + K_f V_f\right)$ in order to obtain the conductive heat flow in fibrous batts which were placed between the two plates having a temperature gradient. He considered the two mechanisms heat flow conduction and radiation and the effect of convection heat transfer can be neglected because there was no significant evidence of convective heat flow even though the experimental conditions were favourable for convection heat transfer.

Stark and Fricke [41] developed three models to calculate the combined thermal conductivity of gas and solid fibre. In their first basic model they considered the mean orientation of fibre in terms of *Z* which defined the fraction of fibre perpendicular to the direction of heat flow. On the basis of the assumptions of Bhattacharyya [61] they developed the relationship of combined thermal conductivity of solid fibre and air in the following equation.

$$\lambda_{sg}^{BM} = K_f \cdot \left(1 + \frac{\alpha - 1}{\beta\left(1 + Z\left(\alpha - 1\right)/\left(\alpha + 1\right)\right)}\right) \qquad 2.7$$

where λ_{sg}^{MB} is the combined thermal (effective) conductivity of solid fibre and air, K_f is the thermal conductivity of solid fibre, α is the ratio of thermal conductivity of air to thermal conductivity of solid fibre (K_a / K_f), β is the ratio of volume fraction of solid fibre (V_f / V_a) and volume fraction of air and *Z* is the portion of fibre oriented upright to the direction of macroscopic heat flow.

In the modified model they considered that the effect of thermal resistance was caused by the contact between fibres; the thermal conductivity of individual solid fibre, gas and coupling effects could be calculated. The diagram of thermal resistance is shown in Figure 2.2.

In Figure 2.2 R_{BM} represents the thermal resistance of basic model, R_{ct} represents the contact resistance between fibres and R_g represents thermal resistance of air. Figure 2.3 demonstrates the unit cell of solid fibre and the contact between the two fibres. In the modified model the unit cell height is *(m+1).2r* but in basic model it was expressed by *m.2r* which is less than that of the modified model.

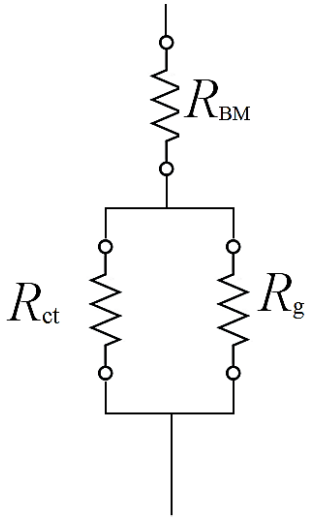

Figure 2.2: Thermal resistances diagram of modified model [41].

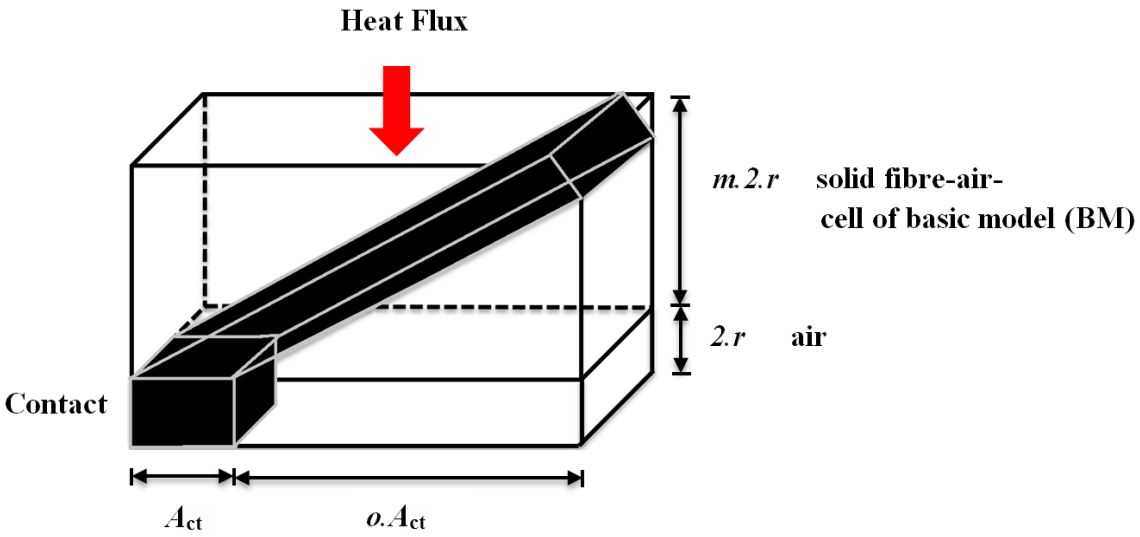

Figure 2.3: Unit cell model of the modified model

From Figure 2.2 and Figure 2.3 the combined thermal conductivity of the modified model can be calculated by:

$$\lambda_{ss}^{MM} = \frac{(m+1)\cdot 2r}{S_{cell}\left(R_{BM} + \left(\frac{1}{R_g} + \frac{1}{R_{ct}}\right)^{-1}\right)} \qquad 2.8$$

where m is the height of air-fibre unit cell in terms of fibre radius (r) and fibre orientation and S_{cell} is the cell area which is equal to area of a fibre-air contact area times contact area between two solid fibres ($S_{cell} = A_{ct} + 0.A_{ct} = (0+1)\cdot A_{ct}$).

In improved modified model they considered the unit cell model of modified model and the effect that in real situation each adjacent fibre was not in contact directly to each other so they sub-divided the cell into eight sub-cells and derived the relation of the effective thermal conductivity of solid fibre and air is following:

$$\lambda_{sg}^{MMC} = (m+1)\left\{\frac{m}{\lambda_{sg}} + \frac{o+1}{o}\frac{1}{K_a + \dfrac{4K_s Ar}{o\pi a_{ct}}}\right\} \qquad 2.9$$

where *A* is the constant connection parameter and its minimum, maximum and mean values are 0.5384, 0.6836 and 0.611 respectively, r is the radius of solid fibre, a_{ct} is the contact radius o+1 is the size parameter calculated by $o+1 = \left(\frac{l}{r}\right)^{\frac{2}{3}} \frac{(0.5\sin\vartheta_o)^{1/3}}{\pi\left(1.5\left(1-\mu_o^2\right)P_{ext}/Y_o\right)^{2/3}}$.

Furthermore they compared the results obtained from the derived model with experimental results for model validation.

Ismail et al. [38] developed a mathematical model which determines the effective thermal conductivity of woven fabric by using unit cell approach. The following assumptions were made to the simple plain woven fabric structure in the model:

(1) no consideration of moisture content;
(2) uniform thermal properties and fibre distribution in fabric elements (warp and weft);
(3) through thickness one dimensional steady state heat transfer;
(4) neglect the effect of temperature change at the boundary radiation and of air and fibre;
(5) the total thermal conductivity of fabric obtained is the combination of conduction, convection and radiative heat transfer; and
(6) in warp element, weft element and at crossover point (combined warp and weft element) were considered two phase element such as air and fibre.

They also transformed the warp and weft elements into equivalent element of uniform thickness in the model.

Kothari and Bhattacharjee [51] considered Peirce's geometrical model based on the fact that fabric at intersection behaves like a plain woven for the prediction of thermal resistance of woven fabrics by using thermal electrical analogy technique. They used second part of the Equation 2.6 to calculate thermal conductivity of yarn. They stated that the thermal resistance of fabric obtained from the developed mathematical model based on the principal of heat transfer gives close results when compared with the experimental results [33].

Yamashita et al. [4] developed structural models of yarns, plain woven fabrics and plain woven fabric/resin composites and theoretical formulas for the effective thermal conductivity which derived from these models. They developed two models to calculate effective thermal conductivity of woven fabrics and their composites. In their model 1 they considered heat is transfer in both longitudinal and transverse direction of yarn and in model 2 only considered heat flow in transverse direction of the yarn. They concluded that model 1 is more effective than model 2 in order to calculate the effective thermal conductivity in comparison to the existing experimental results. They also concluded that the influence of fibre anisotropy on the effective thermal conductivity in transverse direction is much less. Zhu and Li [53] developed a fractal effective thermal conductivity model for woven fabrics with multiple layers.

Das et al.[54] developed a mathematical model for the prediction of thermal resistance of multilayer clothing in non-convective environment without consideration of geometrical parameters of woven fabric. Ran et al. [56] developed a 3D mathematical model to measure the coupled heat and mass transfer in woven fibrous materials by taking into consideration of its geometrical parameters. The finite volume method was utilised to separate the governing equations and Tri-Diagonal Matrix Algorithm was used to solve the linear individual equations. They assumed that the cross-section of yarn is non-deformable circular and isotropic thermal conductivity of the fibre.

Matusiak [57] developed a thermal resistance model of woven fabrics and assumed that the yarn cross-section shaped in square referred to the research work taken by Yamashita [4]. However in reality the cross-section of yarn in a woven fabric is hardly in square shape. They also applied the same method on twill woven fabric and claimed that the developed model can be used to predict the thermal resistance of single layer plain woven fabric and their derived woven structures; however it's not applicable to multi-layered fabric and fabrics with complex woven structures.

Baxter [34] measured the thermal conductivity of wool felt against different level of bulk density and moisture regain; he found that the thermal conductivity increases with the increase of bulk density and moisture regain.

Prakash and Ramakrishnan [59] studied the effect of blend ratio, loop length, and yarn linear density on thermal comfort properties of single jersey knitted fabrics. It was found that the thermal conductivity of fabric decreases when the bamboo component in the yarn increases and also decreases as the yarn linear density increases because more air entrapped in the yarn. The thermal conductivity increased with the increase of loop length.

Fayala et al. [49] and Majumdar [55] developed a model to predict the thermal conductivity of knitted fabrics based on artificial neural network (ANN). Artificial neural network is a tool to predict the response on a given set of input data after the training of model. During training the model learns the pattern between the input and their output responses. Artificial neural network required abundant amount of data to train the model.

Stankovic et al. [50] analysed the thermal properties of plain knitted fabrics made of natural and regenerated cellulose fibres. They concluded that the heat transfer phenomenon across the fabric depends on the air volume distribution within the fabric, capillary structure of component fibers and yarns, as well as yarn surface geometry. Oglakcioglu and Marmarali [46] analysed and compared the thermal properties of cotton and polyester based single jersey, 1x1 rib and interlock knitted fabrics. They found that the thermal insulation properties of different structure depend on the amount of fibre per unit area. With the amount of fibre increases the amount of entrapped air decreases, therefore the thermal conductivity would be higher for thicker fabric. They also concluded that there was almost no relationship of yarn twist on thermal conductivity of fabric.

Dias and Delkumburewatte [45] developed a theoretical model as shown in Equation 2.10 to predict the thermal conductivity (K) of knitted fabric in terms of porosity (p), thickness and moisture content in pores (w). They found that the thermal conductivity of knitted fabric increases with the increase of thermal conductivity of fibre and moisture content, and thermal conductivity also increases while the porosity of fabric decreases.

$$K = \frac{K_m K_a K_W}{(1-p)K_a K_W + (p - pw)K_m K_W + pwK_m K_a} \qquad 2.10$$

where K_m, K_a and K_W are thermal conductivity of material, air and water respectively.

Li et al. [43] reported that heat and moisture transport in porous textile material were significantly influenced by fabric thickness and porosity. Ucar and Yılmaz [62] determined the natural and forced convection of rib knit fabric. They also analysed the effect of fabric parameters on the thermal behaviour of fabric and concluded that the conductive heat loss due to fibre and entrapped air was more important than the convective heat loss.

Cimilli et al. [48] analysed the heat transfer of plain knitted fabric by finite element method, their objective is to investigate the applicability of a FEM to textile problems. For that purpose they developed the model of weft knitted fabric and analysed it and compared with results from experiment. In their analysis there was no consideration of air in the model when the knitted fabric was placed between the two plates.

Hasani et al. [58] analysed the heat transfer behaviour of interlock weft knitted fabric by using finite element method. They developed the model of knitted structure and analysed the steady heat transfer analysis by applying temperature on one side of the fabric and placed in air which has temperature less than the applied temperature which allows the heat to flow, using two modes of heat flow i.e. conduction and convection. They ignored the interaction between the air and fabric considering fabric space was not removed from the air domain which was unrealistic.

Bogaty et al. in 1957 [35] studied the effect of pressure on thermal conductivity of fabric by using two plates method. They used the results of thermal conductivity of fabric obtained from the experimental device at different levels of pressure to find out the effective fraction of fibres parallel (*x*) and perpendicular (*y*) to the direction of heat flow by using Equation 2.11.

$$K_m = x\left(K_a V_a + K_f V_f\right) + y\left(\frac{K_a K_f}{K_a V_f + K_f V_a}\right) \qquad 2.11$$

where K_a is the thermal conductivity of air, K_f is the thermal conductivity of fibre, V_a is the fractional volume of air, V_f is the fractional volume of fibre

They conclude that:

1) thermal conductivity of fabric increases with the increase of proportion of fibres which are parallel to the heat flow at higher bulk density;
2) thermal resistance of fabric can be improved by using low thermal conductive fibres which are arranged parallel to the surface or perpendicular to the direction of heat flow; and
3) at a given bulk density the insulation property of fabric can be improved by using higher density of fibre because fibre volume fraction is dependent on the bulk and fibre density. The fact is that the fibre volume fraction is inversely proportional to fibre density. It means that the higher the fibre density at given bulk density the less will be the fibre volume fraction and the more volume fraction of air.

In the above model there is no consideration of thermal anisotropy of fibre in fabric. Imakoma [40] developed a unit cell model as shown in Figure 2.4, to determine the effective thermal conductivity of fibrous insulation by considering the conduction heat transfer. Two semi cylinders represent two fibres which are parallel to the surface of the material. In this unit cell model there is no consideration of contact between fibres. In order to compensate this issue they proposed another unit cell in which contact between the fibres was considered but it was assumed that the thermal resistance at contact point was much higher than that of within fibres. In their models random orientation of fibre was taken however they also did not take into consideration of the thermal anisotropy nature of fibre.

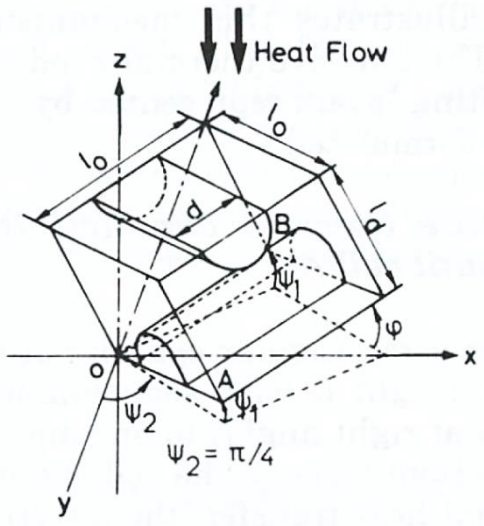

Figure 2.4: Conduction heat transfer unit cell model [40]

Naka and Kamata [36] analysed the thermal conductivity of wet fabric by varying the water content. In their model the effect of thermal anisotropy of fibre was considered in order to calculate the thermal conductivity of fabric normal (K_v) and parallel (K_w) to the surface by:

$$K_v = \frac{a}{2} K_{e\parallel} + \left(1 - \frac{a}{2}\right) K_{e\perp} \qquad 2.12$$

$$K_w = d_w \left\{(1-a) K_{e\parallel} + a K_{e\perp}\right\} + d_f \left\{\frac{a}{2} K_{e\parallel} + \left(1 - \frac{a}{2}\right) K_{e\perp}\right\} \qquad 2.13$$

where $K_{e\parallel}$ is the thermal conductivity of fibre parallel to the fibre axis, $K_{e\perp}$ is the thermal conductivity of fibre normal to the fibre axis, d_w is the thickness of warp layer, d_f is thickness of weft layer and a is the ratio of fibre which are parallel and normal to the yarn.

In the above described model there was no consideration of actual orientation of fibre. Kawabata [30] evaluated the thermal anisotropy of fibre by measuring the thermal conductivity of fibre along and perpendicular to the fibre axis and the result of thermal conductivity of fibres obtained shows strongly anisotropy. It is believed that in order to calculate the effective thermal conductivity of fibrous material it is necessary to consider the thermal anisotropy of fibre.

Kawabata measured the longitudinal thermal conductivity of fibres by clamping the parallel fibres in the copper chuck. The distance between the chucks/clamps or sample length is around 3~7 mm, sample width about 30 mm and cross-sectional area of fibres is about 3~5x10^{-6} m^2. Base chuck has constant flow of water and the temperature difference of 10°C was maintained by a built-in chuck sensor as shown in Figure 2.5 (a). The longitudinal thermal conductivity of fibre can be calculated by following equation:

$$K_L = \frac{Qt}{\Delta T A} \qquad 2.14$$

where t is the thickness of the specimen, Q is the heat flow , ΔT is the temperature difference and A is the sum of the cross-sectional area of fibres .

In Kawabata's work the transverse thermal conductivity of fibre contained in composite plate which was measured. The composite plate was composed of parallel fibre bundles which impregnated in epoxy at high pressure about 1 ton/cm^2 and cured. The thickness of plate is around 0.5-1 mm and the surface area of 5 x 5 cm^2 was placed between the plates as shown in Figure 2.5 (b).

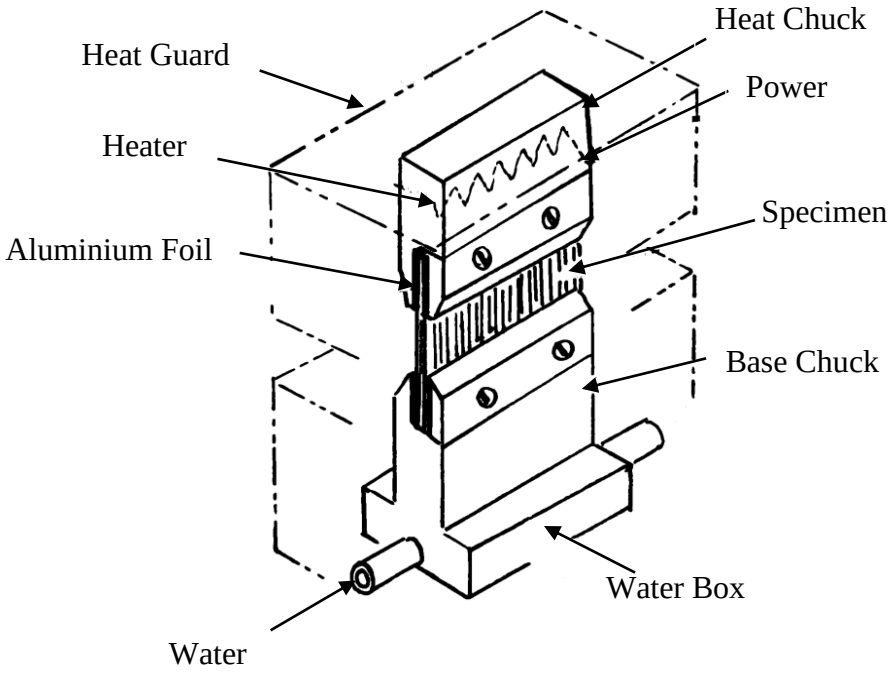

(a)

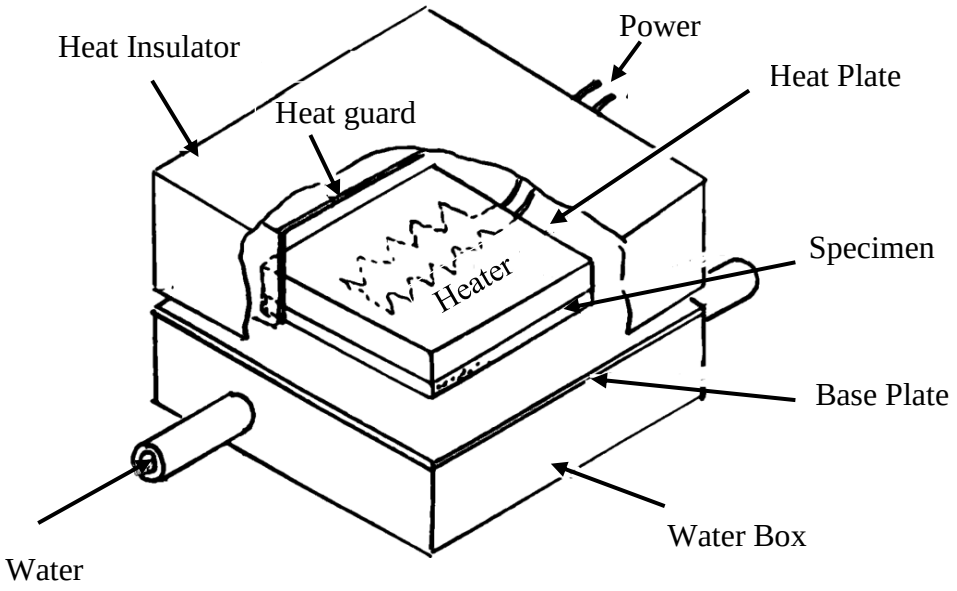

(b)

Figure 2.5: Measuring head for measurement of thermal conductivity: (a) Longitudinal and (b) Transverse

The transverse thermal conductivity of fibres was calculated by:

$$K_T = V_F\left(\frac{\Delta T \cdot A}{qt} - \frac{1-V_F}{K_R}\right)^{-1} \qquad 2.15$$

where V_F is the volume fraction of fibre, K_R is the thermal conductivity of resin, t is the plate thickness, A is the area of plate sample and ΔT is the temperature difference (10°C) .

Woo et al. [31] developed an analytical model for the thermal conductivity of nonwoven fabric in the transverse direction by considering fibre orientation, thermal anisotropy of fibre and fabric orthotropic effect as shown in Equation 2.16.

$$\begin{aligned} K_{oz} = {} & K_a \sin^2\phi P_i \\ & + K_{\parallel}\cos^2\phi\,\alpha X_f/(1+\alpha) + \sin^2\phi(1-P_i)^2 \\ & \times\left\{1/\left[X_f/K_{|} + (1-P_i-X_f)/K_a\right]\right\} \\ & + \cos^2\phi(1+\alpha-\alpha X_f)^2/\left\{(1+\alpha)\left[X_f/K_{|} + (1+\alpha)/K_a\right]\right\} \end{aligned} \qquad 2.16\ (a)$$

and

$$P_i = \left[1-(8/\pi)X_f + (8/\pi)^2 X_f{}^2\alpha/(1+\alpha)^2\right]^{t/(2d)} \qquad 2.16\ (b)$$

where K_{oz} is the thermal conductivity through the fabric, K_a is the thermal conductivity of air, $K_{|}$, and $K_{\parallel}$ are the thermal conductivities of the fibres along and across their axes, X_f is the fibre volume fraction, α is the anisotropy factor, $\cos^2\phi$ is the polar orientation parameter, t is the fabric thickness, and d is the fibre diameter.

They analysed the effect of fabric geometry on thermal conductivity of the nonwoven fabric and concluded:

1) the conduction is the prominent mode of heat transfer, there is no evidence of convective heat transfer and radiative transfer was only effective when the fibre volume fraction is less than 3%;
2) the thermal conductivity of fabric is affected by the fibre volume fraction; and
3) the thermal conductivity of fabric is influenced by fibre orientation and thermal anisotropy of fibre. The overall thermal conductivity of the nonwoven fabric

would increase for fibres arranged parallel to heat flow compared to that of the fibres arranged perpendicular to heat flow.

2.3 Measurement of Thermal Conductivity by Experimental Methods

The overall thermal conductivity of fabric can generally be measured by three different methods [18]:

1) two plate method, in which a fabric placed between the two metallic plates where there is temperature gradient;
2) cooling method, in which fabric is placed on hot surface and the other face of fabric is exposed to air; and
3) constant temperature method, in which fabric is wrapped around the heating source.

There are several commercial instruments are available which work on the principles on above mentioned methods.

2.3.1 Two Plate Method

In two plate method, fabric is placed between the two plates which have temperature gradient, heat flow from hot plate to cold plate. In this method thermal conductivity can be determined by steady-state method or transient method.

There are several devices available under two plate category but they have different arrangements to measure the thermal conductivity and thermal resistance of fabrics:

1) hot plate with reference samples;
2) hot plate with guarded heater; and
3) hot plate with heat flow meter or transducer;

In order to determine the thermal conductivity and thermal resistance of fabric it is necessary to know the heat flow rate per unit area (heat flux). It is difficult to measure the heat flux in a specific direction even with the use of heater with which power is known because it dissipates heat in all directions. There are two different ways to measure the heat flow through the fabric: one is to use reference sample of known thermal resistance to compare with the testing sample and the other is to eliminate the heat loss which does not pass through fabric to be tested [22].

Togmeter is the device which works on the principle of reference sample. The testing arrangement of the apparatus is that all the conductors (fabrics) are placed in series with respect to the direction of heat flow and with fixed pressure to avoid the convection heat loss.

Thermal resistance of the fabric is equal to the ratio of the temperature difference across the two conductors next to the two faces of tested fabric which equals to the ratio of their thermal resistance which is analogous to the electrical circuit when two conductors are connected in series. The sketch of Togmeter with two plates is shown in Figure 2.6.

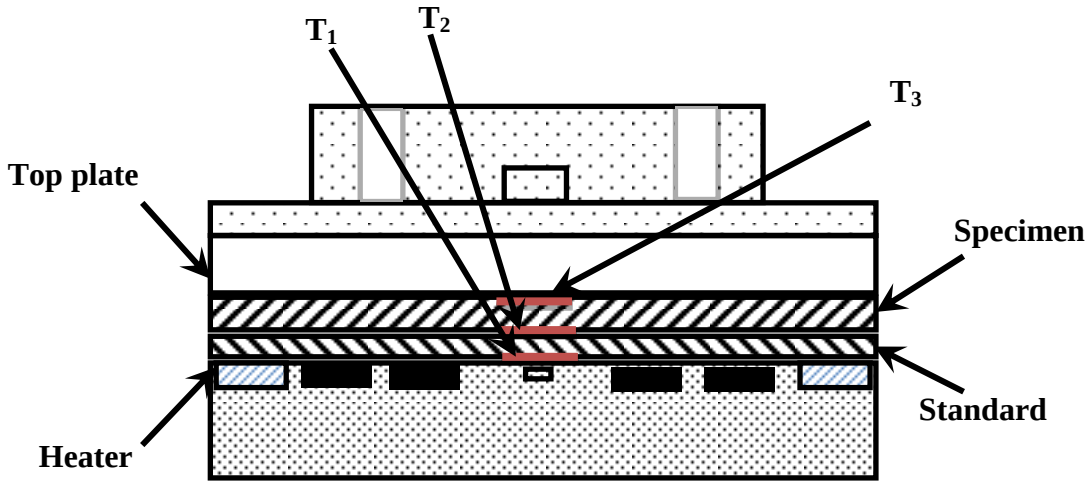

Figure 2.6: Togmeter: two plate method

During the testing, the sample (330 mm in diameter) is placed on the reference fabric (with known thermal resistance) which is heated by a temperature controlled hot plate. The top plate (insulated) needs to be closed gently to avoid the compression of fabric.

The following three temperatures are obtained at steady-state condition:

1. $T_{1:}$ the temperature at hot plate;
2. $T_{2:}$ the temperature between the upper surface of reference fabric and lower surface of tested specimen; and
3. T_3: the temperature in between the upper surface of the test specimen and top plate.

Thermal resistance of the test specimen is calculated by:

$$\frac{R_f + R_c}{R_s} = \frac{T_2 - T_3}{T_1 - T_2} \qquad 2.17$$

where R_f, R_c and R_s are the thermal resistance of the specimen, contact and standard respectively.

The detailed about the testing method can be found in BS 4745:2005 [63].

KES-F7 Thermo-Lab-II (manufactured by Katotech Ltd.) works on two plate method with guarded heater to ensure that heat only passes through the tested fabric. The testing arrangement is that fabric sample (5 x 5 cm) is placed on cold plate which is attached with a water box at room temperature. The temperature controlled hot plate (B.T- Box) with the accuracy of ±0.1ºC is placed over the fabric sample as shown in Figure 2.7 (a).

When steady-state condition achieved the heat loss from the B.T- Box will be displayed on the panel. The heat loss is calculated on the principle of how much power is supplied to the heater by using multiplier as illustrated in Figure 2.7 (b).

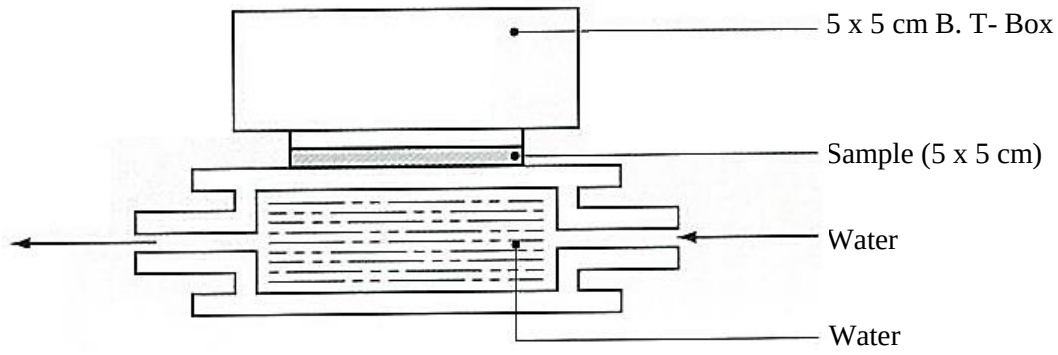

(a)

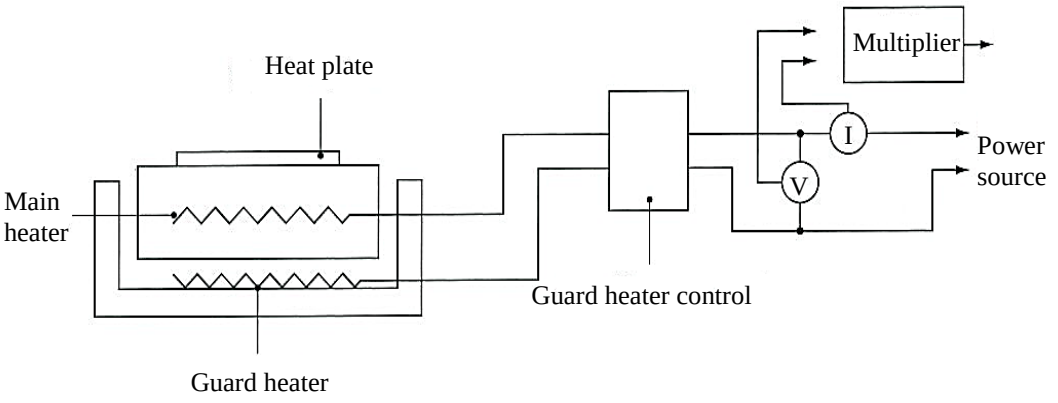

(b)

Figure 2.7: Thermo-Lab-II (a) Thermo-Lab-II for thermal conductivity measurement and (b) Circuit- diagram of B. T. Box [64]

The thermal conductivity (K) of fabric sample can be calculated by:

$$K = \frac{Q \cdot t}{A \Delta T} \qquad 2.18$$

where Q is the heat loss , t is the thickness of sample, A is the area of B.T- heat plate and ΔT is the temperature difference across the sample.

DTC-25 (TA Instruments) works on the principle of heat flow meter method in which heat flux sensor is attached to a heat sink cooled by liquid; heat flow meter method is highly accurate method for the measurement thermal conductivity of anisotropic materials [65]. The testing arrangement is that sample (50 mm in diameter) is placed between the two plates under compressive load and uses thermal interface pastes to avoid the contact thermal resistance as shown in Figure 2.8 (a). An axial temperature difference achieved between the two plates, heat flow from heat source (the hot plate) to the cold plate, presented in Figure 2.8 (b). When steady-state condition reached the temperature difference across the sample is measured by the temperature sensor installed on the surface of plates; heat flux is measured by the heat flux sensor. The thermal conductivity of sample can be calculated by Equation 2.18.

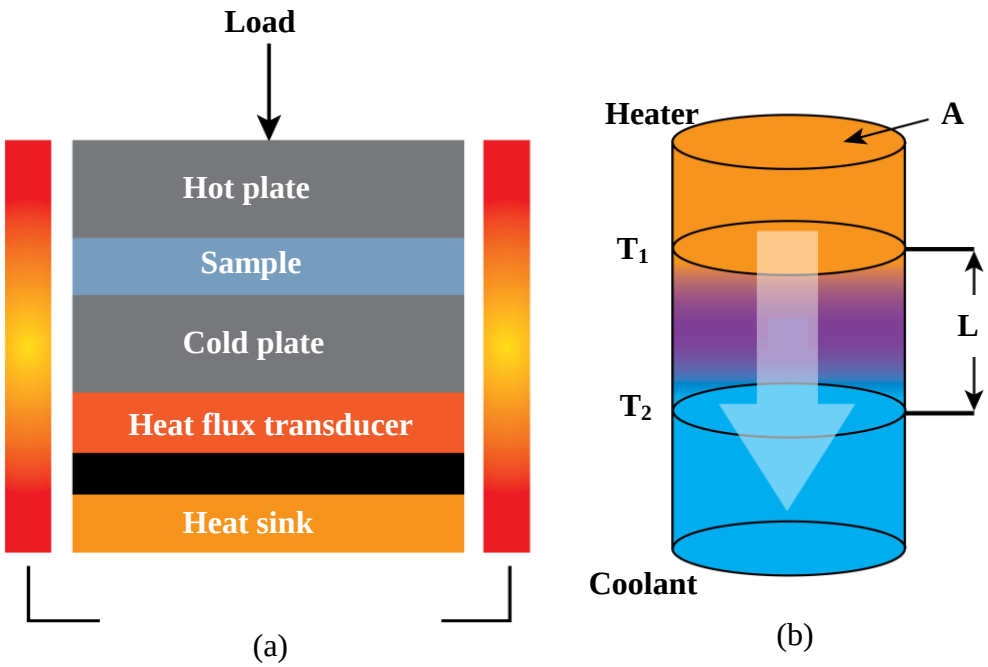

Figure 2.8: DTC-25: (a) Test section schematic and (b) Heat flow mechanism [66].

The detailed about the testing method can be found in ASTM E1530 [67].

Alambeta developed at the Technical University of Liberec (Czech Republic) is used to simulate the first moment of the contact of skin with fabric (warm-cool-feelings) by using the term thermal absorptivity, shown in Figure 2.9 (a).

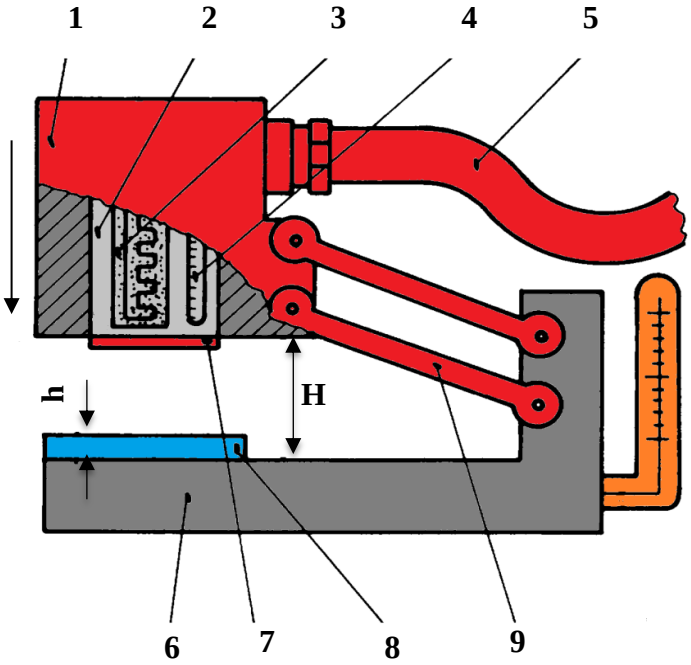

1: measuring head, 2: copper block, 3: heater, 4: temperature sensor,
5: connection with computer, 6: metal plate, 7: heat flow sensor,
8: sample and 9: parallel guide

(a)

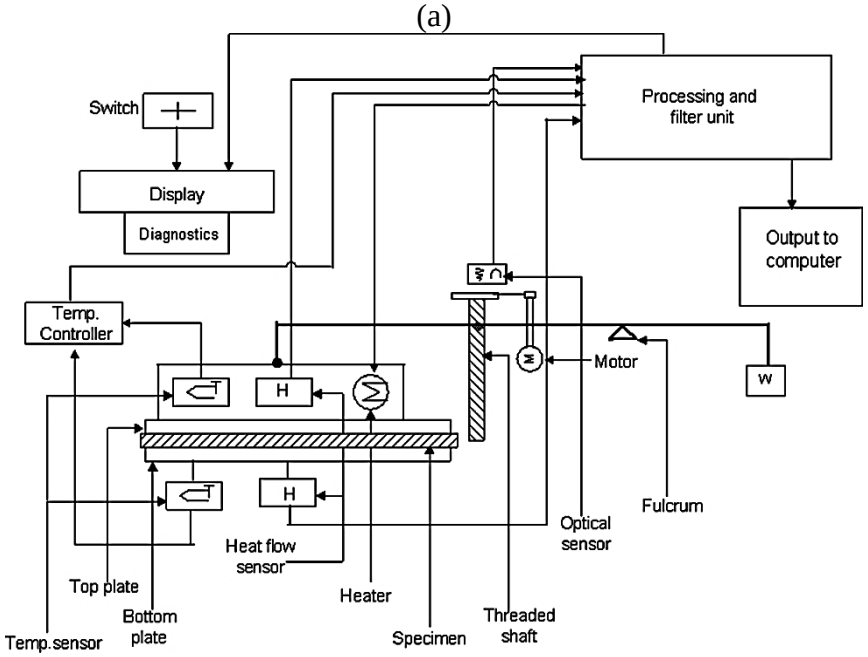

(b)

Figure 2.9: Alambeta (a) Schematically diagram of Alambeta [68] and (b) Line diagram of Alambeta [69]

Heat flow from skin to fabric, which has lower temperature than skin. Alambeta is used to measure transient and steady-state thermo-physical properties of fabric. The arrangement of device is that sample (5) is placed on a plate located at the instrument base (6) and top plate with heat flow sensor (7) connected to copper block (2) which has temperature controller maintaining the constant temperature difference from the sample.

During the testing the sample is paced between the two measuring heads both have heat flow sensors as shown in Figure 2.9 (b). When top measuring head comes down and touches the sample, the sudden transient heat flow is measured by Alambeta and different parameters are evaluated such as: thermal conductivity, thermal absorptivity, ratio of maximum heat flow density to stationary heat flow density $(q_{\max}/q_{st})$, thermal diffusion, thermal resistance, and thickness of sample by photoelectric sensor.

2.3.2 Cooling Method

Guarded hot plate method has also been used to evaluate the thermal transmittance of textile fabrics. It works on the principle that the fabric is placed over the heated plate maintained at constant temperature in the range of human skin temperature (33-36ºC) and the upper surface of the fabric is exposed to the air. The arrangement of the apparatus is that the heater is sandwiched between two aluminium plates and test plates is surrounded by guard ring to ensure that the all heat passes through the fabric and no heat loss, illustrated in Figure 2.10. A test apparatus placed inside the chamber for maintaining nearly still air conditions has a temperature range between 4.5 to 21.1°C (40 to 70°F).

During testing when equilibrium or steady-state condition is reached, the temperature of the hot plate and air above 500 mm from test plate inside the chamber is measured. The heat flux value determined by power supplied to the heater to maintain the temperature and the overall thermal transmittance of fabric with air can be calculated by:

$$U_1 = \frac{P}{A \times (T_p - T_a)} \qquad 2.19$$

where P is the power loss from test plate, A is the area of test plate, T_p is the test plate temperature and T_a is the air temperature.

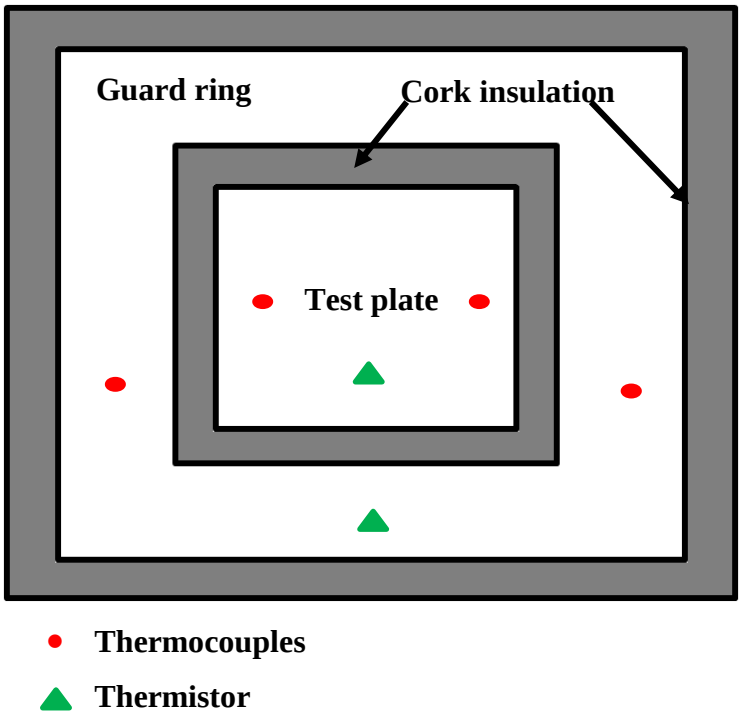

(a)

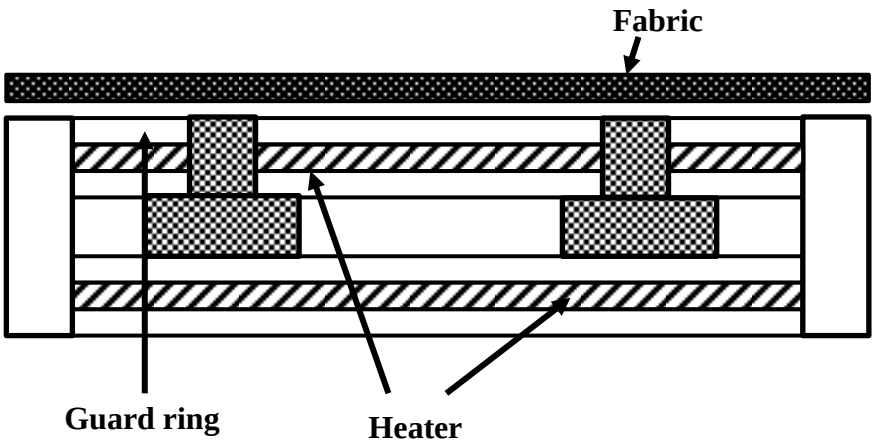

(b)

Figure 2.10: Guarded hot plate instrument: (a) Top view and (b) Side view

The thermal transmittance of fabric alone can be calculated by subtracting the thermal transmittance of bare plate (U_{bp}):

$$U_2 = \frac{U_1 U_{bp}}{U_{bp} - U_1} \qquad 2.20$$

The intrinsic thermal conductivity (K) of the fabric alone can be calculated by following equation.

$$K = \frac{U_2 \times t_i}{1000} \qquad 2.21$$

where t_i is the thickness of sample (mm).

The detailed about the testing method can be found in ASTM D 1518-85 [70].

2.3.3 Constant Temperature Method

The basic concept of constant temperature method is that fabric sample is to wrap around the hot body and the amount of energy required maintaining the constant temperature difference between the fabric and coolant normally used is air.

The general arrangement of apparatus consists of cylinder heater on which fabric sample is wrapped, the end of the cylinder properly insulated and the chamber. The cylinder is heated electrically and at steady-state conditions, the thermal conductivity of fabric can be calculated by measuring the amount of energy required to maintain the temperature difference between the cylinder surface and air in the chamber [18].

2.4 Effect of PCM on Heat Transfer Behaviour of Textiles

Microencapsulated phase change materials (MicroPCMs) are thin wall spherical particles consisting of core phase change material (PCM) and the wall. The wall is inert and high temperature resistant polymeric material, which prevents leakage of the core material while in liquid phase. MicroPCMs are widely used to regulate the temperature and heat storage in many applications such as building materials [71], electronics [72], thermal energy storage system [73], solar heating system [74], coating of fabrics [75, 76] and fibres [77, 78].

The MicroPCMs technology was first incorporated inside textile fibres in 1987 to improve their thermal performance [79] and MicroPCMs can also be incorporated in textile fabric by coating [8]. When PCM fabric is exposed to hot environment it absorbs heat and keeps the temperature of fabric constant until PCM melts and similarly when it is subjected to cold environment, where the temperature below the crystallization

temperature of PCM it converts from liquid to solid [2]. Thermal performance of PCM fabric mainly depends on the amount of PCM used in the fabric.

Heat and moisture transfer in PCM fabric have been investigated by many researchers. In 1990, Lamb and Duffy-Morris [80] measured the heat loss through fabrics with and without PCM additives. Pause [81] investigated the development of heat and cold insulating membrane structures with phase change materials. For that he carried out research to develop a new membrane material with improved thermal properties by the application of phase change material.

Nuckols [82] developed an analytical model of a diver dry suit enhanced with micro-encapsulated phase change materials to predict their thermal performances in simulated ocean environments. Kim and Cho [83] developed thermostatic garments using MicroPCMs and assessed their temperature sensing properties and compared to the garments without MicroPCMs. Ghali et al [84] studied the effect of phase change materials on clothing during periodic ventilation.

Li and Zhu [85] developed a mathematical model to predict the heat and moisture transfer through PCM textile on the basis of finite volume difference method. The purpose of that work was to develop a tool which numerically computed the distributions of temperature, moisture concentration and water content in the fibres for different amounts of PCM applied in porous textiles.

Fengzhi and Yi [86] developed a mathematical model that analysed the heat and moisture transfer in porous textiles with PCM microcapsules and analysed the effect of fibre hygroscopicity on the distributions of water vapour concentration in the fabrics, water content in the fibres and on the effect of PCM microcapsule in delaying fabric temperature variation during environment transient periods.

Fengzhi [87] established a dynamic model to analyse the mechanisms of heat and moisture transfer in PCM incorporated clothing and investigated the effect of PCM distribution by considering the effect of water content on physical parameters of textiles and heat transfer with phase change. Ying et al [88] developed a dynamic mathematical model of heat and moisture transfer in multi-layer porous textiles, in which some layers incorporated PCM. A finite element volume difference scheme was used to numerically simulate the thermal regulating performance.

Bendkowska and Wrzosek [89] studied the thermo-regulating properties of nonwovens treated with microencapsulated PCM and determined the temperature regulating factor and thermal resistance. Sánchez et al [17] developed a thermo-regulating textile by using PCM microcapsules through a coating technique. The thermoregulatory effect was studied by using an infrared thermography (IR) camera.

Salaün et al [75] manufactured the thermo-regulating textile fabric based on different mass ratio of binder to microcapsules and analysed the effect of the amount of microcapsules and binder on the thermal response of the fabric.

Alay et al [90] analysed the thermal comfort properties of the fabrics incorporating microencapsulated phase change materials (MicroPCMs) and studied the thermal conductivity and thermal resistance under steady-state condition. Yoo et al [91] investigated the thermo-regulating properties of four-layer garments and analysed the effects of the number of layer and position of fabrics treated with PCM in a garment. Their work showed that the location of the PCM-treated fabric in a garment is an important factor in determining the rate of heat loss.

More recently, Hu et al [92] developed an one dimensional mathematical model to analyse the thermal insulation property of protective clothing embedded with PCM for firefighters. The research was focused on temperature variation by comparing different thicknesses and position conditions of PCM in the clothing, as well as the melting state of PCM and human irreversible burns.

2.5 Discussion and Identification of Research Gap

All the foregoing research works related to the modelling of thermal conductivity of textile fabrics are lack of accuracy and there were no consideration of the following:

(a) The actual cross-section of yarn in woven fabric and actual parametric geometric model of knitted fabric

Cross-section of yarn has significant influence on the fibre content in the model. Fibre content or volume fraction of fibre in the model can be defined as the ratio of fibre volume to the total volume of model. A textile fabric as non-homogeneous material contains heterogeneous mixture of fibre substance and air, usually the thermal conductivity of air is less as compared to the thermal conductivity of textile fibre. If the inaccurate or non-realistic cross-section of yarn were used for geometrical modelling of

woven fabric this would give more amount of fibre than the actual. The resulted overall thermal conductivity of the fabric will be more than it should be because the model has less air or vice versa. Similar effect may happen in geometrical modelling of knitted fabric by using the generic geometric modelling approach which gives more deviation in stitch length and also has significant impact on the fibre content in the model.

(b) Fibre orientation and influence of fibre anisotropy behaviour on effective thermal conductivity of fabric

Textile fibres are transversely isotropic in nature; transversely isotropic material is a special kind of orthotropic material. Orthotropic material is subset of anisotropic material. Transversely isotropic materials are those in which properties are symmetrical in one plane and different in plane which is perpendicular to this plane. Thermal conductivity of fibre is more in longitudinal direction than the transverse direction therefore it is necessary to get the material orientation assigned for material property during finite element modelling process. The assumption of yarn and fabric as isotropic material made by those published research work was incorrect and it will give more deviation from the experimental results.

(c) Temperature dependent thermal conductivity of fibre

Thermal conductivity of fibre increases with the increase of temperature and similar pattern is followed by the air therefore in realistic estimation of effective thermal conductivity in high temperature environment it is necessary to consider the temperature dependent thermal conductivity.

2.6 Research Methodology

This chapter also summarizes the methodological approaches of the research work which gives the better understanding to the reader on how the overall objectives of the research will be achieved as described in the section 1.3.

The research methodology contains three parts: the first to describe the design and development of experimental setup for thermal conductivity measurement; second part to address the development of finite element models to simulate and predict the effective thermal conductivity and thermal resistance of textile structures; and third part to describe the creation of plug-ins for the generation of the geometrical models of different textile structures.

2.6.1 Development of an Experimental Setup

Thermal conductivity testing of fabrics is one of the objectives as described in section 1.3. The literature review suggested that there are three methods available to test the thermal conductivity of textile materials. The design concept of the in-house experimental setup in this research adopted the heat flow meter method because heat flow meter method is the most accurate method to obtain the thermal conductivity of anisotropic material when temperature gradient is applied in one direction as described in the literature review. The design aim, selection of components and testing procedure will be discussed in Chapter 3.

2.6.2 Finite Element Modelling

Finite element method is a numerical technique for solving complex problems by dividing them into finite number of simple elements that can be solved in relation to each other. Its practical approach is Finite Element Analysis (FEA).

In this work a commercial software Abaqus/CAE is used to evaluate the thermal property and analyse the heat flow mechanism of textile structures. The most important benefit of FEA is that it is able to determine some of the properties which cannot be easily obtained through experimental studies. The detailed background information regarding the evaluation of thermal property and heat flow mechanisms by using finite element method will be covered in Chapter 4 and Chapter 5.

2.6.3 Plug-ins Development

In this research GUI plug-ins have been developed to automatically generate and predict the effective thermal conductivity of textile structures. Plug-ins are developed by using Python script. In Abaqus/CAE python script allows to create interactive user interface which takes input from user and can be used to generate geometrical models, extract results from output data base and many more. The design aim, development and validation of plug-ins will be discussed in detail in Chapter 6.

2.7 Summary

In this chapter, relevant literature has been reviewed which provides better understanding about the heat transfer analysis of different textile structures and the overall needs for this research.

The literature review discusses the factors which influence the effective thermal conductivity of textile fabrics such as fibre orientation, thermal anisotropy of fibre etc. Different methods of experimental measurement have been described. Development of thermo-regulating smart textiles and their improved heat transfer behaviour have also been discussed.

In addition this chapter provided the foundation and overall plan to achieve the aim and objectives of this research work. The next chapter contains the information about the design and development of experimental setup.

Chapter 3 Development of Experimental Setup for Thermal Conductivity Measurement

3.1 Introduction

Development of an experimental setup to measure the thermal conductivity across the thickness of the fabric was one of the objectives in this research. This chapter introduces an in-house experimental setup for the measurement of the thermal conductivity of fabric by using two plates heat flow meter method. It was based on the heat flow meter principle which is a highly accurate and reliable method in determining the thermal conductivity of anisotropic material when heat flows in one direction. The design, development and selection criteria of components of the set up will be discussed. Testing procedure and data acquisition is also elucidated.

3.2 Rationale

The knowledge of thermo-physical properties of textile materials is important to understand thermal comfort of the fabric. Accurate and highly efficient thermal measurement of material is the key for the development of products that have thermal transport applications such as thermo-regulation, thermal comfort, thermal protection, thermal insulation and more. Thermal property evaluation technique should be reliable and accurate. According to the literature, thermal conductivity is one of the thermal properties influencing the heat transfer behaviour of fabrics. For this purpose, an experimental setup was designed and developed which is capable of testing thermal conductivity by using one plate and two plate methods.

The developed experimental setup is different from commercial available instruments mentioned in Chapter 2. A Proportional-Integral-Derivative (PID) controller and highly sensitive heat flux sensor were used to control the temperature of heater, and it is designed with the consideration of small sample size, fast testing, highly accuracy and reproducibility of testing results.

3.3 Design and Development of Experimental Setup

Figure 3.1 shows the 3D model of the experimental setup. Based on the motivation discussed above, the experimental setup was developed in three steps:

1. hot plate development;

2. cold plate development; and
3. heat flow data acquisition.

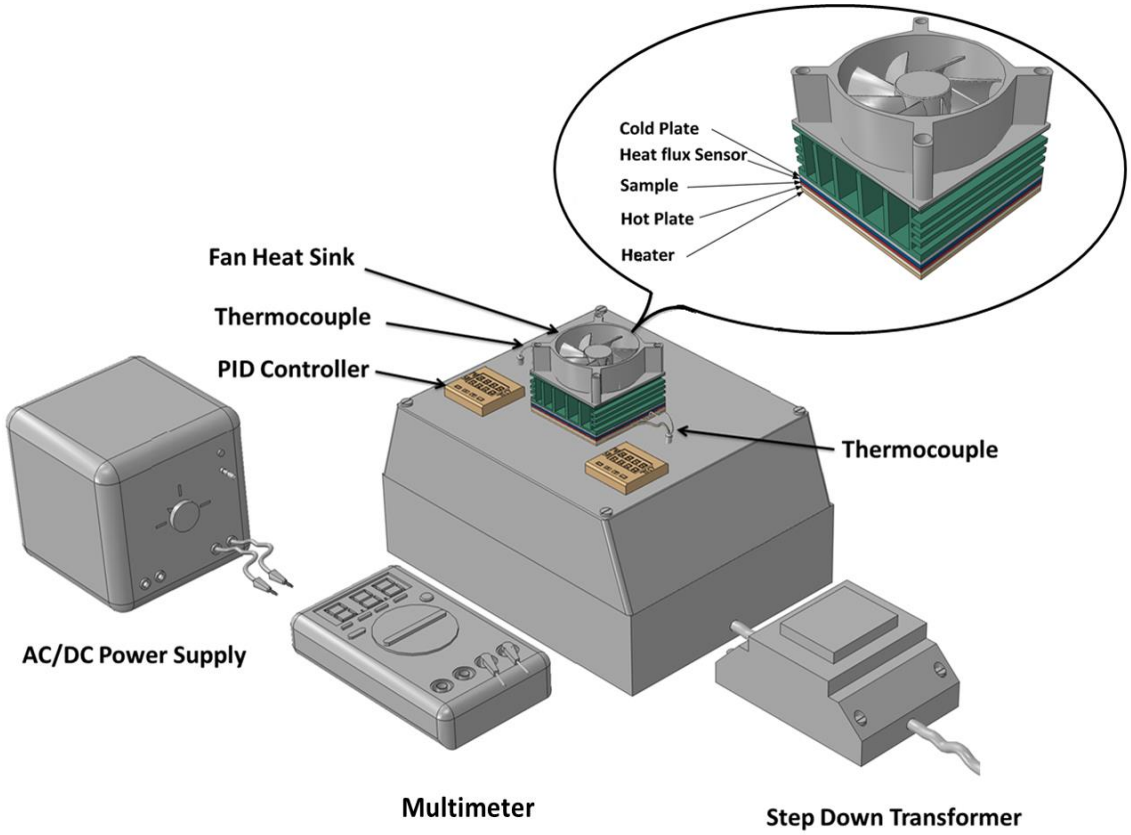

Figure 3.1: 3D model of experimental setup

3.3.1 Hot Plate Development

A halogen free thermoplastic box was used to enclose the controller, it provides the base of the hot plate. A fibre glass insulation plate is fastened in the centre of the box to avoid the effect of excessive heat build-up during the heating process especially in steady-state analysis with one plate as show in Figure 3.2.

A OMEGALUX® Kapton® insulated flexible heater as shown in Figure 3.3 is used to heat the aluminium plate (50×50 mm) acted as hot plate. The construction of flexible heater is that the etched foil element which is encapsulated between the layers of Kapton® and Teflon® adhesives.

The selection criteria are: Kapton® is polyamide film produced by Dupont® which can withstand at high temperature and the operating temperature range of flexible heater is -200 °C to 200 °C.

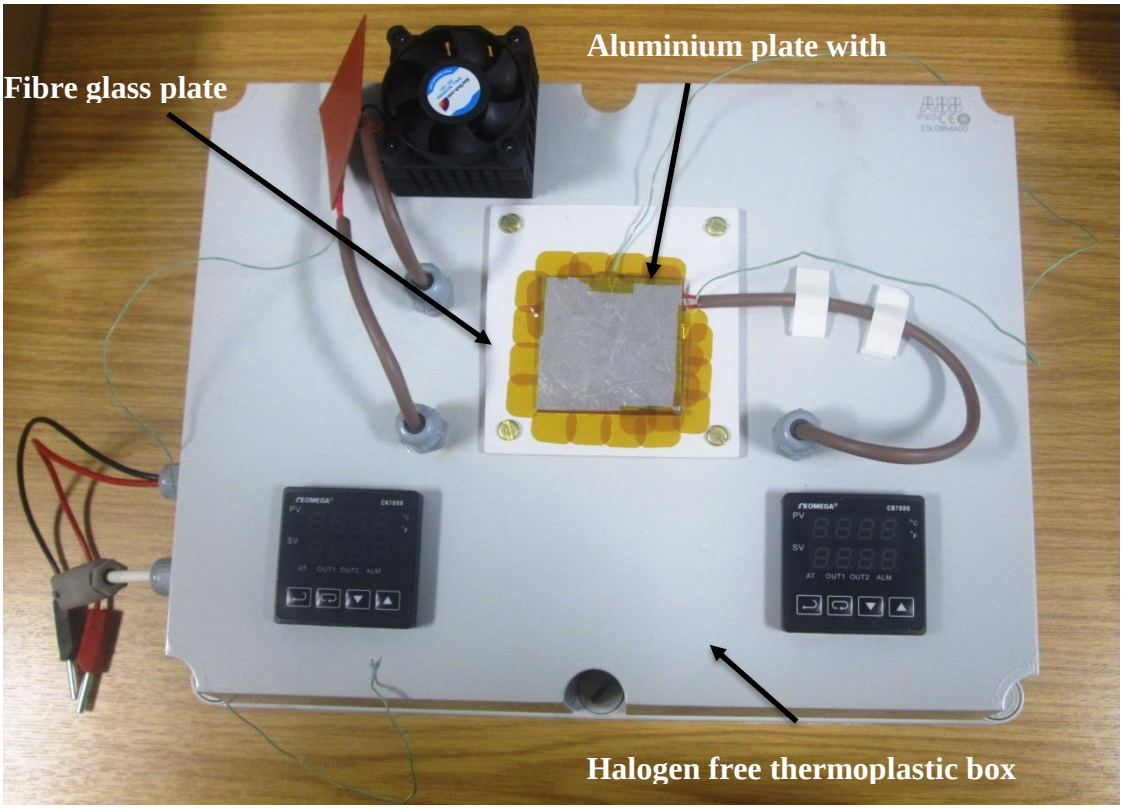

Figure 3.2: Hot plate arrangement of experimental setup

Figure 3.3: Kapton® Flexible heater (50×50 mm)

Heater is mounted on the top of the fibre glass plate and an aluminium plate was placed and fixed over the heater. A slight grove was made on the aluminium plate to fix the K-Type thermocouple which was connected to the controller to maintain the temperature of the hot plate.

A CN7800 controller manufactured by Omega was used to control the temperature of heater as shown in Figure 3.4 . It works with wide variety of thermocouples (B, E, J, K, L, R, S, T, U and W) with temperature covering range from -212 °C to 1820 °C. K-type thermocouples have been used to measure the temperature of hot and cold plates.

The selection criteria are: (1) the available control options of controller are: on/off, PID (Proportional-Integral-Derivative), auto-tune and manual-tune; and (2) the measuring error of the controller is below ±0.25% and the temperature fluctuation of the heater within of ±0.1°C.

Figure 3.4: Omega CN7800 controller

A controller controls the heater by PID operation mode. PID controller provides proportional with integral and derivative control. This controller combines the proportional control with two additional adjustments, enabling the unit automatically compensate any changes in the system.

The proportional, integral and derivative terms must be individually adjusted or "tuned" to a particular system, using a "trial and error" method. It provides the most accurate and stable control over on/off and proportional controller.

In fact the temperature of the hot plate is controlled indirectly by a heater which gives more stable temperature control of ±0.1°C of the surface of hot plate.

3.3.2 Cold Plate Development

A fan heat sink was used to maintain the temperature gradient between hot and cold plates. An aluminium plate was connected with fan heat sink which has a K-type thermocouple. Thermocouple was connected similarly to the hot plate. A fan heat sink from StarTech.com as shown in Figure 3.5 is used to connect to the aluminium plate acted as cold plate.

The selection criteria are: the dimension of the aluminium heat sink is 50×50 mm and fan speed is around 5000 rpm to meet design specification of sample size and capable of maintaining the surface temperature of cold plate which is up to 25 ºC.

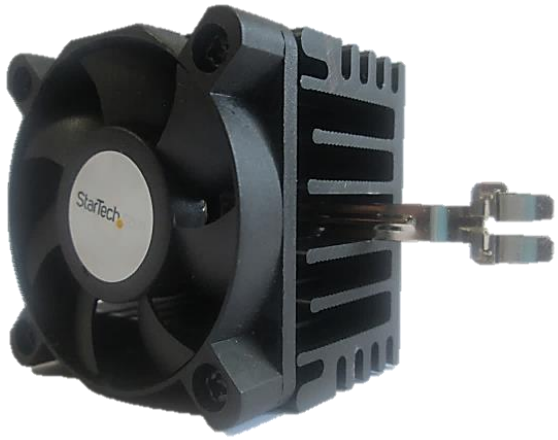

Figure 3.5: Fan heat sink

AC/DC power supply is used to supply the 12V DC to fan heat sink. Kapton® Flexible heater works on 115Vac input voltage and CN7800 PID controller works in the range of input voltage of 100-240Vac, therefore Step-down transformer is used to step down the voltage from 230 to 115 Vac.

3.3.3 Heat Flow Data Acquisition

A CAPTEC flat plate heat flux sensor (50×50 mm) as shown in Figure 3.6 is used to measure the heat flux passed through the fabric. The sensor is constructed by a thin foil sensor which is sandwiched between two copper plates. The thin foil sensor is made of thermoelectric panel which is laminated between the polymeric layers.

When sensor comes in contact with the surface of fabric sample which produces or absorbs heat, therefore it creates the temperature difference across the surface of sensor. The temperature difference generates voltage which is proportional to the heat flow through the sensor.

The selection criteria are: (1) the operating temperature range and sensitivity of sensor are -180 °C to 200 °C and 16.8 $\mu volt/(W/m^2)$ respectively; and (2) the operating temperature range and size of the sensor match with the heater.

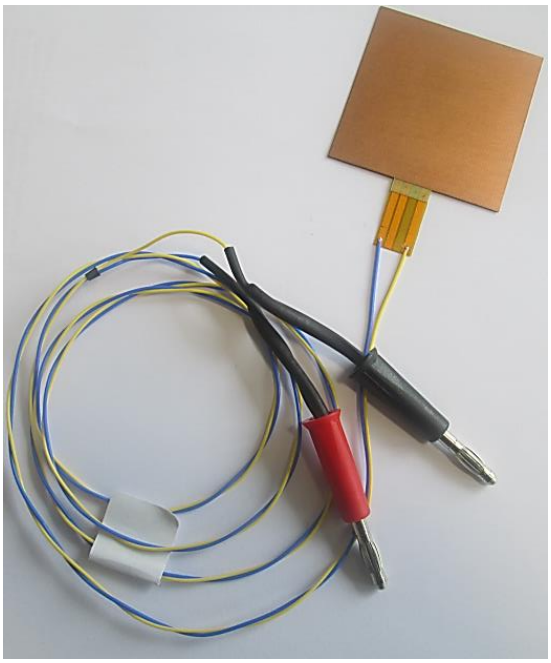

Figure 3.6: Flat plate heat flux sensor

A MASTECH MS8218 Multimeter as shown in Figure 3.7 is used to measure the voltage generated from the heat flux sensor.

The selection criteria are: (1) It has 50000 counts measurement capability with maximum 0.01Ω resistance resolution and 1μV voltage resolution; (2) it can be connected to a computer by RS-232C connector; and (3) it is able to record and analyse collected data by software MS2818 V1.6.

Figure 3.7: MASTECH MS8218 Multimeter

3.4 Testing Procedure for Thermal Conductivity and Thermal Resistance Measurement

The entire test was conducted in standard conditions at a room temperature of 20±2ºC and 65±2% relative humidity. The samples were cut in a defined square shape 50×50 mm dimension and conditioned for 24 hours before they were tested. During the testing, sample was placed between the hot and cold plate as shown in Figure 3.8.

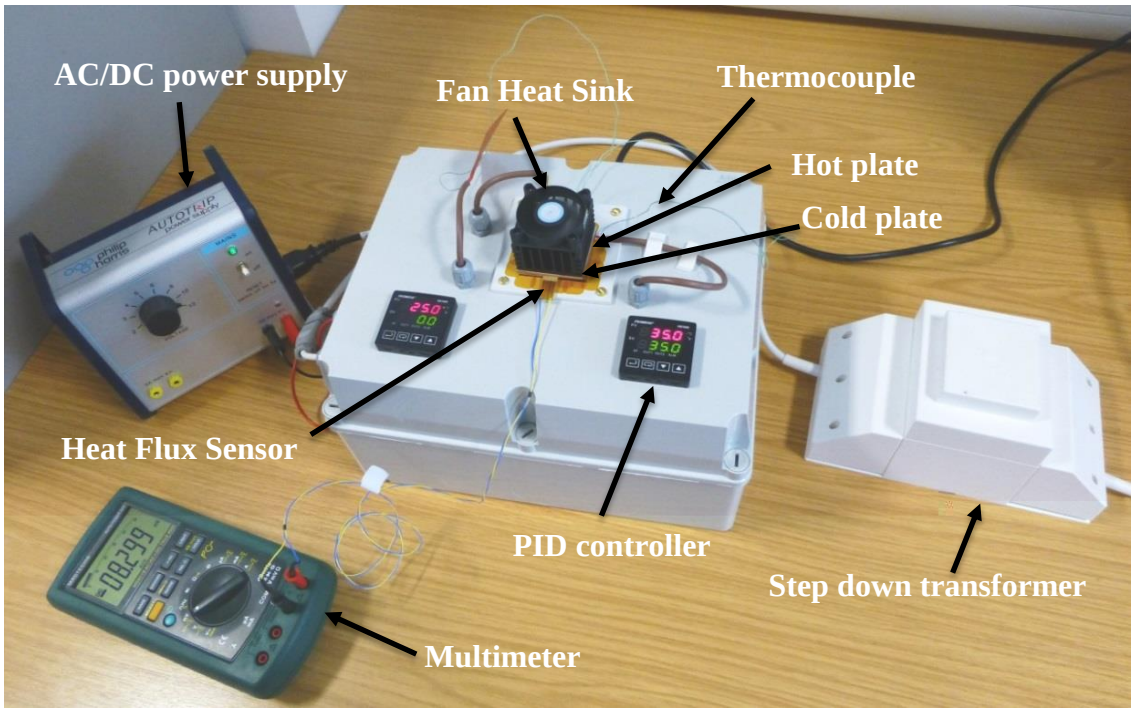

Figure 3.8: Photograph of experimental setup during testing

The hot plate temperature was maintained by the PID controller at 35 °C which is within range of normal human body temperature. The temperature of the cold plate is controlled by a fan heat sink. A heat flux sensor with sensitivity of 16.8 $\mu volt/(W/m^2)$ was used with cold plate to measure the amount of heat flow through the sample caused by the temperature difference. Temperature sensors were connected with hot and cold plates to measure the temperature difference across the sample.

When steady–state condition has been achieved the voltage generated from the heat flux transducer will be obtained from software MS2818 V1.6 as shown in Figure 3.9.

MS2818 V1.6 is capable of generating voltage report received from the heat flux sensor, the voltage report is then exported in CSV (Comma Separated Values) file which can be

analysed in Microsoft Excel spread-sheet applications. It is very useful to obtain the heat flux values with respect to time for MicroPCMs coated fabric.

The data obtained from the heat flux sensor in millivolt needs to be converted to heat flux in order to calculate the thermal conductivity. Voltage value can be converted into heat flux by dividing the sensitivity value of heat flux sensor as shown in Equation 3.1.

$$Q = \frac{V}{S} \tag{3.1}$$

where V is the output of heat flux sensor and S is heat flux sensor sensitivity.

The effective thermal conductivity (K_{eff}) and thermal resistance of samples can be calculated by Equation 2.1 and 2.3 presented in Chapter 2.

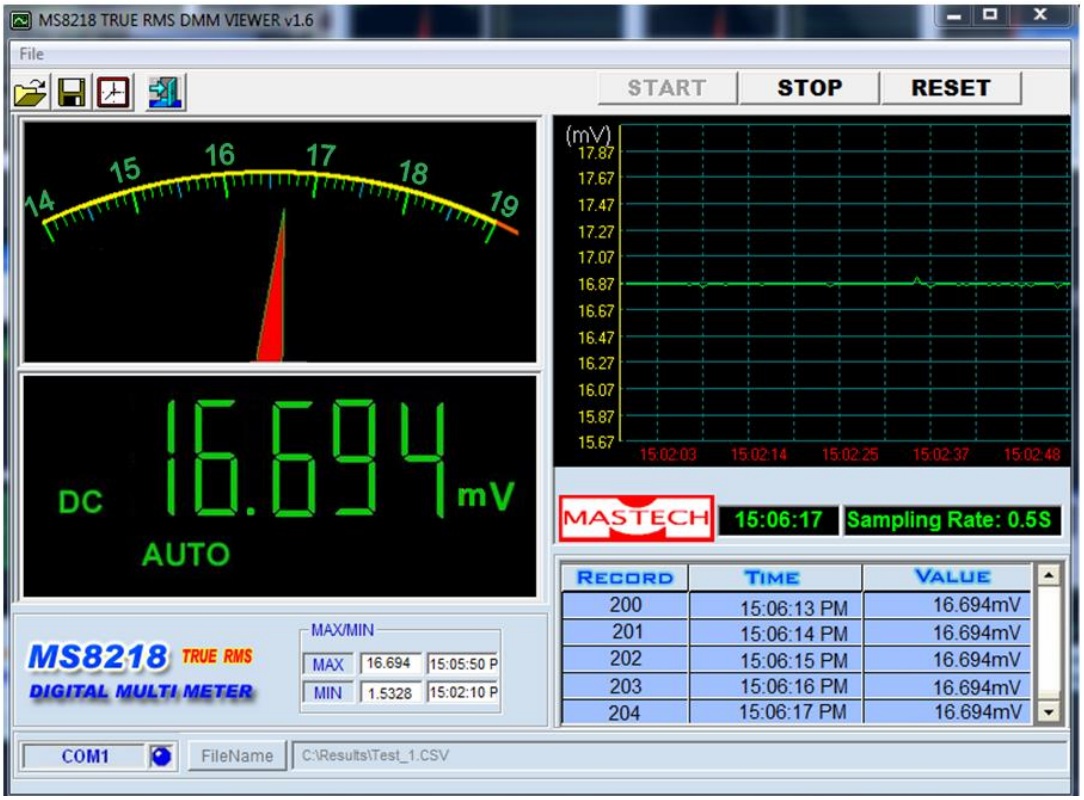

Figure 3.9: Main software environment of MS2818 V1.6

The details of the fabric specifications are given in Table 3.1 to Table 3.4. The purpose of selecting fabrics with different structures has been briefly described in Chapter 1 and Chapter 2. The details regarding the criteria of fabric selection will be covered in Chapter 4. Table 3.5 shows the experimental results obtained from the experimental setup.

Table 3.1: Fabric specifications of plain weave fabric

Specifications	Nomex® III	Twaron®	Cotton	Wool	Poly-Viscose
Areal density (g/m^2)	170±3	150±4	132±4	130±3	98.0±2
Warp/Weft sett (per inch)	59/59	19.8/19.8	65/55	70/45	75/85
Warp/Weft Yarn linear density (Tex)	33.3/33.3	93/93	25.5/25.5	27.8/27.8	7.798/19.6

Table 3.2: Specifications of plain weft knitted fabrics

Fabric Code	Fibre Type	Yarn Count (Tex)	wpc	cpc	SL (mm)	t (mm)	Areal Density (g/m^2)
F1	Polyester (MF)	27.0	3.2	5.6	8.220	0.49	40.4
F2	Polyester (MF)	20.0	6.4	9.6	4.930	0.47	61.0
F3	Polyester (MF)	27.0	7.4	9.0	5.020	0.49	92.0
F4	Cotton (SF)	40.0	6.0	7.5	5.910	0.8	104.62
F5	Viscose (MFF)	33.5	6.0	9.6	5.083	0.648	102.3

MF: Monofilament; MFF: Multifilament; SF: Staple fibre; SL: Stitch length wpc: Wales per cm; cpc: Course per cm; and t: thickness

Table 3.3: Fabric specifications of plain weave PCM coated fabric

Specifications	Nomex® III	Twaron®	Cotton
Thickness	0.68	0.575	0.56
Warp/Weft sett (per inch)	59/59	19.8/19.8	65/55
Warp/Weft Yarn linear density (Tex)	33.3/33.3	93/93	25.5/25.5

Table 3.4: Fabric specifications of nonwoven fabric

Specifications	Sample-1	Sample-2	Sample-3
Areal density (g/m^2)	78.133	38.265	77.280
Thickness (mm)	0.54	0.35	0.57
Fibre Material	polypropylene	polypropylene	polypropylene

Table 3.5: Experimental results of effective thermal conductivity and thermal resistance of fabrics

Fabric Code	Experimental effective thermal conductivity, K_{eff} (W/m.K)	Experimental thermal Resistance of Fabric, R_z (m^2.K/W)
Nomex®III	0.05000	0.010000
Twaron®	0.04100	0.008486
Cotton	0.05600	0.008643
Wool	0.04140	0.009855
Poly-Viscose	0.04840	0.007045
F1-Polyester (MF)	0.03500	0.014000
F2-Polyester (MF)	0.03770	0.012467
F3-Polyester (MF)	0.04030	0.012159
F4- Cotton (SF)	0.04300	0.018605
F5- Viscose (MFF)	0.04120	0.015728
Nomex® III with PCM	0.08900	0.007640
Cotton with PCM	0.08700	0.006609
Wool with PCM	0.07200	0.007778
Sample-1 (polypropylene)	0.037335	0.014464
Sample-2 (polypropylene)	0.036146	0.009683
Sample-3 (polypropylene)	0.033889	0.016820

MF: Monofilament; MFF: Multifilament; SF: Staple fibre

3.5 Validation of Experimental Setup

In order to test the accuracy of the experimental setup the thermal conductivity of fabric samples were tested using the developed device and the results were compared to that of tested by commercial instruments.

Table 3.6 shows the material specification of samples that were tested for the validation of the in-house developed device. It is worth to note: although not all of the fabric samples used for this project were tested for the purpose of device validation, fabrics made by all types of construction methods were selected for testing by commercial instruments for comparison due to limited availability of testing facilities.

Table 3.6: Fabric specifications

Fabric Code	Fabric Construction
Nomex® III	Plain weave
Twaron®	Plain weave
Wool	Plain weave
Poly-Viscose	Plain weave
F1-Polyester (MF)	Plain weft knitted
F2-Polyester (MF)	Plain weft knitted
F3-Polyester (MF)	Plain weft knitted
F4- Cotton (SF)	Plain weft knitted
F5- Viscose (MFF)	Plain weft knitted
Nomex® III with PCM	PCM Coated Woven
Wool with PCM	PCM Coated Woven
Sample-1 (polypropylene)	Nonwoven

MF: Monofilament; MFF: Multifilament; SF: Staple fibre

Table 3.7 and Table 3.8 show the comparison between the results obtained from developed experimental setup and commercial available instruments. Different construction methods of samples have been tested to evaluate the effectiveness of the developed instrument. The results obtained from the Togmeter have higher absolute error because high pressure was applied on the top plate of Togmeter therefore fabrics were compressed and gave higher thermal conductivity because of less air present in samples.

The low mean absolute error between the newly developed experimental setup and commercial instruments tested results of thermal conductivity and thermal resistance were found 7.94 and 8.55 respectively. A very high correlation coefficient and coefficient of determination between results obtained by the developed experimental setup and commercial instruments are shown in Figure 3.10 and Figure 3.11.

Table 3.7: Comparison of thermal conductivity obtained from developed experimental setup and commercial instruments

Fabric Code	In-house developed Experimental Setup (W/m.K) (A)	Commercial Instruments (W/m.K) (B)	Absolute Error $\lvert(B-A)/B\rvert\times100$ (%)
Nomex® III	0.0500	0.0521(Togmeter)	4.03071
Twaron®	0.0410	0.048 (Togmeter)	14.58333
Wool	0.0414	0.049 (Togmeter)	15.5102
Poly-Viscose	0.0484	0.042 (Togmeter)	15.2381
F1-Polyester (MF)	0.0350	0.0383(Alambeta)	8.616188
F2-Polyester (MF)	0.0377	0.0401(Alambeta)	5.985037
F3-Polyester (MF)	0.0403	0.0418(Alambeta)	3.588517
F4- Cotton (SF)	0.0430	0.044 (Alambeta)	2.272727
F5- Viscose (MFF)	0.0412	0.0399(Alambeta)	3.25815
Nomex® III with PCM	0.089	0.09 (DTC-25)	1.111111
Wool with PCM	0.072	0.08 (DTC-25)	10.00000
Sample-1 (polypropylene)	0.037335	0.042 (Alambeta)	11.10714
Mean Absolute error (%)	-	-	7.942

MF: Monofilament; MFF: Multifilament; SF: Staple fibre

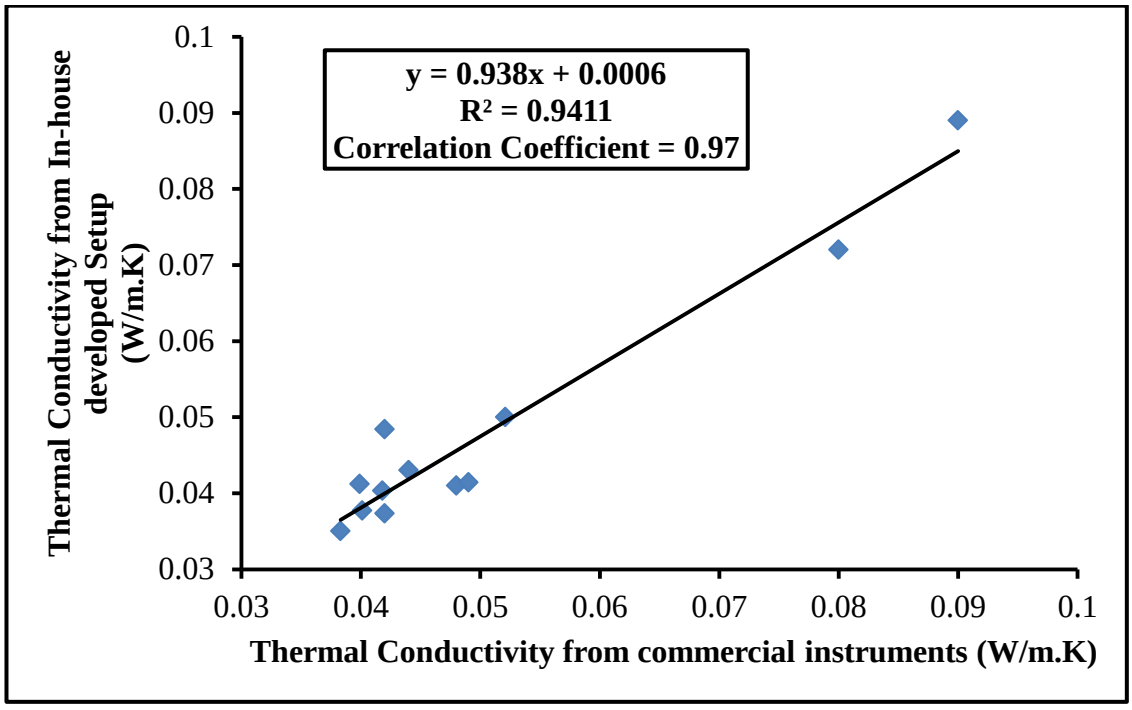

Figure 3.10: Comparison of thermal conductivity between developed experimental setup and commercial instruments

Table 3.8: Comparison of thermal resistance obtained from developed experimental setup and commercial instruments

Fabric Code	In-house developed Experimental Setup (m^2.K/W) (A)	Commercial devices (m^2.K/W) (B)	Absolute Error $\lvert(B-A)/B\rvert\times100$ (%)
Nomex® III	0.009597	0.0100 (Togmeter)	4.2
Twaron®	0.00725	0.00849 (Togmeter)	17.0732
Wool	0.008327	0.00985 (Togmeter)	18.3575
Poly-Viscose	0.008119	0.00704 (Togmeter)	13.22314
F1-Polyester (MF)	0.012794	0.01400 (Alambeta)	9.42857
F2-Polyester (MF)	0.011721	0.01247 (Alambeta)	6.36605
F3-Polyester (MF)	0.011722	0.01216 (Alambeta)	3.72208
F4- Cotton (SF)	0.018182	0.01861 (Alambeta)	2.32558
F5- Viscose (MFF)	0.016241	0.01573 (Alambeta)	3.15534
Nomex® III with PCM	0.007556	0.00764 (DTC-25)	1.1236
Wool with PCM	0.007	0.00778 (DTC-25)	11.1111
Sample-1	0.012857	0.01446 (Alambeta)	12.495
Mean Absolute error (%)	-	-	8.54843

MF: Monofilament; MFF: Multifilament; SF: Staple fibre

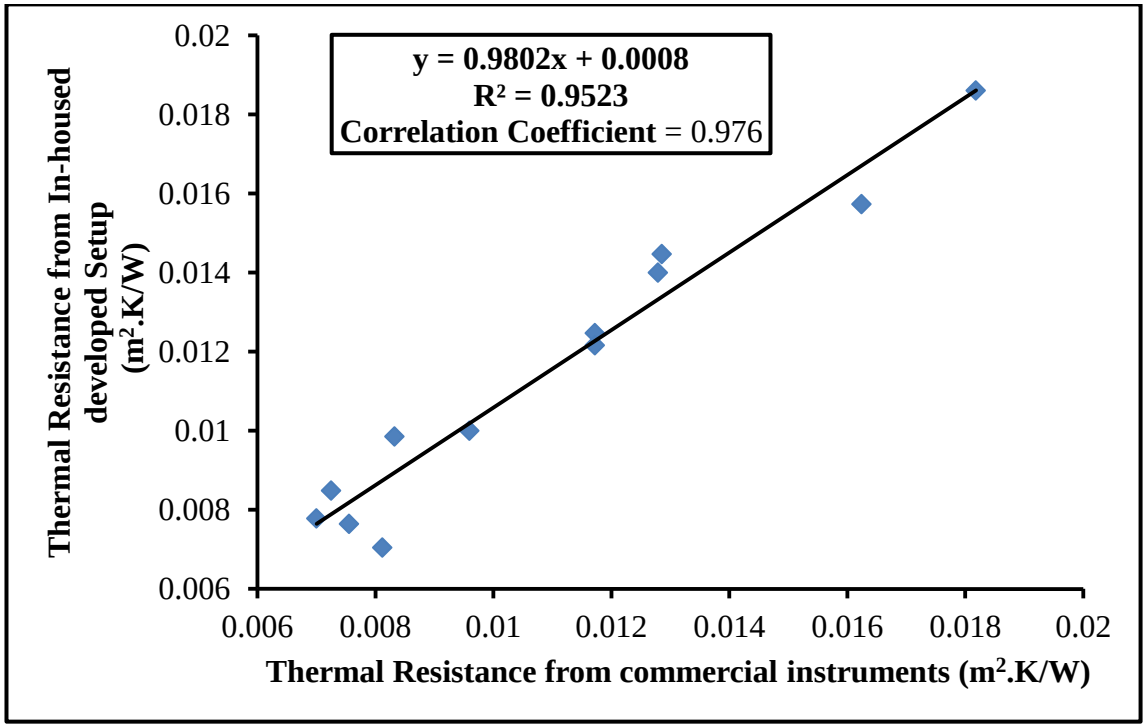

Figure 3.11: Comparison of thermal resistance between developed experimental setup and commercial instruments

3.6 Summary

In this chapter the detailed design and development of an experimental setup have been described for the evaluation of the thermal conductivity and thermal resistance of textile structures. A good correlation coefficient and coefficient determination between the results obtained from developed device and commercial instruments show the success and reliability of the developed setup in determining the thermal conductivity and thermal resistance of fabrics. The setup can also be used for transient heat transfer analysis by using the software to evaluate the heat flow rate with respect to time.

The next Chapter will describe the development of the finite element geometrical structures.

Chapter 4 Geometrical Modelling

4.1 Introduction

Textile fabrics can be classified as: woven, nonwoven and knitted fabrics. In case of woven and knitted fabrics, fabrics are composed of yarns which contain individual fibres; these fibres may be staple and continuous filament. But in case of nonwoven fabrics they are composed of bulk fibres bonded together by means of mechanically, chemically and thermally. Woven fabrics are composed of two sets of yarns which interlace with each other at 90 degrees. Knitted fabrics are produced by the inter-looping of yarn. This Chapter describes the development of finite element geometrical model of woven, MicroPCMs coated woven, knitted and nonwoven fabric.

4.2 Geometrical Modelling of Plain Woven Fabrics

Physical, mechanical and thermal properties of fabrics mainly depend on their structural parameters once a specific fibre material has been selected. In order to predict these properties accurately it needs to define the realistic geometrical models of the fabric structures. In this section a brief review of geometrical modelling of plain woven fabric will be carried out.

The first attempt was made by Peirce in 1937 [93] to study a geometrical model of plain woven fabric by considering yarns cross-section as circular; yarns were highly incompressible and absolutely flexible. Yarn path of fabric defined by a tangent line followed by arcs at crossover point is shown in Figure 4.1.

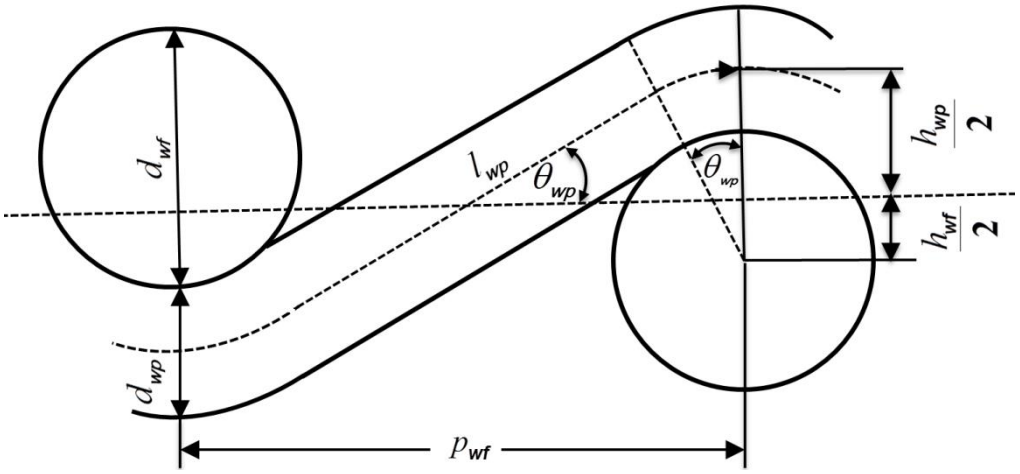

Figure 4.1: Peirce's circular cross-sectional model of plain woven fabric

Peirce established the relationship between different geometrical parameters such as warp/weft yarn spacing, warp/weft yarn crimp, woven angle and fabric thickness of the above defined two-dimensional unit cell geometrical model of plain woven fabric. The main advantage of this model considering simple circular geometry is that it can be used to evaluate the relative resistance of fabric against water, air and light [94], but it only implies to very open woven structures [95].

The list of symbols used in the equations of geometrical parameters are:

d_{wp} : diameter of warp yarn
d_{wf} : diameter of weft yarn
a_{wp} : major diameter of flatend warp yarn
a_{wf} : major diameter of flatend weft yarn
a_{wp} : minor diameter of flatend warp yarn
a_{wp} : minor diameter of flatend weft yarn
e_{wp} : warp yarn flattening effect $\left(a_{wp}/b_{wp}\right)$
e_{wf} : weft yarn flattening effect $\left(a_{wf}/b_{wf}\right)$
p_{wp} : warp spacing
p_{wf} : weft spacing
θ_{wp} : maximum angle of the warp axis to plane of cloth in radians
θ_{wp} : maximum angle of the weft axis to plane of cloth in radians
c_{wp} : warp yarn crimp (fractional)
c_{wf} : weft yarn crimp (fractional)
h_{wp} : warp crimp height
h_{wf} : weft crimp height
l_{wp} : length of the warp axis between plane containing the consecutive cross threads
l_{wf} : length of the weft axis between plane containing the consecutive cross threads

Based on the Peirce's model, the relationships of the above parameters are presented in the following Equations from 4.1 to 4.7.

$$D = d_{wp} + d_{wf} = h_{wp} + h_{wf} \tag{4.1}$$

$$c_{wp} = \frac{l_{wp}}{p_{wf}} - 1 \tag{4.2}$$

$$c_{wf} = \frac{l_{wf}}{p_{wp}} - 1 \tag{4.3}$$

$$p_{wp} = \left(l_{wf} - D\theta_{wf}\right)\cos\theta_{wf} + D\sin\theta_{wf} \tag{4.4}$$

$$p_{wf} = \left(l_{wp} - D\theta_{wp}\right)\cos\theta_{wp} + D\sin\theta_{wp} \tag{4.5}$$

$$h_{wp} = \left(l_{wp} - D\theta_{wp}\right)\sin\theta_{wp} + D\left(1 - \cos\theta_{wp}\right) \tag{4.6}$$

$$h_{wf} = \left(l_{wf} - D\theta_{wf}\right)\sin\theta_{wf} + D\left(1 - \cos\theta_{wf}\right) \tag{4.7}$$

The limitation of this model is that the yarn cross-section is not regular circular in a woven fabric because of the sufficient pressure or normal force acted on yarns that are introduced during weaving process and the yarns flattened [96]. Peirce's, in his later research, addressed this issue with the replacement of circular cross-section shaped yarn by elliptical as shown in Figure 4.2. However it is too complex to establish any relationship within the geometrical parameters of the yarn.

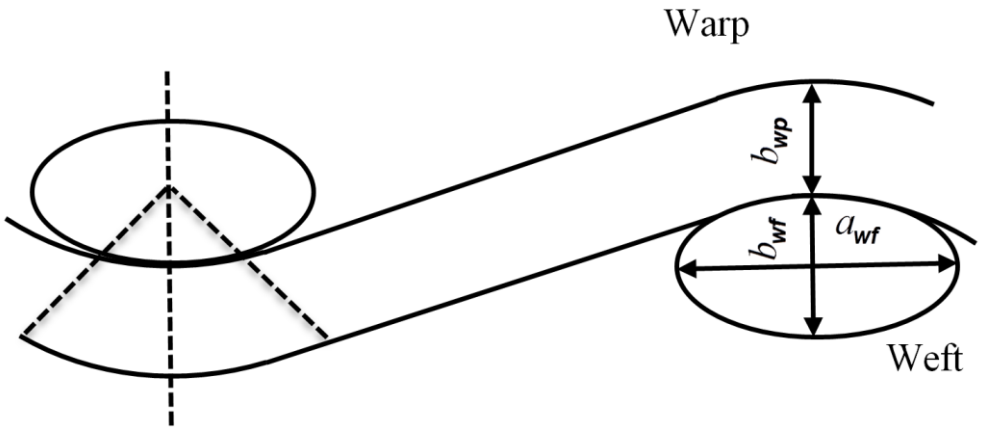

Figure 4.2: Peirce's elliptical cross-sectional model of plain woven fabric

Kemp in 1958 [97] modified Peirce geometrical models of plain woven fabric by replacing the circular or elliptical yarn cross-section by racetrack. Racetrack cross-sectional shape consists of a closed rectangle with two semi-circles. It has also been found that Peirce's elliptical model doesn't work well with high sett plain woven structure. The yarn geometrical structure developed by Kemp is shown in Figure 4.3.

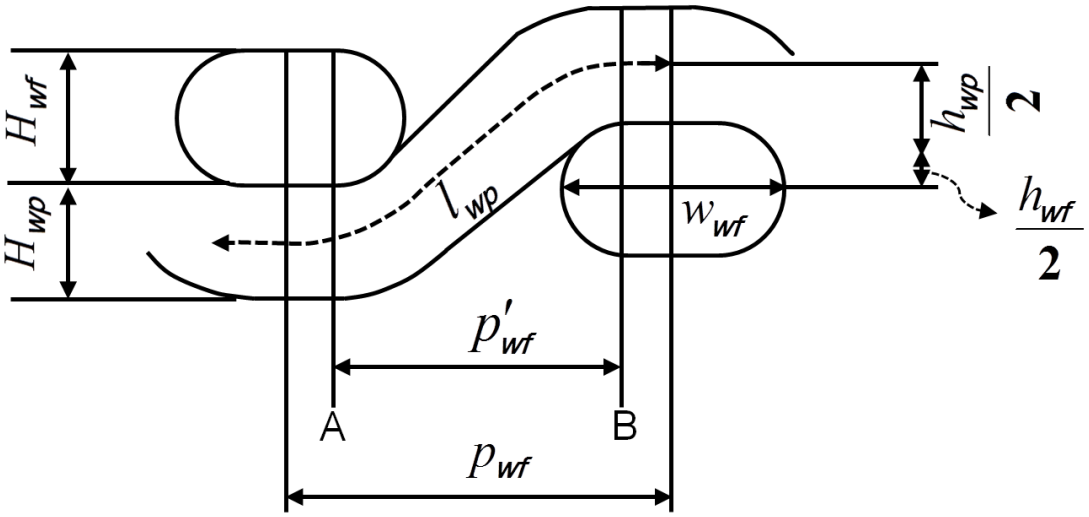

Figure 4.3: Kemp's racetrack cross-sectional model of plain woven fabric

The list of symbols used in the equations of geometrical parameters is given below:

w_{wp} : width of the cross-section of warp yarn
w_{wf} : width of the cross-section of weft yarn
H_{wp} : height of the cross-section of warp yarn
H_{wf} : height of the cross-section of weft yarn
c'_{wp} : warp yarn crimp between A and B
c'_{wf} : weft yarn crimp between A and B
p'_{wp} : warp spacing between A and B
p'_{wf} : weft spacing between A and B
l'_{wp} : length of the warp path between A and B
l'_{wf} : length of the weft path between A and B

Note: Rest of the notation have same as described for Peirce's model.

The following relationships can be built up based on Kemp's model:

$$p'_{wp} = p_{wp} - \left(w_{wp} - H_{wp}\right) \tag{4.8}$$

$$p'_{wf} = p_{wf} - \left(w_{wf} - H_{wf}\right) \tag{4.9}$$

$$l'_{wp} = l_{wp} - \left(w_{wf} - H_{wf}\right) \tag{4.10}$$

$$l'_{wf} = l_{wf} - \left(w_{wp} - H_{wp}\right) \tag{4.11}$$

$$c'_{wp} = \frac{l'_{wp} - p'_{wf}}{p'_{wf}} = \frac{c_{wp} p_{wf}}{p_{wf} - \left(w_{wf} - H_{wf}\right)} \quad 4.12$$

$$c'_{wf} = \frac{l'_{wf} - p'_{wp}}{p'_{wp}} = \frac{c_{wf} p_{wp}}{p_{wp} - \left(w_{wp} - H_{wp}\right)} \quad 4.13$$

$$D = H_{wp} + H_{wf} = h_{wp} + h_{wf} \quad 4.14$$

The limitation of Kemp's racetrack model is that in many cases yarns are flattened in a woven fabric therefore racetrack cannot simulate close to the actual yarn cross-section. Many other researchers also reported their work related to yarn geometry in a woven fabric structure. Olofson in 1961 [98] reported that yarn cross-sectional path could be considered as circular arcs. Shanahan and Hearle in 1978 [99] proposed a geometrical model of plain woven fabric by considering yarn cross-section as lenticular in order to calculate the fabric mechanics by using energy method, shown in Figure 4.4. Lenticular shape gives more realistic yarn geometry with flattened cross-section in woven fabrics.

The list of symbols used in the equations of geometrical parameters is given below:

a_{wp} : widht of warp yarn
a_{wf} : widht of weft yarn
a_{wf} : major diameter of flatend weft yarn
h_{wp} : warp crimp height
h_{wf} : weft crimp height
R_{wp} : lenticular radius of warp yarn
R_{wf} : lenticular radius of weft yarn
t : thickness of fabric
Note : Rest of the notation have same as described for Peirce's model

The following relationships can be built up based on Hearle's model:

$$D_{wp} = 2R_{wp} + b_{wf} \quad 4.15$$

$$h_{wp} + h_{wf} = b_{wp} + b_{wf} \quad 4.16$$

$$a_{wp} = 2R_{wp} \sin\theta_{wp} \quad 4.17$$

$$a_{wf} = 2R_{wf} \sin\theta_{wf} \quad 4.18$$

$$p_{wp} = \left(l_{wf} - D_{wf}\theta_{wf}\right)\cos\theta_{wf} + D_{wf} \sin\theta_{wf} \quad 4.19$$

$$p_{wf} = \left(l_{wp} - D_{wp}\theta_{wp}\right)\cos\theta_{wp} + D_{wp} \sin\theta_{wp} \quad 4.20$$

$$c_{wp} = \frac{l_{wp}}{p_{wf}} - 1 \qquad 4.21$$

$$c_{wf} = \frac{l_{wf}}{p_{wp}} - 1 \qquad 4.22$$

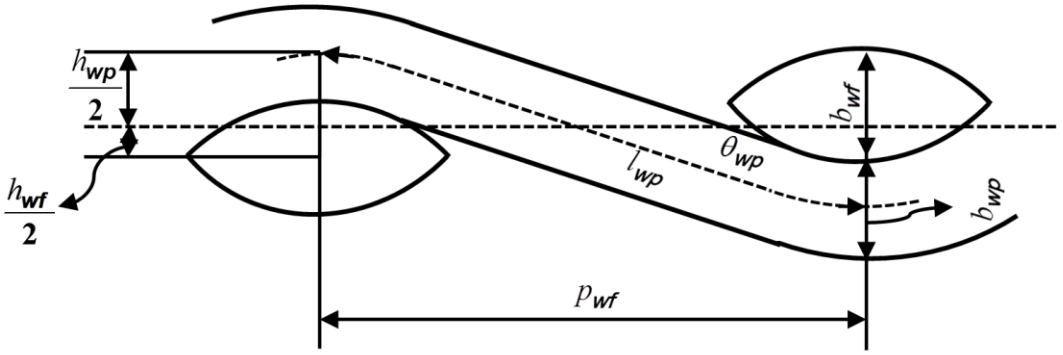

(a)

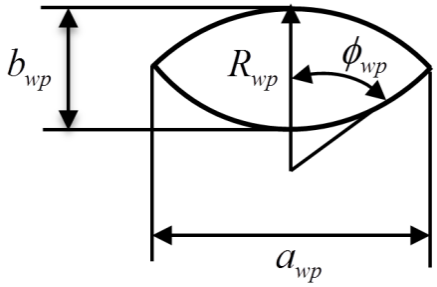

(b)

Figure 4.4: Hearle's lenticular cross-sectional model of plain woven fabric

Searles et al. [100] developed a method which described the tow cross-section by using cubic spline curves and polynomial functions. They used 8 harness satin woven fabric composites and analysed the SEM micrograph of the composites. They divided yarn cross-section into upper and lower portions and two natural cubic spline curves were used to define the yarn cross-section and centreline of tow was also defined by spline curve, shown in Figure 4.5.

Lin and Newton [101] developed a method in which the three dimensional plain woven fabric structures were generated by taking necessary input parameters of fabrics. They defined yarn path by using cubic B-spline curves with control points and assumed the cross-section of yarn as circular, shown in Figure 4.6.

Hofstee and Keulen [102] proposed a 3D geometrical model of plain woven fabric in which yarn cross-section varies throughout the fibre bundle centre line. They assumed that the relative location of fibre within the yarn was constant and packing fraction of fibre in yarn was also constant throughout the cross-section.

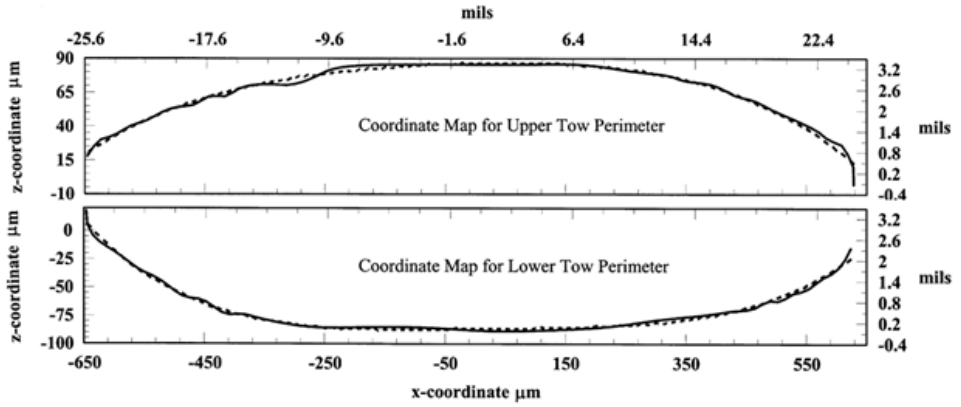

(a)

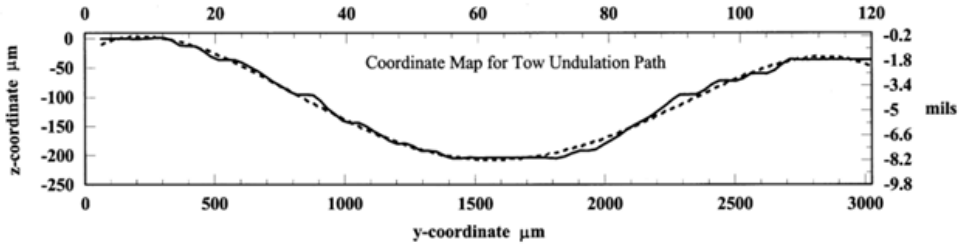

(b)

Figure 4.5: Fourth order polynomial fits: (a) Upper and lower cross-section of tow, and (b) Tow undulation path [100]

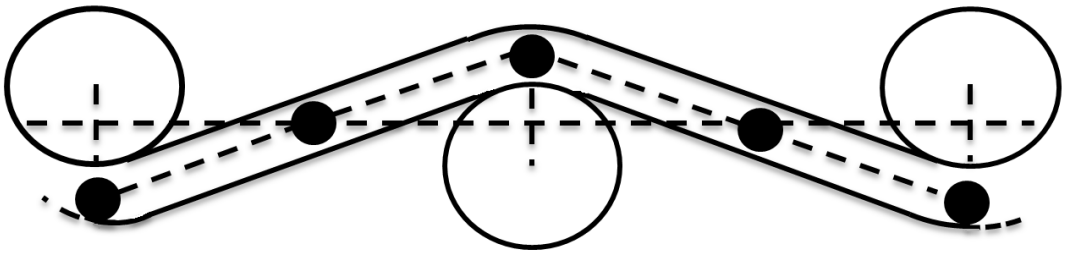

Figure 4.6: Plain woven fabric unit cell [101]

Gong et al. [103] developed algorithms which created the realistic yarn model from fabric image obtained by a synchrotron technique. They developed the model by

analysing the image in ImagePro and tracing the yarn path by using the tracing features available in the software and converted the lines into coordinate by Matlab. For 3D reconstruction elliptical shapes were fitted on the centre line which created by image processing. The significance of that study was the cross-sectional shape of yarn which was made variable throughout the yarn path.

However the fabric geometry is very complicated and it is difficult to consider a single cross-section of yarn because yarn cross-section is dependent on many factors such as the level of twist in yarn, normal force induced during the weaving process, and the measurement of accurate geometrical parameter is not an easy task. If we consider one factor only e.g. level of twist in yarn, for the sake of argument, then yarn would form round bundle of fibre if yarn has higher twist because it will be less subjected to force which will flatten the yarn. On the other hand, in case of lower level of twist of yarn, the yarn crimp is also low and as a result yarn will be flatter up to single level of fibre [104].

In this research the unit cell model of plain woven fabric is developed by using TexGen [105]. TexGen is open source software, distributed under the general public license and developed by Textile Composite Research group at the University of Nottingham. TexGen can generate woven geometrical structure by taking few input parameters such as: yarn width, yarn height, yarn spacing and thickness of fabric.

In TexGen yarns are generated by two dimensional cross-sectional shape of yarn sweep along the path of yarn. Yarn path can be defined by more flexible and generic way using discrete points and these points are interpolate by: Bezier spline, natural cubic spline and linear spline [106].

Figure 4.7 shows a plain woven structure generated from TexGen. The developed model of woven structure can be exported to CAD (Computer Aided Design) software. The woven structures can also be created by other well-known software such as TexEng [107] (weave Engineer and TechText CAD [108]) and WiseTex [109] as shown in Figure 4.8.

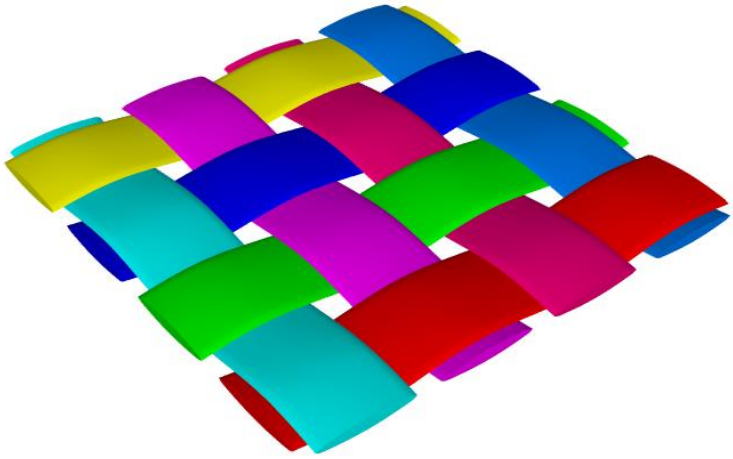

Figure 4.7: Plain woven structure generated from TexGen

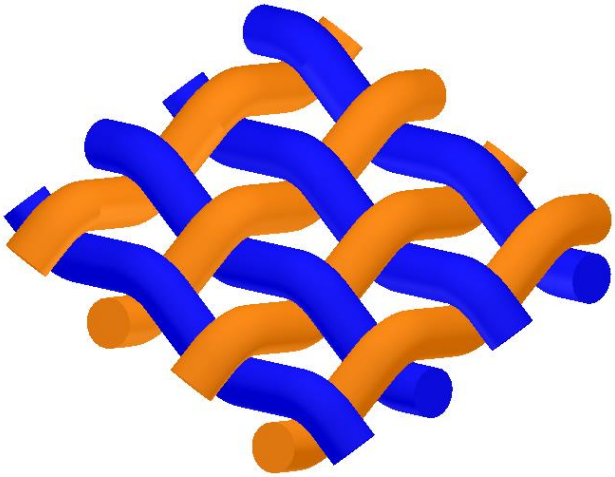

(a)

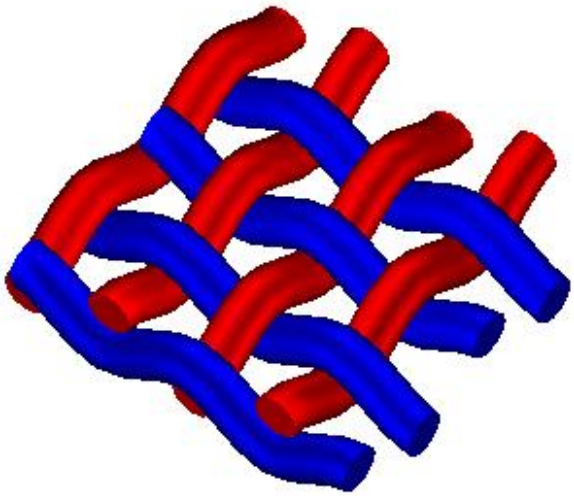

(b)

Figure 4.8: Plain woven structure generated by: (a) TechText CAD [108], and (b) WiseTex [109]

TexGen has the following advantages over other software packages mentioned above.

(1) Yarn can be created with variable and combination of different shape cross-section because it contains hybrid section.
(2) Control point can be adjusted manually.
(3) Intersections between yarns can be avoided by using the above two options.

4.2.1 Finite Element Model

In order to develop the finite element model of plain woven fabric it needs to find out the geometrical parameters which would be used as input parameters in TexGen.

4.2.1.1 Fabric Geometric Parameters

In this work, effective thermal conductivity and thermal resistance of plain woven fabric was examined, the fabric specifications were listed in Table 3.1 to Table 3.4, Chapter 3. Woven fabrics were selected by considering the different applications such as: fire protective clothing, body armour clothing and normal wearing.

Nomex® III fabric is widely used for protective clothing which provides protection against fire. The purpose of selecting Nomex® III fabric in this study is to simulate the realistic effect of heat transfer when it is subjected to extreme temperature environment. The thermal conductivity of fibre will increase with the increase of temperature; this effect will be discussed in detail in Chapter 7.

Protective clothing made of Twaron® fibre used in body armour for ballistic protection. There is a common issue of thermal stress with body armour because of their almost impermeable structure which required for high ballistic resistance therefore which provide insulation to the body and reduces the heat loss to the environment. Clothing insulation property can be determined by thermal resistance and thermal conductivity so as to develop better thermal comfort body armour.

Poly-viscose fabric is also used in this research along with cotton and wool fabrics. These fabrics are used for normal wear clothing. In Poly-viscose fabric a special core spun yarn was used as weft yarn and simple polyester yarn as warp.

To understand the thermal behaviour of the fabrics is important so as to determine their specific applications. Unit cell models of plain woven fabrics were created by using the

actual parametric values of the fabric. For that purpose the following parameters are needed:

(1) Warp and weft yarn spacing (Wf_s / Wa_s);

(2) fabric thickness (t); and

(3) width of the warp and/weft yarn (Wa_d / Wf_d) and yarn cross-sectional shape.

4.2.1.1.1 Yarn Spacing

The warp and weft yarn spacing (Wf_s and Wa_s) were calculated by using method-A described in British standard BS EN 1049-2:1994 [110]. Five random samples were selected and conditioned according to the BS EN ISO 139:2005 [111]. The length of the sample is more than 0.4 to 0.6 cm longer than the minimum length defined in standard against method-A (Dissection of fabric). Yarns from specified length were removed from the fabric and counted. Warp and weft spacing were calculated by using Equations 4.23 & 4.24,

$$Wa_s = \frac{1}{S_{wa}} \qquad 4.23$$

$$Wf_s = \frac{1}{S_{wf}} \qquad 4.24$$

where S_{wa} and S_{wf} are the warp and weft density respectively.

4.2.1.1.2 Fabric Thickness

Fabric thickness (t) was tested by FAST-1 compression meter under 2gf/cm^2 or 0.196 KPa over the surface area of 10 cm^2. Figure 4.9 shows the working principle of FAST-1 testing device.

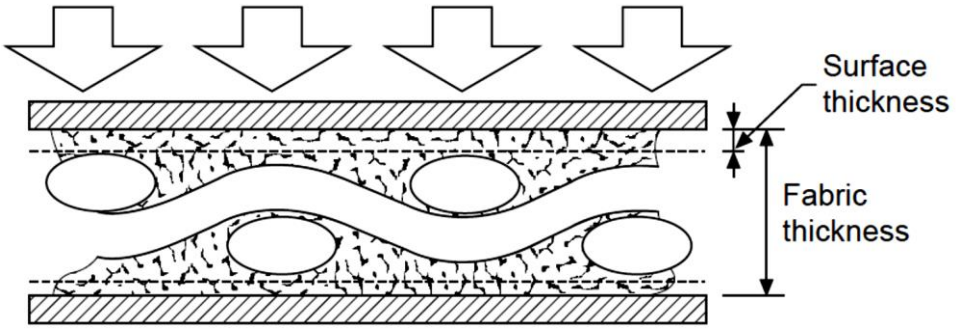

Figure 4.9: Working principle of FAST-1 compression meter [112]

It measures the thickness of fabric by placing the fabric on the reference surface. Below the reference surface there is a non-contact electronic sensor which measures the thickness of fabric by lowering the appropriate weight on to the fabric. Measured thicknesses of fabrics are given in Table 4.1.

4.2.1.1.3 Width of the Warp/Weft Yarn and Yarn Cross-Sectional Shape

There are several techniques available such as MicroCT, microscope, electron microscope etc. which can be used to find out the cross-sectional image for further study of yarn width, yarn height and yarn path through image analysis.

In this work Hitachi S-4300 SEM (Scanning electron microscope) was used to examine the geometry of yarn cross-section. Scanning electron microscope generates images of samples by using the beam of electron which generated from electron gun and passes through the electron column where they are focused into tight beam by the help of electromagnetic lenses. Then the tight beams of electron strike on the surface of sample and are collected by the detector which generates the image on a monitor demonstrated in Figure 4.10.

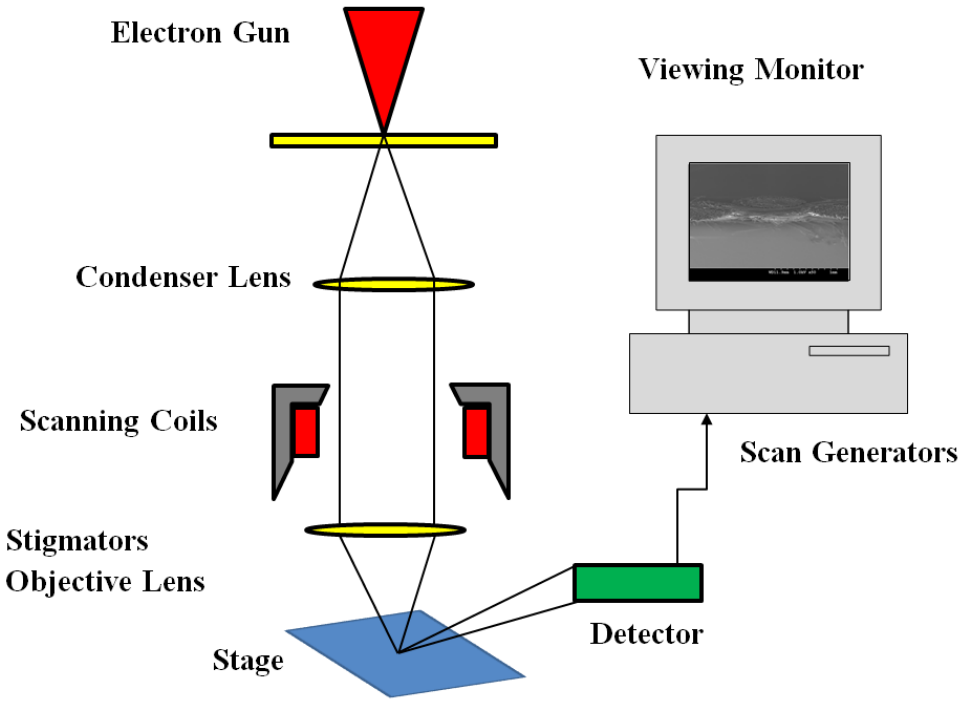

Figure 4.10: Schematic diagram of the SEM

It is very difficult task to obtain very clear cross-sectional image of fabric because when the fabric is cut fibre opens apart and correct dimension of the yarn cross section will not be obtained. In order to avoid this problem fabric was first coated with acrylic

binder without applying pressure. Acrylic binder was applied by brushing manually on one side of the fabric then dried and the same procedure was applied on other side of the fabric. When fabric dried fully it was then cured under specified temperature before the cross-sectional image was taken by SEM. The image was further analysed by ImageJ [113] which was developed at the National Institutes of Health. It is a public domain, Java-based image processing program. The yarn spacing, width, height and fibre volume fraction of the SEM image were measured in ImageJ. Figure 4.11 shows the micrograph of Twaron® plain woven fabric. During the image analysis yarn cross-section was examined carefully because all the fabrics except Twaron® have asymmetrical cross-sectional shape of yarn.

The measured geometric dimensions for unit cell of the fabrics are listed in Table 4.1. Unit cell model of Twaron® plain woven fabric was generated from TexGen by using the actual parameters measured by using the technique mentioned above and shown in Figure 4.12.

The cross-sectional image of the developed unit cell model of Twaron® fabric is comparable to the cross-sectional micrograph image from SEM. SEM image digitized in plot digitizer [114] which is a general public licensed software being used to find out the length of yarn in one unit cell. The length obtained from SEM image and model is 2.586 and 2.603 respectively.

Table 4.1: Measured geometric dimensions of an unit cell model

Dimensions	Nomex® III	Twaron®	Cotton	Wool	Poly-Viscose
Wa_s / Wf_s (mm)	0.431/0.431	1.282/1.282	0.390/0.462	0.363/0.564	0.339/0.299
Wa_d / Wf_d (mm)	0.337/0.337	1.2154/1.2154	0.26/0.277	0.3/0.33	0.1591/0.219
t (mm)	0.5	0.348	0.484	0.408	0.341
Total length of unit cell (mm)	0.862	2.564	0.924	1.128	0.675
Total width of unit cell (mm)	0.862	2.564	0.78	0.726	0.598
Unit cell volume (mm^3)	0.3715	2.2878	0.3488	0.3441	0.13766

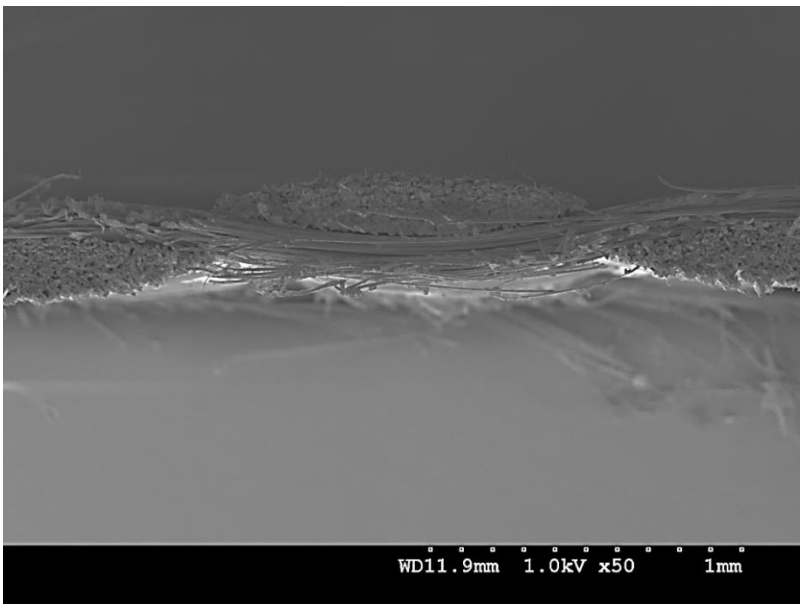

Figure 4.11: Micrograph of the cross-section of Twaron® fabric

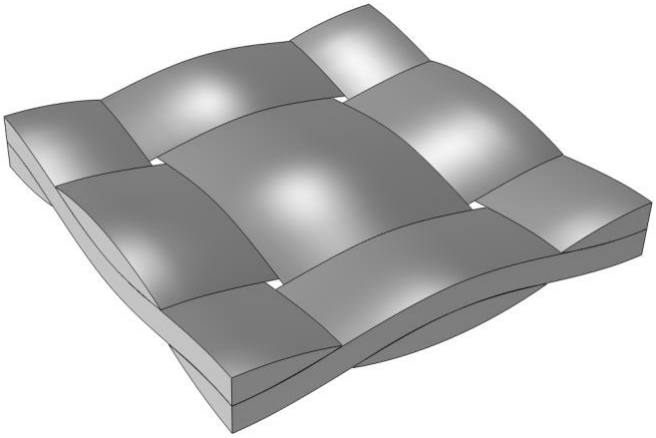

(a)

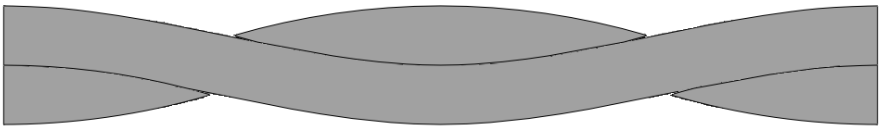

(b)

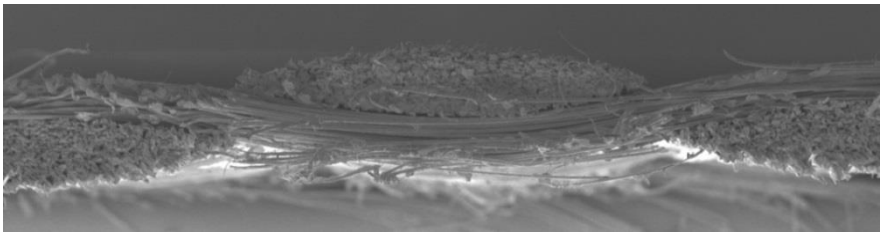

(c)

Figure 4.12: Twaron® fabric (a) Unit cell model of Twaron® fabric, (b) Cross-sectional view of Twaron® model, and (c) Crosss-sectional view of micrograph of Twaron® fabric

Figure 4.13 (a) Shows the cross-sectional micrograph of Nomex® III fabric which clearly indicates that the cross-section of yarns is not exactly lenticular, initially considered the yarn cross-section was lenticular but there were huge interference between the yarn at cross over point because of crimp. In order to remove the interference between yarns hybrid cross-sectional shape was used which has the combination of power ellipse. Figure 4.13 (b) shows the unit cell model of Nomex® III fabric.

The effective thermal conductivity of yarn was calculated based on the generated unit cell model of plain woven fabric developed by using actual parameters of the fabric.

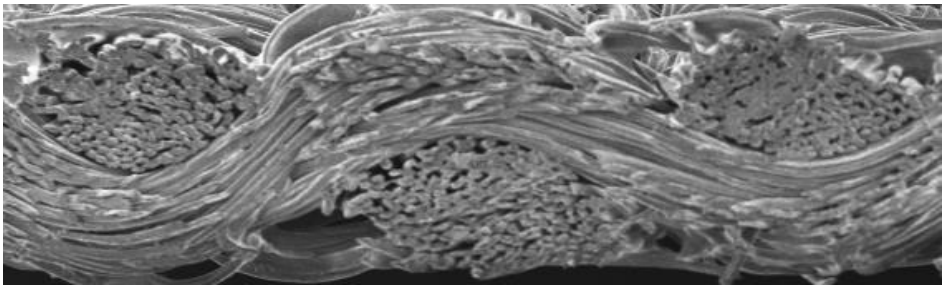

(a)

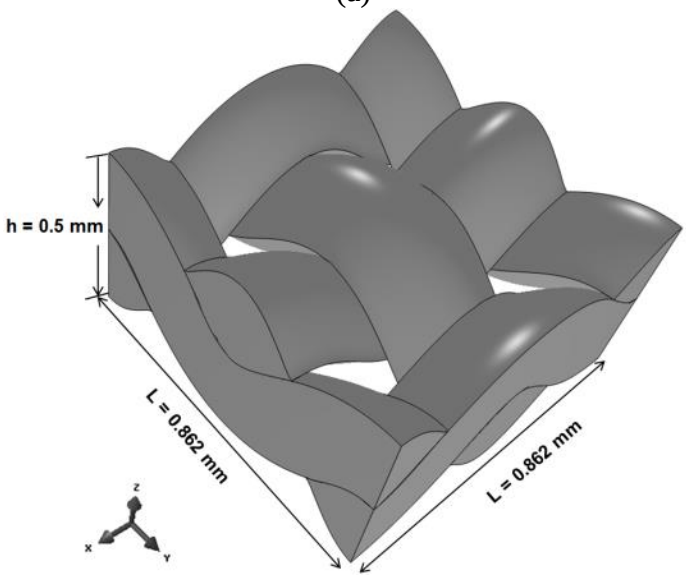

(b)

Figure 4.13: Nomex® III fabric (a) Micrograph of the cross-section of Nomex® III fabric, and (b) Unit cell model of Nomex® III

4.2.2 Geometrical Modelling of MicroPCMs Coated Composite Fabric

Phase change material is used to develop thermo-regulating textile materials as mentioned in Chapter 2. The fabric specifications are shown in Table 4.2. As discussed earlier, due to the property of high performance materials used for protective clothing,

heat do not transfer easily from body to environment when it is subjected to high temperature environment. The use of PCM material can reduce the thermal strain in heat protective clothing [115, 116] and it can also be used for normal wear to keep the wearer in a micro-temperature stable environment. MicroPCMs are composed of n-octadecane as core material and melamine formaldehyde as shell material. The properties of MicroPCMs are listed in Table 4.3.

In this research work fabrics were coated both sides with MicroPCMs obtained from Microtech laboratory Inc. Fabrics were coated by using the rotary screen coating technique. The coating mixture contains binder and microcapsules which uniformly mixed and forced through the screen by using circular metal rod. In order to remove the very fine dot configuration a wiper blade was used to spread the dots into continuous coat after coating fabric was dried and cured.

The core (PCM) content (in percentage) of MicroPCMs can be calculated by using the following equation [117]:

$$C = \frac{|\Delta H_m|}{\Delta H_o} \times 100 \qquad 4.25$$

where C is the core content in percentage; ΔH_m and ΔH_o are the enthalpy of MicroPCMs and pure PCM respectively.

The diameter and shell thickness of MicroPCMs can be calculated by the following equations [118, 119]:

$$\left(\frac{d_p}{d_c}\right)^3 = 1 + \frac{\rho_c(1-\alpha_c)}{\rho_s \alpha_s} \qquad 4.26$$

$$T_s = \frac{d_p}{2}\left(1 - \sqrt[3]{\frac{C \times \rho_s}{\rho_c - C\rho_c + C\rho_s}}\right) \qquad 4.27$$

where d_p and d_c are the diameter of microcapsule and core, respectively; ρ_c and ρ_s are the density of core and shell, respectively; T_s is the shell thickness and αc is the mass fraction of core.

Table 4.2: Fabric specifications

Specifications	Nomex® III	100 % Cotton	100% wool
Areal density (g/m^2)	170	132	130
Thickness* (mm)	0.50	0.484	0.408
Warp/Weft sett (per inch)	59/59	65/55	70/45
Warp/Weft Yarn linear density (Tex)	33.3/33.3	25.5/25.5	27.8/27.8

*Fabric thickness was the thickness without MicroPCMs coating

Table 4.3: Physical properties of MicroPCMs

Properties of microcapsules	
Capsule composition	85-90% wt.% PCM
Core material	n-octadecane
Shell material	Melamine Formaldehyde
Particle size	17-20 (μm)
Melting point	28.2 °C
Heat of Fusion	180-195 J/g
Specific Gravity	0.9

4.2.2.1 Finite Element Modelling

In order to compute the effective thermal conductivity of MicroPCMs coated composites fabrics finite element models of MicroPCMs coated composite fabric were developed. For geometrical model generation, the SEM images of coated composite fabrics were analysed and it was found that the MicroPCMs were only at the surface of the fabric due to the fact that it was surface coating only and air was entrapped inside the yarn as shown in Figure 4.14.

For finite element modelling the following steps were followed:

1) first to develop a unit cell model of MicroPCMs and binder, then analyse the model;
2) unit cell modelling of uncoated fabric;
3) unit cell modelling of fabric with coated materials; and
4) combine the above three steps together to developed complete finite element model.

The method was adopted to develop the finite element model of MicroPCMs coated composite fabrics and the detailed steps were illustrated in Figure 4.15.

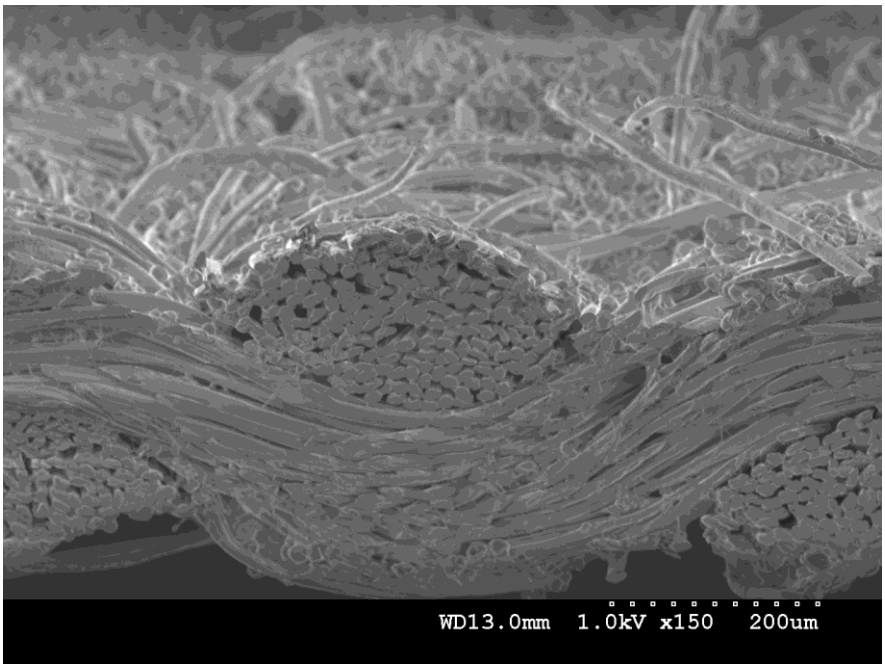

(a)

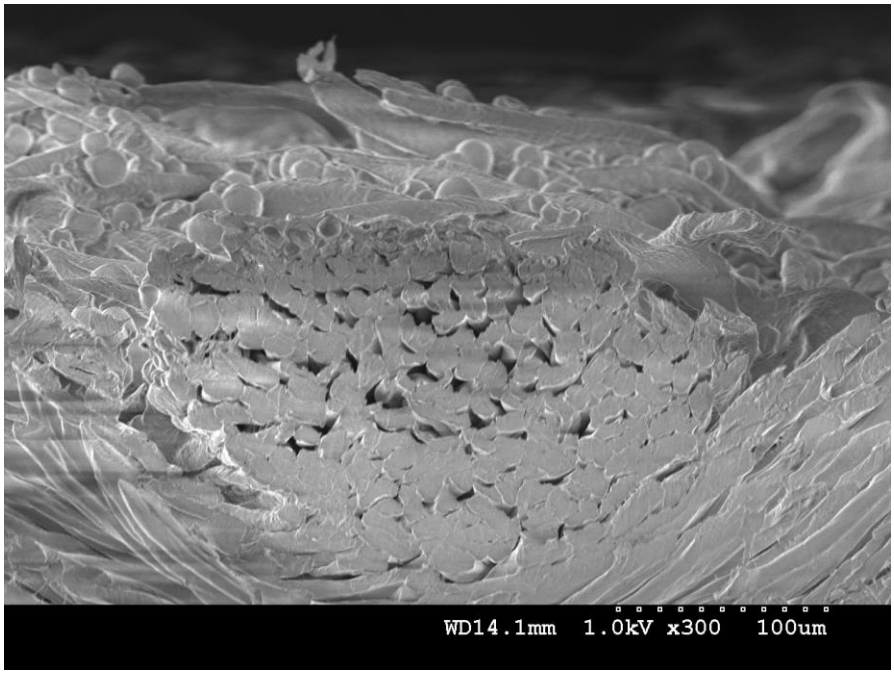

(b)

Figure 4.14: Micrograph of the cross-section of composite fabric coated with MicroPCMs: (a) Nomex® III fabric; and (b) Close view of cotton cross-section which shows the sandwich structure

.

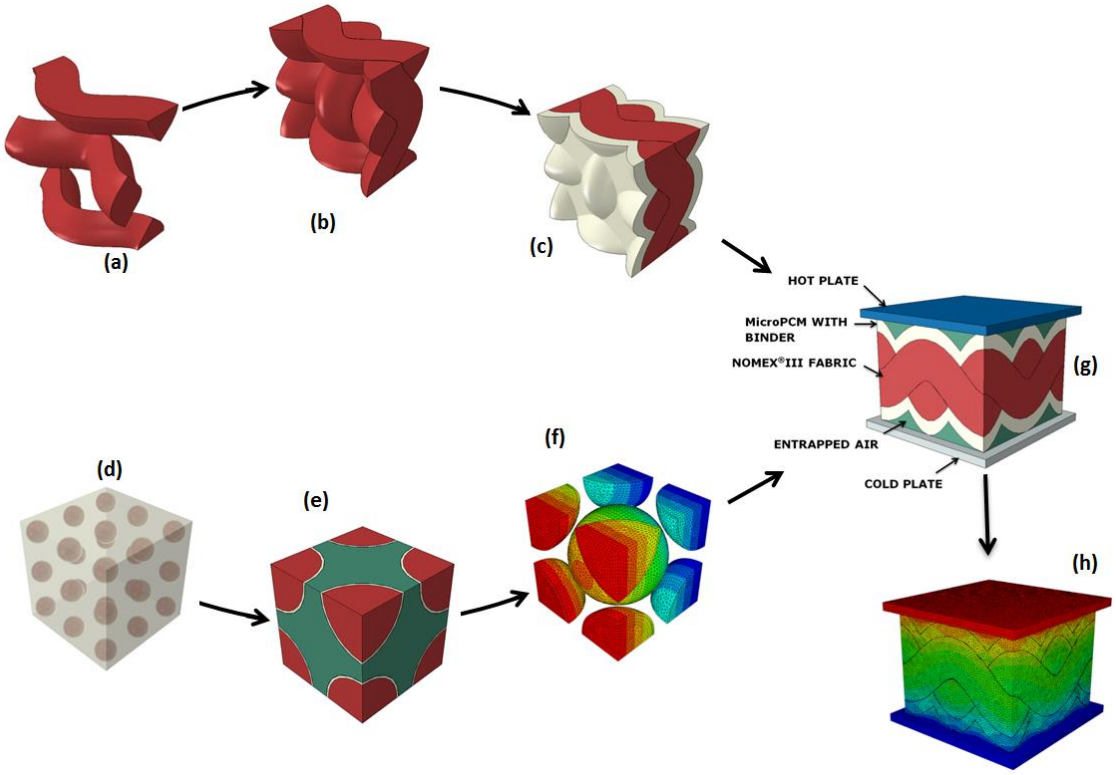

Figure 4.15: Stages of modelling: (a) Model of yarn; (b) Unit cell model of woven fabric only; (c) Unit cell model of woven fabric with coated material; (d) Binder and MicroPCMs composite; (e) Unit cell model of binder and MicroPCMs composite; (f) Simulated temperature profile of fabric composite

4.2.2.1.1 Unit Cell Model of Binder and MicroPCMs composite

The fabrics were coated with mixture of MicroPCMs and binder in which contained 60% MicroPCMs as volume fraction. The unit cell model for binder and MicroPCMs was developed through micro-sphere filled composite material approach with the consideration of Acrylic binder as matrix and MicroPCMs as filler which is homogenously distributed.

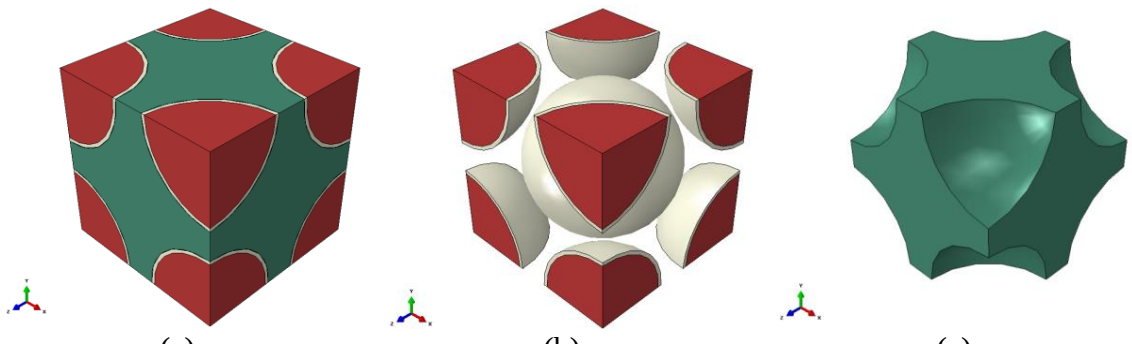

(a) (b) (c)

Figure 4.16: Unit cell model of MicroPCMs and Binder: (a) MicroPCMs with Binder; (b) MicroPCMs only; and (c) Binder only

4.2.2.1.2 Unit Cell Model of Fabric with and without Coated PCM

For the development of coated composite fabric models the following assumptions were made when coated PCM composite fabrics to be placed between the hot and cold plates:

i) no compression applied to fabric from the plates; and
ii) entrapped air exists between the plate and fabric as shown in Figure 4.17.

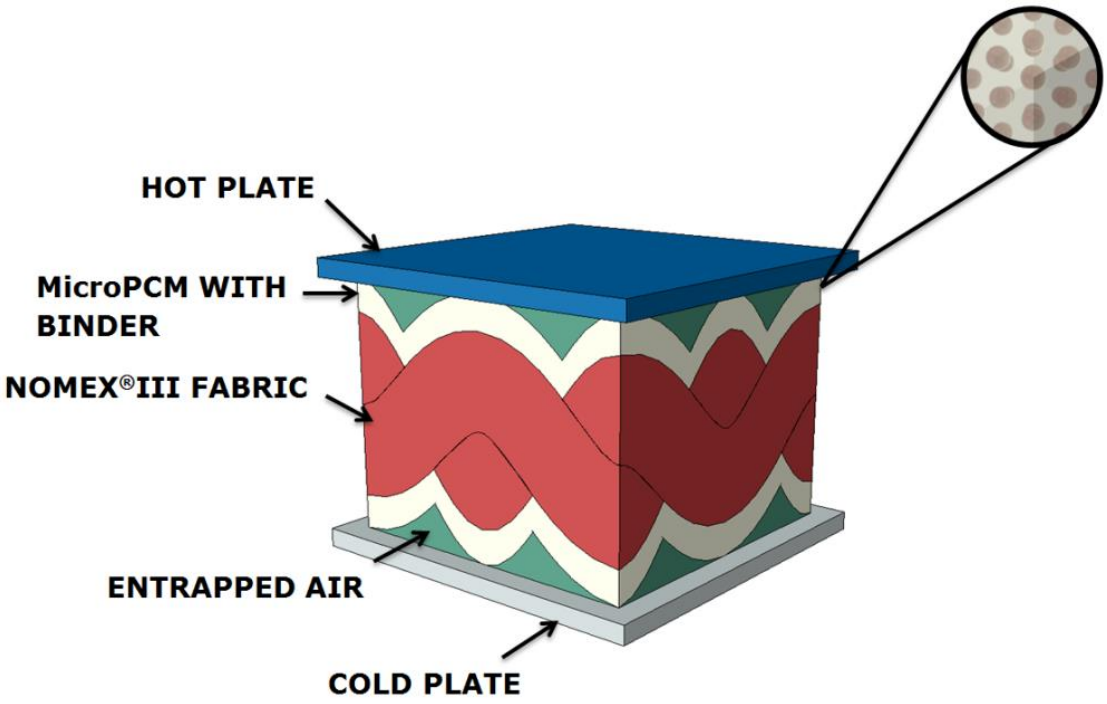

Figure 4.17: Experimental setup of MicroPCMs coated composite fabric

Unit cell of model of fabric was created by using the data shown in Table 4.4. Figure 4.18 shows the geometrical model of MicroPCMs coated Nomex® III fabric.

Table 4.4: Geometric dimensions of models

Dimensions	Nomex® III	Cotton	Wool
Warp/weft Spacing (mm)	0.431/0.431	0.390/0.462	0.363/0.564
Warp/weft width (mm)	0.337/0.337	0.26/0.277	0.3/0.33
Fabric thickness (mm)	0.68	0.575	0.56
Total length of unit cell (mm)	0.862	0.924	1.128
Total width of unit cell (mm)	0.862	0.78	0.726
Unit cell volume (mm^3)	0.505	0.4144	0.458

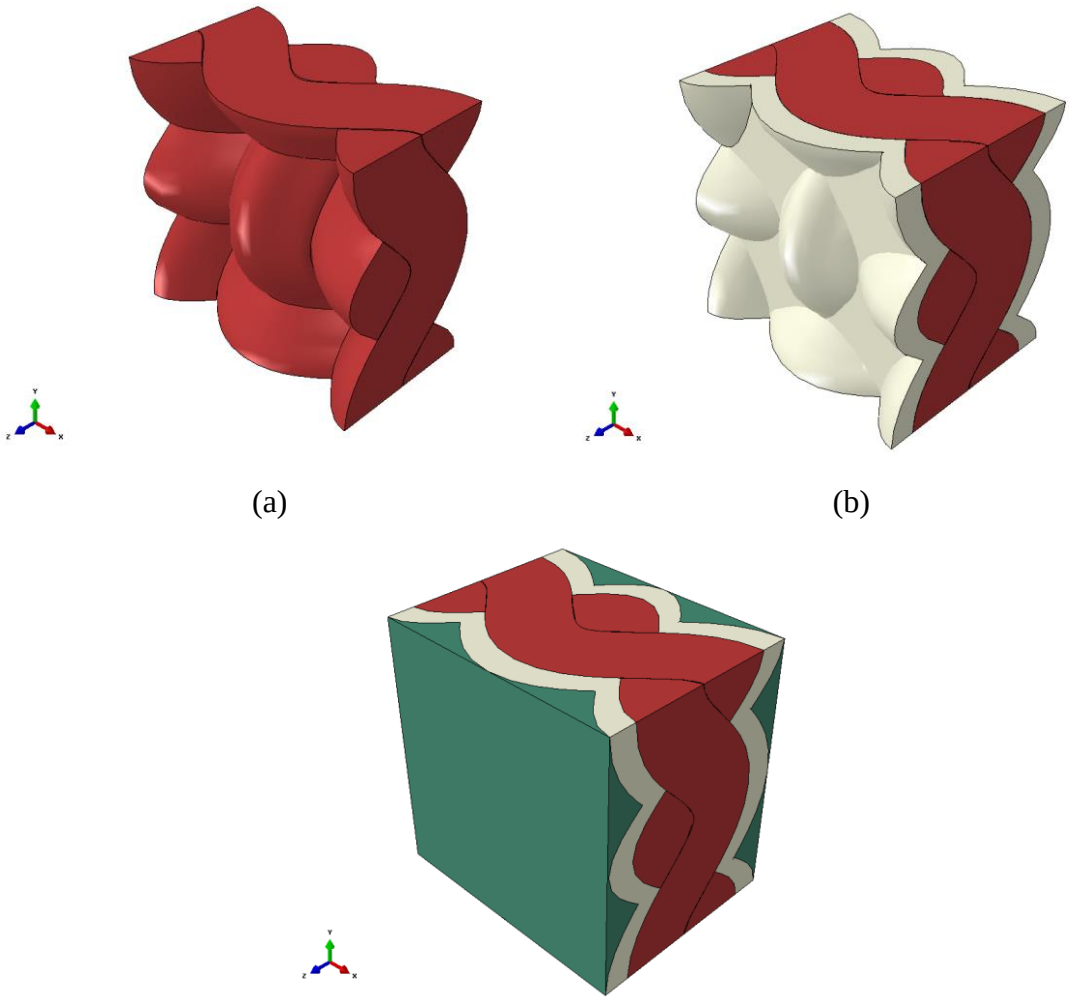

(a) (b)

(c)

Figure 4.18: MicroPCMs coated Nomex® III fabric (a) Unit cell model of Nomex® III fabric without MicroPCMs; (b) Unit cell model of Nomex® III fabric with MicroPCMs only; and (c) Unit cell model of Nomex® III fabric with MicroPCMs and air fluid matrix

4.3 Geometrical Modelling of Plain Weft Knitted Fabrics

Knitted fabrics have a good stretch property which offer better conformability and avoid excessive pressure between the garment and body [120]. Many researchers analysed the geometrical model of knitted fabrics. In 1926 Chamberlain [121] presented a two dimensional loop structure of plain knitted fabric. He proposed that the theoretically correct fabric as shown in Figure 4.19**,** in which GH represent the distance between the centres of two loops, GKH represent the equilateral triangle and KJ bisect the equilateral triangle. In order to produce the fabric with maximum cover factor with minimum weight it's only possible when GH is the distance between the loops in

horizontal direction and KJ is the correct length between the loops in longitudinal direction.

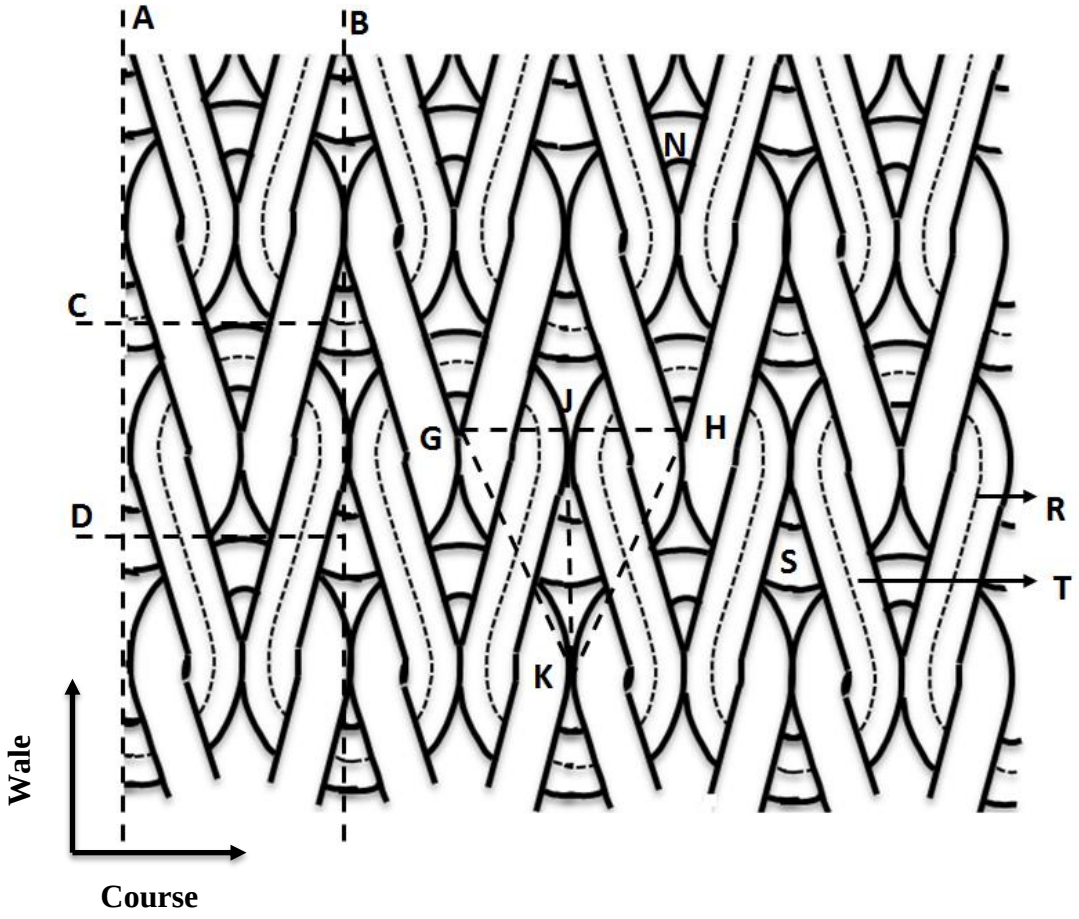

Figure 4.19: Chamberlain's jammed plain knitted loop

The minimum area of intersection obtained when;

$$\mathrm{JK} = \frac{\sqrt{3}}{2} \times \mathrm{GH} \tag{4.28}$$

The relationship between course and wale in the fabric is expressed:

$$\frac{\text{Courses}}{\text{Wales}} = \frac{2}{\sqrt{3}} \tag{4.29}$$

Diameter and stitch length of the yarn can be calculated by the following equations [121].

$$\text{Diameter of yarn}\,(d) = \frac{\text{Width of wale}}{4} \tag{4.30}$$

$$\text{stitch length of yarn}(l) = \pi \times \text{mean diameter of loop circle and combined lengths of side loop (R and T)} \quad 4.31$$

$$\text{stitch length of yarn}(l) = \frac{3\pi \text{w}}{4} + 2\sqrt{\left(\frac{\text{w}}{4}\right)^2 + \left(\frac{\text{w}\sqrt{3}}{2}\right)^2} \quad 4.32$$

$$\text{stitch length of yarn}(l) = \frac{3\pi \text{w}}{4} + \frac{\text{w}\sqrt{13}}{2} \quad 4.33$$

$$\text{stitch length of yarn}(l) = \frac{\text{w}\left(3\pi + 2\sqrt{13}\right)}{4} \quad 4.34$$

where w is the wale spacing.

In Chamberlain's model there was no consideration of loop in third dimension so the length of loop cannot be predicted with high accuracy. In 1947 Peirce [122] developed geometrical model of plain weft knitted fabric on the assumption that the loop composed of circular arc and straight line and the yarn central axis follows a path on the surface of cylinder following the direction of a course. In order to develop the relationship of stitch length in terms of yarn diameter, wales and course spacing he considered the flat structure of plain weft knitted fabric as shown in Figure 4.20. In his compact planned structure the course (p') and wales (w) spacing can be calculated by Equation 4.35 & 4.36 respectively,

$$p' = \sqrt{(4d)^2 - (2d)^2} = 3.4643d \quad 4.35$$

$$w = 4d \quad 4.36$$

Stitch length of loop can be calculated by the following equations.

$$l/4 = 3d(\pi - \theta) + 2d\ \sin(\theta - \psi) \quad 4.37$$

ψ and θ as shown in Figure 4.20 can be calculated by the following expressions:

$$\psi = \sin^{-1}\frac{1}{2} = 30° = 0.5236 \text{ radians}$$
$$\theta - \psi = \cos^{-1} 1.5/2 = 41° 24.58' = 0.7228 \text{ radians} \quad 4.38$$
$$\theta = 1.2464 = 71°24.6'$$

Hence stitch length becomes:

$$l/4 = 2.8428\,d + 1.3229\,d = 4.1657\,d$$
$$\text{Stitch length } (l) = 16.6628d \quad 4.39$$

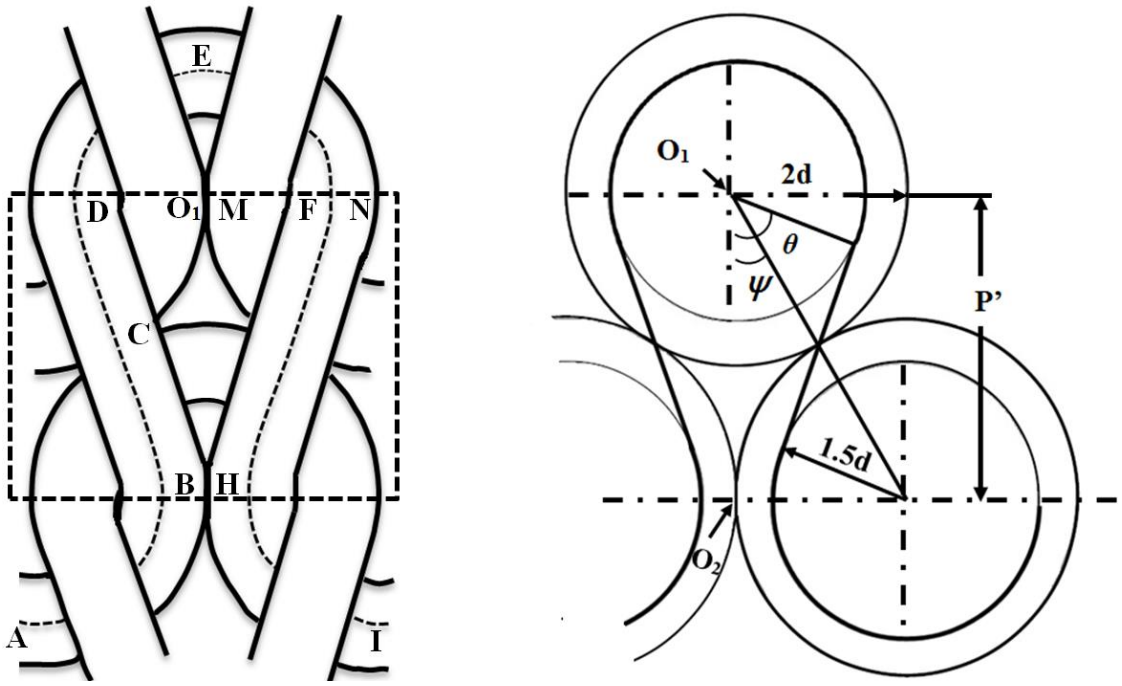

Figure 4.20: Planed structure of Peirce's loop

In all the above equations there was no consideration of the bending effect of yarn. In order to include this effect he assumed that these loops laid on the cylinder which gives three dimensional effects to the knitted loop. He found that radius of curvature *R* was only satisfied in order to provide space for interlocking when it equals to 4.172 times the diameter of yarn as shown in Figure 4.21.

The wales spacing is not effected in three dimensional loop structure but course spacing as it was observed by him in plane of the cloth is:

$$p = 3.364\ d \quad 4.40$$

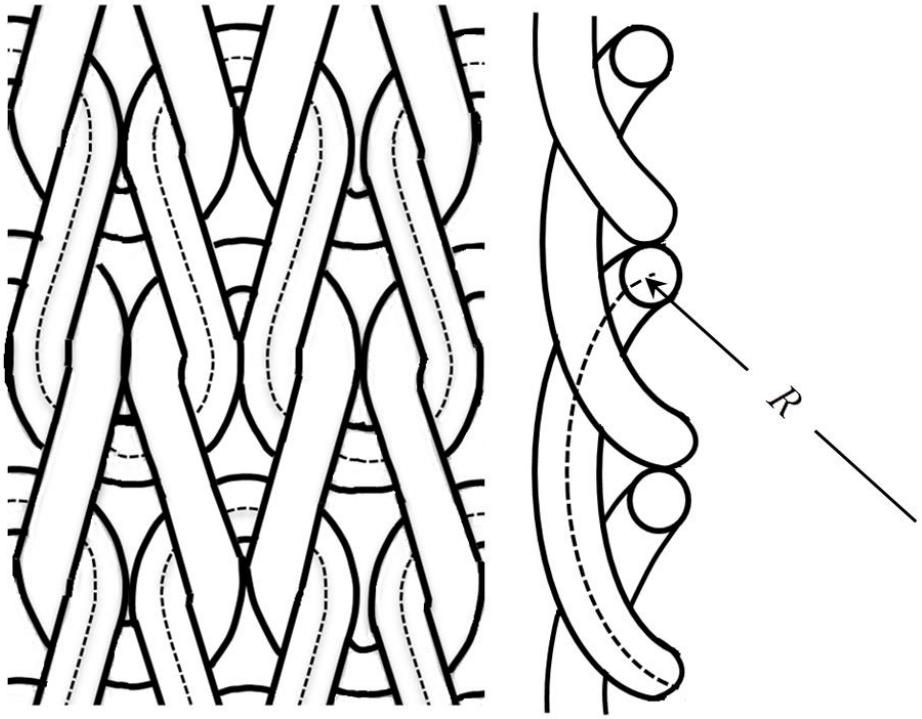

Figure 4.21: 3D dimensional Peirce's loop structure of plain weft knitted fabric

He also developed a relationship of wales spacing, course spacing and stitch length for open structure plain weft knitted fabric as shown in Equation 4.41 , 4.42 and 4.43 respectively. Peirce suggested that more open structures than the one he considered could be examined by inserting a straight yarn with the length of εd in the crown of the loop, and a length ξd in the sides of the loop. So, he reported to open up the structure by inserting a space εd along the wale line O_1O_2 and by inserting a straight line parallel to the course line. Similarly a straight length ξd was inserted in the centre of each loop. The increase in course spacing was virtually equal to the added length of yarn.

$$\frac{w}{d} = 4 + 2\varepsilon \tag{4.41}$$

$$\frac{p}{d} = 3.364 + \xi \tag{4.42}$$

$$l = 2p + w + 5.94d \tag{4.43}$$

Shinn [123] also analysed the two dimensional geometrical model of plain weft knitted fabric based on by Peirce's model [122]. He compared the experimental results with the theoretical results obtained from expression generated from the Peirce two dimensional

geometrical models. He also modified the Tompkins's formula [124] by which weight per square yard was predicted by using relations of stitch length, courses and wales spacing developed by Peirce.

In 1955 Leaf and Glaskin [125] pointed out that the stable knitted fabric loop structure could not be produced by the model proposed by the Peirce [122]. They showed that the Peirce considered the radius of curvature $R = 4.172d$ for all types of loop which gave the discontinuity in the torsion of yarn and eventually affected the shape of loops. They proposed a geometrical model of plain weft knitted fabric in which central axis of yarn passes over a series of circular cylinder and their model composed of circular arcs as shown in Figure 4.22.

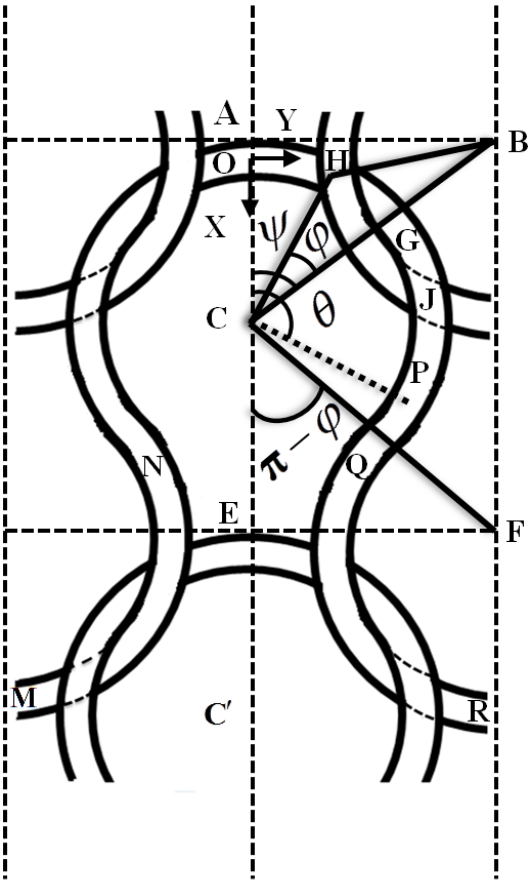

Figure 4.22: Leaf and Glaskin's model of plain weft knitted fabric

$$\varphi = \pi + \sin^{-1}\left\{\frac{C^2 d}{\left[C^2 + W^2\left(1 - C^2 d^2\right)^2\right]^{1/2}}\right\} - \tan^{-1}\frac{C}{W\left(1 - C^2 d^2\right)} \qquad 4.44$$

$$a = 1/4Wd\sin\phi \tag{4.45}$$

$$l = 4\cdot\left[1/\left(4Wd\sin\varphi\right)\right]\cdot\left[\pi+\sin^{-1}\left\{\frac{C^2 d}{\left[C^2+W^2\left(1-C^2d^2\right)^2\right]^{1/2}}\right\}-\tan^{-1}\frac{C}{W\left(1-C^2d^2\right)}\right]\cdot d \tag{4.46}$$

where d is the diameter of yarn, W and C are the courses and wales spacing respectively.

In 1959 Munden [126] developed the relationships between stitch length and wale and course spacing. He proved that the ratios between course and wale spacing per stitch length were independent of fabric cover factor. The developed relationships are as follows:

$$\text{Stitch density}(\text{N}) = cpi\times wpi = \frac{K_1}{l^2} \tag{4.47}$$

$$cpi = \frac{K_2}{l} \tag{4.48}$$

$$wpi = \frac{K_3}{l} \tag{4.49}$$

$$K_2\times K_3 = K_1 \tag{4.50}$$

$$\frac{cpi}{wpi} = \frac{K_2}{K_3} = K_4 \tag{4.51}$$

where K_1, K_2, K_3 and K_4 are constant values which can be determined experimentally on the basis of actual configuration (wet or dry relax state) of knitted loop.

Hurd and Doyle [127], Postle [128] and Kurbak [129] also studied the geometry of plain weft knitted fabrics. Furthermore, Demiroz and Dias [130] developed a mathematical model to generate 3D images of plain weft knitted fabric. They developed a stitch model by using cubic-spline as the central axis. The software relating to their developed model required input parameters such as: yarn diameter, stitch length, course and wales spacing and other fabric parameters were calculated by a software program developed using C programing language.

Choi and Lo [131] developed a model of plain weft knitted fabric to describe the mechanical properties and dimensional change in a fabric through energy approach. Their model is also capable of predicting biaxial tensile property of knitted fabrics.

Kyosev et al. [132] developed two models of plain weft knitted fabrics. Their first model is pure geometrical model based on research work done by Choi and Lo [131] taking into consideration of the yarn cross-section as elliptical. Their second model was made in considering discretization of yarn into small element and mechanical interaction between the yarns.

Lin et al. [133] developed geometrical models of weft knitted fancy structures on the basis of Non-uniform Rational B-splines (NURBS) curve. They generated the yarn central axis by using a set of points at intermeshing position of yarn adopting NURBS method and created the solid shape of knit loop by sweeping the sphere along the yarn. They developed a program to generate 3D surface loop model by using Visual C++ programing language and OpenGL.

Plain weft knitted fabrics were used in this study. Plain weft knitted structure is normally used for single jersey fabrics for sportswear. Different types of yarns were used to develop weft knitted fabrics to evaluate the effectiveness of the developed method.

The fabric specifications are shown in Table 3.2 and their surface macrostructures are illustrated in Figure 4.23.

4.3.1 Finite Element Model

The parametric model of plain weft knitted fabric created by using the central axis of yarn is defined by the path shown in Figure 4.24 (a); but the actual parameters of the fabric such as, courses and wales per centimetre were used. Parameter '*e*' can be determined by the average loop height (*H*) through image analysis using the following equation:

$$H = C + 2e \qquad 4.52$$

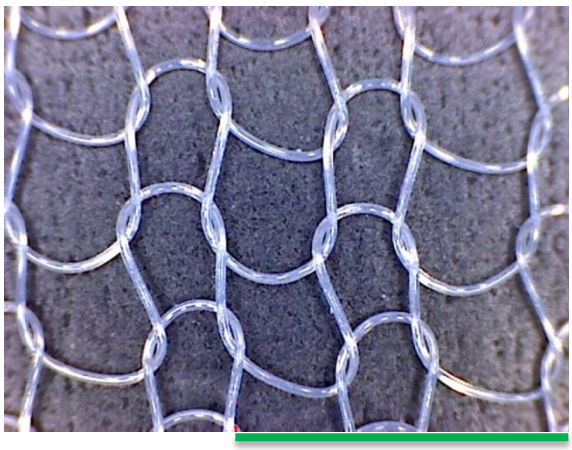

F1

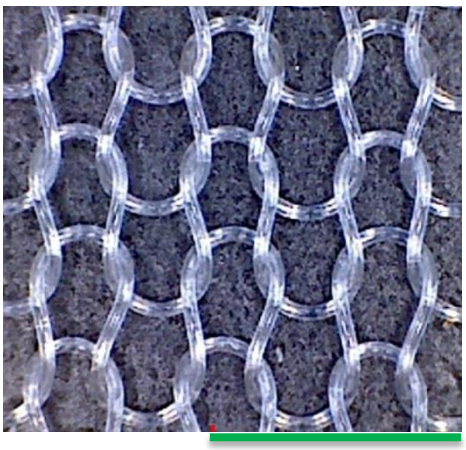

F2

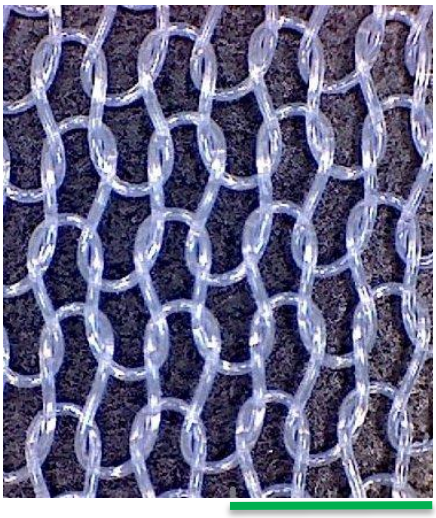

F3

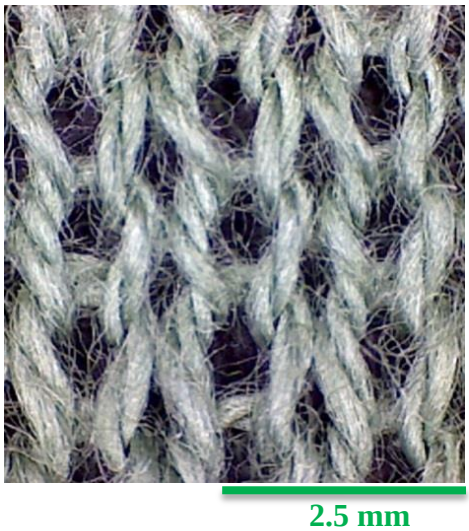

F4

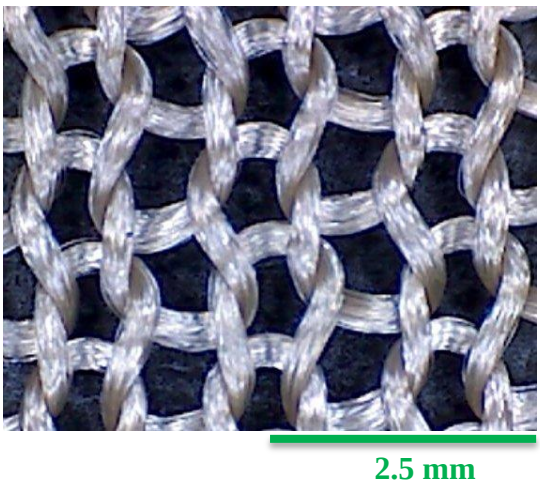

F5

Figure 4.23: Macrostructures of plain weft knitted fabrics

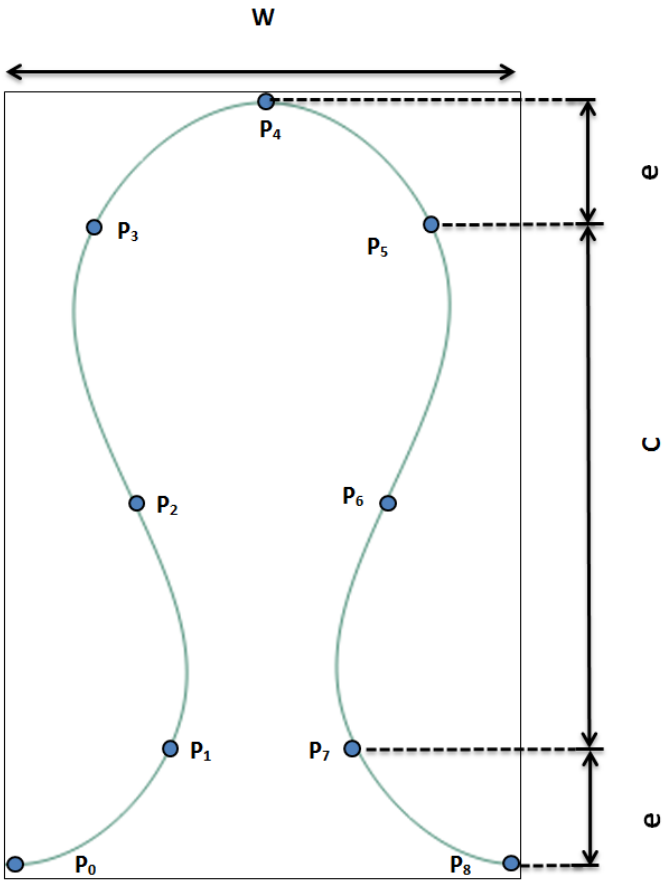

(a)

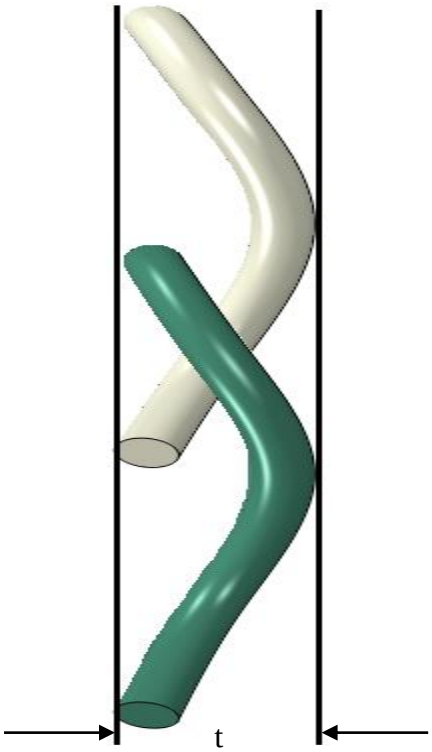

(b)

Figure 4.24: Geometrical parameter (a) Yarn central axis; and (b) Thickness of fabric

The coordinate values of the points illustrated in Figure 4.24 (a) were calculated which define the central axis of yarn using spline curve in Abaqus/CAE. Abaqus/CAE calculates the shape of the curve using a cubic spline fit between all points along the spline; in addition, the first and second derivatives of the spline are continuous. The 3D models of plain weft knitted fabrics can be generated by sweeping the circular cross-section of the yarn along the central axis of the yarn. Yarns were assumed to be incompressible in nature.

A polyester plain weft knitted fabric (F3) model generated by the plug-in is shown in Figure 4.25.

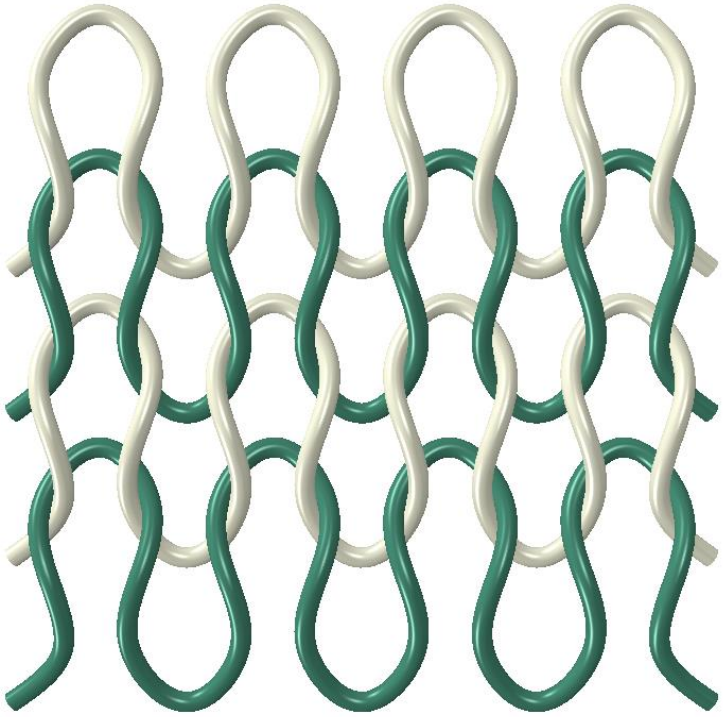

Figure 4.25: Geometrical model of fabric F3

4.3.1.1 Effect of 'e' Value on Loop Structure

In Figure 4.26 the effect of 'e' value on loop structure of fabric F3 was analysed by increasing and decreasing the 'e' value from the actual value of 0.4245.

It can be observed clearly that when the value decreases loops become more compact and loop length decreases or vice versa.

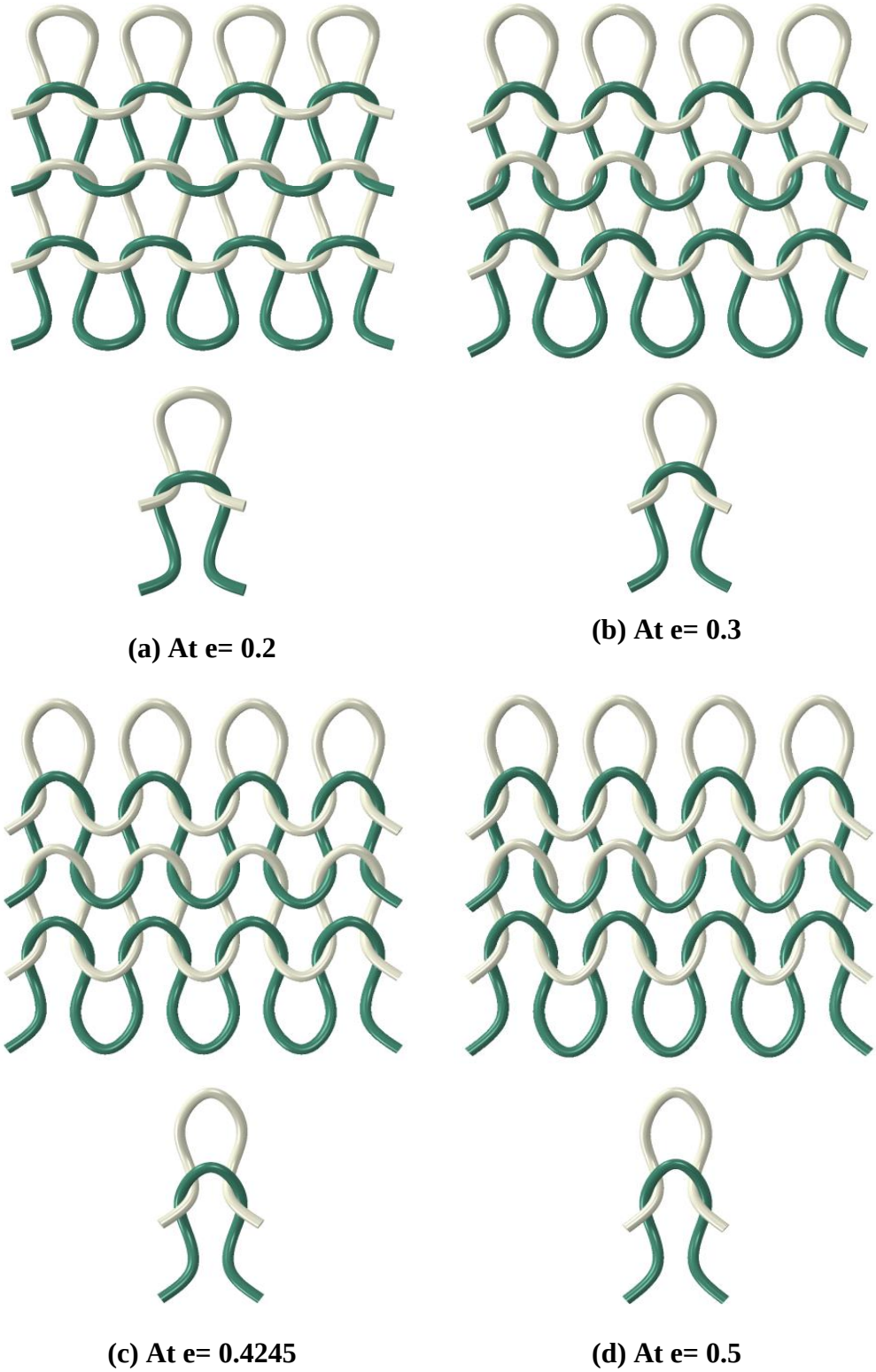

(a) At e= 0.2 **(b) At e= 0.3**

(c) At e= 0.4245 **(d) At e= 0.5**

Figure 4.26: Effect of parameter ‘e' on loop structure of fabric F3

4.4 Geometrical Modelling of Nonwoven Fabrics

Nonwoven fabrics are widely used in many application areas such as, insulation, filtration, health care, protective clothing, automotive interiors, consumer and industrial

wipes because of its specific thermal property, filtering, bacterial barrier, flame retardancy, resilience, stretch, softness, strength, and absorbency [134].

They are several definitions available of nonwoven fabric. According to BS EN ISO standard 9092:2011 nonwoven fabrics can be defined as: "nonwovens are structures of textile materials, such as fibres, continuous filaments, or chopped yarns of any nature or origin, that have been formed into webs by any means, and bonded together by any means, excluding the interlacing of yarns as in woven fabric, knitted fabric, laces, braided fabric or tufted fabric"[135].

According to American Society for Testing Materials (ASTM D 1117-80) nonwoven fabric can be defined as: "A nonwoven is a textile structure produced by the bonding or interlocking of fibres, or both, accomplished by mechanical, chemical, thermal or solvent means and combinations thereof. The term does not include paper or fabrics that are woven, knitted or tufted" [136].
According to INDA : **"**Nonwoven fabrics are broadly defined as sheet or web structures bonded together by entangling fibre or filaments (and by perforating films) mechanically, thermally, or chemically. They are flat, porous sheets that are made directly from separate fibres or from molten plastic or plastic film. They are not made by weaving or knitting and do not require converting the fibres to yarn" [137].

4.4.1 Production of Nonwoven Fabric

Nonwoven fabric can be produced in three stages: web formation, web bonding and finishing (optional) as shown in Figure 4.27.

In this research thermal bonded nonwoven fabrics were used due to their unique structural properties and applications. Thermally bonded fabrics have been used for protective clothing, cloth interlining, insulation etc. According to the literature review the heat transfer behaviour of thermally bounded nonwoven fabric has been not studied by numerical analysis except randomly distributed nonwoven fabric. Therefore the research of heat transfer behaviour of thermally bonded nonwoven fabric using numerical method will contribute to the knowledge base of academic research. It will be useful for nonwoven textile industry due to the rapid market growth of nonwoven fabrics and their applications [138]. Figure 4.28 shows the process flow of thermal point bonding of nonwoven fabric. Two rollers one smooth and other engraved roller are used. A web which contains thermoplastic fibre is passed through these two heated

rollers; the web melts at the contact points and binds thermoplastic fibres to form a nonwoven fabric. The fabrics produced by this method are relatively softer than the fabric produced by thermal bonding with high pressure.

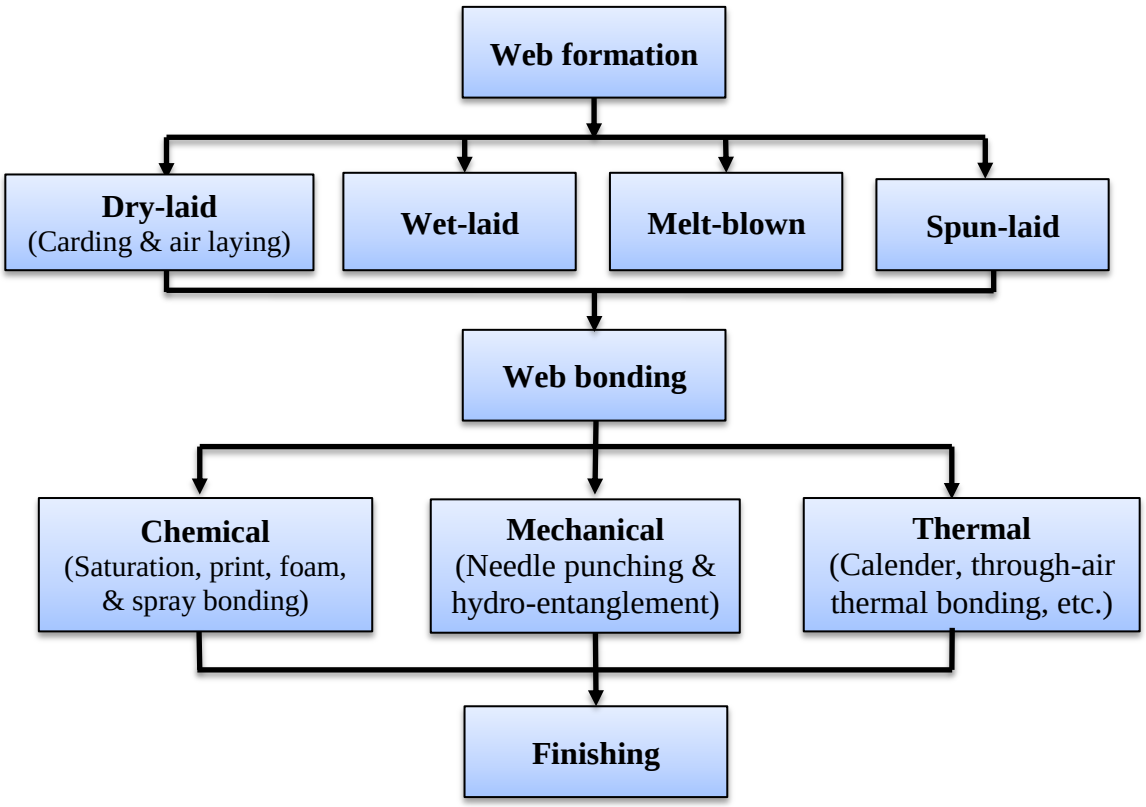

Figure 4.27: Stages of nonwoven fabric manufacturing process

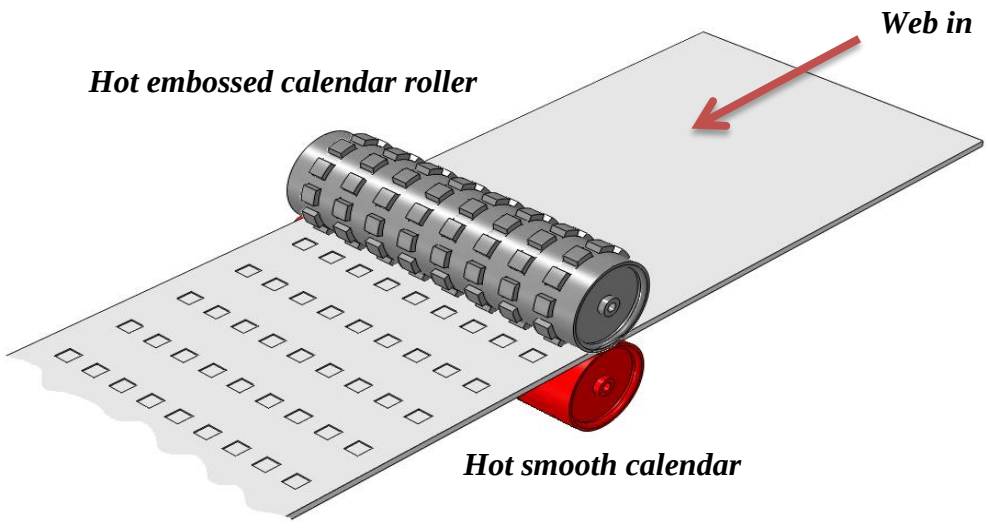

Figure 4.28: Thermal point bonding process of nonwoven fabrics

The advantages of thermal bonding over other bonding techniques are:

1) thermal bonding process are energy efficient process as compared to chemical bonding because in chemical bonding high amount of energy is required to evaporate the water from adhesive [139];

2) they have high production rate as compared to chemical bonding [139];
3) thermal bonding processes are environmental friendly because there is no use of chemical; and
4) the end product developed by thermal bonding have soft feel.

In this study thermally bonded nonwoven fabrics made of polypropylene fibre (PP) were used. The fabric specifications and fibre properties are shown in Table 3.4 (Chapter 3) and Table 4.5 respectively.

Table 4.5: Fibre properties of polypropylene

Property	Symbol	Values
Fibre density (Kg/m^3)	ρ	910
Axial fibre thermal conductivity (W/m.K)	K_{fa}	1.241
Transverse fibre thermal conductivity (W/m.K)	K_{ft}	0.111
Anisotropy	K_{fa}/K_{ft}	11.18
Fibre specific heat (J/Kg.K)	C_{pf}	1680

4.4.2 3D Reconstruction of Nonwoven Fabric

Nonwoven fabrics have complex structures as compared to woven and knitted fabrics. In this work the geometrical models of nonwoven fabrics were obtained by 3D reconstruction through High-resolution X-ray Computer Tomography (CT). In X-ray CT the samples are rotated around a vertical axis in front of X-ray source and the reconstructed data come as slices and cut to normal to that axis, illustrated in Figure 4.29.

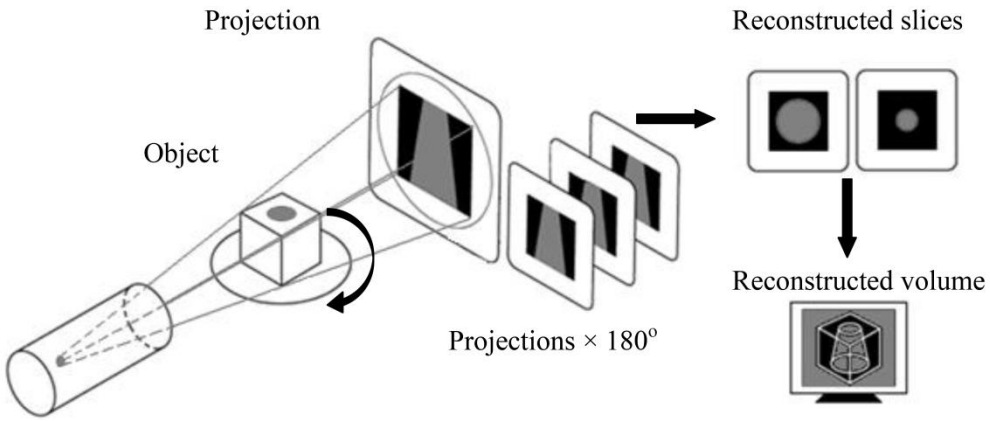

Figure 4.29: Schematic of X-ray tomography [140]

In order to develop the 3D reconstructed nonwoven fabrics, the fabric samples were cut in small strips with a scalpel and placed in boron nitride cup to hold (BN is extremely low in density and almost x-ray transparent). A small angle cone X-ray beam source is used and samples are rotated around the vertical axis. Images are generated on the basis of X-ray attenuation showing the density of nonwoven fabric samples. These projection images are used to generate 2D slices which reflect the inside of the samples when it's cut to normal to the axis of rotation. The resolution of the data collected was 3.713 microns per voxel (a voxel is the volume equivalent of a pixel). Figure 4.30 shows the 3D rendering of grey scale image achieved by ImageVis3D [141].

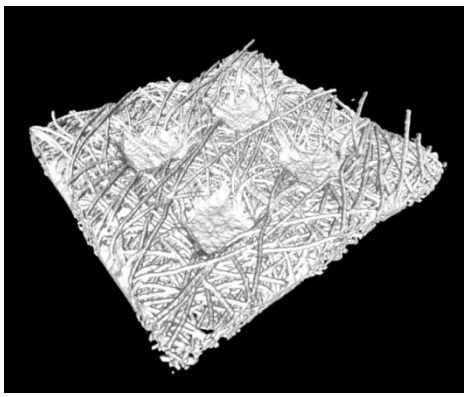

(a)

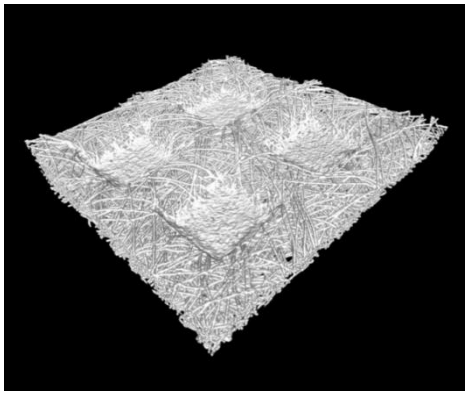

(b)

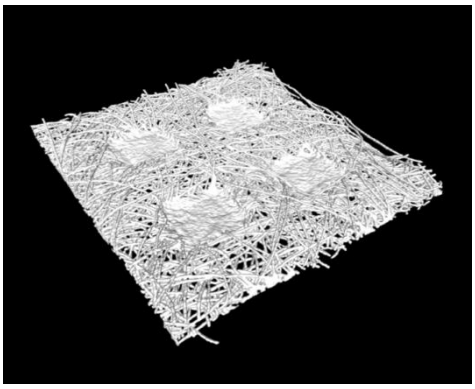

(c)

Figure 4.30: 3D Rendering of: (a) Sample-1; (b) Sample-2; and (c) Sample-3

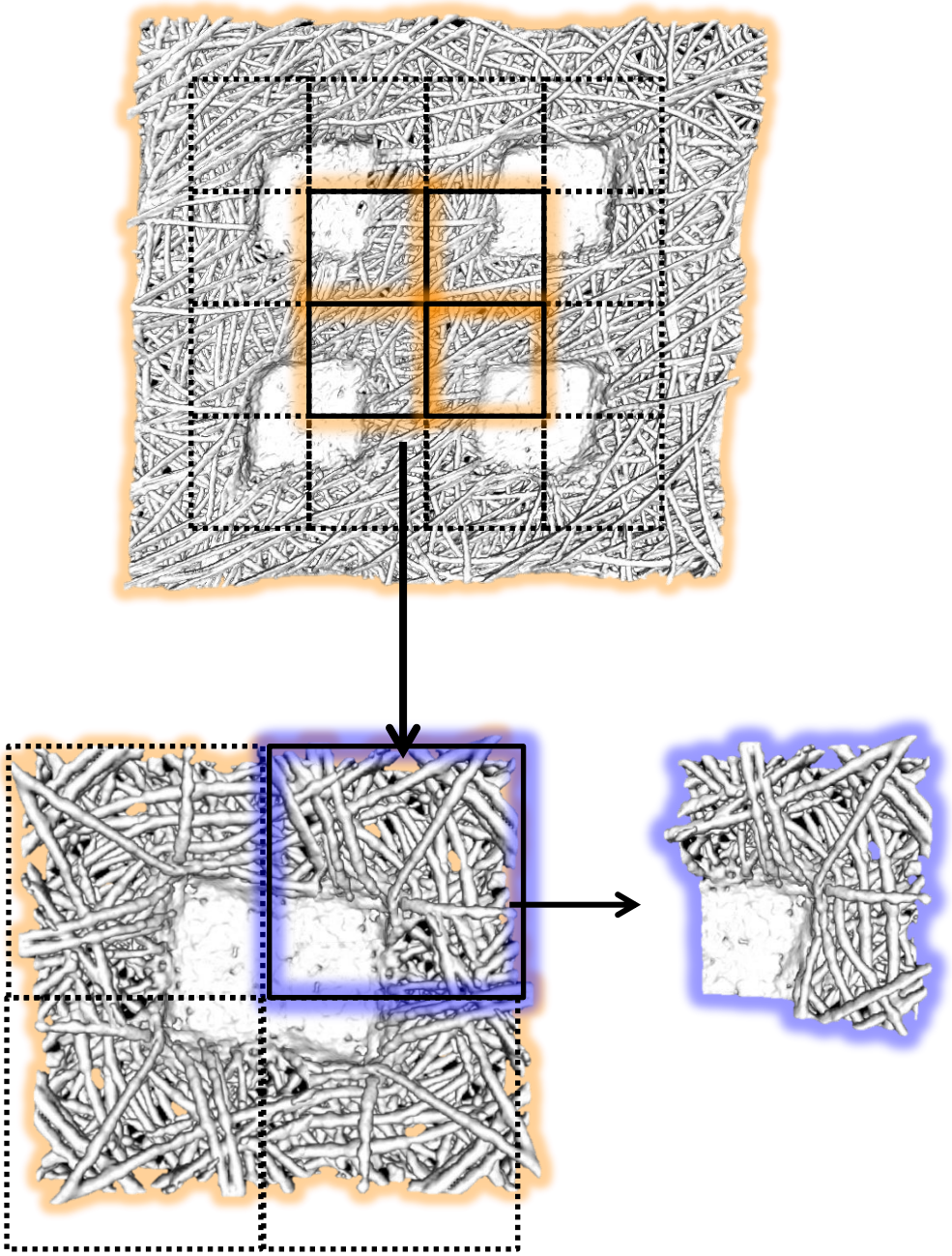

Figure 4.31: Unit cell model of thermally bonded nonwoven fabric

4.4.3 Unit Cell Model of Thermally Bonded Nonwoven Fabric

The unit cell models of thermally bonded nonwoven fabrics have been developed by using repeat unit cell approach, shown in Figure 4.31. The following two techniques were used:

1) X-ray Computer Tomography (CT); and
2) solid model generation by using 3D reconstructed STL mesh model.

4.4.3.1 Unit Cell Model from X-ray Computer Tomography (CT)

Unit cell model of thermally bonded nonwoven fabrics created from the data obtained from the X-ray Computer Tomography (CT) in four steps:

1) image collection, 2D slice reconstruction and segmentation;
2) 3D reconstruction and STL surface mesh generation;
3) restoration and simplification of STL surface mesh; and
4) solid unit cell model formation of STL surface mesh.

4.4.3.1.1 Image Collection, 2D Slice Reconstruction and Segmentation

1429 2D grey scale sliced images obtained from CT scan were assembled in ImageJ [142] to develop the stack. These stack images were binarised/segmented in order to extract the solid fibrous portion from their backgrounds by using sufficient thresholds of grey levels. In this work Otsu algorithm [143] was utilized to binarises the stack of images as shown in Figure 4.32. Otsu algorithm binarises the image by the following steps:

1) calculate the grey level of normalized histogram of the input image;
2) find the potential threshold level of input image and categorize the pixel into two groups (background and foreground);
3) calculate the mean of each group;
4) calculate the between-class variance (σ_B^2);
5) obtain the optimal threshold that maximises the between-class variance (σ_B^2) or minimises the weighted within class variance; and
6) use the optimal threshold to binarise the input image.

The drawback of Otsu's method is that it fails in case of the object and background pixels are extremely unstable (unimodality of the object function). During the segmentation of the stack images in ImageJ by using Otsu's method it is important to use the optimum threshold level to ensure that the fibre volume fraction of thermally bonded nonwoven fabric will not be changed. If the fibre volume fraction is changed during the segmentation process, the effective thermal conductivity will be affected significantly.

4.4.3.1.2 3D reconstruction and STL Surface Mesh Generation

After the segmentation step, stack images were cropped and the slices were reduced in order to obtain the quarter unit cell of thermally bonded nonwoven fabric. A 3D viewer plugin [144] of ImageJ was used to generate surface mesh (shell) of sample-1 in STL

(stereolithography/Standard Tessellation Language) format which contains 254388 triangular faces, 381582 edges and 126778 vertices.

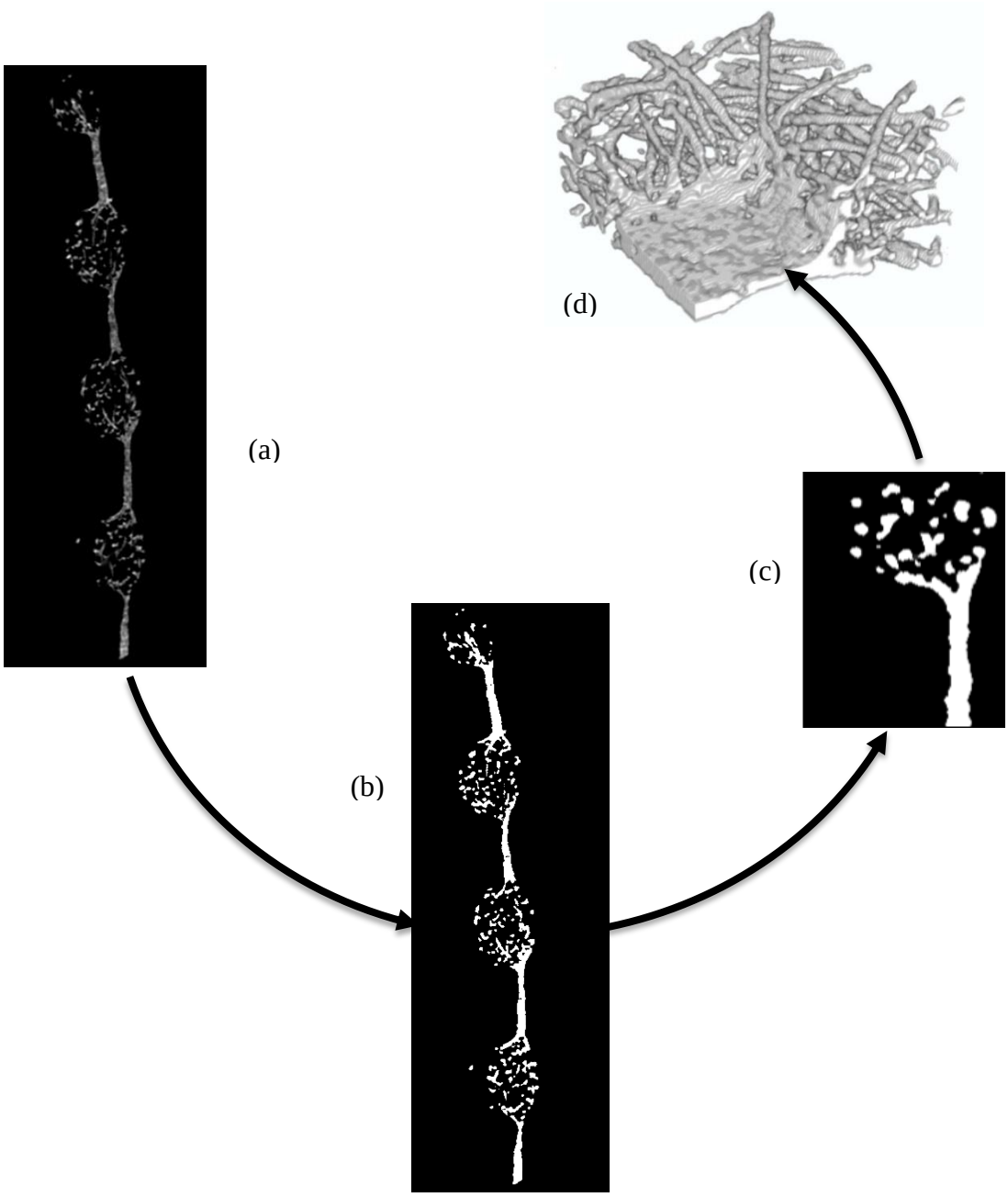

Figure 4.32: 3D reconstruction steps (a) 2D grey scale stack slice image of sample-1; (b) Segmented image by Otsu's method; (c) Cropped unit cell segmented image of sample-1; and (d) 3D reconstructed unit cell of sample-1

4.4.3.1.3 Restoring and Simplification of STL Surface Mesh

Surface mesh file was imported in MesLab [145] and filters were applied to remove the duplicate faces, zero area faces and self-intersecting faces. Quadratic edge collapse decimation was also used to reduce the number of faces which ultimately reduced the

computing cost and time. Figure 4.33 shows how this Quadratic edge collapse decimation filter works. When quadratic edge collapse decimation filter was applied it was important to make sure that the geometric parameter mesh volume keeps no change because it represents the fibre volume fraction. After applying Quadratic edge collapse decimation filter the faces of sample-1 reduces from 254388 to 40000.

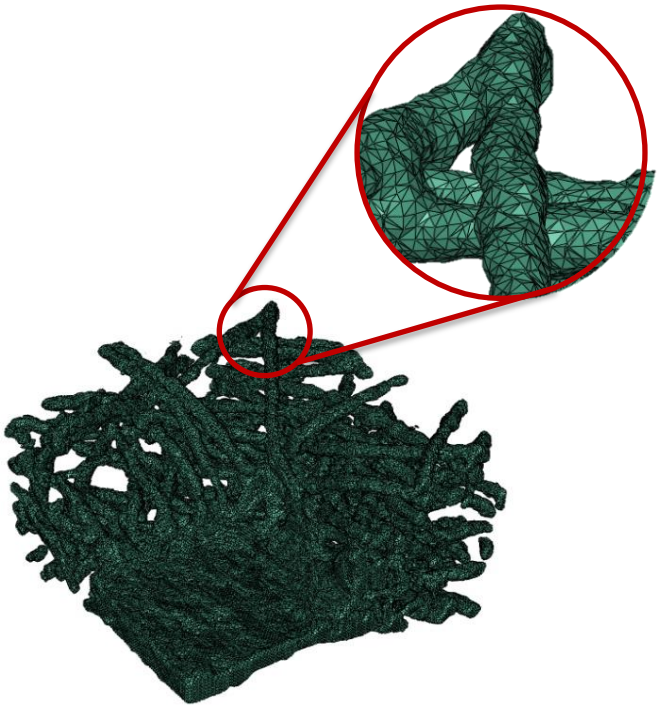

(a)

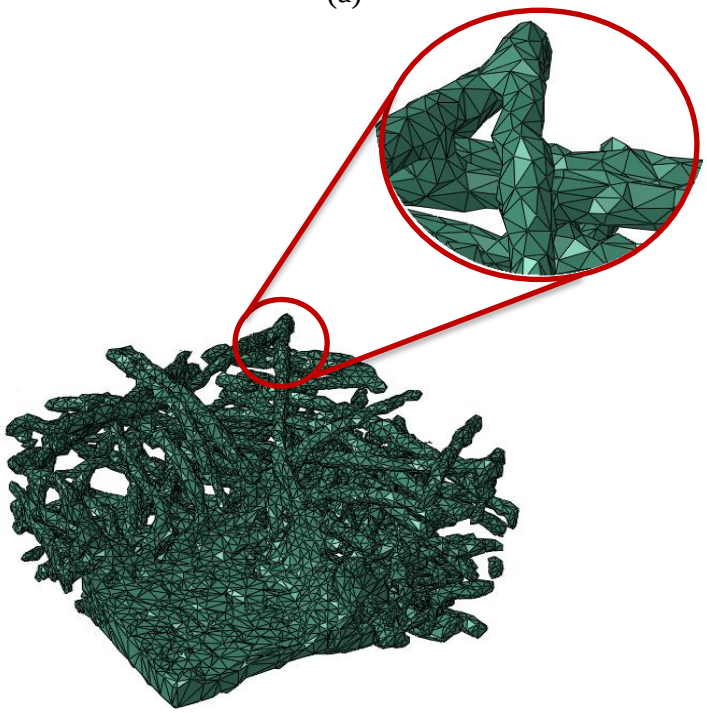

(b)

Figure 4.33: Faces reduction: (a) Sample-1 with 254388 faces and (b) Sample-1 with 4000 faces after quadratic edge collapse decimation filter

4.4.3.1.4 Solid Unit Cell Model form STL Surface Mesh

After the application of filter and face reduction in MeshLab the STL file was imported into Abaqus/CAE by using STL import plug-in which enables to import a model from Stereolithography (*.stl) file into Abaqus/CAE by using node merge tolerance of $1x10^{-6}$ as shown in Figure 4.34. A plug-in was used to convert STL mesh model into shell geometrical model and the volume was added to make the shell solid, shown in Figure 4.35. Some portion of the model is still in shell form after conversion by plug-in therefore the built-in GUI function of Abaqus/CAE "shape solid from shell" has been utilised to further convert shell portion into solid.

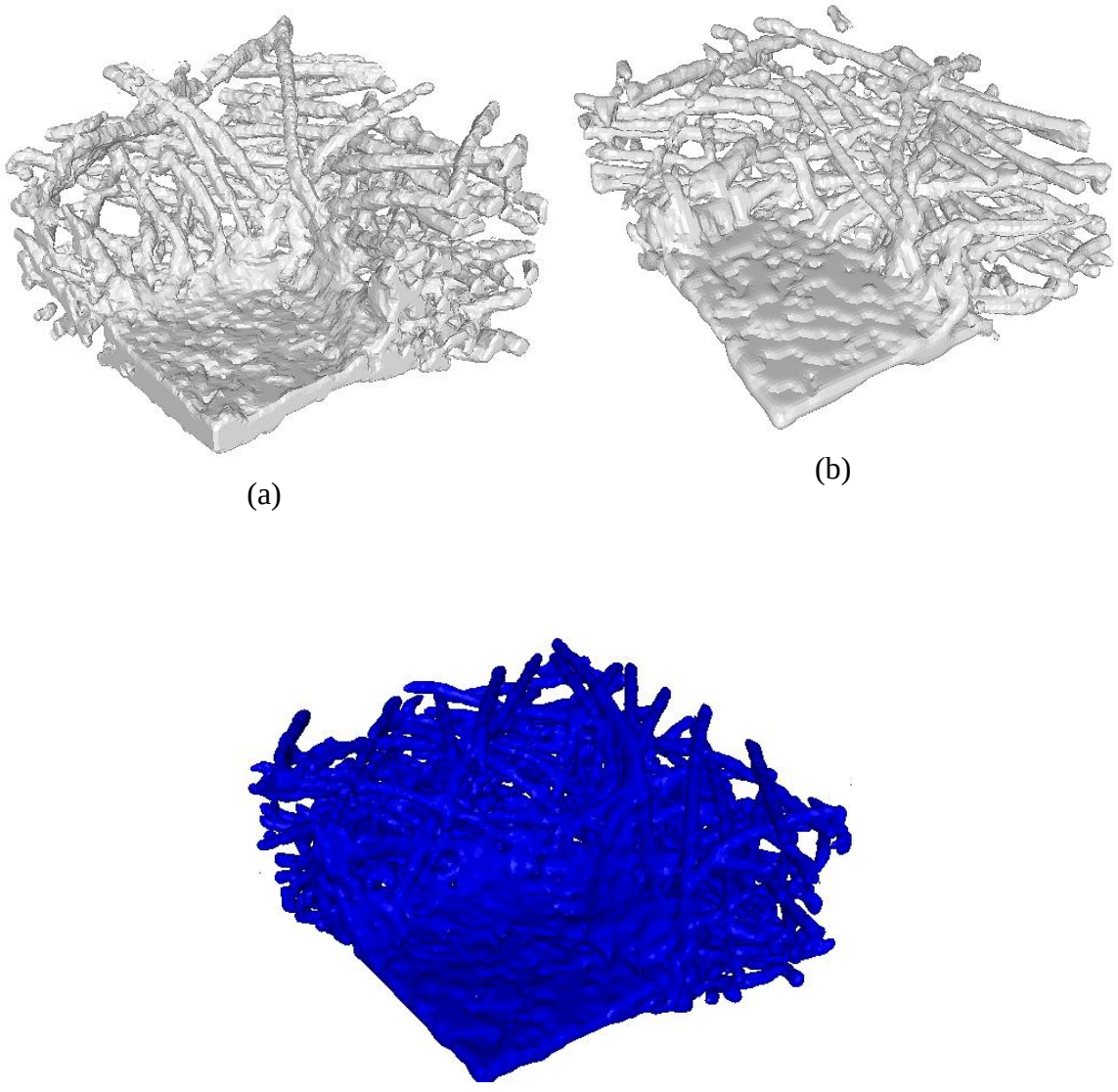

(a) (b)

(c)

Figure 4.34: STL mesh model: (a) Sample-1; (b) Sample-2; and (c) Sample-3

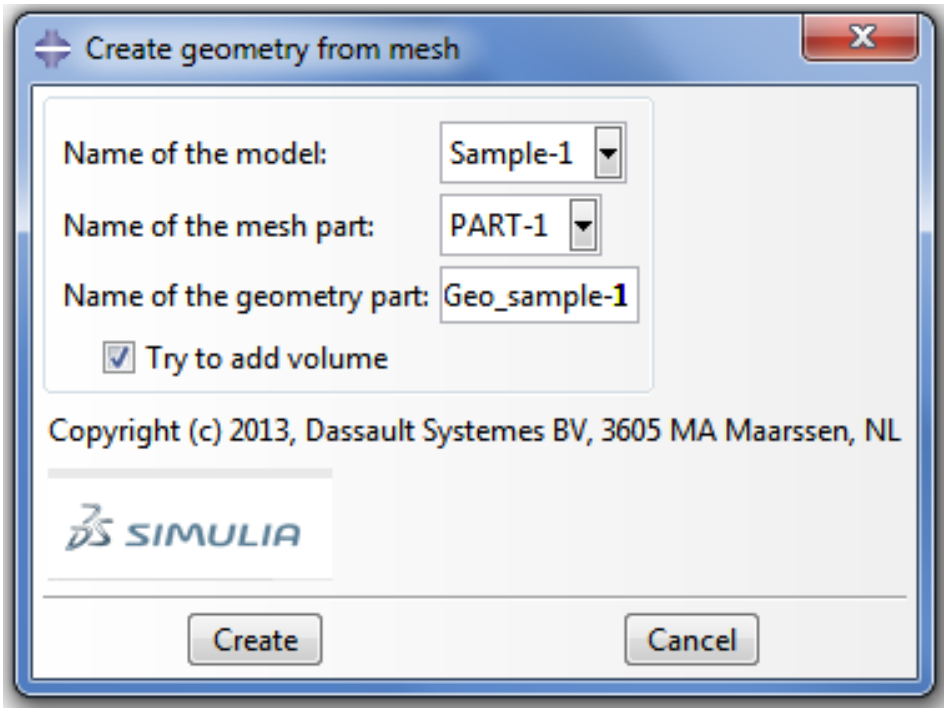

Figure 4.35: Create geometry from mesh plug-in

4.4.3.2 Unit Cell Model by Using 3D Reconstructed STL Mesh Model

Solid unit cell model was developed by using STL mesh model as shown in Figure 4.34. The parametric dimensions of thermally bonded nonwoven fabrics were determined in MeshLab by using STL mesh models and described in Table 4.6. It is assumed that the bond points were solid without any porosity because they were melted during the production and became a polymeric sheet, while the fibrous part is considered as solid, shown in Figure 4.36 (b).

Table 4.6: Sample geometric dimensions

Samples	Fibre diameter d_f (mm)	t (mm)	l (mm)	w (mm)	h (mm)	v_{SF} (mm^3)
Sample-1	0.028	0.54	0.720	0.3560	0.0550	0.150
Sample-2	0.026	0.35	0.787	0.4185	0.0322	0.104
Sample-3	0.024	0.57	0.904	0.5130	0.0430	0.213

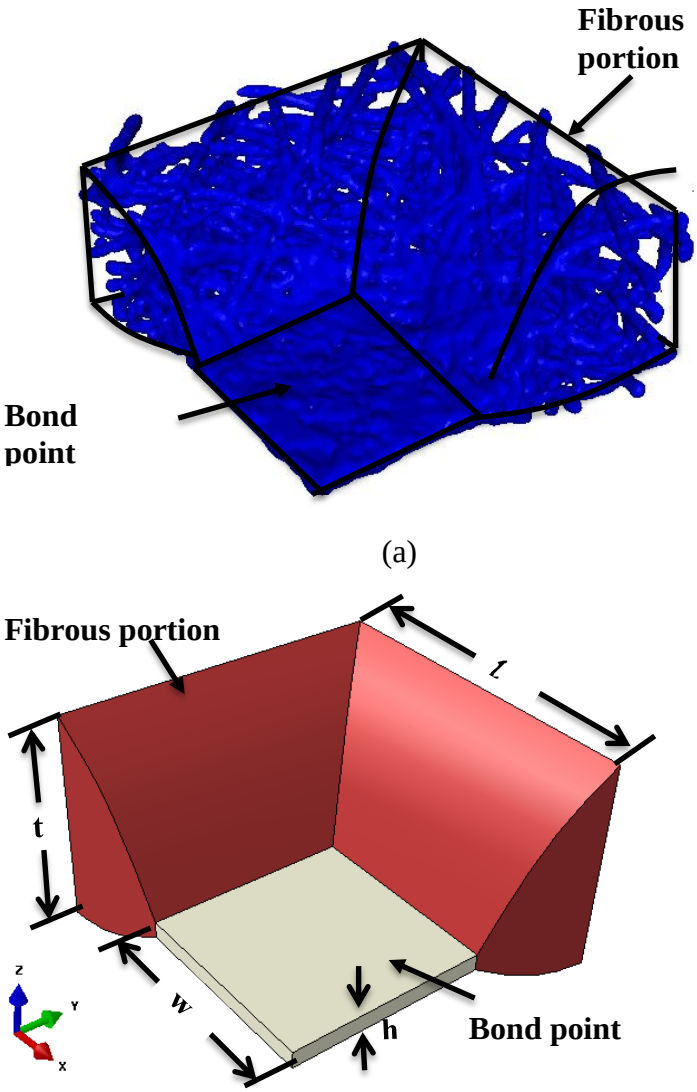

Figure 4.36: Nonwoven models: (a) STL mesh model of sample-3 and (b) Solid model of sample-3

4.5 Summary

One of the objectives of the research was to develop a finite element models of textile structures by using the actual geometrical parameters. Different techniques have been used to acquire the structural parameters of the fabrics such as: SEM, microscope, x-ray microtomography and experimental method for the development of the accurate finite element models.

Woven fabric models were developed in TexGen by using variable cross-section of yarn in order to minimize the interference between warp and weft yarns due to yarn crimp in the fabric. Plain weft knitted fabric models were developed by the parametric modelling approach using the actual fabric parameters to ensure the accuracy of the geometrical

models. In addition nonwoven fabric models were also generated through two different approaches 3D reconstruction and solid modelling. Solid models were generated by using the actual parameters obtained from 3D reconstructed surface mesh models. The developed models will be used to analyse the heat transfer behaviour of the fabrics, this will be discussed in next Chapter.

Chapter 5 Heat Transfer Analysis of Textile Structures

5.1 Introduction

Development of finite element models of textile structures was one of the objectives of the research. This Chapter describes the heat transfer analysis and prediction of effective thermal conductivity and thermal resistance of developed models. The methodology is adopted to calculate the effective thermal conductivity and thermal resistance of woven, MicroPCMs coated woven composites, knitted and nonwoven fabrics as shown in the following block diagram in Figure 5.1.

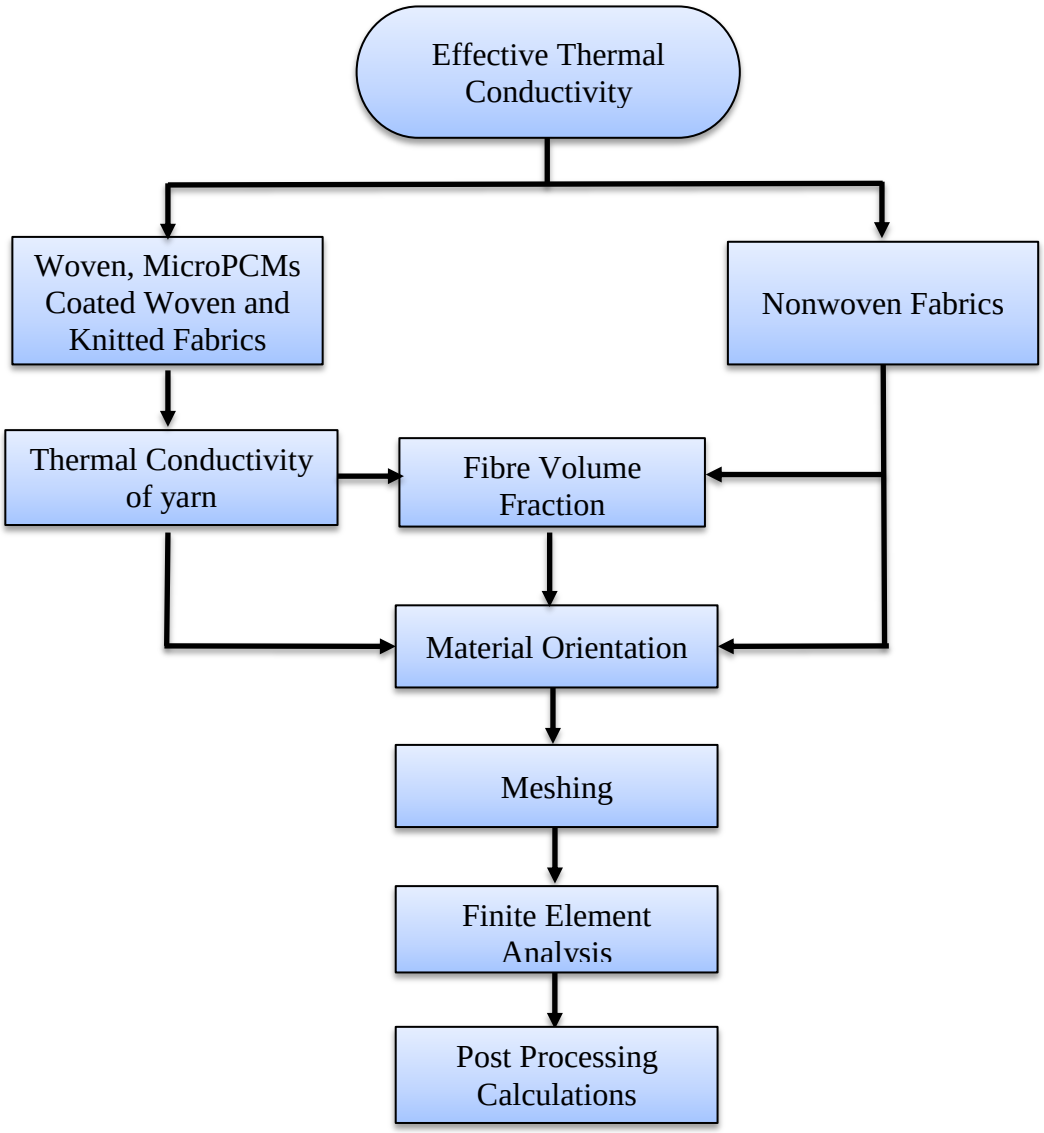

Figure 5.1: Research methodology for effective thermal conductivity and thermal resistance of fabrics by using finite element method

5.2 Effective Thermal Conductivity of Yarn

The effective thermal conductivity of textiles mainly depends on two components: conductive heat transfer through solid fibres and air within the fabric [146]. Therefore it is substantial to determine the amount of fibre content or fibre volume fraction in the unit cell of a woven fabric.

5.2.1 Fibre Volume Fraction of Woven, MicroPCMs Coated and Knitted Fabric

Fibre volume fraction in a fabric (V_f) was calculated by using Equation 5.1.

$$V_f = \frac{\rho}{\rho_f} \tag{5.1}$$

where ρ and ρ_f are the fabric and fibre density respectively.

Fabric density can easily be calculated by the areal density of fabric and fabric thickness as shown in Equation 5.2.

$$\rho = \frac{\text{Fabric Areal Density}}{\text{Fabric Thichkness}} \tag{5.2}$$

Fibre volume fraction of yarn (V_{fy}) in a fabric can be calculated in two ways, i.e. (i) through image analysis [147] and (ii) find out the unit cell fibre volume fraction/Fibre volume fraction of fabric (V_f) using Equations 5.3 & 5.4 respectively,

$$V_{fy} = \frac{\text{Total Fibre Volume in Yarn}}{\text{Yarn Volume}} \tag{5.3}$$

$$V_{fy} = \frac{V_f \times V_{uc}}{V_y} \tag{5.4}$$

where V_f, V_{uc} and V_y are the fibre volume fraction of fabric, volume of the unit cell and volume of yarn respectively.

5.2.1.1 Fibre Volume Fraction of Different Yarn Count

Fibre volume fraction of same yarn count and equal number of warp/weft set of fabric can be calculated by the above Equation 5.3 and 5.4. However in case of cotton, wool and poly-viscose fabric they have different yarn count and warp/weft set; yarn counts is utilised to calculate the fibre volume fraction in yarn by following steps:

(1) calculate the individual length of yarn;
(2) calculate the individual volume of yarn;
(3) multiply the length of yarn with the yarn count which gives the mass of fibre in yarn;
(4) convert the mass of fibre in yarn into volume of fibre in yarn by dividing the mass of fibre in yarn by the density of fibre ; and
(5) finally divide the volume of fibre in yarn by volume of yarn.

Fibre volume fraction of yarn for different yarn count and different number of warp/weft per unit length can be calculated following the above mentioned steps using Equations 5.5, 5.6 and 5.3.

$$\text{Mass of fibre in yarn} = \text{Yarn count} \times \text{Lenght of yarn} \tag{5.5}$$

$$\text{Volume of fibre in yarn} = \frac{\text{Mass of fibre in yarn}}{\rho_f} \tag{5.6}$$

then, fibre volume fraction of yarn with different yarn count can be calculated by Equation 5.3.

5.2.1.2 Fibre Volume Fraction of Core Spun Yarn

The weft yarn in the poly-viscose fabric is a core-spun yarn and warp yarn is simple polyester yarn shown in Figure 5.2. The core part of the spun yarn is polyester filament covered by viscose fibres. The effective density of fibres for the whole yarn was calculated on the basis of weighted proportion by using Equation 5.7 [148].

$$\rho_{feff} = w_{af}\rho_{af} + w_{bf}\rho_{bf} \tag{5.7}$$

where w_{af}, w_{bf}, ρ_{af}, and ρ_{bf}, are the weight proportion and density of fibre 'a' and 'b' respectively.

Weight proportion of fibre in core-spun yarn was calculated by using image analysis of SEM image. During image analysis the area of respective fibre within the yarn was calculated firstly and then the weight proportion which was calculated by using Equations 5.8 and 5.9.

$$m_{af} = A_{af} \times l_{af} \times \rho_{af} \tag{5.8}$$

$$w_{af} = \frac{m_{af}}{T_y \times l_y} \qquad 5.9$$

where m_{af}, A_{af}, l_{af}, l_y and T_y are mass of fibre 'a', cross-sectional area of fibre 'a', length of fibre 'a', length of yarn and yarn count in Tex respectively. In case of multifilament yarn it was assumed that the length of both yarn and filament fibre was same.

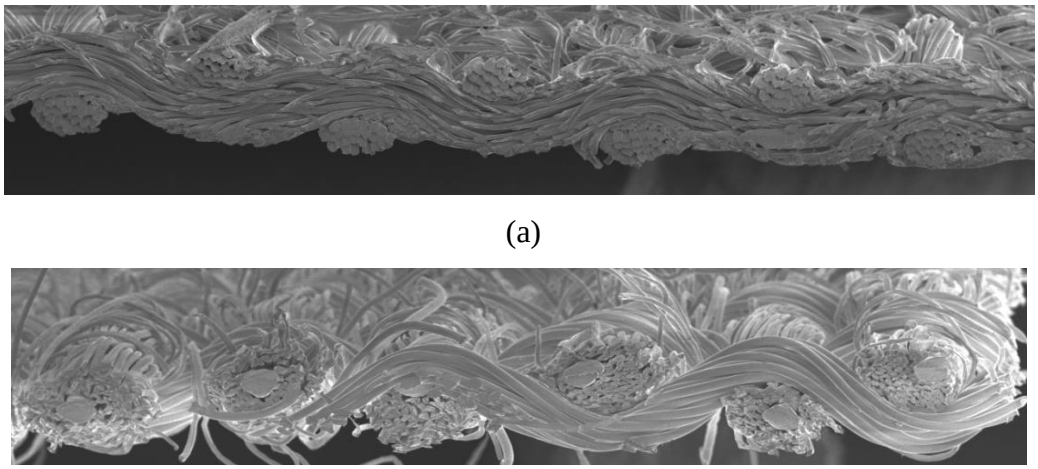

(a)

(b)

Figure 5.2: Micrograph of poly-viscose fabric; (a) Cross-section of warp yarn, and (b) Cross-section of core spun weft yarn

Table 5.1 shows the value of fibre volume fraction in a yarn of woven fabric calculated by aforementioned technique. The fibre volume fraction value of yarn was used to calculate the axial and transverse thermal conductivity of yarn.

Table 5.1: Fibre volume fraction of yarn and unit cell of woven fabric

Fabrics	Fibre volume fraction of yarn, V_{fy} (%)		Fibre volume fraction of unit cell, V_f (%)
	warp	weft	
Nomex® III	40.00	40.00	24.6
Twaron®	50.87	50.87	30.00
Cotton	40.69	36.4	17.94
Wool	57.50	45.71	24.32
Poly-Viscose	44.34	41.67	20.17

Yarn packing/ volume faction (V_{fy}) of knitted fabrics F4 and F5 can be calculated by Equation 5.10 which are 0.213 and 0.274 respectively.

$$d = 2 \times \sqrt{\frac{T_y}{10^3 \pi \rho k}} \tag{5.10}$$

where T_y is the yarn count (Tex), ρ is the density of fibre (g/cm^3) and k is the fibre packing fraction in the yarn.

Table 5.2 shows the thermal properties of fibres which were used to determine the effective thermal conductive of yarns. The material of yarn orthotropic in nature with consideration of transversely isotropic was taken so the thermal conductivity of yarn can be defined by the following tensor Equation 5.11:

$$K = \begin{bmatrix} K_{11} & 0 & 0 \\ 0 & K_{22} & 0 \\ 0 & 0 & K_{33} \end{bmatrix} \tag{5.11}$$

where K_{11} , K_{22} and K_{33} are the thermal conductivity of the yarn along the fibre direction and perpendicular to the fibre direction respectively.

Combined thermal conductivity of component fibres of the core spun yarn can be calculated by Equation 5.12:

$$K_{feff} = w_{af} K_{af} + w_{bf} K_{bf} \tag{5.12}$$

where K_{af} and K_{bf} are thermal conductivity of fibre ‘a’ and ‘b’ respectively.

After the fibre volume fraction and air fraction in the yarn were calculated, the axial and transverse thermal conductivity of the yarn can then be calculated by a number of models which have been developed.

Yarn axial thermal conductivity (K_{ya}) can be calculated by Parallel model:

$$K_{ya} = K_{fa} V_{fy} + K_{air} (1 - V_{fy}) \tag{5.13}$$

Yarn transverse thermal conductivity (K_{yt}) can be calculated by the Series model, Clayton model and Pilling model [149-151] as shown in Equations 5.14-5.16.

$$K_{yt} = \frac{K_{ft} K_{air}}{V_{fy} K_{air} + (1 - V_{fy}) K_{ft}} \tag{5.14}$$

$$K_{yt} = K_{air} \left[\frac{\sqrt{(1 - V_{fy})^2 \left(\frac{K_{ft}}{K_{air}} - 1 \right)^2 + 4 \frac{K_{ft}}{K_{air}}} - (1 - V_{fy}) \left(\frac{K_{ft}}{K_{air}} - 1 \right)}{2} \right]^2 \tag{5.15}$$

$$K_{yt} = K_{air} \frac{(1 - V_{fy}) + (1 + V_{fy}) \left(\frac{K_{ft}}{K_{air}} \right)}{(1 - V_{fy}) \left(\frac{K_{ft}}{K_{air}} \right) + (1 + V_{fy})} \tag{5.16}$$

Table 5.2: Thermal properties of fibres

Symbol	Nomex® III [152]	Tawron [152]*	Cotton [153]	Wool [153]	Viscose [153]	polyester [153]
ρ_f (kg/m^3)	1380	1440	1520	1310	1490	1390
K_{fa} (W/m.k)	1.3[a]	3.05	2.88	0.48	1.89	1.26
K_{ft} (W/m.k)	0.13	0.192	0.243	0.165	0.289	0.157
C_{pf} (J/kg.K)	1200	1420	1350	1360	1590	1030

[a]Assumed axial thermal conductivity value 10 times than the transverse [30]
*Thermal conductivities values of Twaron® assumed same as Kevlar
K_{fa} : Thermal conductivity along fibre axis
K_{ft} : thermal conductivity perpendicular to the fibre axis

Table 5.3, Table 5.4 and Table 5.5 shows the thermal conductivity value in both the yarn axial and transverse directions calculated by the equations mentioned above. In Table 5.3 cotton, wool and poly-viscose yarns show different values of thermal conductivity in warp and weft directions due to the yarn count difference. The material of yarn is transversely isotropic, hence:

$$K_{22} = K_{33} = K_{yt}$$

$$K_{11} = K_{ya}$$

Table 5.3: Yarn thermal conductivity of woven fabrics

Fabrics	Yarn thermal conductivity in axial direction, K_{ya} (W/m.K)		Yarn thermal conductivity in transverse direction, K_{yt} (W/m.K)	
	warp	weft	warp	Weft
Nomex® III	0.5356	0.5356	0.0382	0.0382
Twaron®	1.5643	1.5643	0.0358	0.0358
Cotton	1.1875	1.0646	0.0408	0.0385
Wool	0.2871	0.2335	0.0504	0.0423
Poly-Viscose	0.5732	0.7356	0.0413	0.0405

Table 5.4. Thermal conductivity of yarn of F4 and F5 of knitted fabric

Fabric Code	Fibre Volume Fraction of Yarn V_{fy} (%)	Yarn thermal Conductivity in axial direction K_{ya} (W/m.K)	Yarn thermal Conductivity in transverse direction K_{yt} (W/m.K)
F4	0.213	0.63390	0.032107[a]
F5	0.274	0.53674	0.03463[a]

[a] Calculated by Series model

Table 5.5: Fibre volume fraction and yarn thermal conductivity of MicroPCMs coated composite fabric

Fabrics	Yarn Fibre Volume Fraction, V_{fy} (%)	Fibre volume fraction of unit cell, V_f (%)	Yarn thermal Conductivity in axial direction, K_{ya} (W/m.K)	Yarn thermal Conductivity in transverse direction, K_{yt} (W/m.K)
Nomex® III	40.00	18.12	0.5356	0.0382
Cotton	38.33*	1510	1.1199	0.0395
Wool	51.00*	17.7	0.2575	0.0456

*Average volume fraction of yarn was used

5.2.2 Fibre Volume Fraction of Nonwoven Fabric

Fibre volume fraction of 3D solid models needs to be calculated. Fibre volume fraction of fibrous portion (V_{fp}) can be determined by the total mesh volume by following steps:

1) calculate the volume of bond point (v_{BP});
2) calculate fibrous portion volume (v_{FP}) by subtracting the volume of bond point from the total mesh volume (v_M); and
3) calculate the volume fraction of fibrous part in solid model by Equation 5.17.

$$V_{fp} = \frac{v_{FP}}{v_{SF}} \qquad 5.17$$

where v_{SF} is the total volume of fibrous portion as solid in solid model.

Table 5.6 shows the fibre volume fraction of thermally bonded nonwoven fabric. The thermal conductivity of their fibrous portion will be used as input material property in Abaqus/CAE.

Table 5.6: Fibre volume fraction and thermal conductivity of nonwoven fabric

Samples	Fibre Volume Fraction of unit cell, V_f (%)	Fibre volume fraction of fibrous portion, V_{fp} (%)	Thermal Conductivity of fibrous portion, K_{fp} * (W/m.K)
Sample-1	15.95	25.112	0.03219
Sample-2	12.01	19.59	0.03059
Sample-3	14.93	27.42	0.032911

* K_{fp} calculated on the bases of transverse thermal conductivity of fibre

5.2.3 Material Orientation

Yarn is considered as solid orthotropic with the consideration of transversely isotropic. Transversely isotropic materials are those which have the equivalent physical properties at every point in the material about an axis that are normal to the plane of isotropy.

Figure 5.3 shows the material orientation in yarn of woven fabric generated in Abaqus/CAE (Computer Aided Engineering), axis 11 refers to the axis which is parallel

to yarn axis, axis 22 and 33 are transverse (perpendicular) to the fibre direction by using discrete orientation technique. Because of the waviness in warp and weft yarn the material principal may vary from point to point. Unit cell model of one repeat unit length of woven fabric was imported in Abaqus in STP (Standard for the Exchange of Product model data) format. A discrete orientation defines a spatially varying orientation at the centroid of each native or orphan mesh element. The orientation is based on the topology of the part, allowing defining a continually varying orientation. Once the normal axis and primary axis are defined, Abaqus/CAE uses these axes to construct a right-handed Cartesian coordinate system [154]. For that purpose the surface of the yarn is divided into small faces by partition and the edges and surfaces are selected for primary and normal axis.

Figure 5.4 (a) shows the material orientation of knitted fabric achieved in Abaqus/CAE. Figure 5.4 (b) and (c) show the fibre direction only along the fibre axis and transverse to the fibre direction respectively.

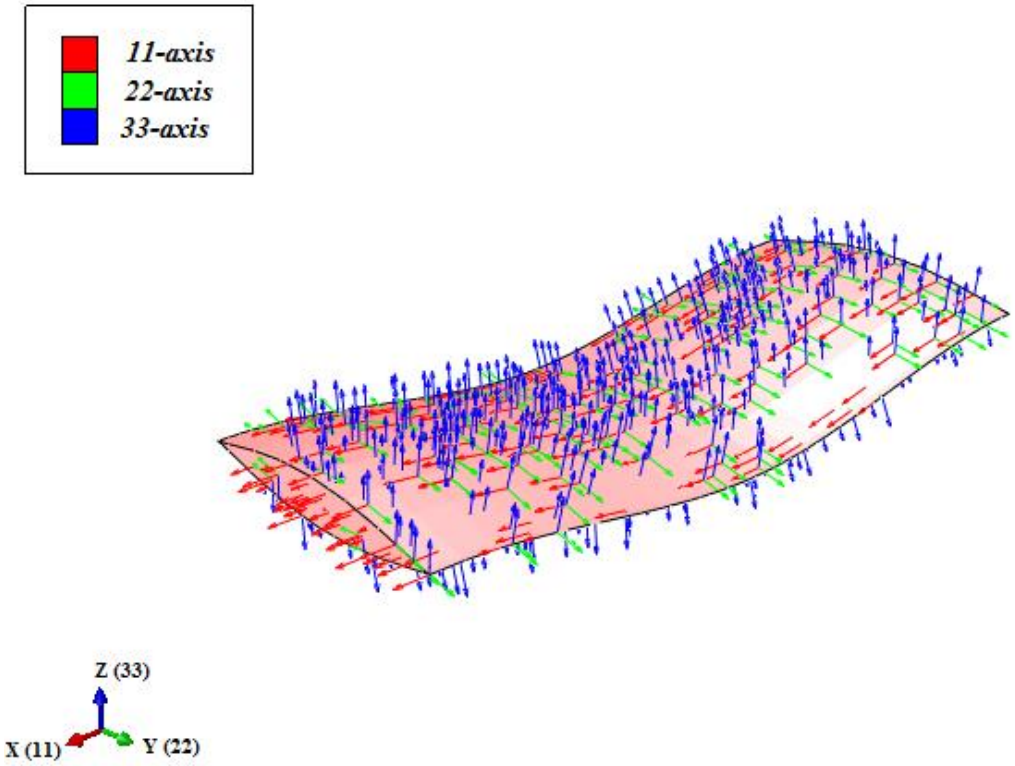

Figure 5.3: Material orientation of yarn in woven fabric

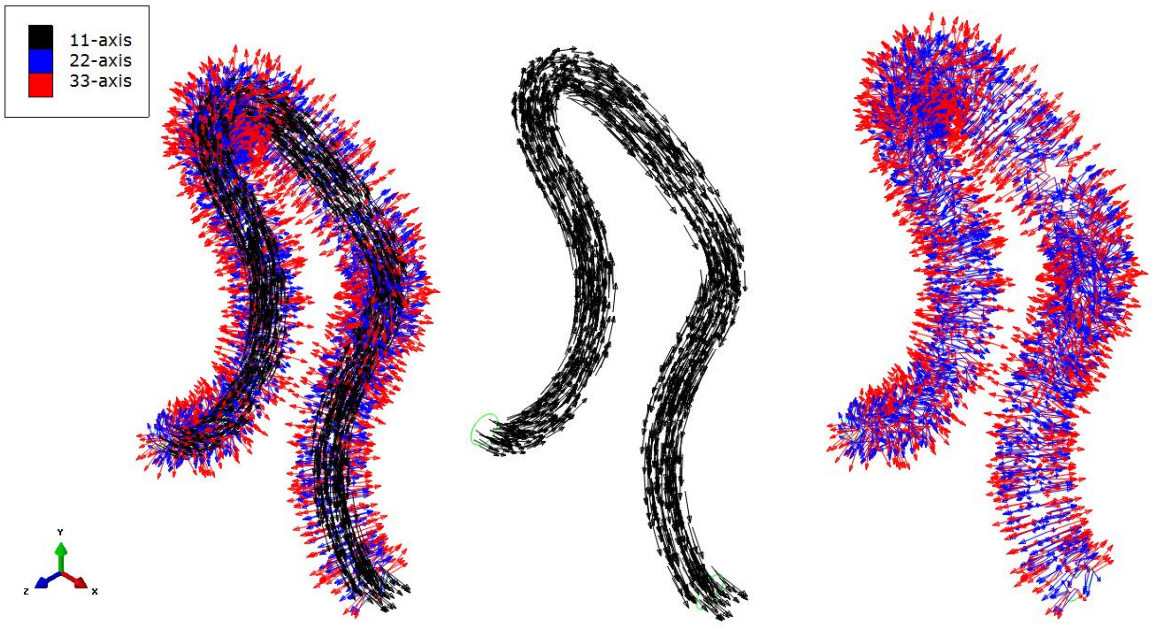

(a) (b) (c)

Figure 5.4. Material orientation of yarn in knitted fabric

The material orientation of nonwoven fabric is evaluate by using 2D Fast Fourier Transform (FFT) was utilized to measure the alignment fibres in nonwoven fabric. A 2D SEM image was utilized and cropped the portion between the two bonding points was taken for analysis of fibre orientation presented in Figure 5.5.

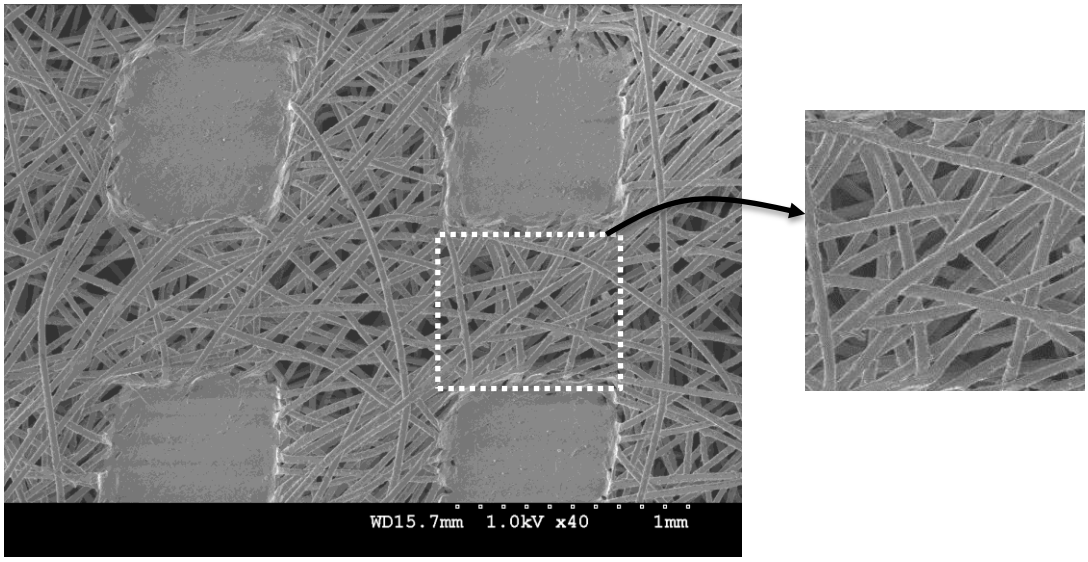

Figure 5.5: Micrograph of sample-1

Fibre orientation of thermally bonded nonwoven fabric has been evaluated by the following steps described by Ayres et al. [155]:

1) 2D-FFT was performed on grey scale image of thermally bonded nonwoven fabric. Only when the cropped image between bond points of 256×256 pixels which within the categories of 2n pixels size, then the good frequency plot

results can be obtained. A 2D Fast Fourier Transform function transforms the spatial information of image into distribution of the points as shown in Figure 5.6 (b);

2) an ImageJ oval plug-in was used to summed pixel intensities along each radius from the origin of circle to the periphery; and
3) a summed pixel intensities value was used to plot FFT alignment with normalization, shown in Figure 5.6 (c).

Figure 5.6 (c) shows that the peaks around 54 degrees but majority of fibres align between 30- 80 degree because lower portion of circumference is almost symmetric to the upper portion.

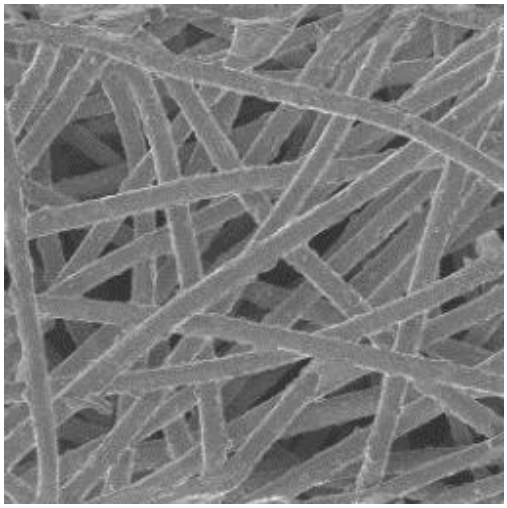

(a)

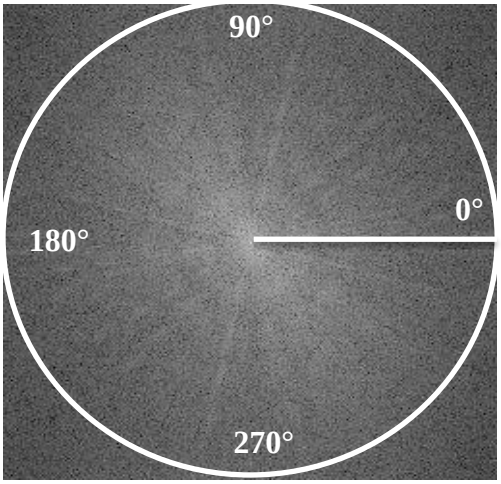

(b)

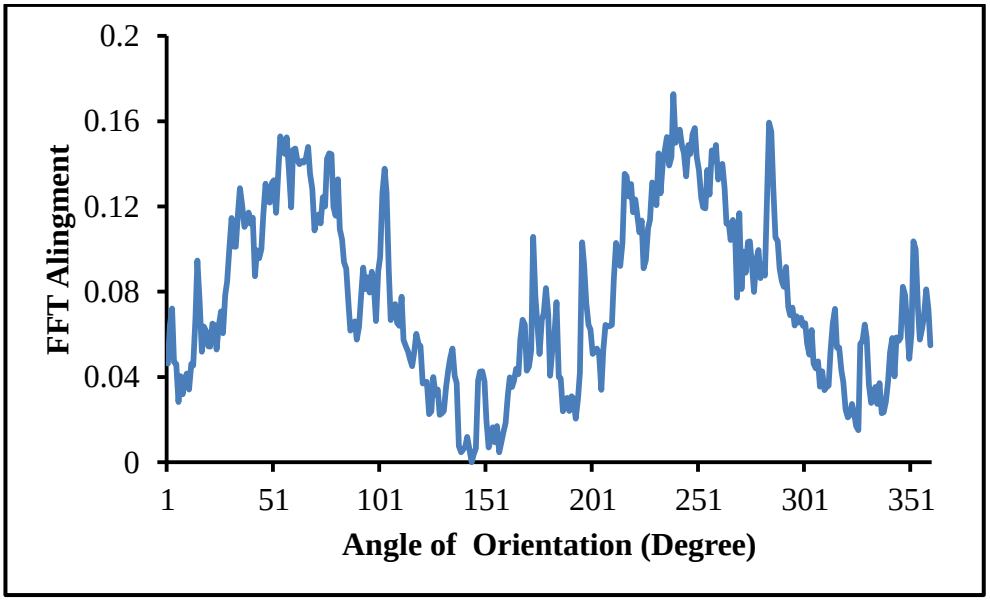

(c)

Figure 5.6: Fibre orientation: (a) Grey scale cropped image of sample-1; (b) 2D FFT frequency plot of sample-1; and (c) 2D-FFT alignment plot of sample-1

This method is unable to give the accurate fibre alignment within the bond point of thermally bonded nonwoven fabric because thermally bonded nonwoven fabric is not in flat structure. In future more research will be required to analyse the 2D reconstructed stack sliced image of nonwoven fabric to give the exact fibre orientation.

5.2.4 Meshing Schemes

4-node linear tetrahedral element (DC3D4) was used to mesh the unit cell of fabric because this is the most suitable mesh element to completely mesh the complex geometrical shape [154]. An optimal mesh density was obtained after the verification that further refinement cannot affect the results. Figure 5.7 shows the meshed unit cell model of Twaron® fabric.

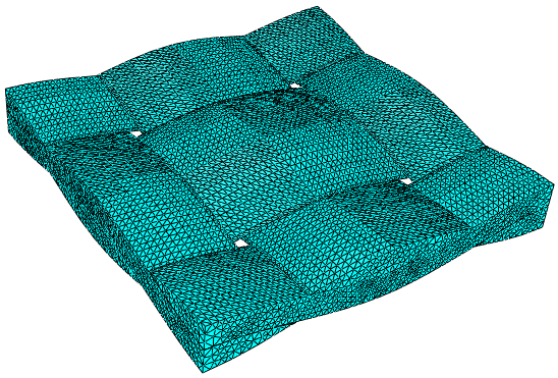

Figure 5.7: Meshed unit cell model of Twaron® fabric

5.3 Finite Element Analysis

5.3.1 Effective Thermal Conductivity of Woven Fabric

As shown in Figure 4.17 in Chapter 4 when fabric is placed between the hot and cold plates during experiment the air is entrapped between the upper and lower surface of the fabric. As mentioned in the literature review there is no significant evidence of convection heat transfer when fibrous material was placed the two plates having a temperature gradient [20]. It was also mentioned in the literature review that radiation heat transfer can be neglected when only small temperature gradient is present [44].

The following assumptions have been made for the finite element analysis of woven fabric thermal properties on the basis of above facts.

1) Consider still air inside and over the surface of fabric so the heat is only transfer by conduction.

2) Only one mode of heat transfer was considered i.e. conduction.
3) Yarn is porous material, considering both fibre and the air.
4) Air in fabric is considered as fluid matrix.

Heat transfer by conduction of fabric is calculated by Equation 1.1.

The unit cell of fabric mentioned in Section 4.2 was imported and meshed in a commercial finite element simulation software Abaqus/CAE by using the mesh schemes described in section 5.2.4. Two material sections were defined for air and fibre. The thermal conductivity value of air is constant which 0.026 W/m.K. In case of yarn three effective thermal conductivity values K_{11} , K_{22} and K_{33} calculated in section 5.2 were taken as the input parameters for analysis.

5.3.1.1 Boundary Conditions and Analysis

For 1-D steady state heat transfer analysis across the thickness of the fabric (t), the specified temperature boundary conditions were used. The two specified temperature values were defined on both side of the fabric with the assumption of all the other surfaces of the fabric are perfectly insulated. The specified temperatures can be expressed as:

$$T(0) = T_0 = Specified\ Value$$
$$T(h) = T_h = Specified\ Value$$

where T_0 and T_h are the specified value at face and back side of the fabric respectively. The effective thermal conductivity across the thickness of fabric can be determined by using Equation 5.18.

$$K_z = Q_z \frac{t}{\Delta T_Z} \qquad 5.18$$

where Q_z, t and ΔT_Z are the overall heat flux value, fabric thickness and the temperature difference in z-direction respectively.

Q_z of unit cell can be calculated by two means [156]:

a) Define the node sets in by adding the following lines:

*node print, NSET=Node-name, freq=1
RFL11

Then sum up all the value of reaction flux across the nodes and then divide by the surface area of unit cell.

b) Define the surface and then add the following lines:

*Section Print, Name=Section_name, Surface=Surface_name, freq=1
SOH, SOAREA
SOH and SOAREA return the total section heat flux and surface area of the unit cell. The overall heat flux value along the z-direction can be calculated by using the Equation 5.19.

$$Qz = \frac{Tatal\ \ Section\ \ Heat\ \ Flux}{Total\ \ Surface\ \ \ Area} \tag{5.19}$$

The effective thermal conductivity and thermal resistance of plain woven fabric predicted by unit cell model are listed in the Table 5.7.

Thermal resistance (R_z) of the unit cell in Z-direction can be determined by:

$$R_z = \frac{t}{K_z} \tag{5.20}$$

Table 5.7: Predicted effective thermal conductivity and thermal resistance of plain woven fabric with consideration of anisotropic condition

Fabrics	Predicted effective thermal conductivity of Fabric across the thickness , K_z / K_{eff} (W/m.K)	Predicted thermal Resistance of Fabric R_z (m^2.K/W)
Nomex®III	0.0552	0.009058
Twaron®	0.0476	0.007311
Cotton	0.065	0.007446
Wool	0.04618	0.008835
Poly-Viscose	0.05088	0.006702

Figure 5.8 shows the heat flux and temperature contour of unit cell of Twaron® under the specified temperature boundary conditions. Figure 5.8 (a), (c), and (d) shows that the heat flux and temperature at cross over points are more compared to the other

portion because less air presents. Figure 5.8 (b) shows the temperature distribution across the thickness of fabric.

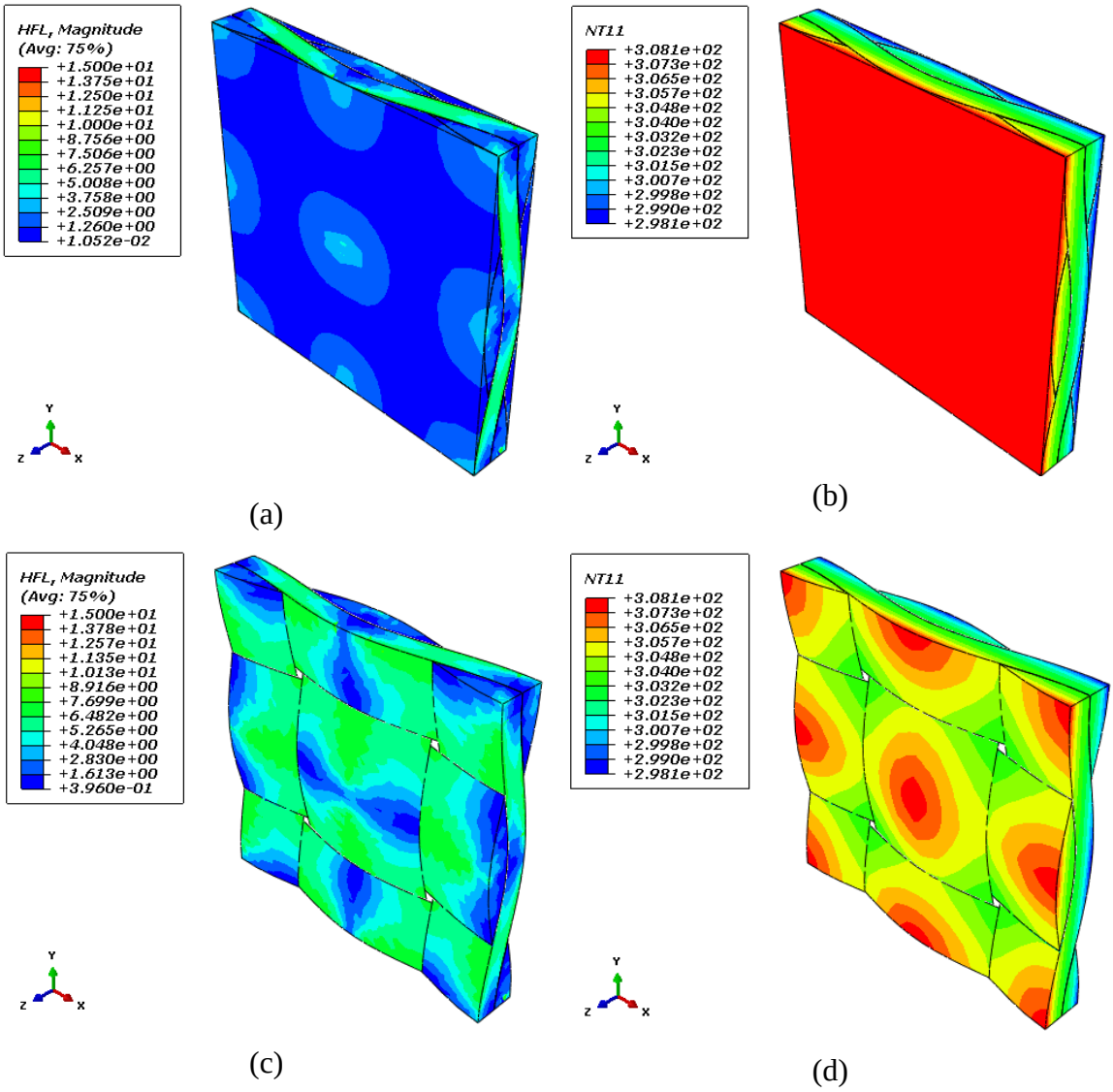

Figure 5.8: Heat flux and temperature distribution of unit cell: (a), (b) Twaron® fabric with air-fluid matrix, (c), and (d) Twaron® fabric without air-fluid matrix.

5.3.2 Effective Thermal Conductivity of MicroPCMs Coated Woven Composites

Effective thermal conductivity of MicroPCMs coated woven composite fabric were calculated in two steps:

1) first step is to calculate the effective thermal conductivity of MicroPCMs and binder; and
2) second step is to use the effective thermal conductivity of MicroPCMs and binder as input material property for coated layer in Abaqus/CAE.

5.3.2.1 Effective Thermal Conductivity of MicroPCMs and Binder

The following assumptions have been taken into consideration in evaluating the effective thermal conductivity of MicroPCMs and binder:

1) acrylic binder as matrix and MicroPCMs as filler which is homogenously distributed.
2) only one mode of heat transfer was consider i.e. conduction
3) no internal heat generation of the model.
4) no PCM density variation with respect to temperature change.

Table 5.8 shows the thermo-physical properties of the core and shell of microcapsules and the acrylic matrix (binder) which were used as the material properties in finite element analysis. Figure 5.9 presents the meshed unit cell model of binder and MicroPCMs with 60% volume fraction of MicroPCMs. It was meshed by 4-node linear tetrahedral elements (DC3D4).

Table 5.8: Thermo-physical properties

Property	n-Octadecane [157]	Melamine Formaldehyde [158]	Acrylic Binder
Density (Kg/m^3)	779	1500	1080
Specific heat (KJ/Kg.K)	1.9 (Solid) 2.2 (Liquid)	1.2	2.4
Thermal conductivity (W/m.K)	0.4 (Solid) 0.3 (Liquid)	0.5	0.155[159]
Latent Heat of Fusion (KJ/Kg)	238.76	-	-
Melting Point (˚C)	28.2	-	-

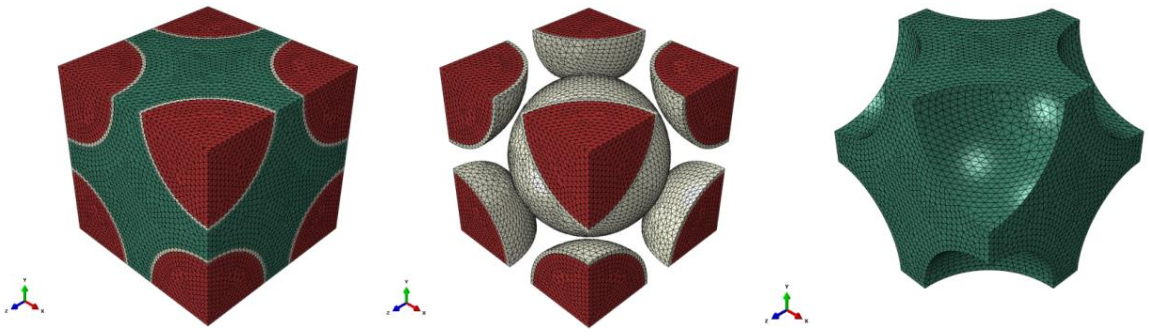

(a) (b) (c)

Figure 5.9: Meshed Unit cell model of MicroPCMs and Binder: (a) MicroPCMs with Binder; (b) MicroPCMs only; and (c) Binder only

For heat transfer analysis the temperature specified boundary conditions were used to define the temperature for hot and cold surface while keeping other surfaces insulated. The predicted effective thermal conductivity was calculated after the post-processing calculation by Equation 5.18. Figure 5.10 illustrates the heat flux and temperature contours of the MicroPCMs and Acrylic binder models from post-processing calculations.

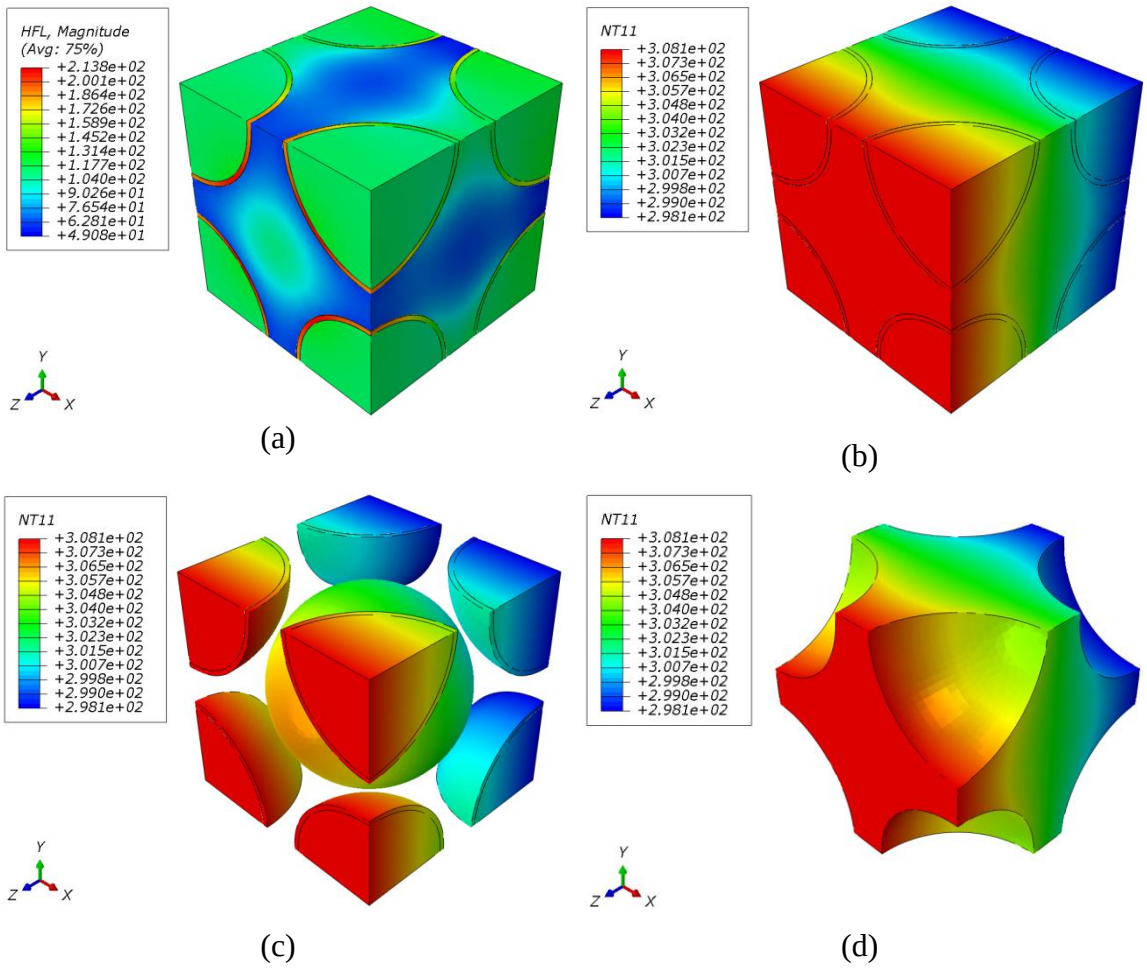

Figure 5.10: Contour plot of MicroPCMs and Binder: (a), (b) Heat flux and temperature contour of unit cell of MicroPCMs and Binder respectively; (c) Temperature contour of MicroPCMs only; and (d) Temperature contour of Binder only

5.3.2.2 Effective Thermal Conductivity of Coated Fabric

The effective thermal conductivity of MicroPCMs and binder is obtained from the unit cell of MicroPCMs and binder which has been used in Nomex® III, cotton and wool MicroPCMs coated fabrics. The effective thermal conductivities value is used as input material property for the coating section as shown in Figure 4.18 (b) (Chapter 4). The thermal conductivity of air 0.026 W/m.K was used as input material property for air

fluid matrix section. A unit cell of MicroPCMs coated composite fabrics were meshed by 4-node linear tetrahedral elements (DC3D4) with the optimum element size so that further refinement will not affect the results. In order to determine the effective thermal conductivity of MicroPCMs coated composite fabric across the transverse direction, temperature specified boundary condition was taken for heat flow. For that purpose temperature gradient was applied at the face and back side of the unit cell, assuming the remaining surfaces are insulated. Figure 5.11 shows the temperature distribution of Nomex® III fabric with MicroPCMs and air fluid matrix. It can be found that temperature decreases evenly along the thickness direction of the unit cell. The inner surface of the fabric has the highest temperature, while the outer surface has the lowest temperature.

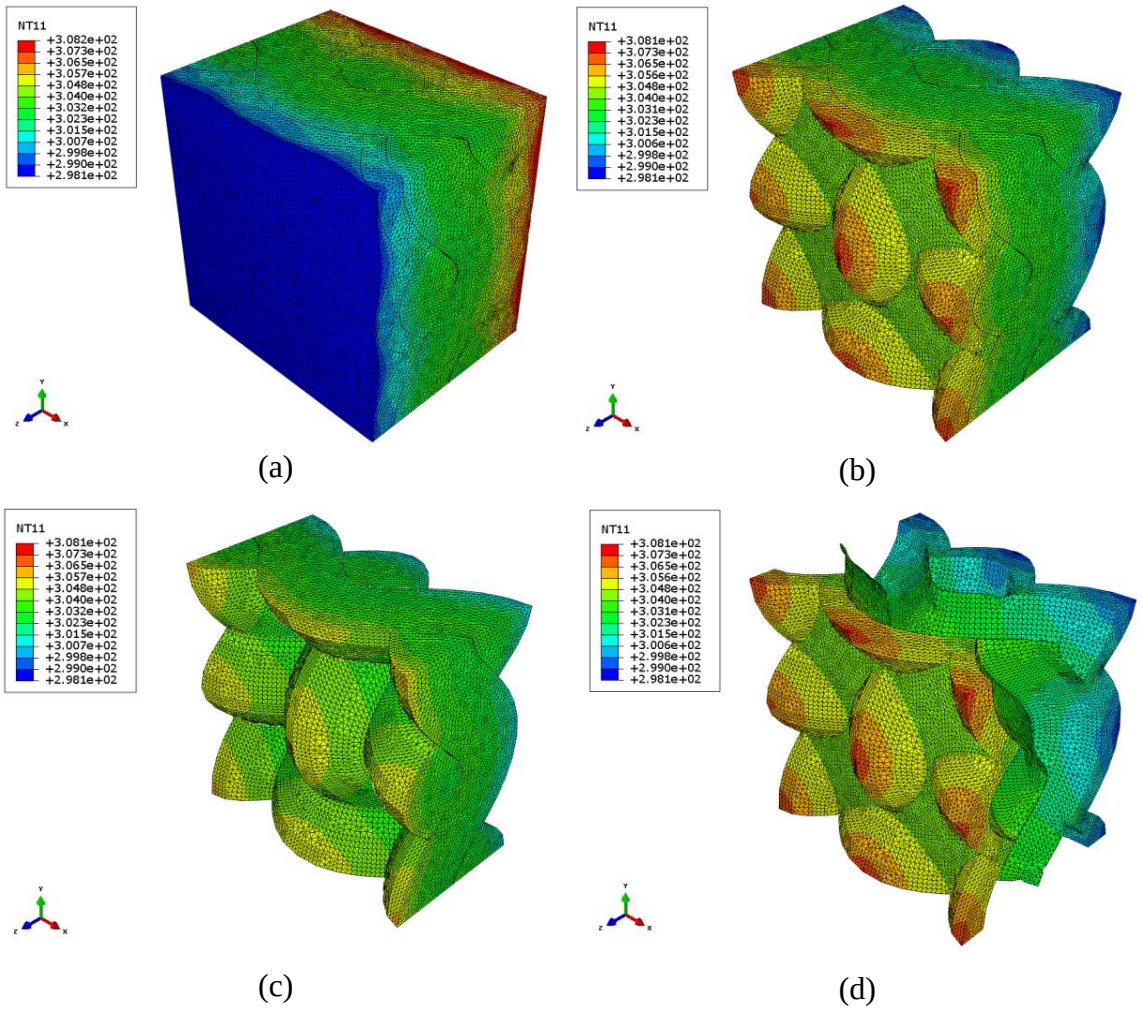

Figure 5.11: Temperature contour of MicroPCMs coated Nomex® III composite fabric

Figure 5.12 shows the heat flux distribution of MicroPCMs coated Nomex® III, cotton and wool composite fabrics. It clearly shows that the heat flux distribution on the surface of fabric is lower as compared to the yarn and MicroPCMs coating due to the

presence of air. In fact yarn and MicroPCMs coating help as main conducting portion in the fabric. The effective thermal conductivity across the thickness of unit cell can be determined by the Equation 5.18. Table 5.9 shows the thermal conductivity from FE model predicted results of MicroPCMs coated composite fabric.

Table 5.9: Effective thermal conductivity values obtained from FEM

Fabrics	Predicted effective thermal conductivity of MicroPCMs coated composite fabric K_{eff} (W/m.K)
Nomex® III	0.085
Cotton	0.081
Wool	0.077

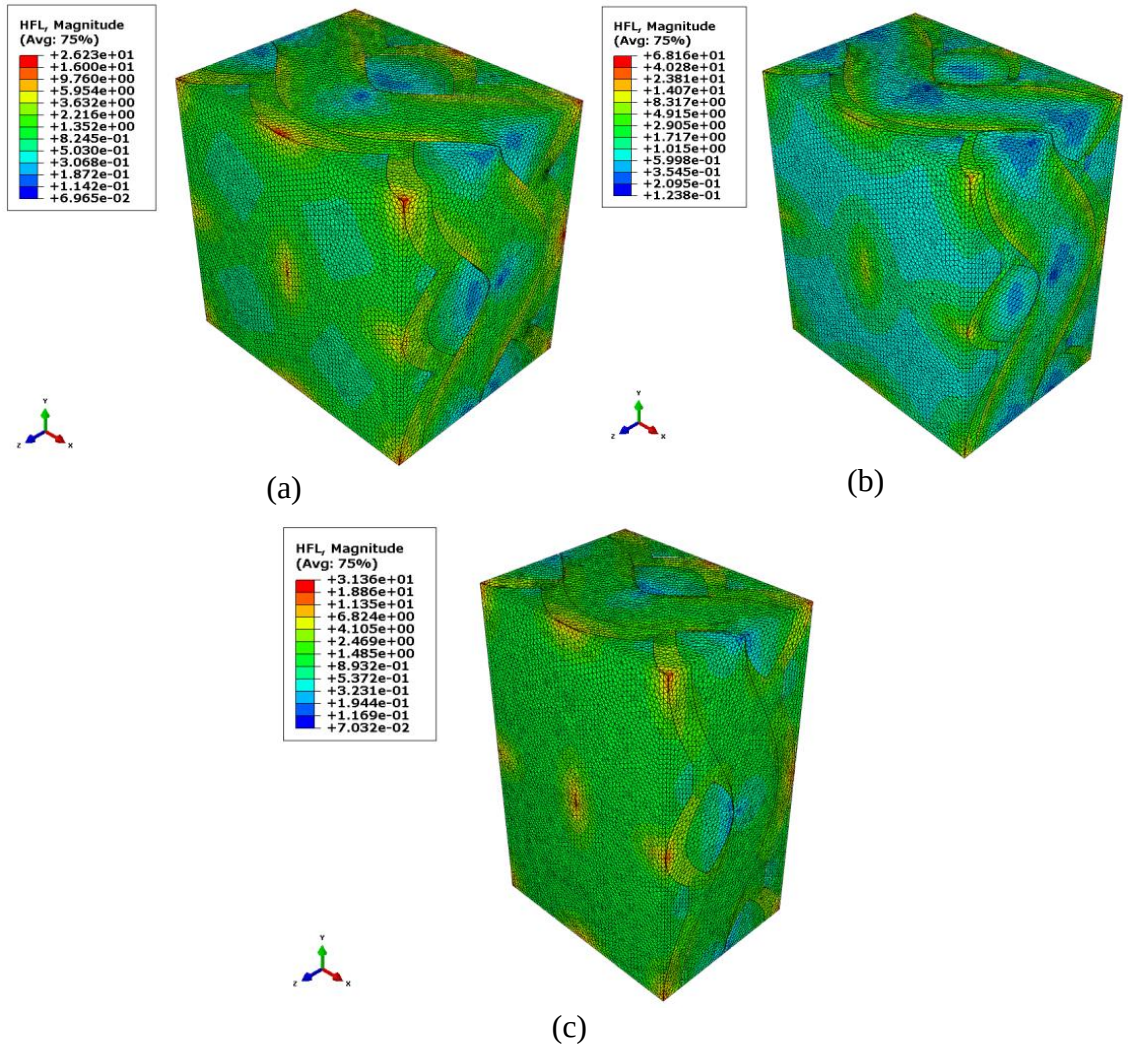

Figure 5.12: Heat flux contour of MicroPCMs coated composite fabric: (a) MicroPCMs coated Nomex® III composite fabric; (b) MicroPCMs coated cotton composite Fabric; and (c) MicroPCMs coated wool composite fabric

5.3.3 Effective Thermal Conductivity of Knitted Fabric

The model of plain weft knitted fabric developed has been used to predict the thermal conductivity by using the following two approaches:

i) Conduction heat transfer only
ii) Conjugate heat transfer by using co-simulation application of Abaqus/CAE

5.3.3.1 Conduction Heat Transfer Only

Figure 5.13 shows the unit cell model used to analyse the thermal conductivity of plain weft knitted fabric by considering the conduction heat flow only.

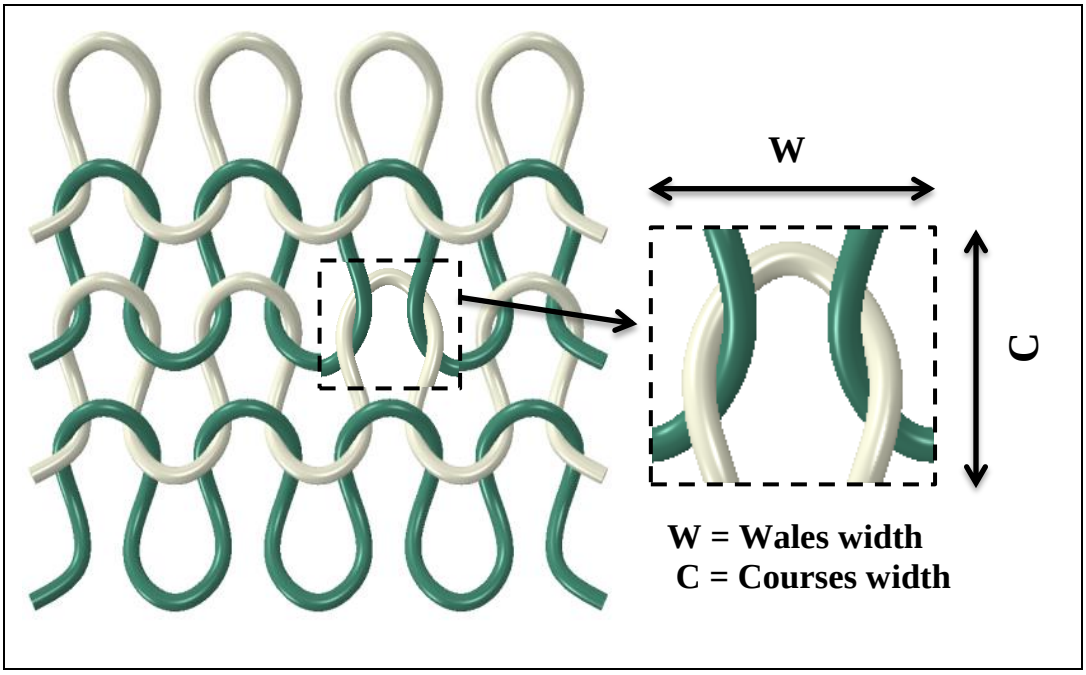

Figure 5.13. Unit cell model of fabric F3

5.3.3.1.1 Boundary Condition and Analysis

Figure 5.14 shows the unit cell model for the analysis with taking into consideration the following assumptions:

i) Consider air as fluid matrix;
ii) Neglect the effect of radiation and convection; and
iii) There is no compression of fabric between the plates.

The material properties assigned to the unit cell of plain weft knitted fabric as mentioned in Table 5.4 were taken by $K_{11} = K_{ya}$ and $K_{22} = K_{33} = K_{yt}$ (transversely isotropic). The thermal conductivity of air 0.026 W/m.k was used. The model was meshed by using 4-node linear tetrahedral elements (DC3D4). For steady state heat transfer analysis temperature specified boundary conditions were used.

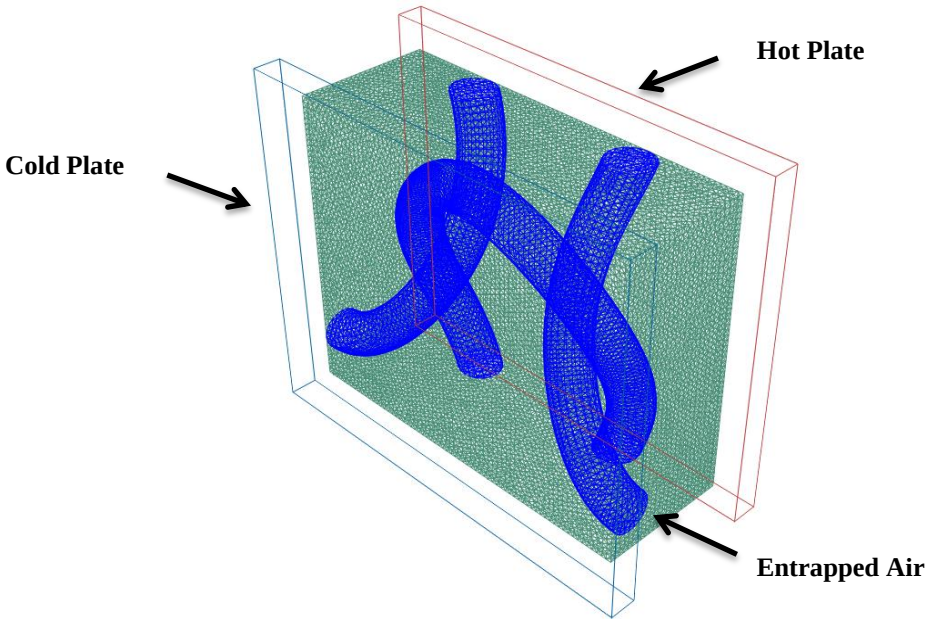

Figure 5.14. Unit cell model for analysis

Table 5.10 shows the effective thermal conductivity obtained from the simulation of plain weft knitted polyester fabric. Figure 5.15 shows the temperature and heat flux distribution of F3 fabric, due to high porosity of knitted fabric it evidently shows that majority of volume of unit cell has less heat flux due to the presence of high volume of air.

Table 5.10: Effective thermal conductivity and thermal reistance of plain weft knitted fabric from FEA

Fabric Code	Effective Thermal Conductivity (W/m.K)	Predicted Thermal Resistance (m^2.K/W)
F1	0.03152	0.015546
F2	0.03821	0.0123
F3	0.04230	0.011584
F4	0.04110	0.019465
F5	0.03845	0.016853

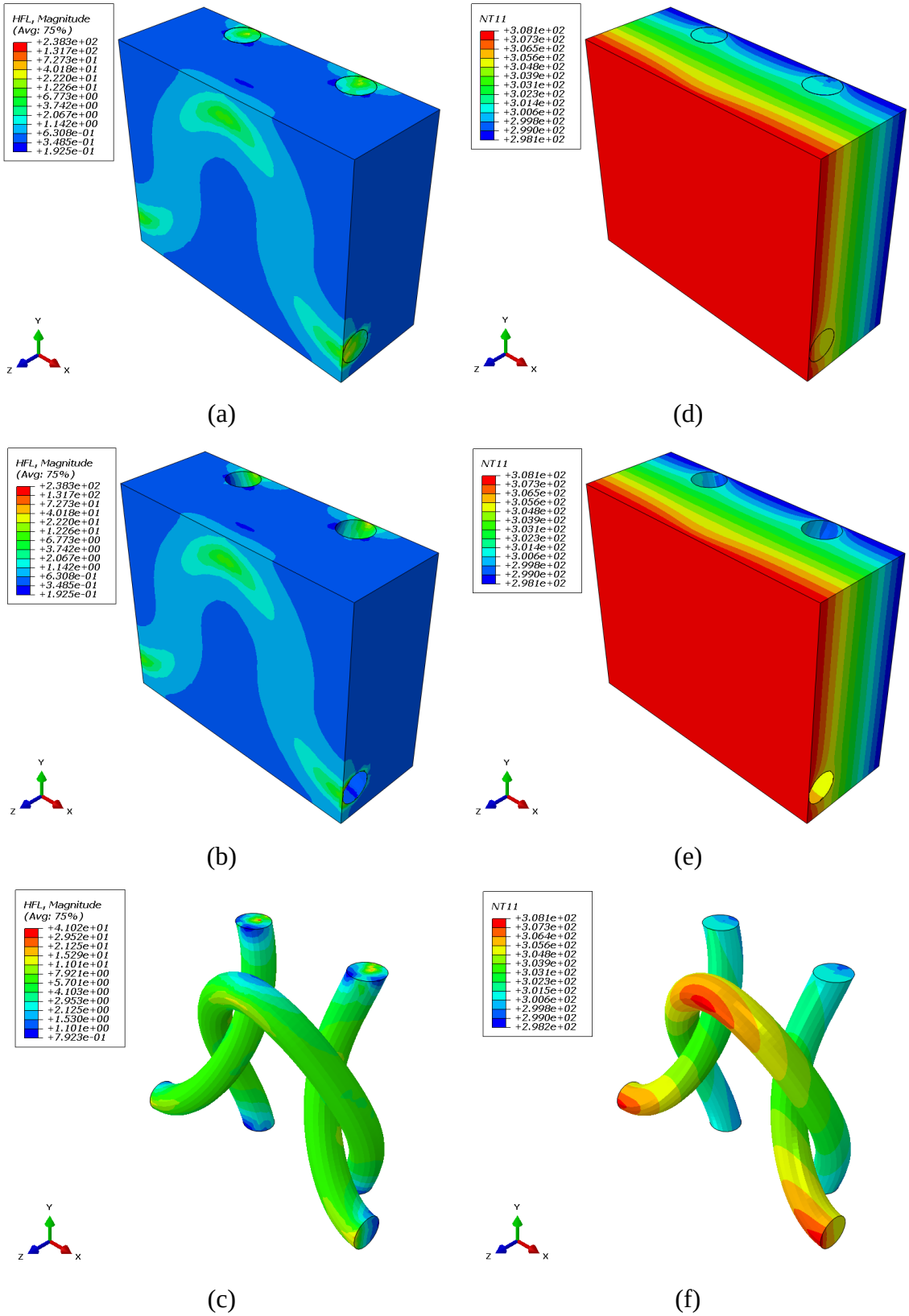

Figure 5.15. Contours: (a), (b) and (c): Heat flux contour of model-I unit cell fabric F3; (d), (e) and (f): Temperature contour model-I Unit cell fabric F3

5.3.3.2 Conjugate Heat Transfer by Using Co-Simulation

In this section conjugate heat transfer analysis of plain weft knitted fabric F3 developed will be analysed by using co-simulation technique in Abaqus/CAE. Conjugate heat transfer refers to the heat transfer between solid (mainly by conduction) and fluid (mainly by convection).

Figure 5.16 shows the experimental setup in which one side of plain weft knitted fabric was placed on a hot plate and the other side was exposed to ambient air which has temperature of 298.15 K. Heat was transferred from hot plate to the solid plain weft knitted fabric mainly by conduction modelled in Abaqus/Standard. The heat flow equation for time dependent heat transfer in solid is:

$$\rho C_p \frac{\partial T}{\partial t} = K\nabla^2 T + Q \qquad 5.21$$

Heat transfer from hot plate and plain weft knitted fabric to the ambient air by buoyancy driven natural convection using Boussinesq approximation and modelled in Abaqus/CFD. The governing equations for fluid flow in CFD are as follows:

$$\rho\frac{\partial \mathrm{V}}{\partial t} + \rho\nabla.\mathrm{V} = 0 \qquad \text{(Continuity equation)} \qquad 5.22$$

$$\nabla.\mathrm{V} = 0 \qquad \text{(Incompressible flows)} \qquad 5.23$$

$$\rho\frac{\partial \mathrm{V}}{\partial t} + \rho\nabla.\mathrm{V} = -\nabla p + \mu\nabla^2\mathrm{V} + \rho g \qquad \text{(Conservation of momentum)} \qquad 5.24$$

(Incompressible Navier-Stokes equation)

$$\rho C_p \frac{\partial T}{\partial t} - K\nabla T = \rho C_p \mathrm{V}.\nabla T \qquad \text{(Conservation of energy)} \qquad 5.25$$

where ρ is the density of fluid, C_p is specific heat of fluid at constant pressure, V is the velocity of fluid, μ is the dynamic viscosity of fluid and ρg is the body force.

In buoyancy driven natural convection heat flow, the density change is caused by temperature and the property of fluid that represent. The variation of density with temperature change is known as volumetric thermal expansion coefficient and it can be expressed by:

$$\beta = -\frac{1}{\rho}\left(\frac{\partial \rho}{\partial T}\right)_p \qquad 5.26$$

Boussinesq approximation is defined as: the density variation is too small in fluid except when evaluating the momentum equation where density multiplied with gravitational acceleration (bouncy force) as shown in Equation 5.27.

$$(\rho - \rho_o)g \approx -\rho_o \beta (T - T_o)g \quad \text{(at constant Pressure)} \qquad 5.27$$

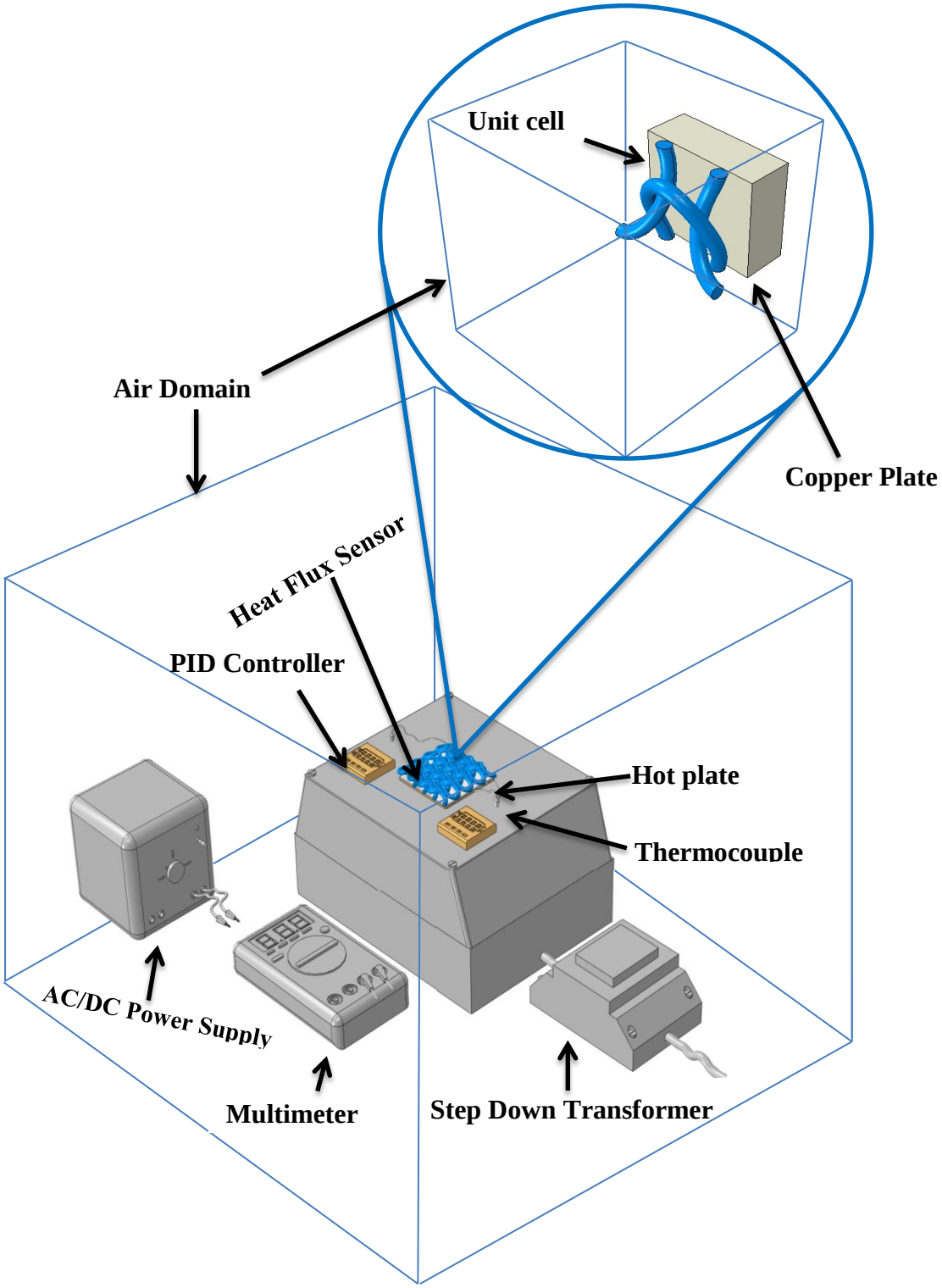

Figure 5.16: Experimental setup for conjugate heat transfer

5.3.3.2.1 Simulation

The enlarged view of Figure 5.16 shows that the unit cell of plain weft knitted fabric with copper plate and air domain was used to analyse the conjugate heat transfer in Abaqus. The copper plate and plain weft knitted fabric was analysed in Abaqus/Standard for transient heat transfer analysis. Table 5.11 shows the material properties of copper and polyester which used for transient heat transfer analysis but all the values will be converted in to CGS unit.

Table 5.11: Thermo-physical property of polyester and copper

Property	Polyester	Copper
Density (Kg/m^3)	1390	8940
Specific heat (J/kg.K)	1030	390
Thermal conductivity (W/m.K)	1.260 (K_{fa}) 0.157(K_{ft})	401
Thermal expansion coefficient (1/K)	20×10^{-6}	16.6×10^{-6}

Figure 5.17 shows a small scaled model of air domain in which plain weft knitted fabric and copper plate has been lessened from the domain and it was analysed in Abaqus/CFD by using the buoyancy driven natural convection (free convection). Table 5.12 shows the property of air which used as input parameter in analysis.

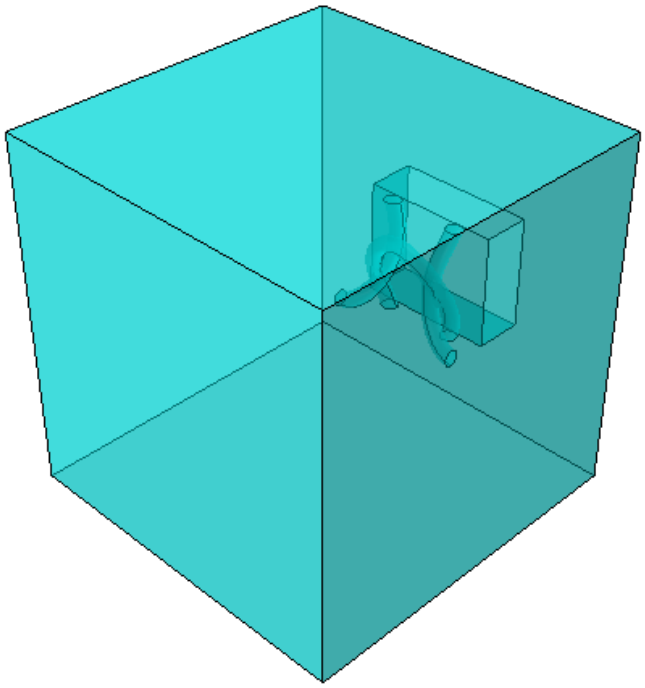

Figure 5.17: Scaled down of air domain model

Table 5.12: Thermo-physical property of air

Property	Air
Density (Kg/m^3)	1.17032
Specific heat (J/kg.K)	1006.96
Thermal conductivity (W/m.K)	0.02614
Viscosity (Kg/m/sec)	1.836×10^{-5}
Thermal expansion coefficient (1/K)	3.337×10^{-3}

5.3.3.2.2 Initial Condition

The initial thermal condition was applied to the plain weft knitted fabric, copper plate and air with a temperature of 298.15 K and considering the initial velocity of air is zero.

5.3.3.2.3 Boundary Condition, Loading and Interactions

No slip condition for interface and air domain wall was considered as shown in Figure 5.18. Acceleration due to gravity was applied as load and pressure at the front surface was set as zero. No boundary conditions have been added to other surfaces in order to allow the air to flow in these directions. Fixed temperature was applied to the copper plate which is connected to the plain weft knitted fabric unit cell allowing the heat flow from hot plate to the plain weft knitted fabric.

Thermal coupling between the solid structure (copper plate and weft knitted fabric) and fluid (air domain) was created in which the common highlighted surface was used as shown in Figure 5.18. Heat will be transferred from solid structure to air domain by buoyancy driven natural convection through the interface.

5.3.3.2.4 Meshes

Solid structure was meshed by using 4-node linear tetrahedral elements (DC3D4) for the transient analysis in Abaqus/Standard. Air domain was meshed by using linear hexahedral (FC3D8) fluid elements in Abaqus/CFD.

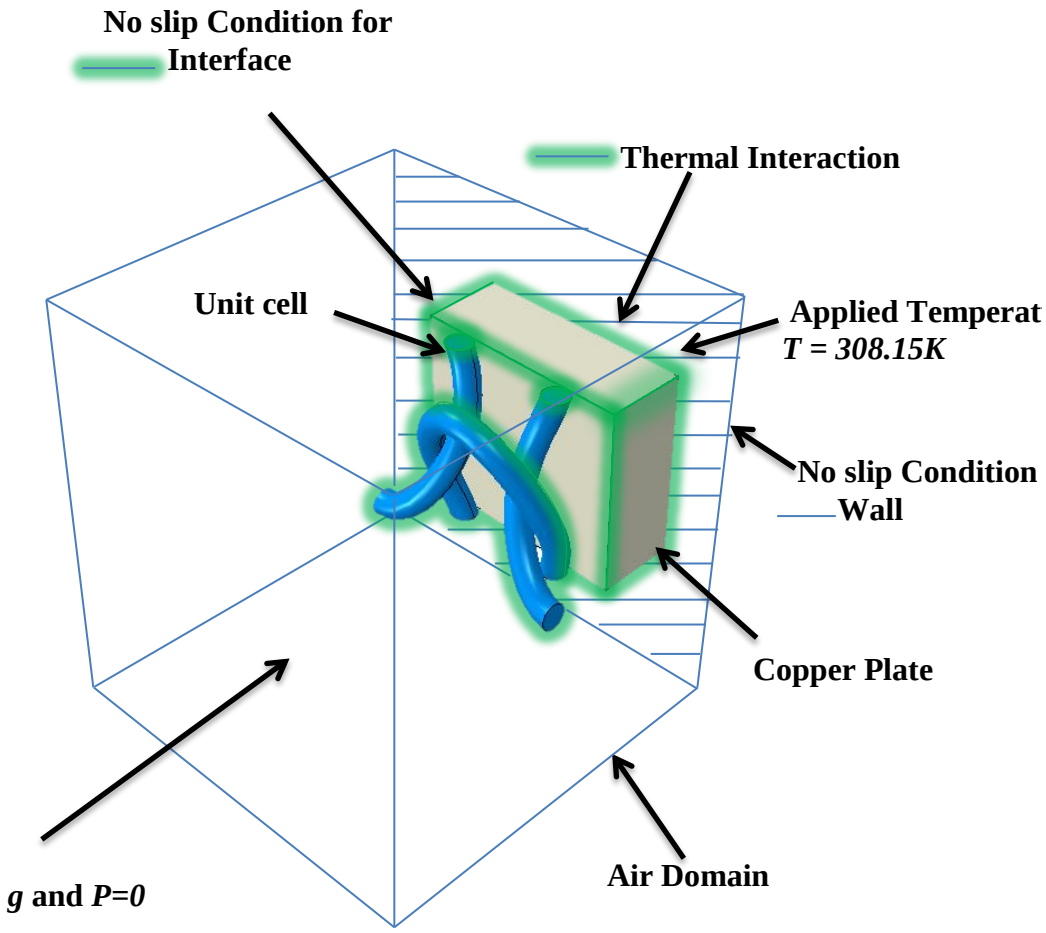

Figure 5.18: Simulation set-up

5.3.3.2.5 Modelling Results

Figure 5.19 shows the conjugate heat transfer in Abaqus through thermal coupling.

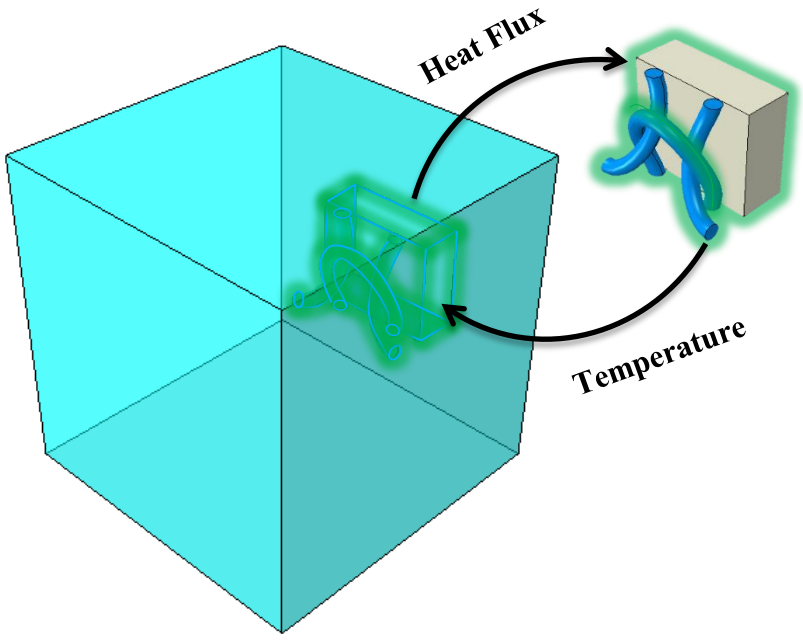

Figure 5.19: Abaqus co-simulation through thermal coupling

Solid structure in Abaqus/Standard exports temperature to fluid domain in Abaqus/CFD and fluid domain exports heat flux to solid structure. When plain weft knitted fabric dissipates heat in the air the air layer which closes to the hot plate and fabric is heated up. The density of the air decreases, as a result, the lighter air moves up and the denser layer moves down, therefore convection current is developed. Figure 5.20 shows the heat flux and temperature contour of plain weft knitted fabric.

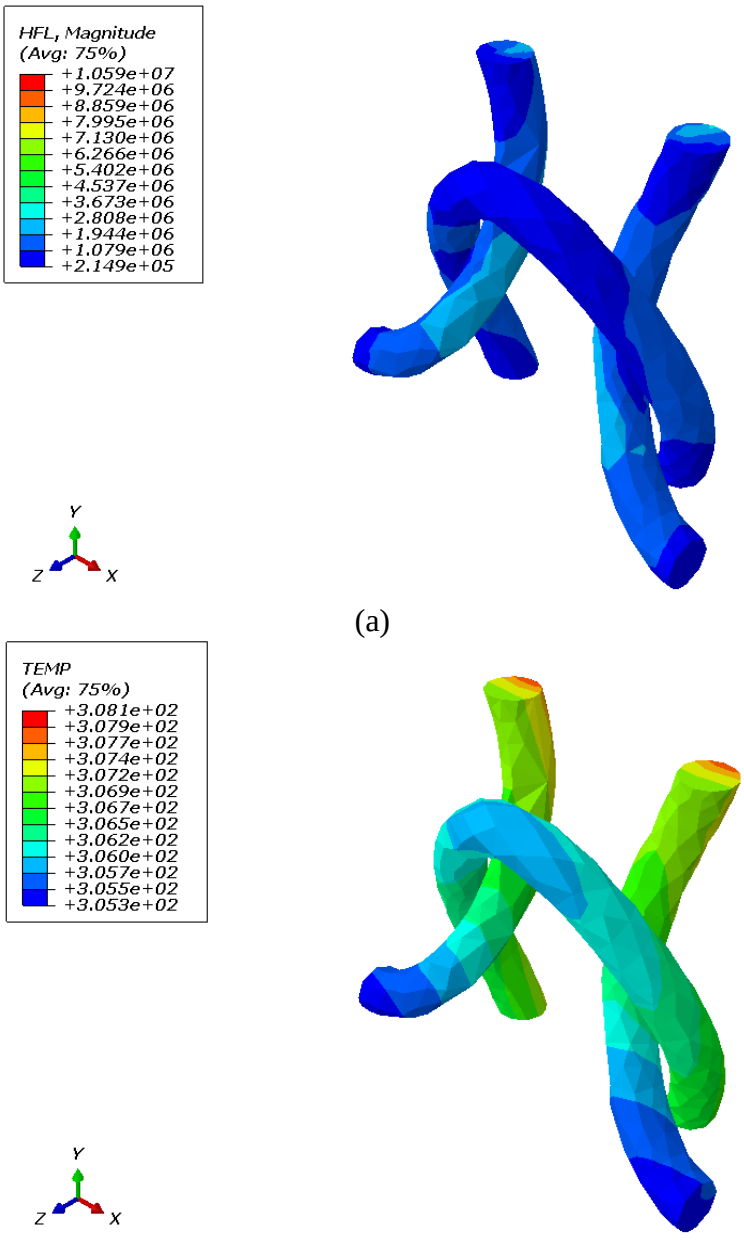

Figure 5.20: Contours (a): Heat flux and (b): Temperature contour of plain weft knitted fabric F3 unit cell

Figure 5.21 shows the temperature contour of half cut view in x-direction of air domain. The enlarge view clearly shows that the temperature is transferred from plain weft knitted fabric and copper plate to air domain through the thermal coupling interface.

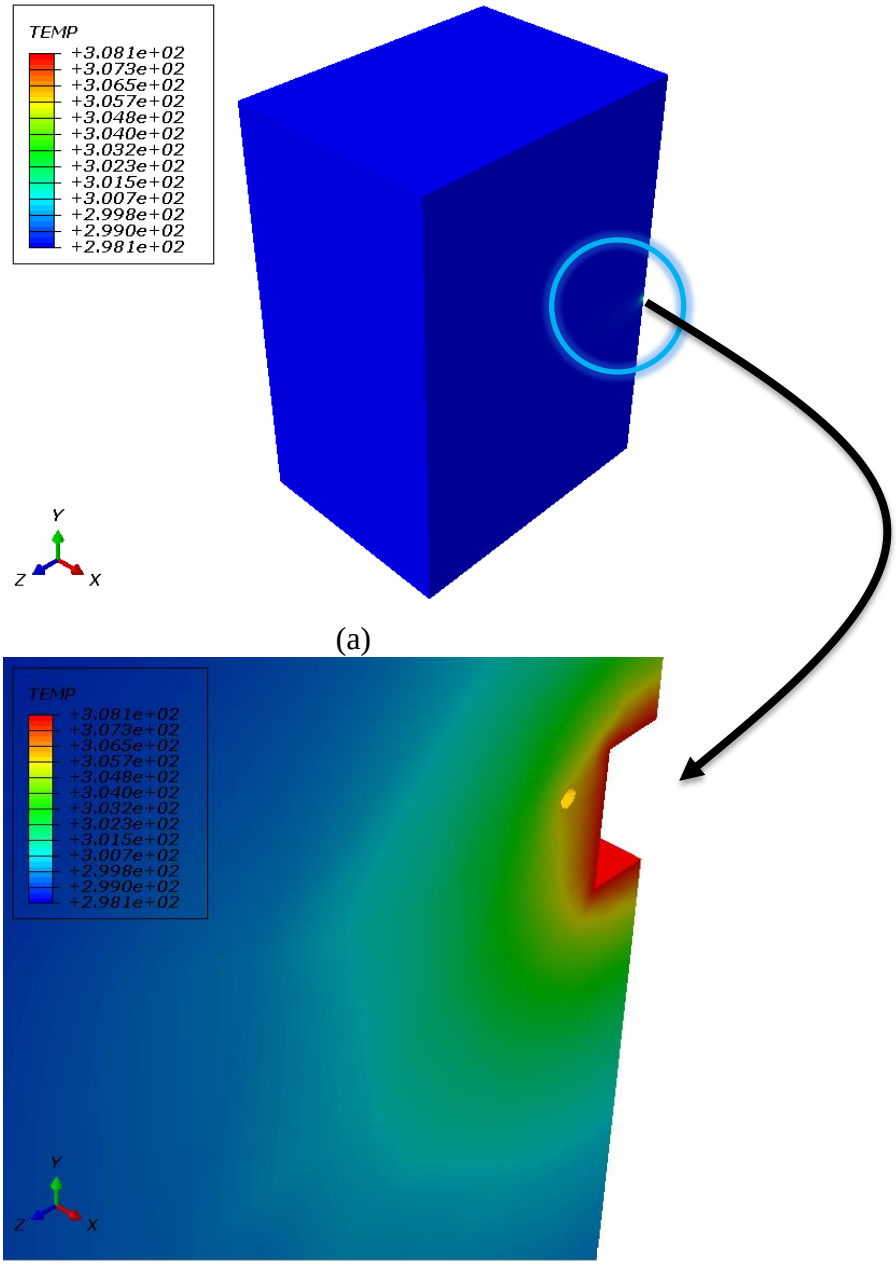

Figure 5.21: Temperature contours: (a) Air domain (half cut view in x-direction) and (b) Enlarge view off highlighted portion

Figure 5.22 shows the velocity contour and velocity vector plot of air domain and Figure 5.23 shows the phenomena of convection current.

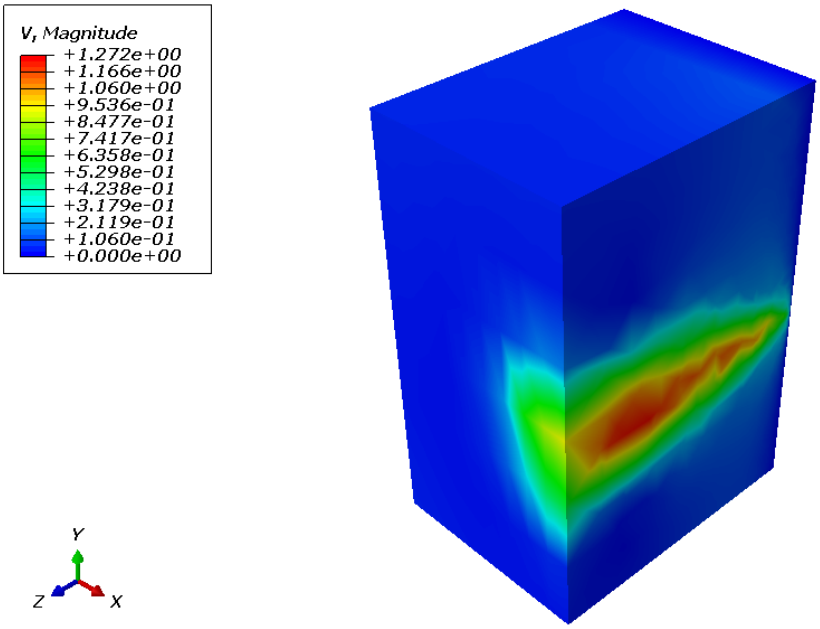

(a)

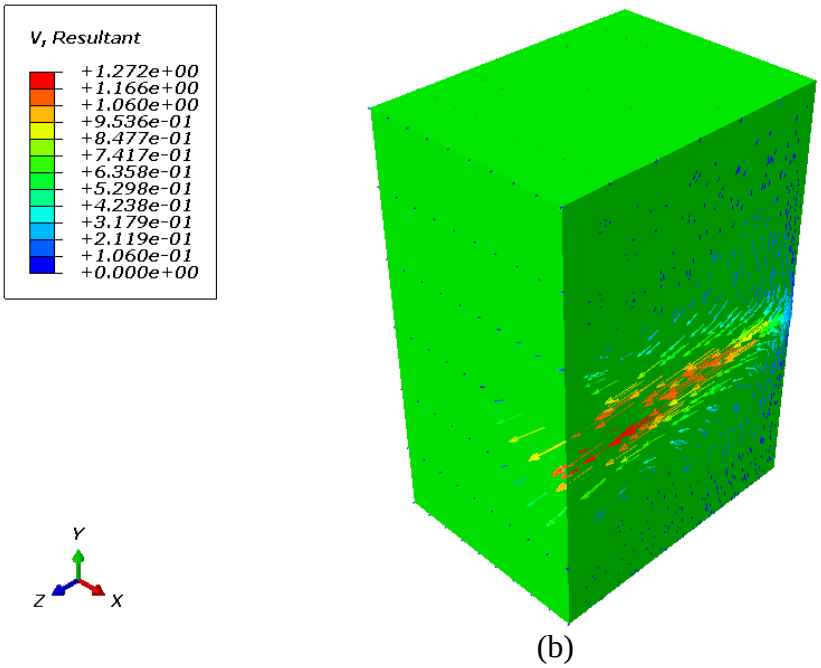

(b)

Figure 5.22: Velocity **c**ontours: (a) Air domain (half cut view in x-direction) and (b) Air domain (half cut view in x-direction)

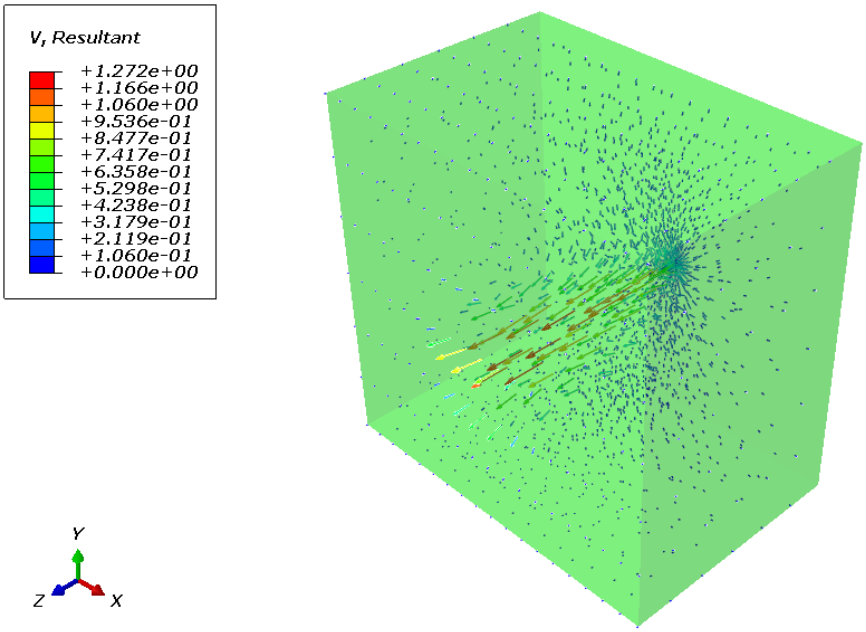

(a)

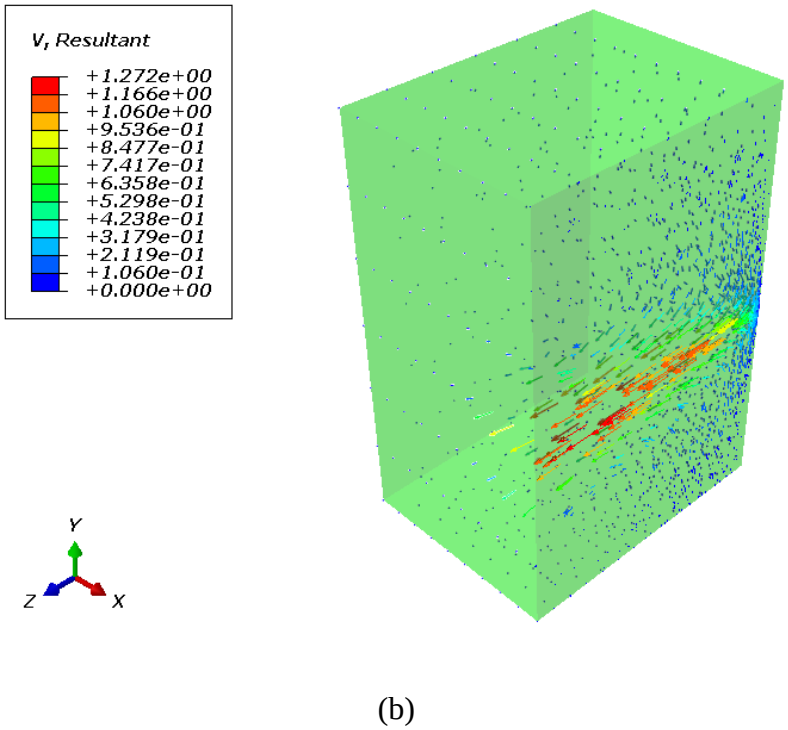

(b)

Figure 5.23: Velocity vector plot: (a) Air domain and (b) Air domain (half cut view in x-direction)

Effective thermal conductivity of plain weft knitted fabric F3 was calculated at steady state, for that purpose out-plane was created over the surface of knitted fabric to monitor the temperature and velocity. Figure 5.24 shows the temperature and velocity reaches the steady state. Heat flux value was evaluated on the surface of copper plate and effective thermal conductivity which can be calculated by Equation 5.18.

The effective thermal conductivity of plain weft knitted fabric predicted from the hybrid finite element and finite volume method is 0.04971 W/m.K.

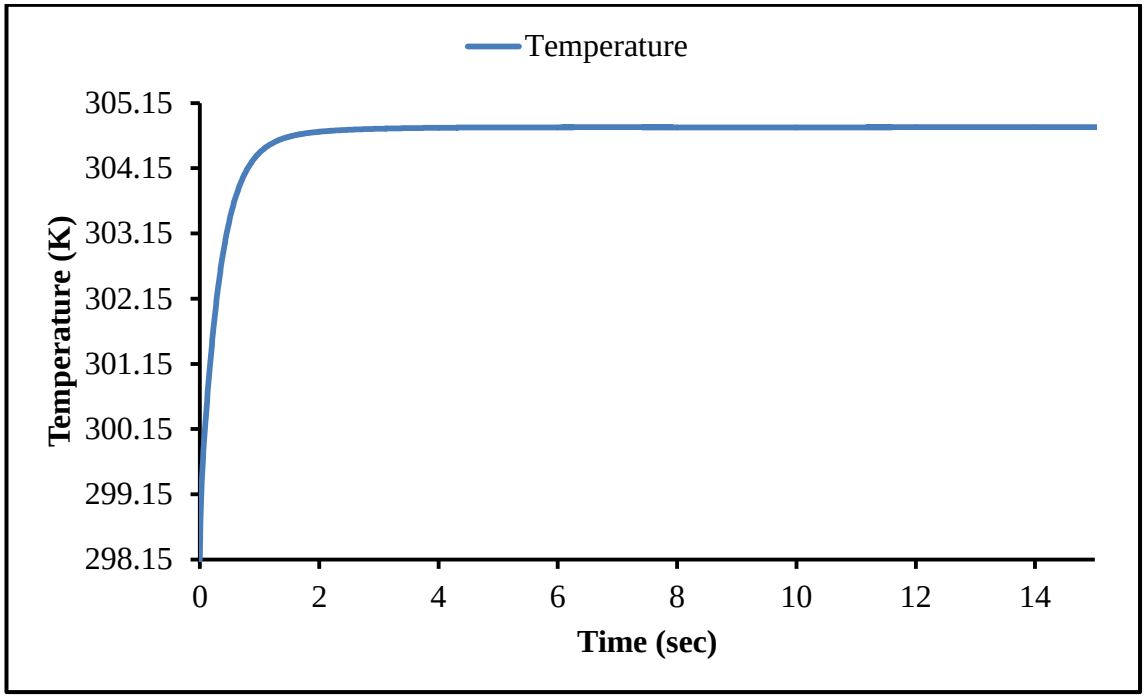

(a)

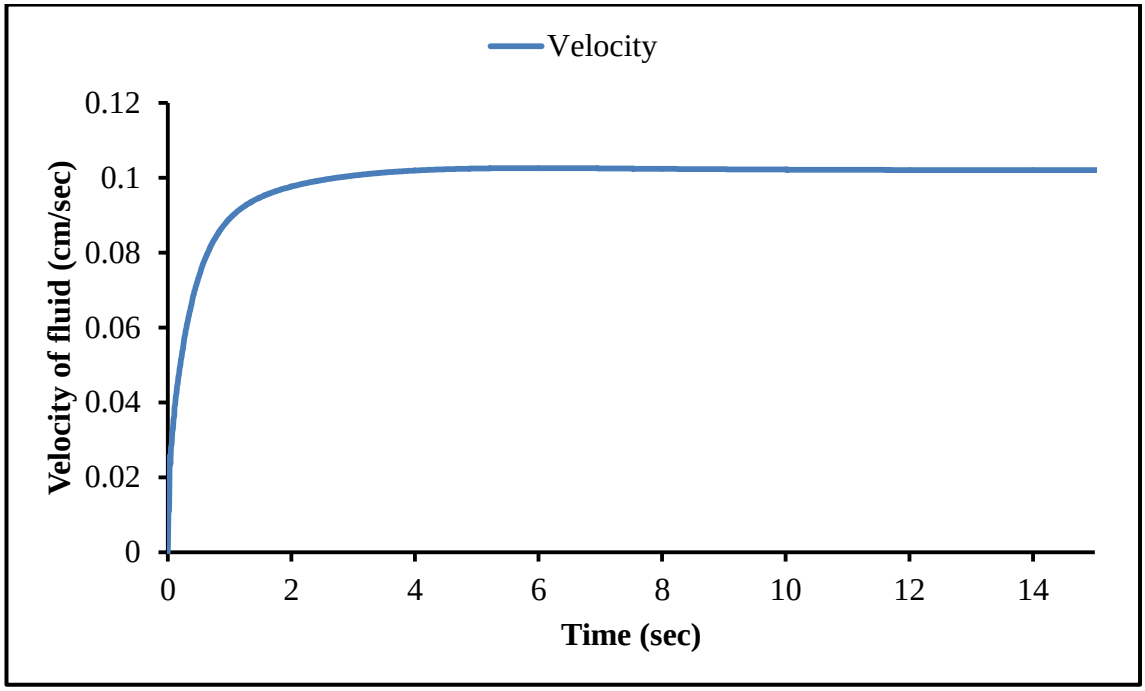

(b)

Figure 5.24: Relationship between time and (a) Average temperature at out-plane and (b) Average velocity of fluid at out-plane

5.3.4 Effective Thermal Conductivity of Thermally Bonded Nonwoven Fabric

Effective thermal conductivity of thermally bonded nonwoven fabric was determined with consideration of the following assumptions:

1) there is no compression in nonwoven fabric when it is placed between the two plates during thermal conductivity testing; and
2) entrapped air between the two plates and within in the fibrous portion of the nonwoven fabrics is considered as fluid matrix, shown in Figure 5.25.

3D reconstructed and solid model with air fluid is shown in Figure 5.26. Thermal conductivity value of fibrous portion (K_{fp}) in solid nonwoven fabric model was calculated by equation:

$$K_{fp} = \frac{K_{ft} K_{air}}{V_{fp} K_{air} + (1 - V_{fp}) K_{ft}} \qquad 5.28$$

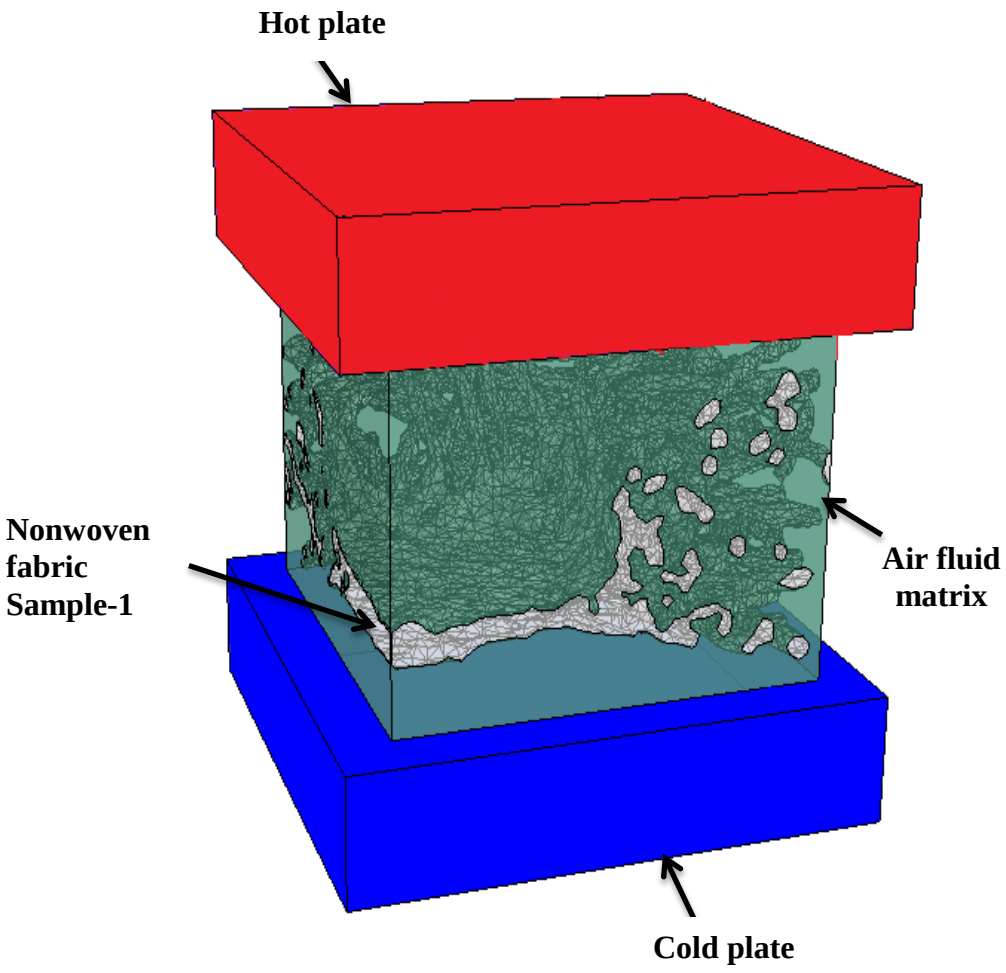

Figure 5.25: Experimental and simulation setup

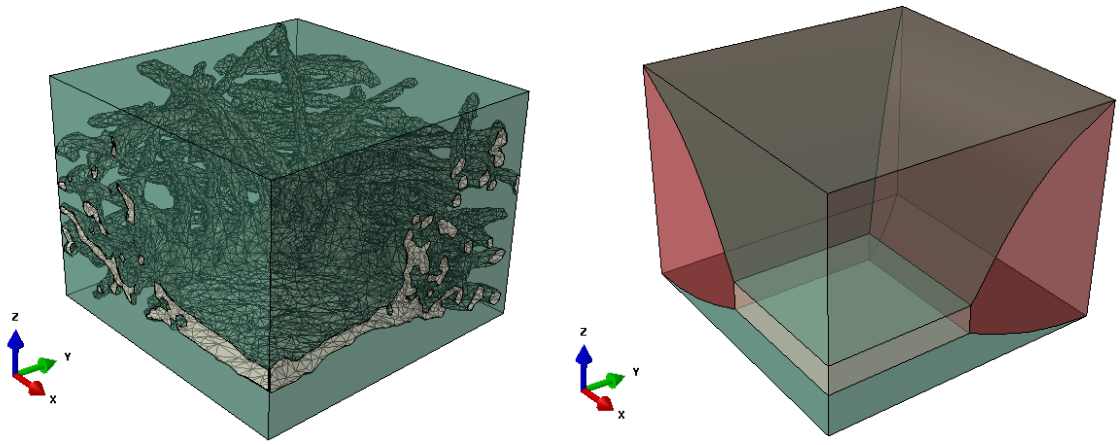

(a) (b)

Figure 5.26: Unit cell model of sample-1 with air fluid matric: (a) 3D reconstructed model and (b) Solid model

Table 5.6 shows the fibre volume fraction of thermally bonded nonwoven fabric. The thermal conductivity of their fibrous portion will be used as input material property in Abaqus/CAE. Only transverse thermal conductivity of fibre was considered because it is very difficult to assign the material orientation to provide anisotropic values of thermal conductivity. Sample-1 was 3D reconstructed and all solid models were meshed by 4-node linear tetrahedral elements (DC3D4). The unit cell was analysed by temperature specified boundary conditions and the effective thermal conductivity was calculated by the Equation 5.18.

Table 5.13 shows the predicted effective thermal conductivity and thermal resistance by FE analysis. Figure 5.27 and 6.16-18 show the heat flux and temperature contour of 3D reconstructed model and solid model respectively.

Figure 5.28 to Figure 5.30 show the heat flux contours of solid unit cell model of thermally bonded nonwoven fabrics. The fibrous portion has less thermal conductivity compared to the solid bond point, as a result, the heat flux profile changed in the contact points between the solid fibrous portion and bond points. This effect is especially significant for sample-1as it has thicker bond point compared to the other two samples.

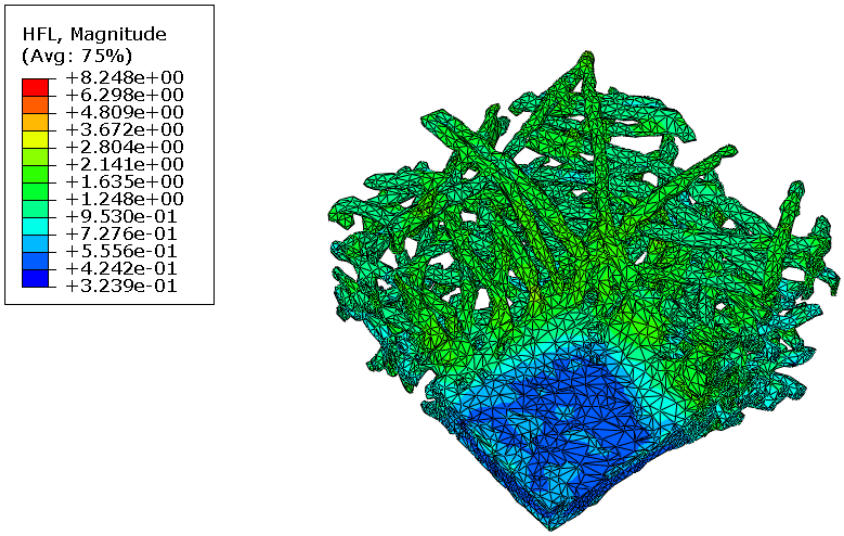

(a)

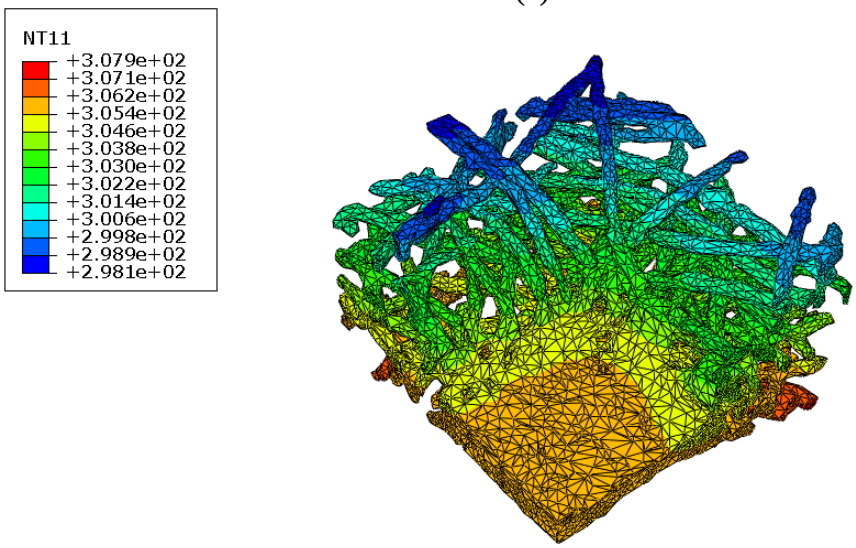

(b)

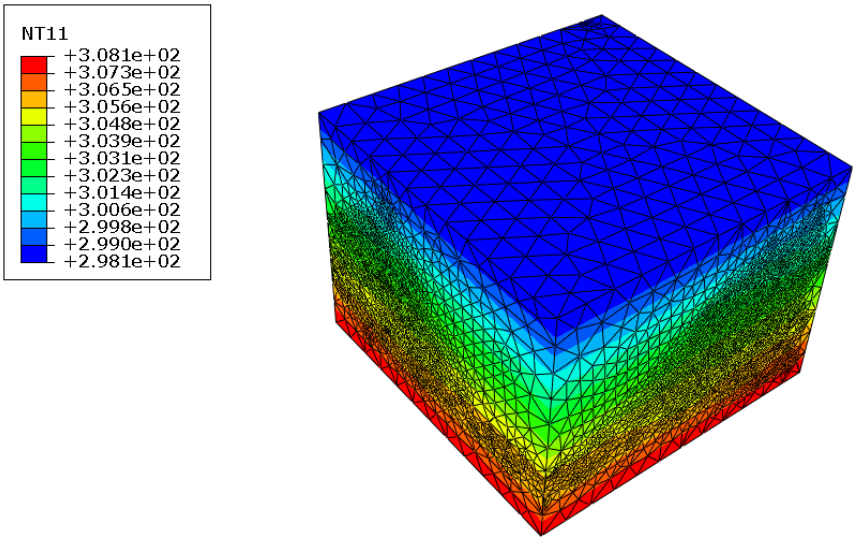

(c)

Figure 5.27: Contours of smaple-1: (a) Heat flux Contour; (b) Temperature contours; and (c) Temperature contours with air fluid matrix

Table 5.13: Predicted effective thermal conductivity and thermal resistance

Samples	Effective thermal conductivity (W/m.K)		Thermal Resistance (m^2.K/W)	
	3D reconstructed model	Solid model	3D reconstructed model	Solid model
Sample-1	0.03368	0.02981	0.01603	0.018115
Sample-2	-	0.02956	-	0.01184
Sample-3	-	0.02873	-	0.01984

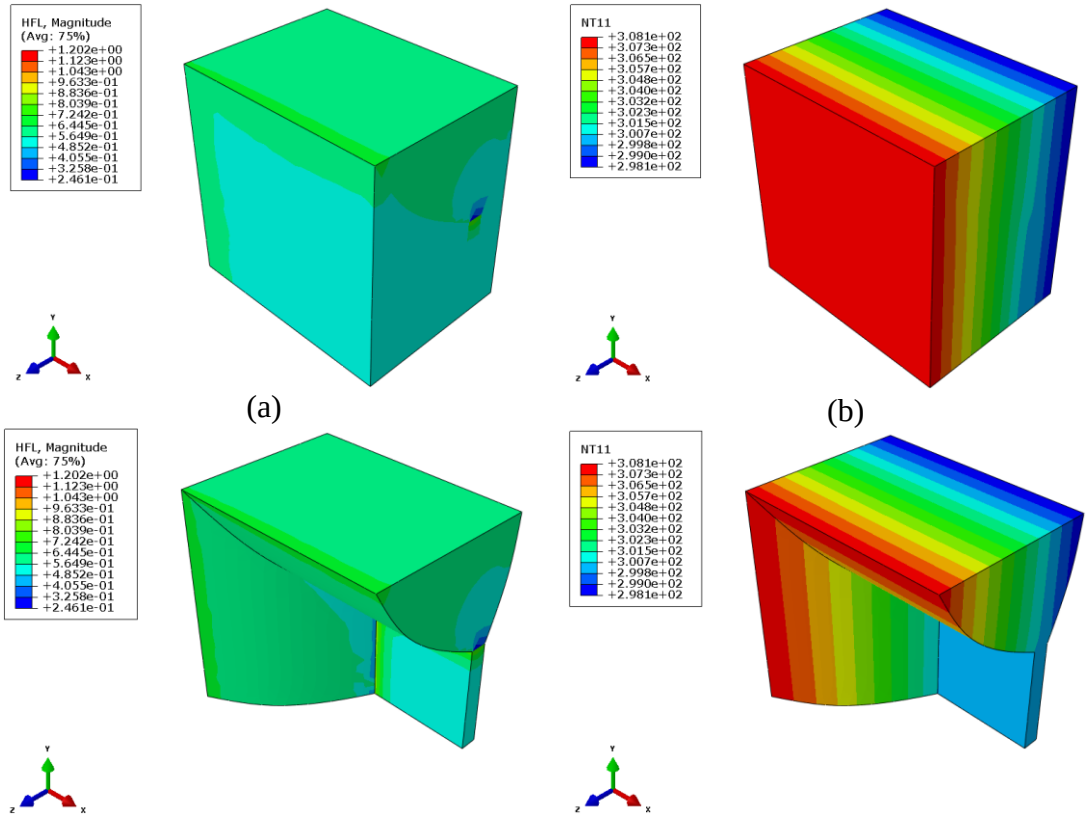

Figure 5.28: Heat flux and temperature contour of unit cell model of sample-1 (a & b) With air fluid matrix and (c & d) Without air fluid matrix

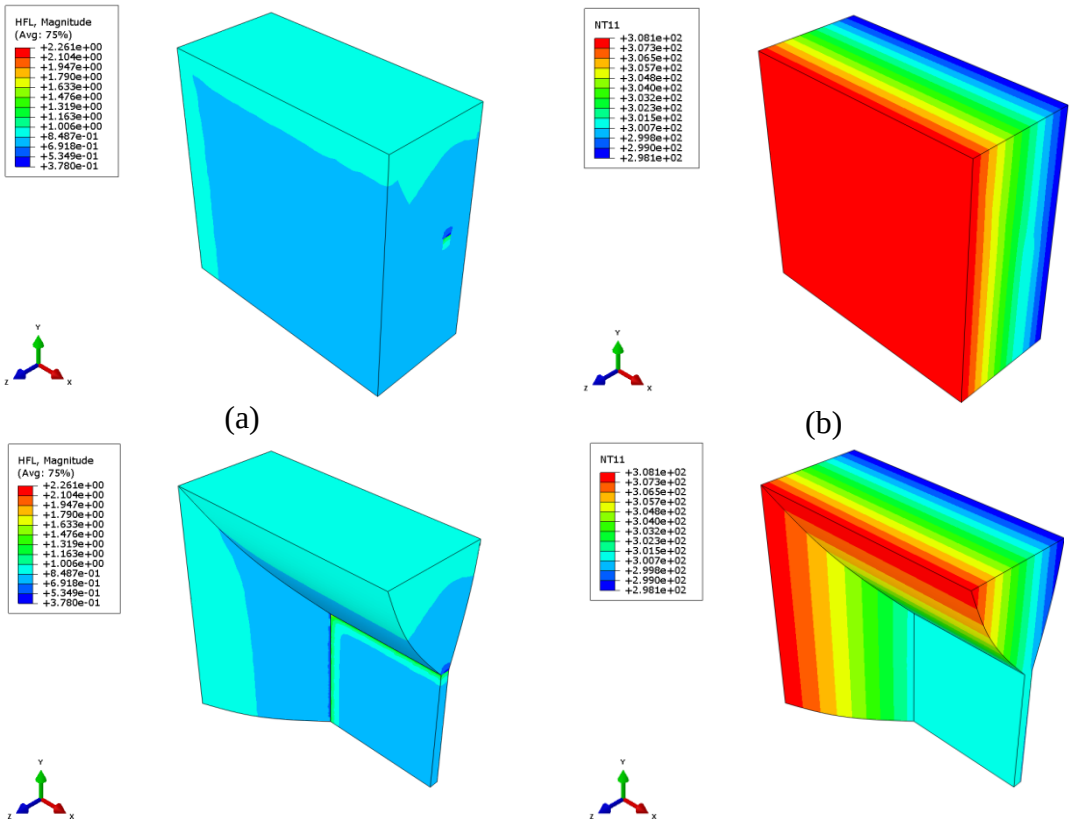

Figure 5.29: Heat flux and temperature contour of unit cell model of sample-2 (a & b) With air fluid matrix and (c & d) Without air fluid matrix

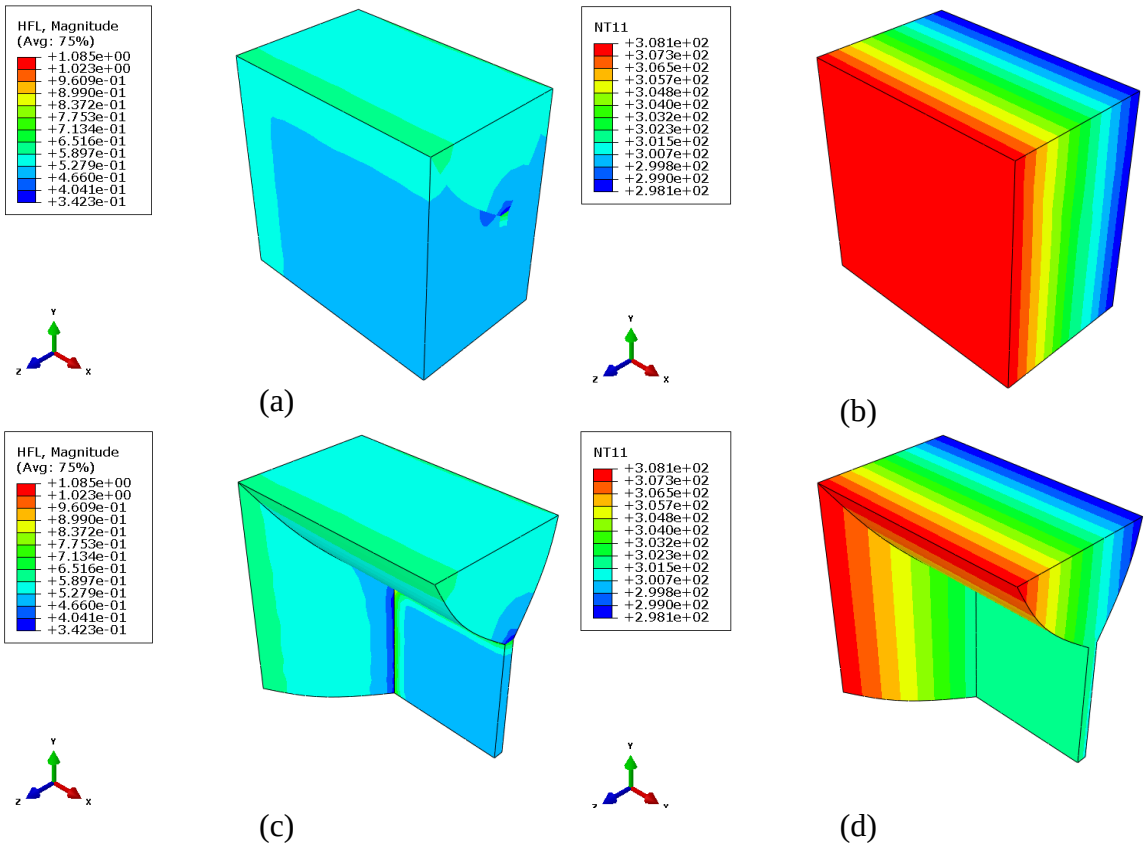

Figure 5.30: Heat flux and temperature contour of unit cell model of sample-3 (a & b) With air fluid matrix and (c & d) Without air fluid matrix

5.4 Summary

This Chapter presents the methodology to evaluate the effective thermal conductivity and thermal resistance of fabrics by using finite element method. One of the aims of this research is to investigate the effect of thermal anisotropy, temperature dependent thermal conductivity and fibre orientation on the effective thermal conductivity of textile structures. For this purpose the predicted results present in this chapter will be validated first by using the experimental results and then analysed the effect of above mentioned factor, this will be discussed in Chapter 7. In next Chapter the design aim, methodology and validation of GUI plug-ins will be presented.

Chapter 6 Design of Plug-ins

6.1 Introduction

One of the aims of this research is to develop user friendly GUI plug-ins. In this chapter the detailed information about how plug-ins were developed and worked in the Abaqus environment will be discussed. A plug-in is a customized software or program which can perform a single or multiple tasks and easily be installed and used as a part of already installed software. This chapter also contains the methodology and validation of models and results obtained from the plug-ins.

6.2 Motivation

More recently, different commercial and open source software packages have been developed for modelling the geometry of textile structures at the mesoscopic TexGen [105], TexEng [107], WiseTex [109] etc. These software packages provide the user friendly environment by using many libraries such as: VTK, wxWidgets, OpenCascade, Python etc. and programs such as: Cmake, SWIG, Visual studio C++ etc. The geometrical models generated from these software packages can be imported into different finite element analysis (FEA) software in required formats. However when these geometrical models are meshed in the finite analysis software it is difficult to mesh due to of the sharp edges in the cross sectional geometry of yarns. If yarn or fabric geometrical models are exported in meshed form to FEA software, meshes are distorted because of too many faces in the geometry. In order to avoid this issue there is necessary to generate geometry of textile structures by inputting yarn and fabric parameters in Abaqus environment, therefore there is need to develop GUI plug-ins incorporated into Abaqus/CAE, in the meantime, the plug-ins are able to automatically predict the effective thermal properties of MicroPCMs and plain weave composites. Furthermore the above mentioned software packages unable to generate any weft knitted geometrical models made of multifilament yarns and this is one more significance of this research work.

Research works have been carried out in different fields to develop the customized tools that used as plug-in in several commercial and open source software [160-166]. There

appears no research work dedicated to plug-ins that can be used to generate textile-based structures in Abaqus/CAE environment; the present study is exploratory in nature.

In this research work five plug-ins have been developed by using python script in Abaqus/CAE environment:

1) plug-in for plain weft knitted fabric;
2) plug-in for Multifilament Weft Knitted fabric;
3) plug-in for porosity of plain weft knitted fabric;
4) plug-in for plain weave composite fabric; and
5) plug-in for MicroPCMs composites.

6.3 Design Methodology of Plug-ins in Abaqus/CAE

Abaqus plug-ins execute Abaqus Scripting Interface and Abaqus Graphical User Interface (GUI) Toolkit commands. They provide ways to customize Abaqus/CAE for the specific needs or preferences. For example, a simple plug-in could automatically print the contents of the current viewport according to some predefined options. A more complex plug-in could provide a graphical user interface to a specialized post-processing routine that you have written [154].

In Abaqus two types of plug-in can be created: kernel and GUI. The kernel plug-in is composed of functions written using the Abaqus scripting interface and requires no GUI infrastructure. In GUI plug-in it will allow the user to input all the necessary data in user interfaces within the Abaqus/CAE environment. In this work a GUI plug-in was developed by using Abaqus GUI toolkit.

It is necessary to understand how the graphical interface of Abaqus works before going into the details of how GUI plug-in was developed and worked in Abaqus. When users start using the Abaqus graphical user interface Abaqus executes two processes, i.e. kernel and GUI process.

GUI process contains GUI command which displays the dialog box; for example, when users click a button a dialog box appears to allow entering the necessary information. When clicked ‘ok’ a kernel command string passes to kernel process containing the data and method which Abaqus uses to perform different operations such as: create part, cut operation, merge operation, meshing and so on.

The process will be continued if there is no error in the input information otherwise a message will be displayed in the form of error dialog box. GUI plug-in works in the same way as Abaqus module works. GUI plug-in comprises of four sets of scripts.

The first script contains form modes that are of the type of AFXForm enabling to launch the dialog box of type AFXDATADIALOG (which is the second script). AFXDATADIALOG collects input data by user and then a command is sent to the Kernel script (third script) from the form mode (AFXForm). The third script performs the operation in Abaqus.

The plug-in registration script (which is the fourth script) is to register the plug-in in the main plug-in menu as shown in Figure 6.1. GUI plug-in execution process is shown in Figure 6.2 .

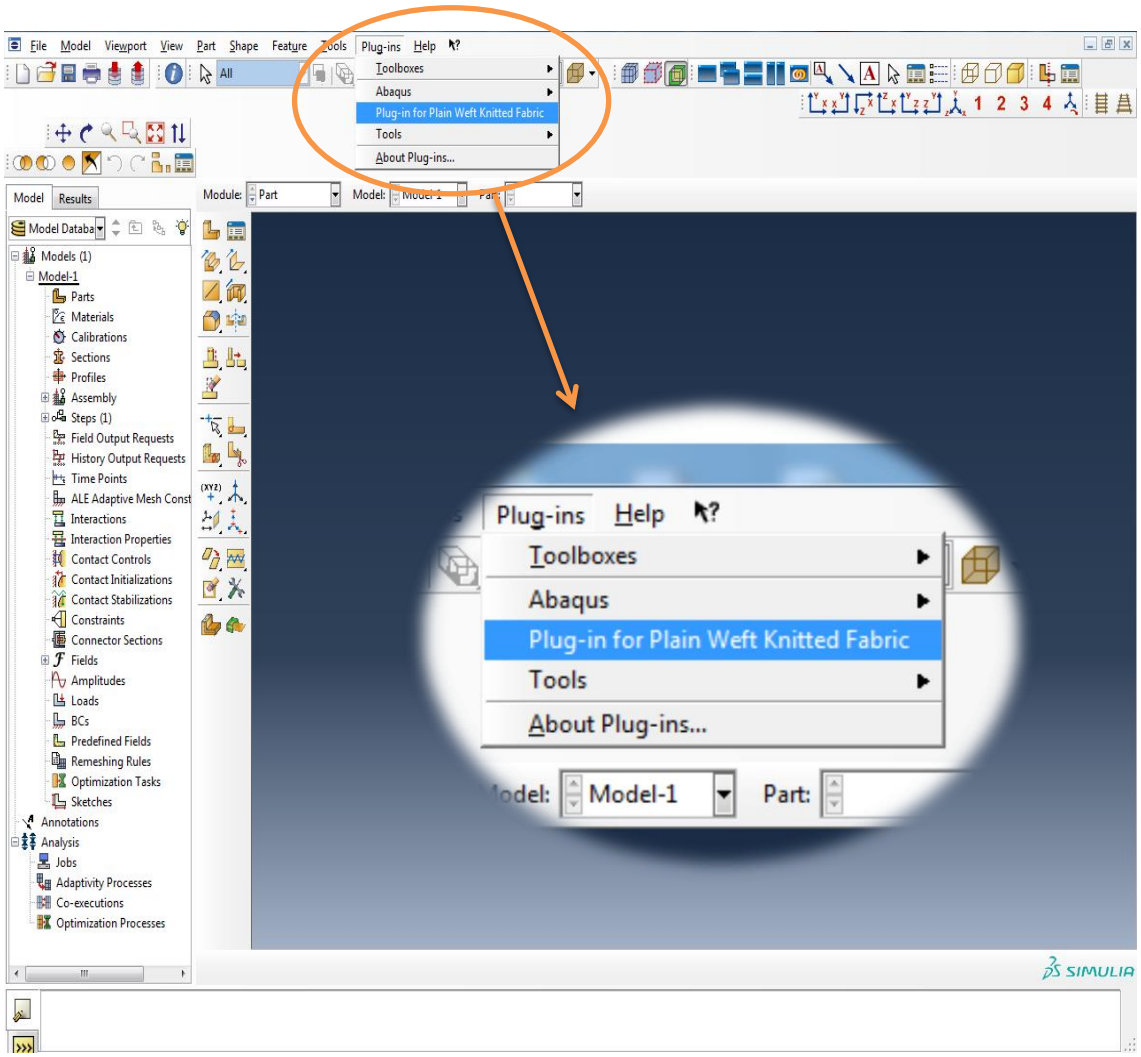

Figure 6.1: Registered plug-in in plug-in menu

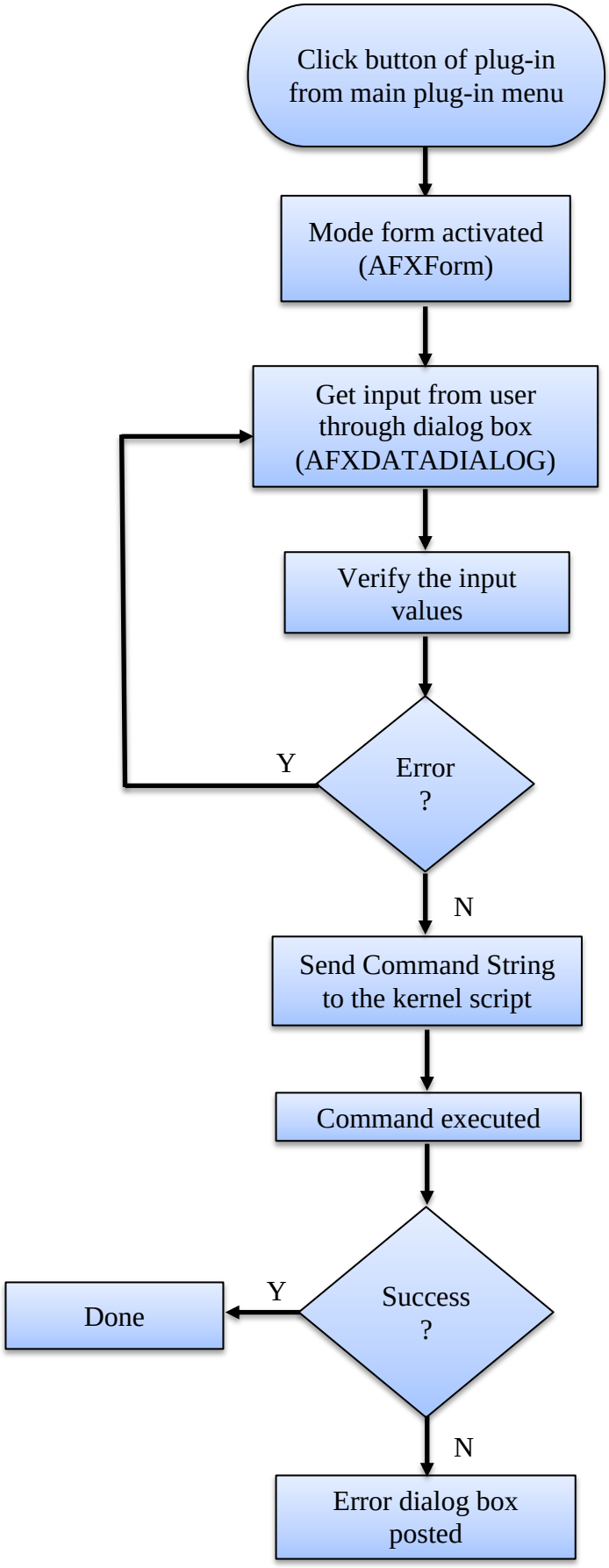

Figure 6.2: GUI plug-in processing sequence

6.3.1 Plug-in of Plain Weft Knitted Fabric

There are software packages available such as TexGen [105], TexEng [107], WiseTex [109] etc. which have been used to generate 3D geometric Models of plain weft knitted fabric geometries. However they can only generate weft knitted structures in their own environment, and the generated geometric models have to be imported into other finite element analysis software packages as part or model. In this work Abaqus/CAE (Computer Aided Engineering) which is powerful software for solving linear and non-linear engineering problems using finite element method was employed as a platform. It has been used for impact, heat transfer, computational fluid dynamics and mechanical (static and dynamic) analysis of complex textile structures. A GUI plug-in was developed and can be used to generate weft knitted fabric geometry in Abaqus environment. The weft knitted fabric geometry generated can be directly used for FE analysis in Abaqus, which is very user-friendly. A Geometrical model of plain weft knitted fabric created by the GUI plug-in developed in Abaqus/CAE is shown in Figure 6.3.

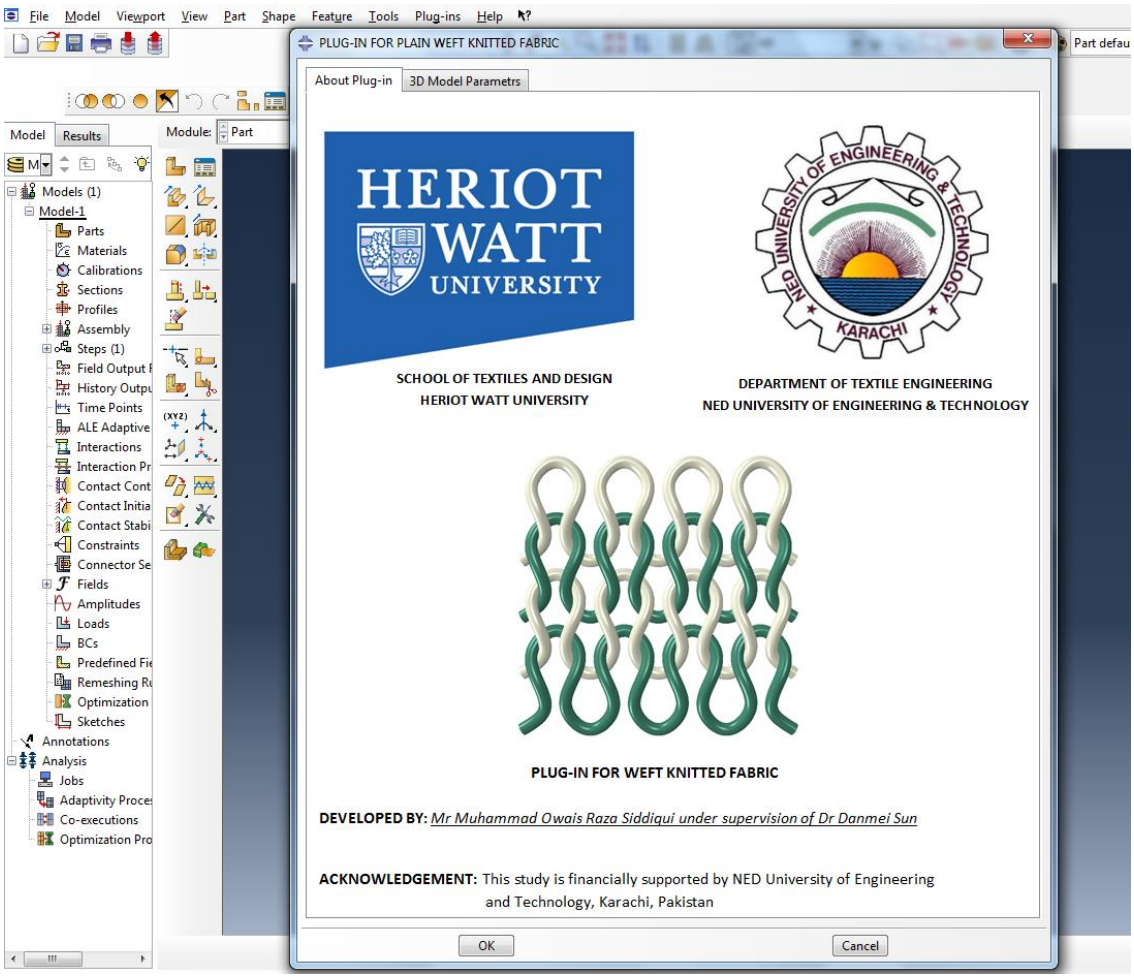

Figure 6.3: Main interface of plug-in for plain weft knitted fabric

The main objective of the developed plug-in is to provide a graphical user interface to enable automatically generating 3D models of plain weft knitted fabrics with only few necessary input parameters. These models can be used to predict the porosity, shrinkage, compression and elongation behaviour of plain weft knitted fabric and composites. There are two options in geometric model creation in the plug-in as shown in Figure 6.4. Both Peirce's and parametric geometric models have been generated by sweeping the circular cross-section of yarn along the yarn central axis, yarn central axis was created by cubic spline curve. The detailed about the geometrical creation has been mentioned in Chapter 4. The scripts related to GUI plug-in of plain weft knitted fabric are attached in Appendix.

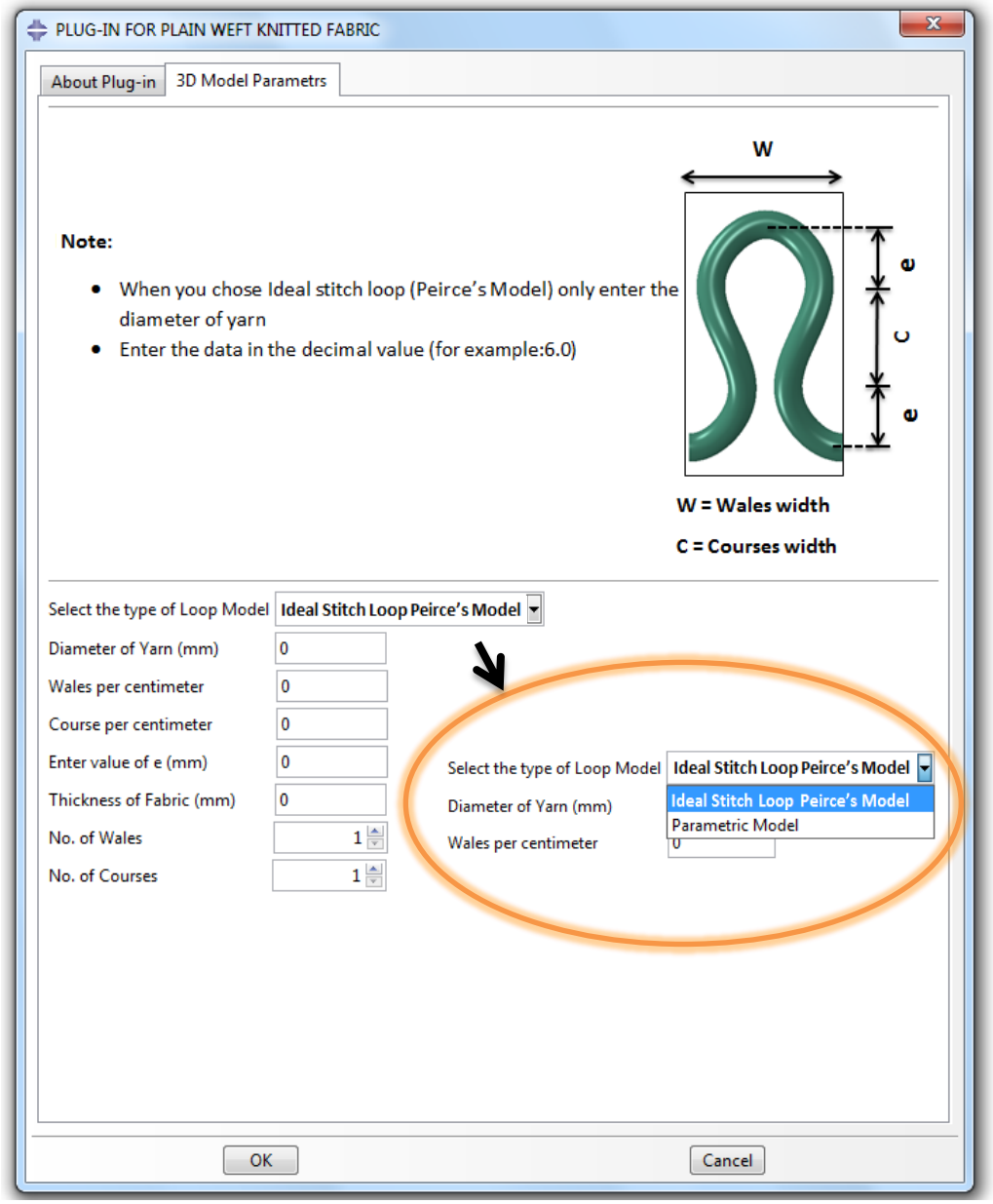

Figure 6.4: Main interface of plug-in for plain weft knitted fabric and highlighted three options for model generation

6.3.2 Plug-in for Multifilament Weft Knitted Fabric

In this GUI plug-in only parametric model option is available. This plug-in requires few more input parameters such as, filament radius (r_f), number of filament in yarn (N) and yarn twist (turns per cm) as mentioned in Figure 6.5, for the creation of 3D model of weft knitted fabric made of multifilament yarns. An idealized packing of circular fibers in yarns was used as described by Schwarz [167, 168], shown in Figure 6.6.

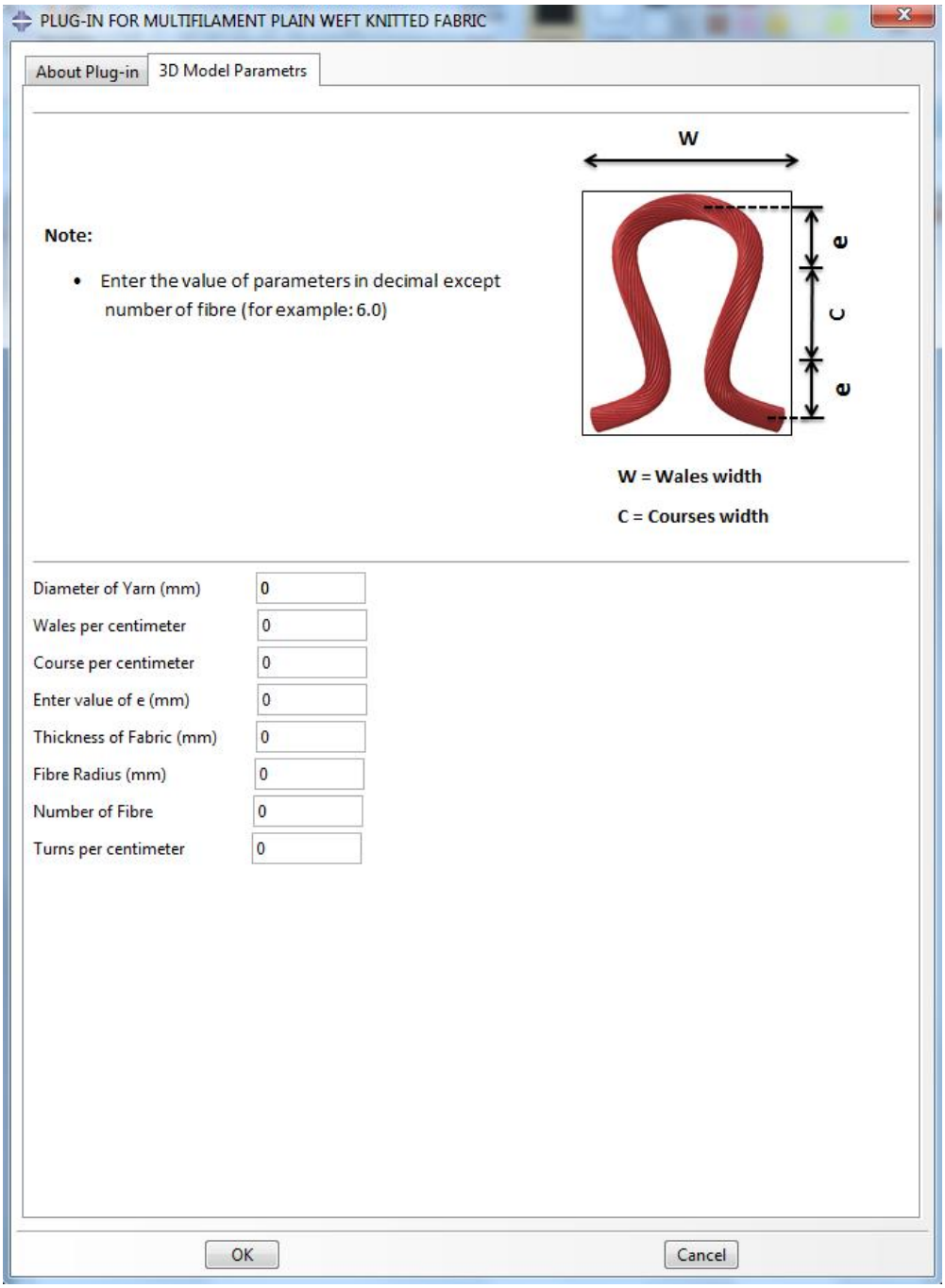

Figure 6.5: Plug-in user interface for generating solid plain weft knitted fabric geometry

The total number of layers (n) and the radius of each layer (r) were calculated by the Equations 6.1 and 6.2 [167, 168] , which were built-in in the plug-in.

$$Number\ of\ Layers = n = \frac{1}{2} \cdot \left(\frac{Yarn\ Rradius\ (R)}{r_f} + 1 \right) \tag{6.1}$$

$$Radius\ of\ Centre\ of\ nth\ Layer = r = 2(n-1)r_f \tag{6.2}$$

Figure 6.7 demonstrates the 3D Model of multifilament weft knitted fabric which can be used for simulation and prediction of heat transfer, air permeability, mechanical properties of fabrics, etc.

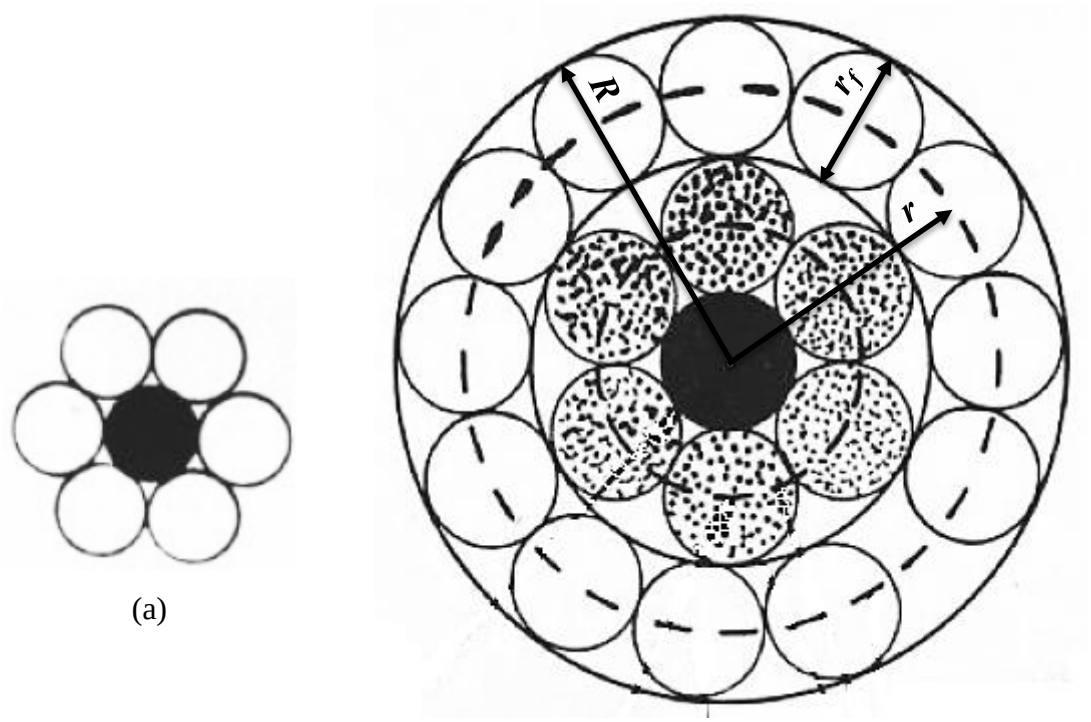

(a)

(b)

Figure 6.6: Ideal packing of circular fibres in yarns: (a) 2 layers with 7 fibres and (b) 3 layers with 19 fibres [167]

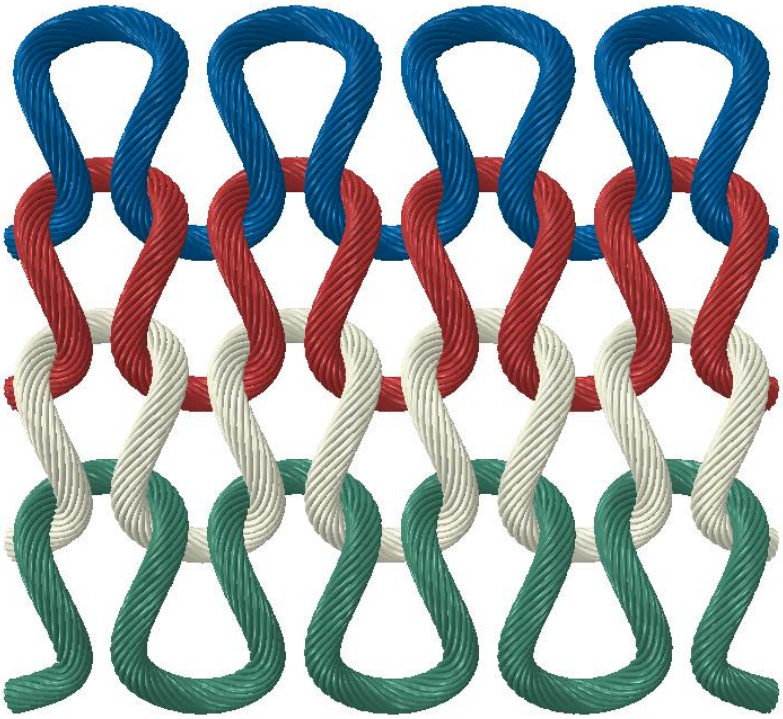

Figure 6.7: Multifilament twisted weft knitted 3D model created from plug-in

6.3.3 Plug-in for Porosity of Plain Weft Knitted Fabric

Porosity is the ratio of void space within the boundaries of solid material to the total volume of solid material including void spaces, defined by Guidoin [169]. He developed equations for porosity of solid material in terms of percentage:

$$porosity\ (\%) = 100\left[\frac{V_v}{V_t}\right] \tag{6.3}$$

$$porosity\ (\%) = 100\left[1 - \frac{M}{L\rho_m}\right] \tag{6.4}$$

where V_v is volume of void space (cm^3), V_t is total volume of porous material (cm^3), M is mass per unit area of porous materials (g/cm^2), ρ_m is density of solid material (g/cm^3) and L is thickness of material (cm).

Benltoufa et al [170] investigated different methods for the estimation of the porosity of jersey fabric. They found that the most effective way for the determination of porosity is the use of geometrical modelling. Furthermore, they found that the loop length has more significant effect on porosity of jersey fabric than the stitch density and the thickness of

fabric. The proposed model for predicting the porosity of plain knitted fabric by Benltoufa is shown in Equation 6.5.

$$porosity\ (\varepsilon) = 1 - \frac{\pi d^2 l}{4t\ C\ W} \tag{6.5}$$

where t is sample thickness, l is stitch length, d is yarn diameter, C is course spacing and W is wale spacing.

Ogulata and Mavruz [171] developed a theoretical model to predict the porosity and air permeability of plain knitted fabric based on D'Arcy's law and they concluded that the air permeability is higher for fabric with lower yarn density (course/cm) and yarn count (Tex). Angelova [172] developed an experimental procedure for the evaluation of pore size and pore distribution in a single layer woven fabric by using image analysis.

Karaguzel [173] developed a structural model for the estimation of pore size of knitted fabric in which Peirce's model was used to calculate the stitch length of fabric and yarns were considered circular in cross-section in her research. She used yarn density of 0.909 g/cm^3 which was used by the Peirce [122] for cotton yarn, due to the fact that the actual values of yarn density are different for both the yarn diameter (width) measured through video microscope and calculated yarn diameter. The results obtained from the model showed the clear difference from the experimental results. In her research, the porosity of plain weft knitted fabric is expressed by:

$$porosity\ (P) = 1 - \frac{S\,l\,\pi R^2}{t} \tag{6.6}$$

where S is the stitch density, l is the stitch length, R is the radius of yarn and t is the thickness of fabric.

Yarn radius R (in mm) can be calculated by the following equation.

$$R = \sqrt{\frac{T_y}{10^3 \pi \rho k}} \tag{6.7}$$

where T_y is the yarn count (Tex), ρ is the density of fiber (g/cm^3) and k is the fiber packing fraction in the yarn.

Dias and Delkumburewatte [174] developed a model which was used to predict the porosity of plain weft knitted fabric by using the repeating unit cell of stitch and analysed the effect of number of courses and wales, fabric thickness, yarn count and fiber density on porosity of plain knitted fabric. They found that the porosity of plain knitted fabric increases with the increase of stitch length and the thickness of fabric. Their theoretical model for porosity of plain weft knitted fabric is shown below.

$$porosity\ (P) = 1 - \frac{T_y . 10^{-5} l}{CWt\rho_f} \tag{6.8}$$

where T_y is the yarn count, l is stitch length, C is Course spacing, W is wale spacing, t is fabric thickness and ρ_f is fibre density.

Abdolmaleki et al. [175] studied the 3D porosity of knitted fabric under different uniaxial extension in course direction. They estimated the porosity of fabric based on the empirical formula developed by Guidoin's [169] and compared the results obtained from Guidoin's empirical formula under different extension with 3D theoretical methods developed by Benltoufa [170] and Karaguzel [173] in their earlier research. They also modified Benltoufa's model due to the fact that it cannot estimate the value close to experimental results under uniaxial extension in course direction of knitted fabric.

Delkumburewatte and Dias [176] developed a theoretical model which used to predict the porosity and radius of capillaries of weft knitted spacer fabric based on the geometrical parameters and they found that the porosity and capillary radius of weft knitted spacer fabric influenced by the number of spacer yarn.

Another GUI plug-in was developed in Abaqus/CAE which can be used to automatically calculate the porosity of plain weft knitted fabric. This Plug-in is the extension of GUI plug-in of plain weft knitted fabric. Comparisons of porosity of plain knitted fabrics are made between results obtained from plug-in and experiment.

In this work plain weft knitted fabrics made of different yarns such as monofilament, multifilament and staple fiber were used in order to evaluate the effectiveness of the developed plug-in as mentioned earlier in Table 3.2. In case of staple fiber yarn intra yarn porosity has been considered in the calculation of porosity.

The Plug-in for the porosity of plain weft knitted fabrics was developed in Abaqus/CAE by using python script. The plug-in comprises of two steps/modules as shown in Figure 6.8, including:

1) 3D solid and multifilament geometrical model creation of plain weft knitted fabric; and
2) Porosity calculation.

Figure 6.8 shows the two steps of plug-in. Step 1 has two options to create 3D model of plain weft knitted fabric such as: Solid geometrical model and multifilament geometrical model discussed earlier. In step 2 porosity of the plain weft knitted fabrics will be calculated.

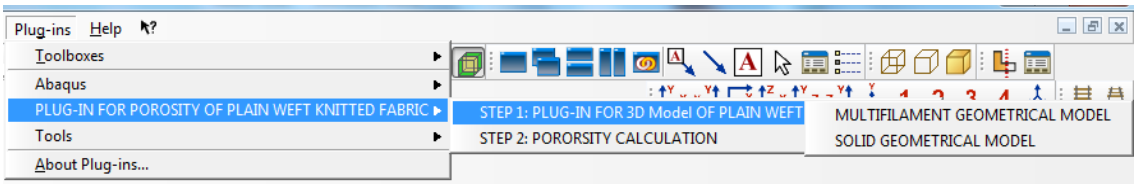

Figure 6.8: Plug-in for porosity of plain weft knitted fabric

6.3.3.1 Porosity Calculation

Porosities of plain weft knitted fabrics were calculated in the second step by the unit cell approach. Yarn inter-porosity was also considered due to the fact that the yarn volumetric density with respect to packing fraction of fibers is different for staple fiber yarns. Figure 6.9 shows the plug-in environment of porosity calculation and equation used for the porosity calculation.

There are two options available for developing of the 3D model of weft knitted fabric as solid and multifilament in the yarn. In case of staple fiber yarn fiber packing fraction is calculated by using Equation 6.7. A command is used in the script which extracts the volume of yarn and unit cell. Porosity of the weft knitted fabric is calculated by equation shown in Figure 6.9.

The Calculated value of porosity and fiber volume fraction will be automatically displayed in the message area of Abaqus/CAE, shown in Figure 6.10.

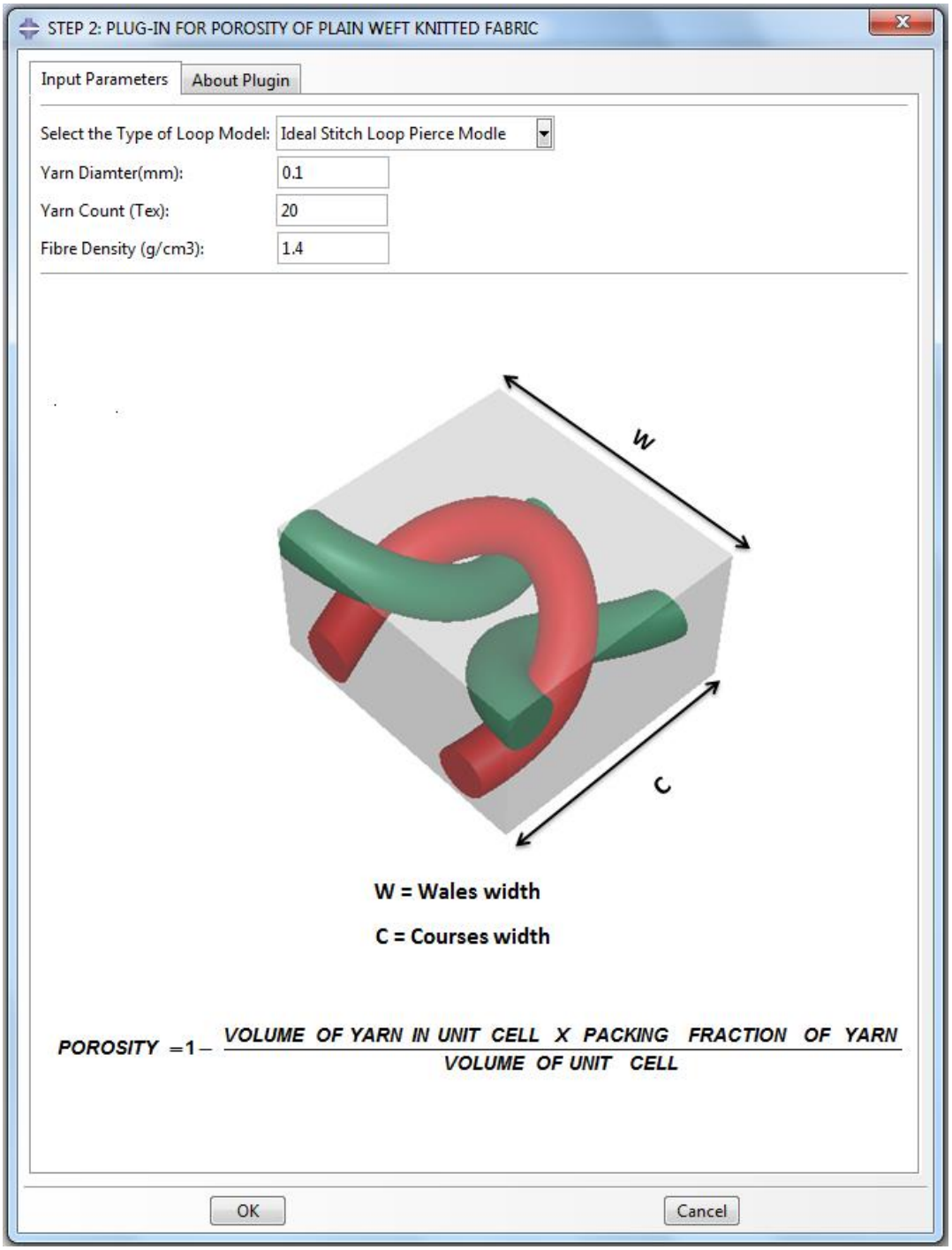

Figure 6.9: Plug-in for porosity of plain weft knitted fabric

Figure 6.10: Printed results of porosity in message area of Abaqus/CAE

6.3.4 Validation

The geometrical models generated with the fabric specification mentioned in Table 3.2 (Chapter 3) from the plug-ins of plain weft knitted fabric and multifilament plain weft fabric were used to predict the porosity by porosity plug-in. In order to validate the plug-ins the predicted results of porosity were compared with the experimental results.

Table 6.1 shows the volume of yarn and unit cell. Table 6.2 and Figure 6.11 show the comparison between the experimental results obtained by using Guidoin's method and predicted results from plug-in in Abaqus/CAE.

In this study the porosity of five different plain weft knitted fabric were calculated. A very high correlation coefficient (0.993) and coefficient of determination (0.986) between predicted results by the developed plug-in and experimental have been found.

Furthermore the predicted results were also compared with results made by other methods as shown in Table 6.3 and Figure 6.12. It is clearly shown that the accuracy of porosity obtained from the plug-in is very close to previously developed method. It is obvious that the results obtained are very close to each other; this means that the models made by plug-ins are reliable and can be used for finite element analysis.

Table 6.1: Yarn and unit cell volume

Fabric Code	Volume of yarn (mm^3)	Volume of unit cell ($W \times C \times t\ mm^3$)
F1	0.1580	2.734375
F2	0.0688	0.764974
F3	0.0961	0.735736
F4	0.7550	1.777778
F5	0.4240	1.125000

Table 6.2: Comparison of porosity between predicted and experiment.

Fabric Code	Plug-in Predicted	Experiment
F1	0.942217	0.940684
F2	0.910062	0.906628
F3	0.869382	0.864924
F4	0.909542	0.913964
F5	0.896732	0.895450

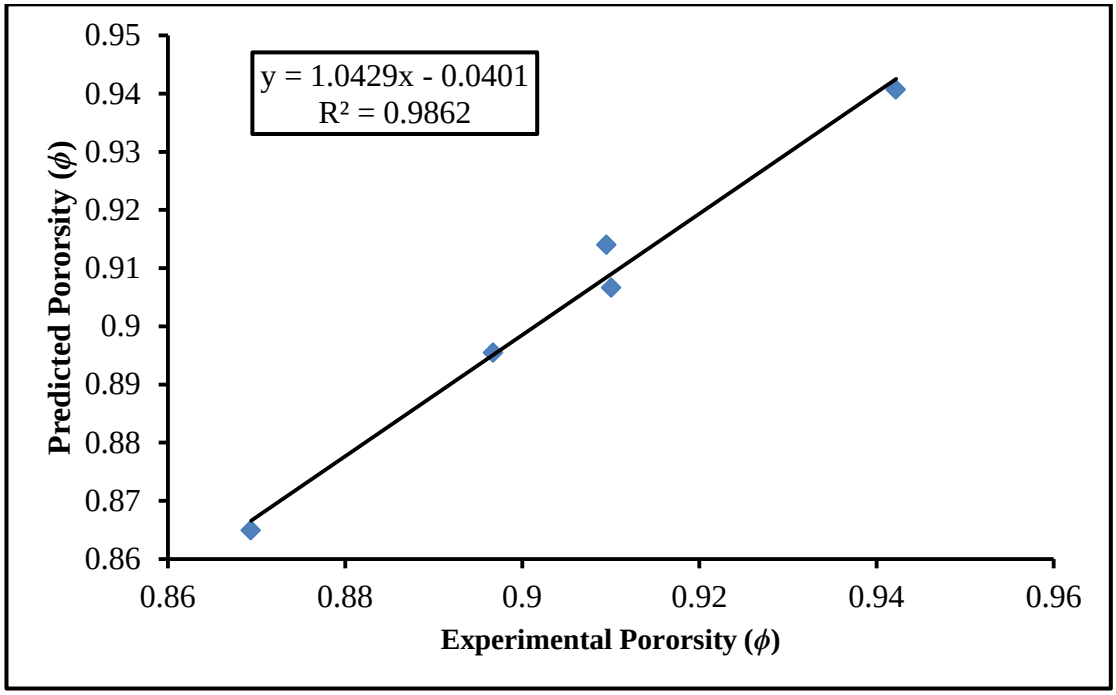

Figure 6.11: Comparison of porosity between plug-in predicted and experimental

Table 6.3: Comparison of porosity between plug-in and other methods

Fabric Code	Plug-in Model	Dias's theoretical model	Guidoin's method
F1	0.942217	0.941606742	0.940684
F2	0.910062	0.907271024	0.906628
F3	0.869382	0.867464924	0.864924
F4	0.909542	0.912516447	0.913964
F5	0.896732	0.899761295	0.895450

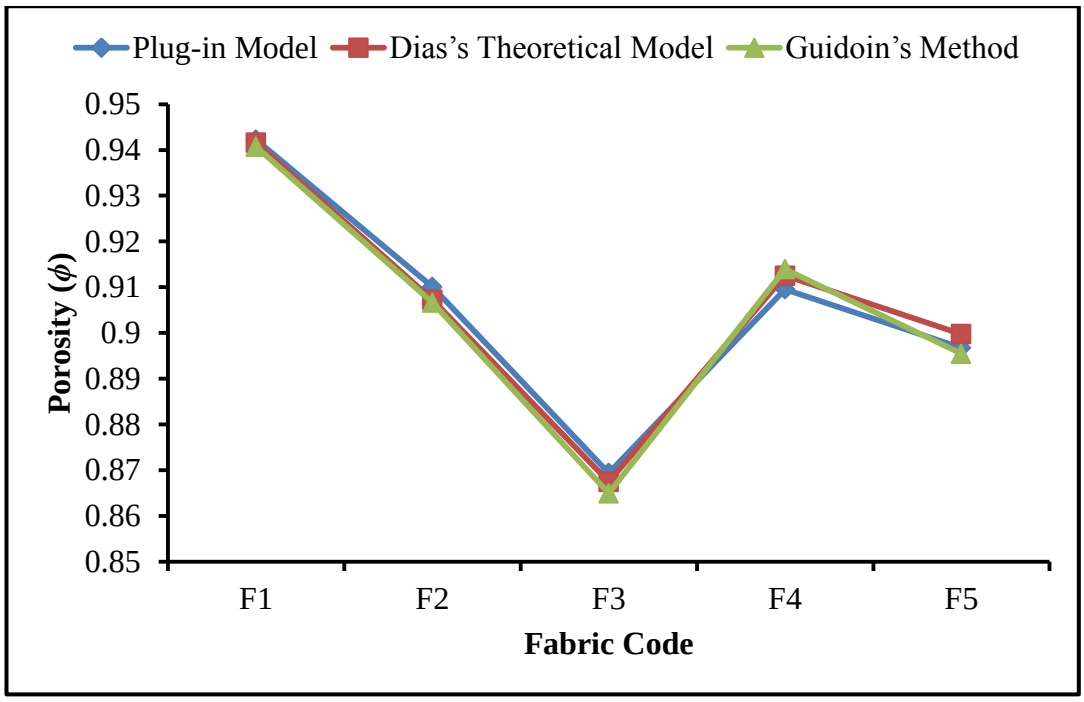

Figure 6.12: Comparison of porosity between plug-in and other methods

6.4 Plug-in for Plain Woven Composite Fabric

Unique properties such as light weight, thermal and high strength of textile composites have been developed to replace many metallic parts in aeronautical, space and automobile industries. Effective thermal conductivity is one of the important thermal properties which describe the thermal behaviour of textile composite.

The aim to develop the plug-in is to create a user friendly environment incorporated into Abaqus/CAE, enabling generate and accurately predict the effective thermal conductivity of plain woven fabric composite.

The main advantages of the plug-in are: it generates a finite element model of single layer or multiple layer composite fabrics by only taking few necessary input parameters which is feasible in term of saving time and it automatically assigns the material orientation, and it is the critical task for woven fabric composite because material principal axis of yarn changes due to the waviness in warp and weft yarns. The Plug-in comprises of three steps.

6.4.1 Step 1

In first step it generates the unit cell model of plain woven fabric composite by sweeping the lenticular cross-section of yarn along the yarn path which is defined by cubic spline curve as shown in Figure 6.13.

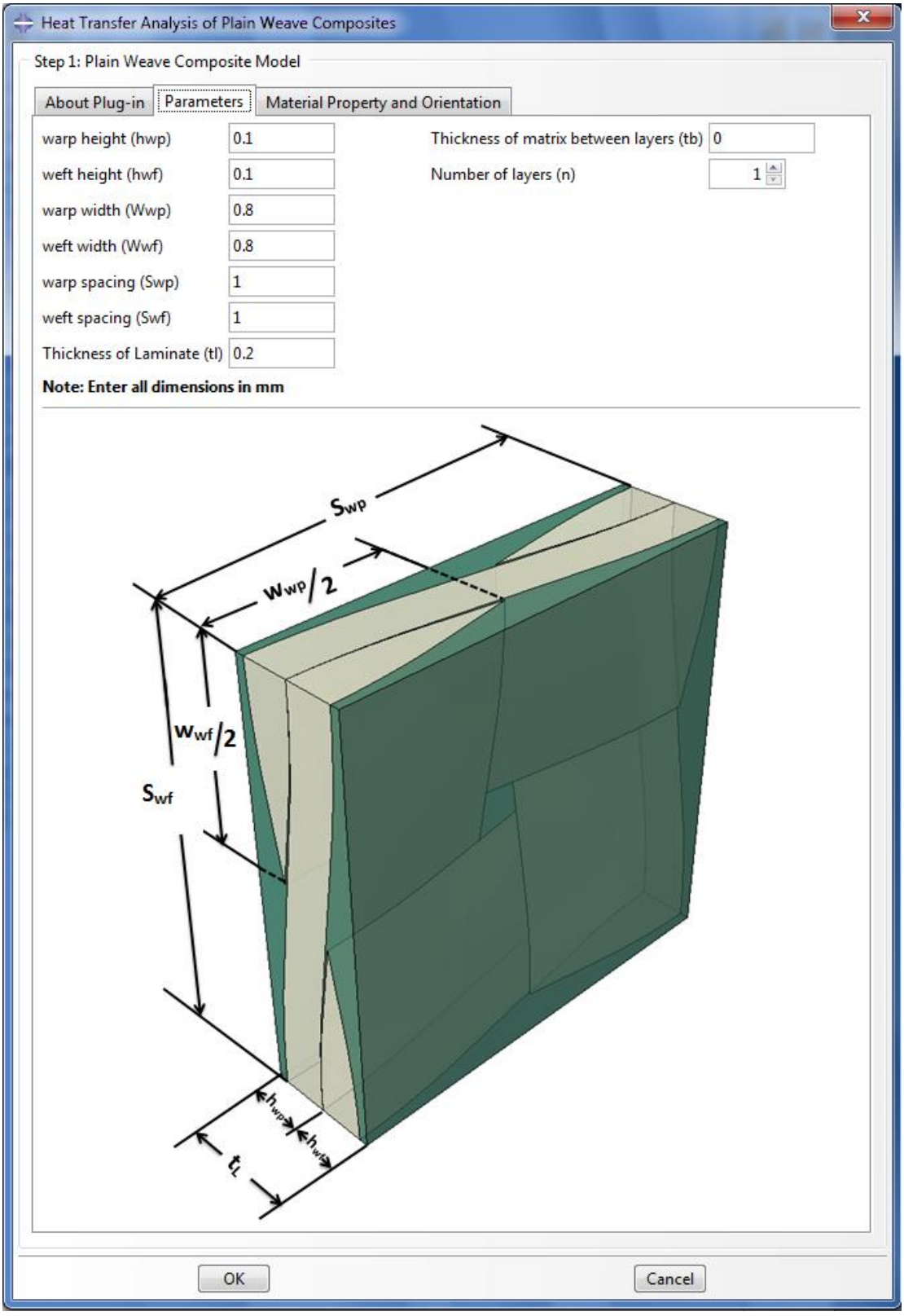

Figure 6.13: Plug-in main interface of plain woven composite fabric

Multilayer plain woven composites can be generated by using the idealized unit cell approach. In the same step material property to the yarn and matrix can be assigned and material orientation can also be defined in this step.

Material orientation was defined by the discrete orientation technique in Abaqus/CAE as shown in Figure 6.14. The details about the material orientation have been discussed in Chapter 5.

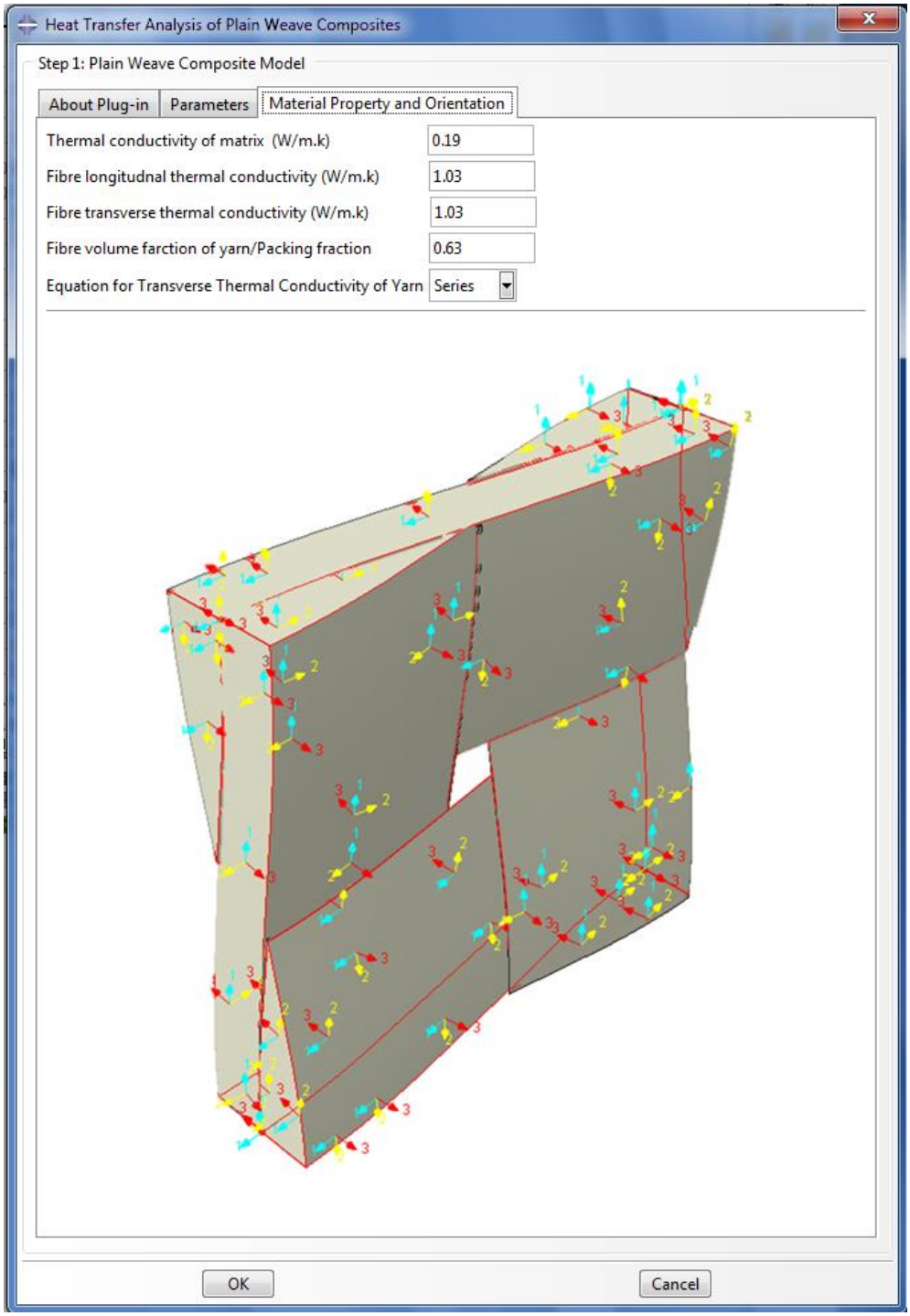

Figure 6.14: Material orientation interface

6.4.2 Step 2

In second step it generates the mesh of unit cell by using 4-node linear tetrahedral elements (DC3D4) as shown in Figure 6.15 .

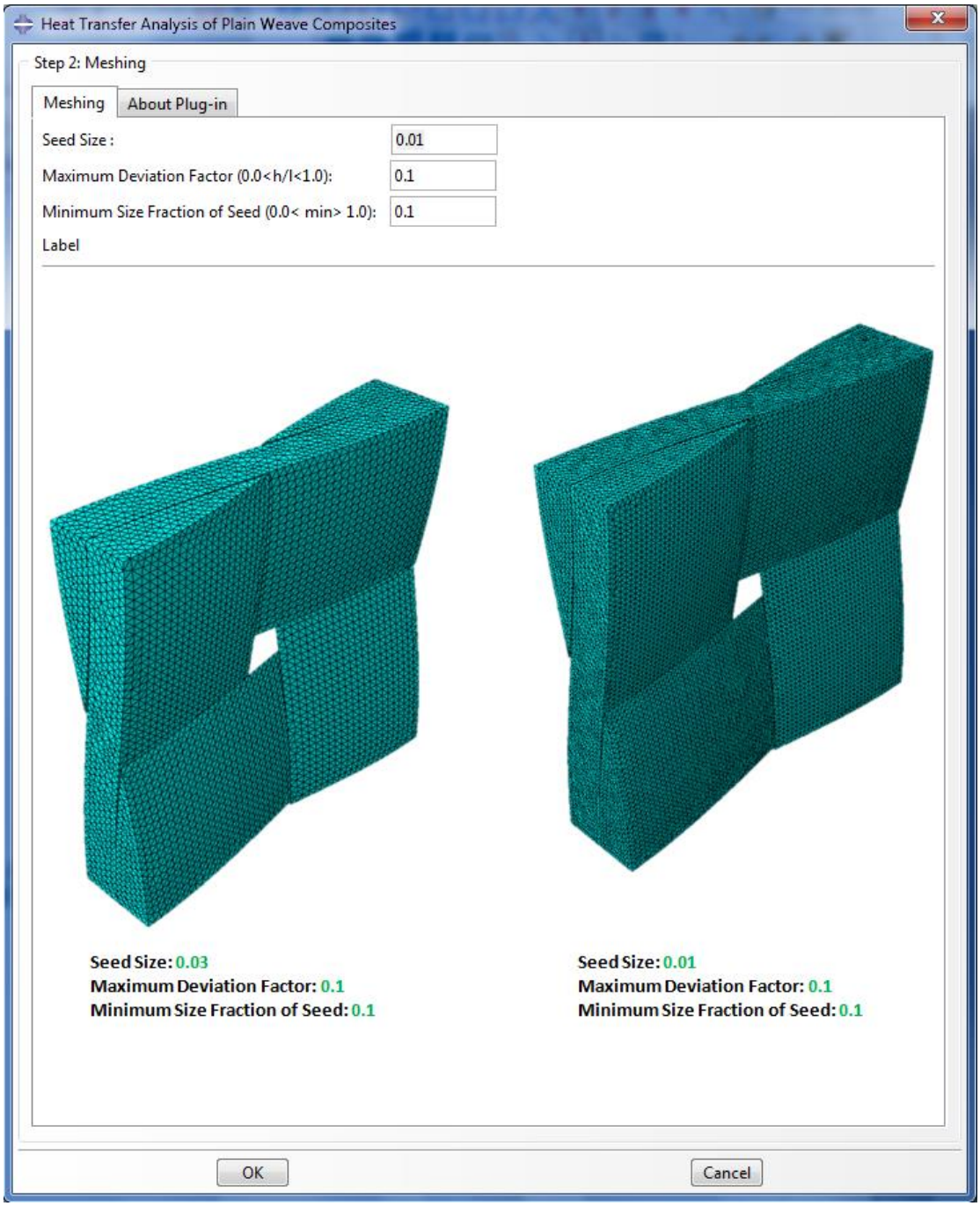

Figure 6.15: Mesh interface

.

6.4.3 Step 3

In this step the temperature specified boundary conditions are applied and job is submitted for analysis. The steady state heat transfer of unit cell will be analysed.

Heat flux and surface area extracted can be obtained by using command within plug-in. The effective thermal conductivity across the thickness can be calculated by Fourier's law of conduction as shown in Equation 6.9 and displayed in the message area of Abaqus/CAE.

$$K_{eff} = \frac{\text{Heat Flux accross the thickness}}{\text{Surface Area} \times \Delta T} \times \text{thickness of composite} \qquad 6.9$$

6.4.4 Validation

In order to validate the predicted effective thermal conductivity of plain woven fabric composite obtained from plug-in, results from FE models generated by the plug-in are compared with Dasgupta's results [177] as shown in Figure 6.16. It was found that they are highly correlated. Figure 6.17 shows the plug-in environment of step 3.

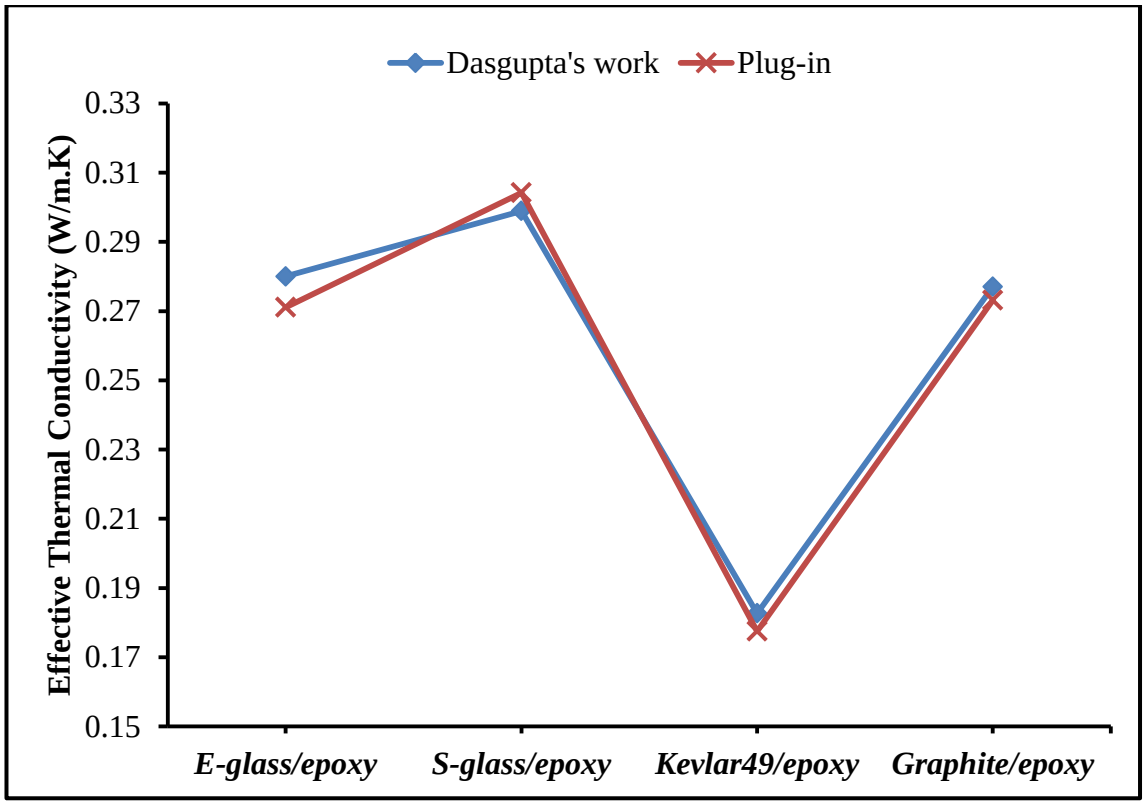

Figure 6.16: Comparison of effective thermal conductivity obtained from plug-in and Dasgupta's work

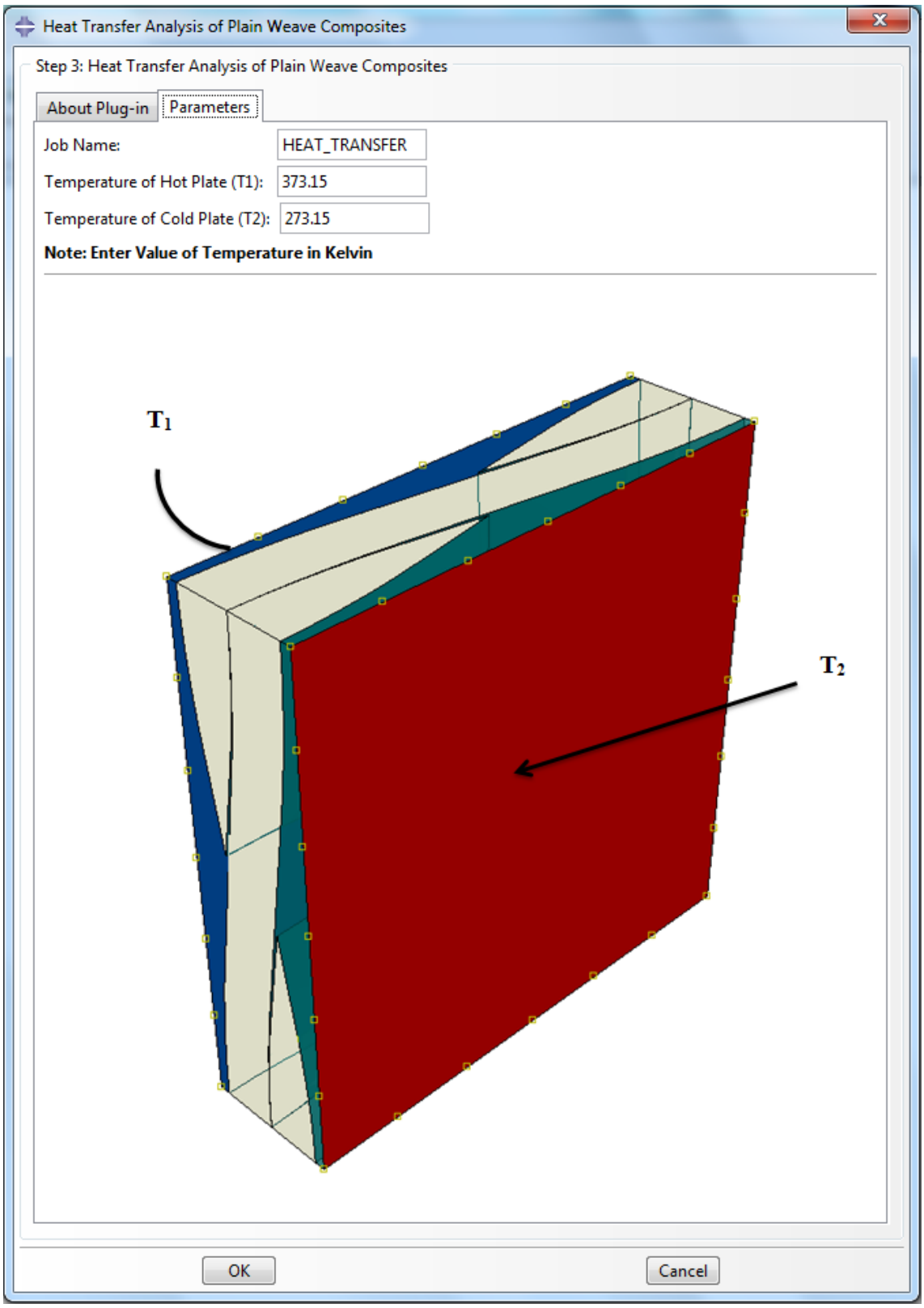

Figure 6.17: Heat transfer analysis interface

Figure 6.18 shows the process sequence of the developed plug-in. The limitation of the plug-in is that it can only generate yarns with lenticular cross-sectional shape and fabrics with low crimp.

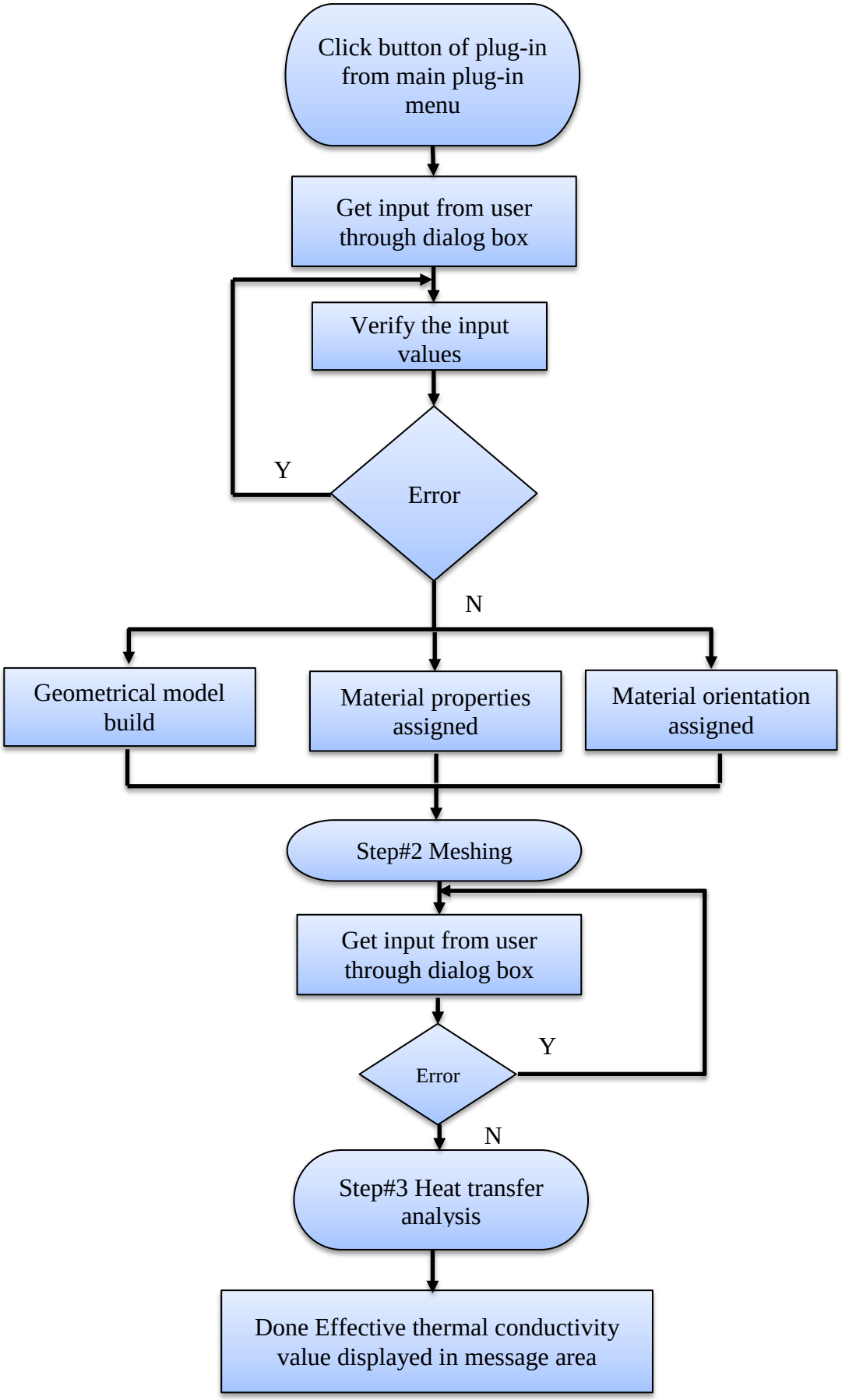

Figure 6.18: Process sequence of the plug-in for plain woven composite fabric

6.5 Plug-in for MicroPCMs Composites

The unit cell model of MicroPCMs composite was created from GUI plug-in through micro-sphere filled composite material approach. Figure 6.19 shows the main interface of GUI plug-in which created in Abaqus/CAE by python script which generate automatically unit cell model of microencapsulated phase change material composites by simple cubic and body-centred cubic (BCC) structure as shown in Figure 6.20. The maximum volume fraction limit in simple cubic structure is 0.52 and in body-centred cubic structure is 0.68.

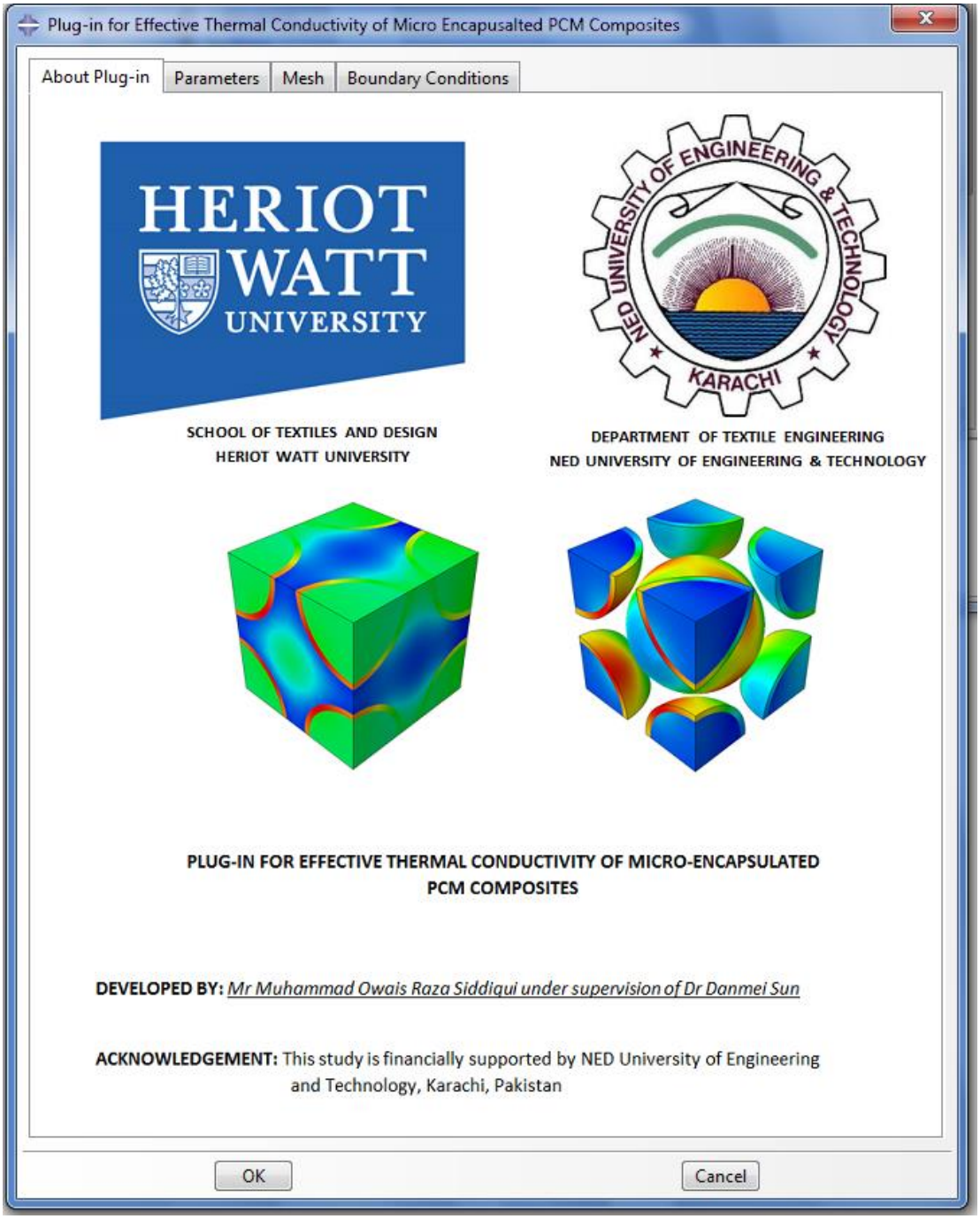

Figure 6.19: Main interface of GUI plug-in for microencapsulate PCM composites

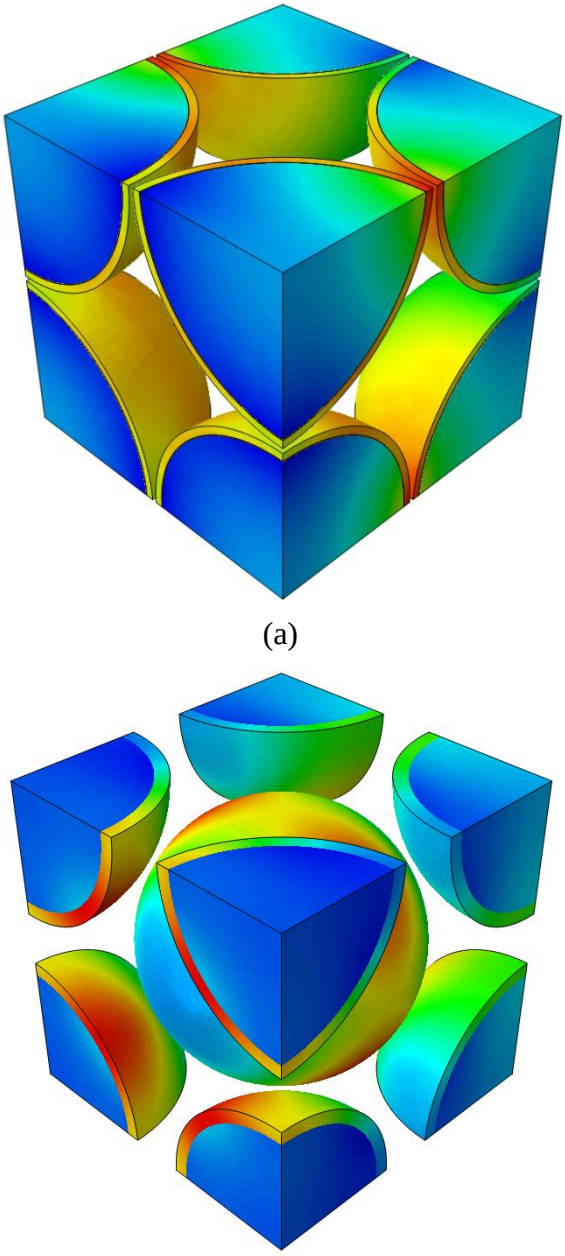

(a)

(b)

Figure 6.20: Packing arrangement: (a) Simple cubic and (b) Body-centred cubic (BCC)

Figure 6.21 shows the material interface of core, shell and matrix. The plug-in is capable to automatically predict the effective thermal conductivity of microencapsulated phase change composites.

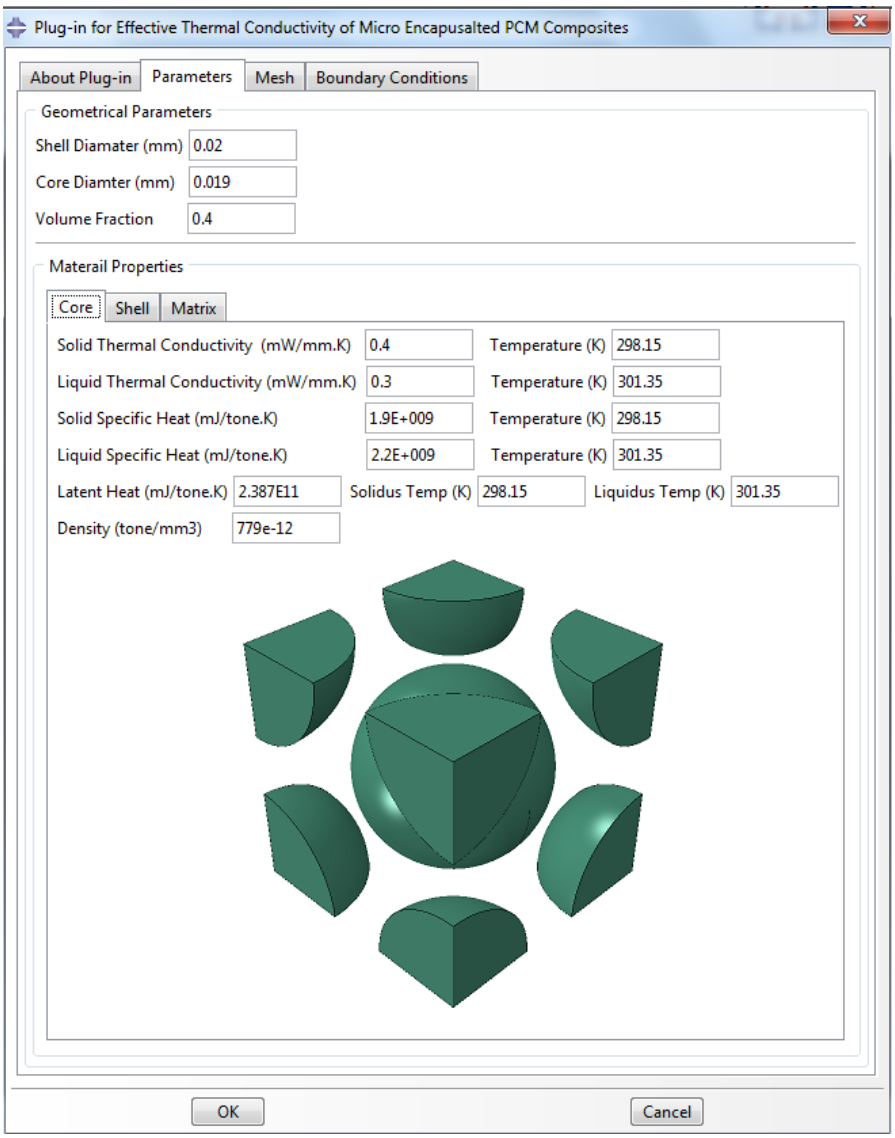

(a)

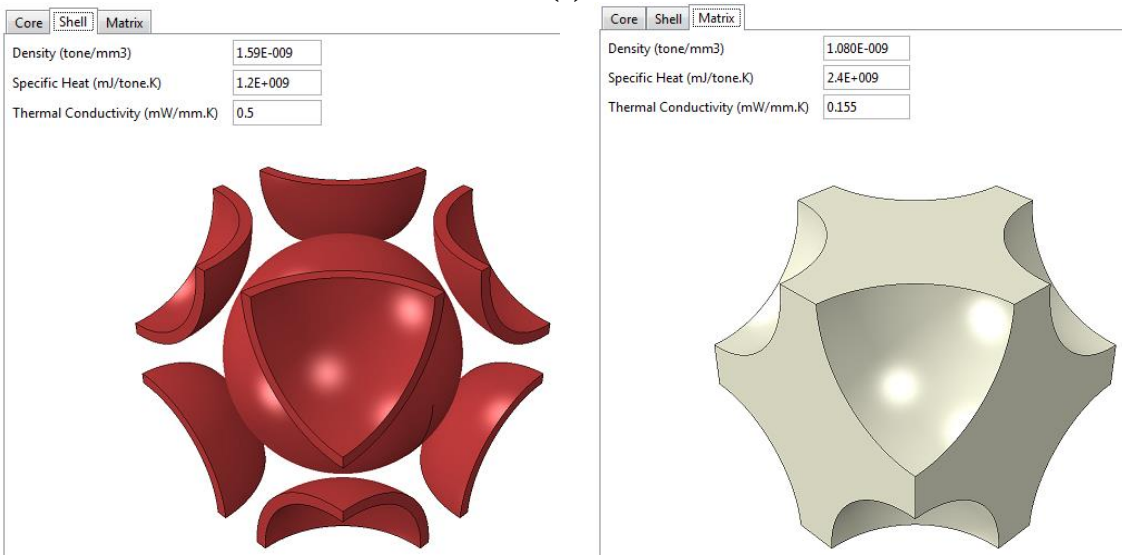

(b) (c)

Figure 6.21: Material property interface: (a) Core; (b) Shell; and (c) Matrix

6.5.1 Validation

In order to validate the models obtained from Plug-in the effective thermal conductivity obtained are compared to results obtained from Maxwell's model at different volume fractions of MicroPCMs (ϕ).

The results from FEA were agreed well with the results obtained from Maxwell's model at lower volume fraction. At higher volume fraction the values obtained from FEA were higher than the Maxwell's model due to the fact that Maxwell's equation was derived based on the assumption that the solid spheres apart from each other so there were no interaction and chain formation between them. The results comparisons between the two methods are shown in Figure 6.22.

The thermal conductivity of MicroPCMs was calculated by composite sphere approach [178] by using the properties given in Table 5.8 in Chapter 5.

$$K_p = \frac{2(1-\phi_c)K_s + (1+2\phi_c)K_c}{(2+\phi_c)K_s + (1-\phi_c)K_c} K_s \qquad 6.10$$

where K_p , K_s and K_c are the thermal conductivity of MicroPCMs, shell and core of PCM microcapsule respectively and ϕ_c is the core volume fraction.

The effective thermal conductivity of acrylic binder and MicroPCMs can be calculated by Maxwell's model [179] using the thermal conductivity of MicroPCMs obtained from Equation 6.11.

$$K_{eff} = K_b \frac{2K_b + K_p + 2\phi(K_p - K_b)}{2K_b + K_p - \phi(K_p - K_b)} \qquad 6.11$$

where K_{eff} is the effective thermal conductivity of binder and MicroPCMs and K_p and K_p are the thermal conductivity of binder and MicroPCMs respectively and ϕ is the volume fraction of MicroPCMs.

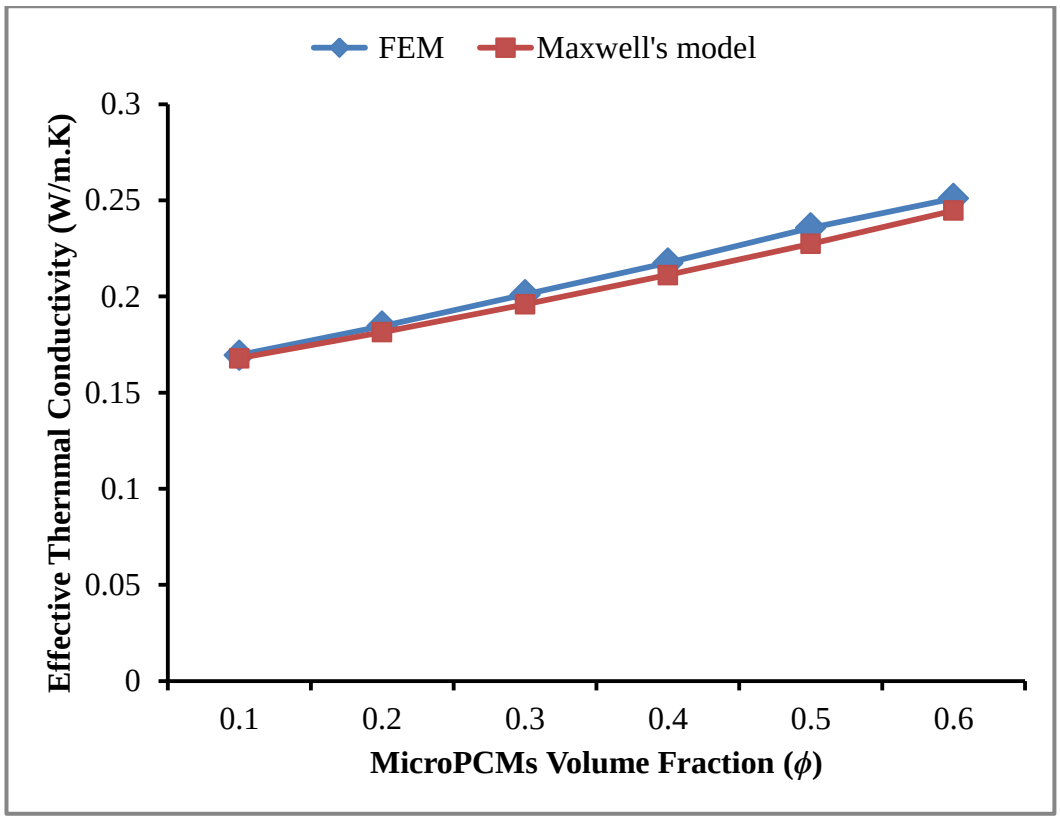

Figure 6.22: Results comparison between FEM and Maxwell's model

6.6 Summary

This chapter describes the development of the Plug-ins which can be used to generate the 3D solid and multifilament weft knitted fabric, predict the porosity of plain weft knitted fabric and automatically compute the effective thermal conductivity of MicroPCMs and plain woven composites.

The plug-in has been created to provide an instinctive and simple way for users to create models and predict fabric properties. The geometrical models and their results generated from the plug-in has showed the same trend as compared to the experimental results and previously established methods. The generated geometric models by plug-in can be directly used for FE analysis in Abaqus/CEA.

Chapter 7 Model Validation and Parametric Analysis

7.1 Introduction

The development of finite element models of textile structures for heat transfer analysis is one of the objectives of the research. This chapter presents the validation of finite element models by comparing the results generated by the FEA models with the experimental results. Furthermore, the detailed studies conducted on the validated models were analysed to find out how the effective thermal conductivity and thermal resistance of textile fabrics affected by fibre orientation, thermal anisotropy of fibre, temperature dependent thermal conductivity and fibre volume fraction. This chapter also contains the evaluation of the influence of PCM on heat transfer behaviour of MicroPCMs composites.

7.2 Model Validation

In order to validate the finite element models of woven, MicroPCMs coated composites, knitted and nonwoven fabrics comparisons have been made between the experimental results and predicted results by FE analysis. Table 7.1 and Table 7.2 show the comparison between predicted and experimental results of effective thermal conductivity and thermal resistance respectively.

The predicted effective thermal conductivity and thermal resistance from the developed FE models were compared with experimental results shown in Figure 7.1. The coefficient of determination between predicted values by using anisotropic thermal conductivity of fibre (transversely isotropic) and experimental results of thermal conductivity and thermal resistance of fabric were found 0.921 and 0.934 respectively which indicate the strong correlations between the experimental and the predicted results. The equation represents the trend line which can be used to estimate the experimental results.

The correlation coefficient of thermal conductivity and thermal resistance between FE and experimental results are calculated 0.959 and 0.966 respectively. Figure 7.2 shows that the simulated results are very close to the experimental results, proving good agreement between the results from FE models and experiments.

Table 7.1: Comparison of effective thermal conductivity between experimental and predicted results by FE models

Fabric Code	Experimental effective thermal conductivity, K_{eff} (W/m.K)	Predicted effective thermal conductivity, K_{eff} (W/m.K)
Nomex®III	0.05	0.0552
Twaron®	0.041	0.0476
Cotton	0.056	0.065
Wool	0.0414	0.04618
Poly-Viscose	0.0484	0.05088
F1-Polyester (MF)	0.035	0.03152
F2-Polyester (MF)	0.0377	0.03821
F3-Polyester (MF)	0.0403	0.0423
F4- Cotton (SF)	0.043	0.0411
F5- Viscose (MFF)	0.0412	0.03845
Nomex® III with PCM	0.089	0.085
Cotton with PCM	0.087	0.081
Wool with PCM	0.072	0.077
Sample-1 (polypropylene)	0.03734	0.02981
Sample-2 (polypropylene)	0.03615	0.02956
Sample-3 (polypropylene)	0.03389	0.02873

MF: Monofilament; MFF: Multifilament; SF: Staple fibre

Table 7.2: Comparison of thermal resistance between experimental and predicted results by FE models

Fabric Code	Experimental effective thermal conductivity, K_{eff} (W/m.K)	Predicted effective thermal conductivity, K_{eff} (W/m.K)
Nomex®III	0.01000	0.00906
Twaron®	0.00849	0.00731
Cotton	0.00864	0.00745
Wool	0.00986	0.00884
Poly-Viscose	0.00705	0.00670
F1-Polyester (MF)	0.01400	0.01555
F2-Polyester (MF)	0.01247	0.01230
F3-Polyester (MF)	0.01216	0.01158
F4- Cotton (SF)	0.01861	0.01947
F5- Viscose (MFF)	0.01573	0.01685
Nomex® III with PCM	0.00764	0.0080
Cotton with PCM	0.00661	0.007099
Wool with PCM	0.00778	0.007273
Sample-1 (polypropylene)	0.01446	0.01812
Sample-2 (polypropylene)	0.00968	0.01184
Sample-3 (polypropylene)	0.01682	0.01984

MF: Monofilament; MFF: Multifilament; SF: Staple fibre

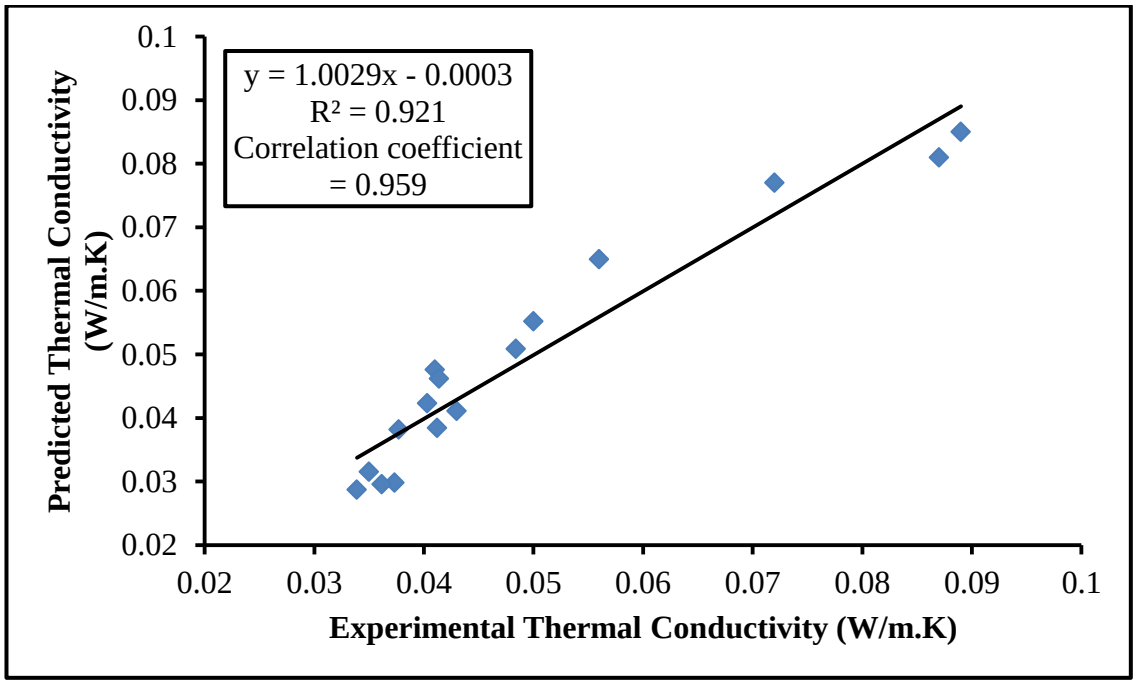

(a)

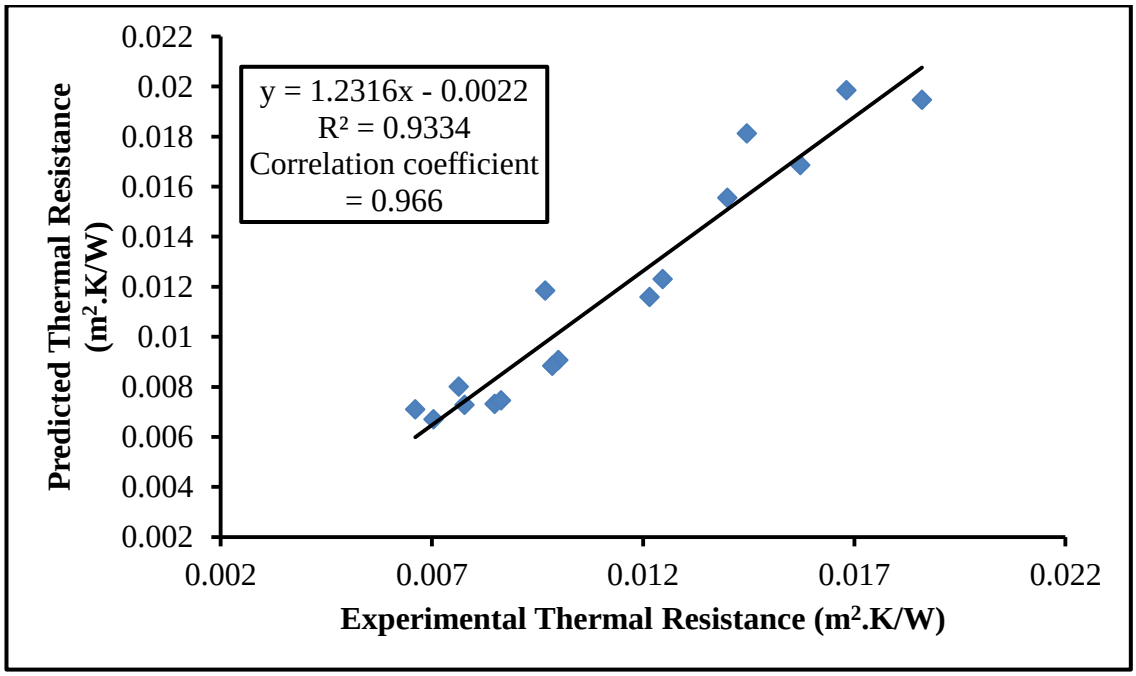

(b)

Figure 7.1: Comparison of FE and experimental results: (a) Effective thermal conductivity of fabric and (b) Thermal resistance of fabric

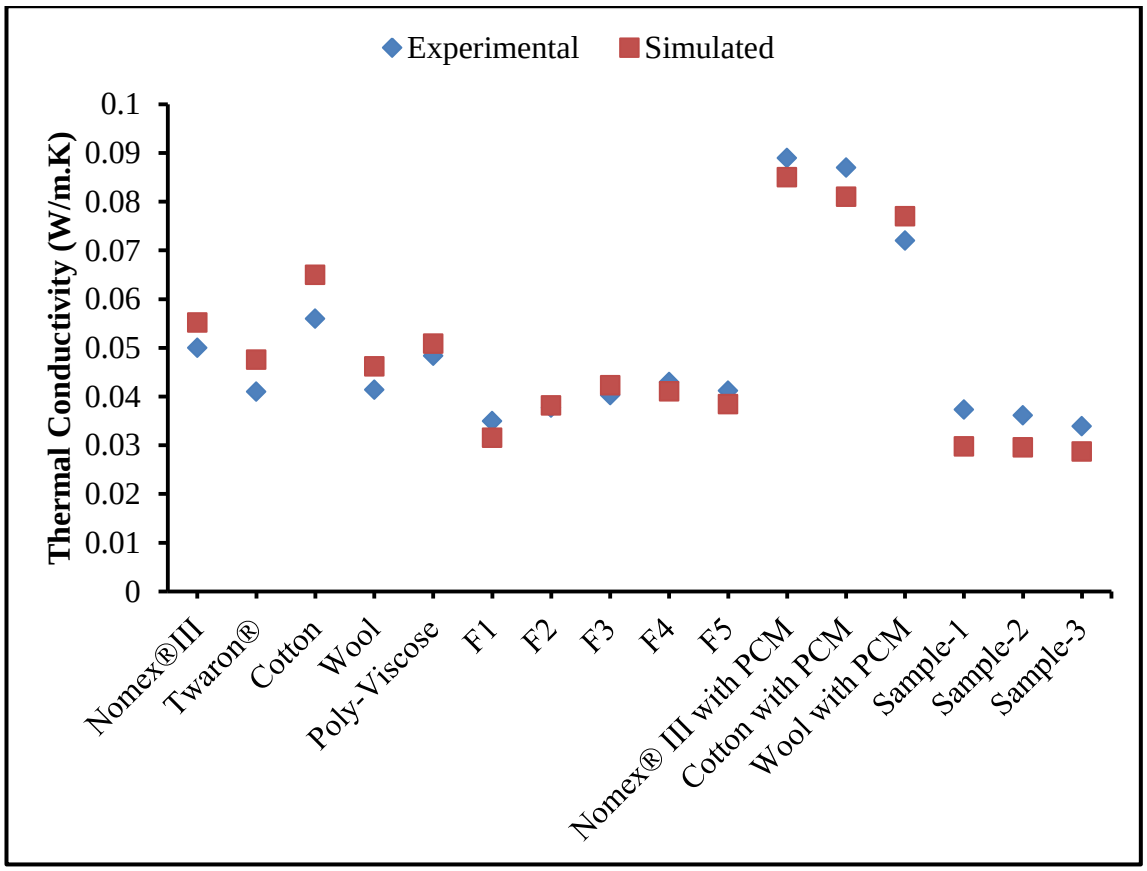

(a)

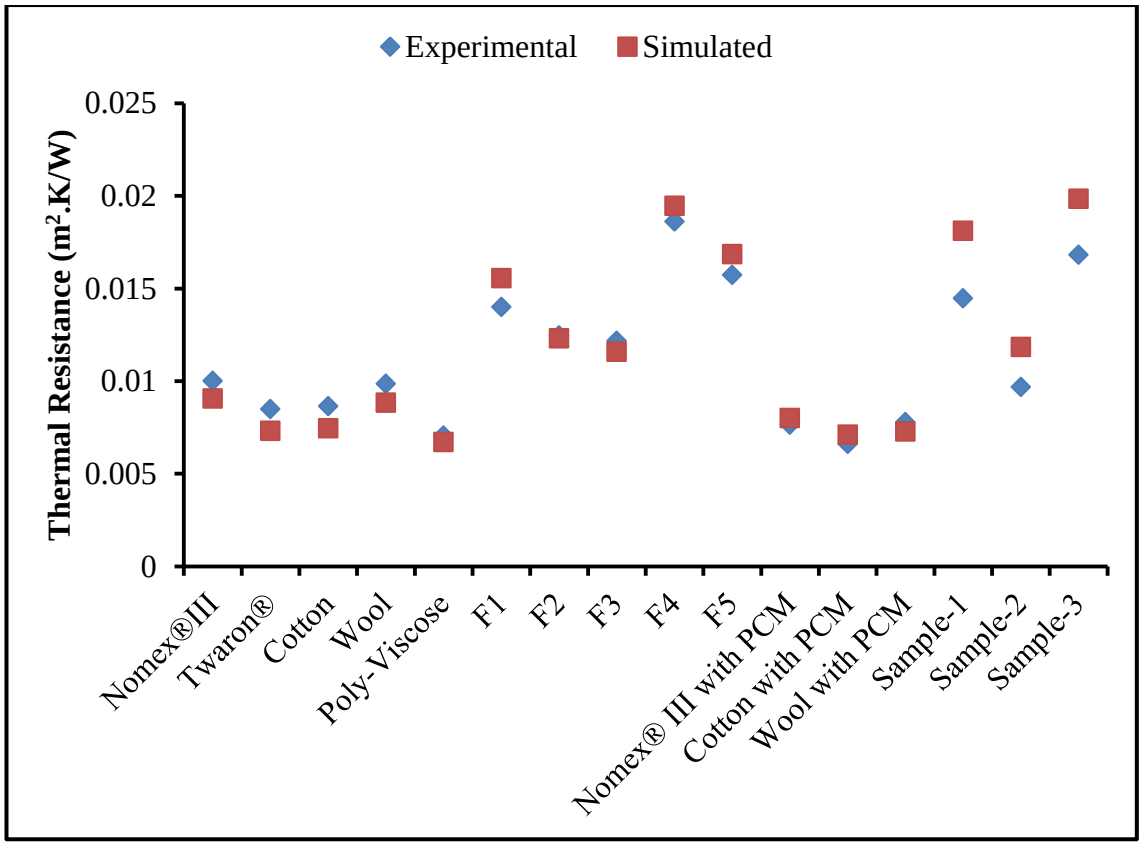

(b)

Figure 7.2: Validation of FE and experimental results: (a) Effective thermal conductivity of fabric and (b) Thermal resistance of fabric

7.3 Parametric Studies

In this section factors such as thermal anisotropy, fibre orientation and temperature dependent thermal conductivity on the effective thermal conductivity of textile structures will be analysed by using the validated models.

7.3.1 Effect of Thermal Anisotropy of Fibre on Effective Thermal Conductivity

To study the effect of thermal anisotropy of fibre on effective thermal conductivity, two finite models have been developed by considering the anisotropic and isotropic material property. Table 7.3 and Figure 7.3 show the comparison between predicted and experimental results with the consideration of anisotropic and isotropic thermal conductivity of fibre.

The absolute error between the FE and experimental results was calculated by Equation 7.1.

$$\text{Absolute Error (\%)} = \left| \frac{\text{Actual value - Predicted Value}}{\text{Actual value}} \right| \times 100 \qquad 7.1$$

Table 7.3: Comparison of effective thermal conductivity of fabrics

Fabric Code	Effective Thermal Conductivity K_{eff} (W/m.K)		
	Experimental	Simulated (Anisotropic)	Simulated (Isotropic)
Nomex®III	0.05	0.0552	0.03213
Twaron®	0.041	0.0476	0.0358
Cotton	0.056	0.065	0.0322
Wool	0.0414	0.04618	0.03541
Poly-Viscose	0.0484	0.05088	0.03204
F1-Polyester (MF)	0.035	0.03152	0.02931
F2-Polyester (MF)	0.0377	0.03821	0.03
F3-Polyester (MF)	0.0403	0.0423	0.03356
F4- Cotton (SF)	0.043	0.0411	0.02825
F5- Viscose (MFF)	0.0412	0.03845	0.0288
Nomex® III with PCM	0.089	0.085	0.0672
Cotton with PCM	0.087	0.081	0.06073
Wool with PCM	0.072	0.077	0.0704
Mean absolute error (%)	-	8.07	24.15

MF: Monofilament; MFF: Multifilament; SF: Staple fibre

High mean absolute error (24.15%) was found between the experimental and predicted results for the case of considering the material of yarn as isotropic in nature. This indicates that the heat did not flow in the transverse direction of yarn. In support of above fact heat also flows in the longitudinal direction of yarn that is why there is low mean absolute error (8.07%) was found when considering the anisotropic thermal conductivity of fibre.

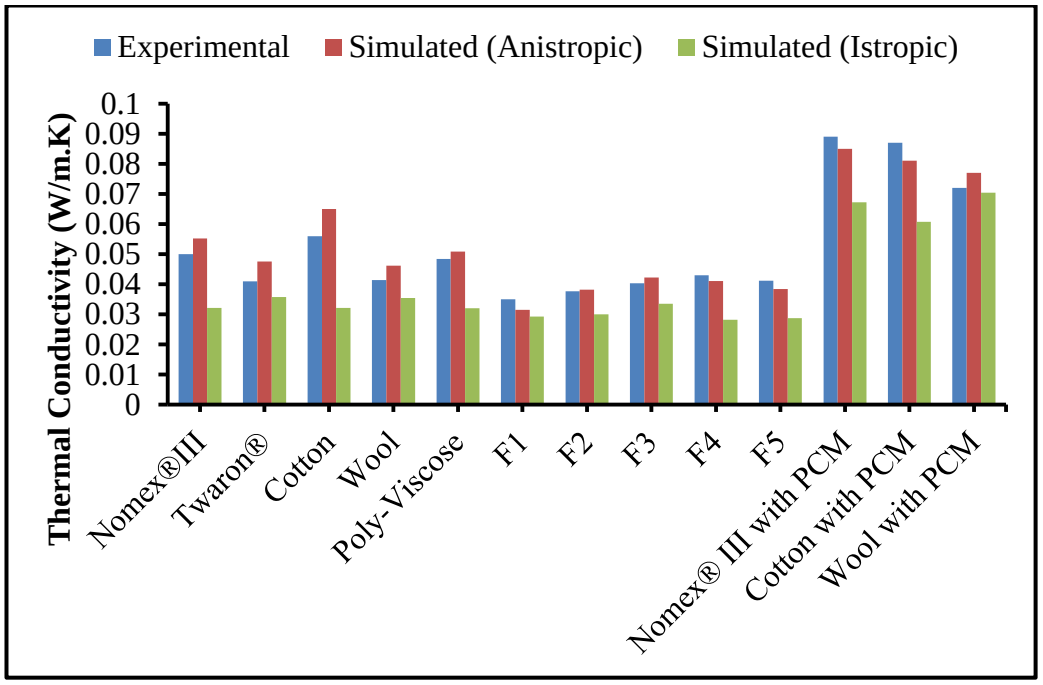

Figure 7.3: Effect of thermal anisotropy of fibre on effective thermal conductivity

7.3.2 Effect of Fibre Orientation on Effective Thermal Conductivity

Three types of models were developed for analysing the effect of fibre orientation on thermal conductivity and thermal resistance of fabrics. In Model-1 material orientation of yarn was considered as described in the material orientation section. In Model-2 global material orientation was considered and in Model-3 fibres were considered as isotropic in nature.

Table 7.4 and Table 7.5 show the mean absolute error (%) of the effective thermal conductivity and thermal resistance of the plain weft knitted polyester fabric obtained from the three models in comparison to results from experiment. Model 1 shows the lowest error as compared to the other two models. Model-1 considered the nature of fibre material as anisotropy as well as actual fibre orientation. There was no consideration of actual fibre orientation in other two models; especially in Model 3 fibres were considered as isotropic in nature. For Model-1 the correlation coefficient

between experimental and predicted thermal conductivity and thermal resistance were 0.839 and 0.977 respectively. Results from Model-1 have already been used to determine the overall coefficient of determination between experimental and predicted results in section 7.2 for model validation. The correlation coefficient of thermal resistance is higher as compared to the thermal conductivity which indicates that the thermal resistance have almost similar trend to the experimental results but both have similar amount of mean absolute error as shown in Table 7.4 and Table 7.5 . Figure 7.4 and Figure 7.5 show that Model-1 has less difference with the experimental results as compared to the other two models.

Table 7.4: Comparison of the effective thermal conductivity and mean absolute error (MAE)

Fabric Code	Effective Thermal Conductivity K_{eff} (W/m.K)			
	Model-1	Model-2	Model-3	Experimental
F1	0.03152	0.02951	0.02931	0.035
F2	0.03821	0.03199	0.03000	0.0377
F3	0.04230	0.03402	0.03356	0.0403
F4	0.04110	0.02890	0.02825	0.043
F5	0.03845	0.02940	0.02880	0.0412
MAE (%)	5.470	21.57	23.56	-

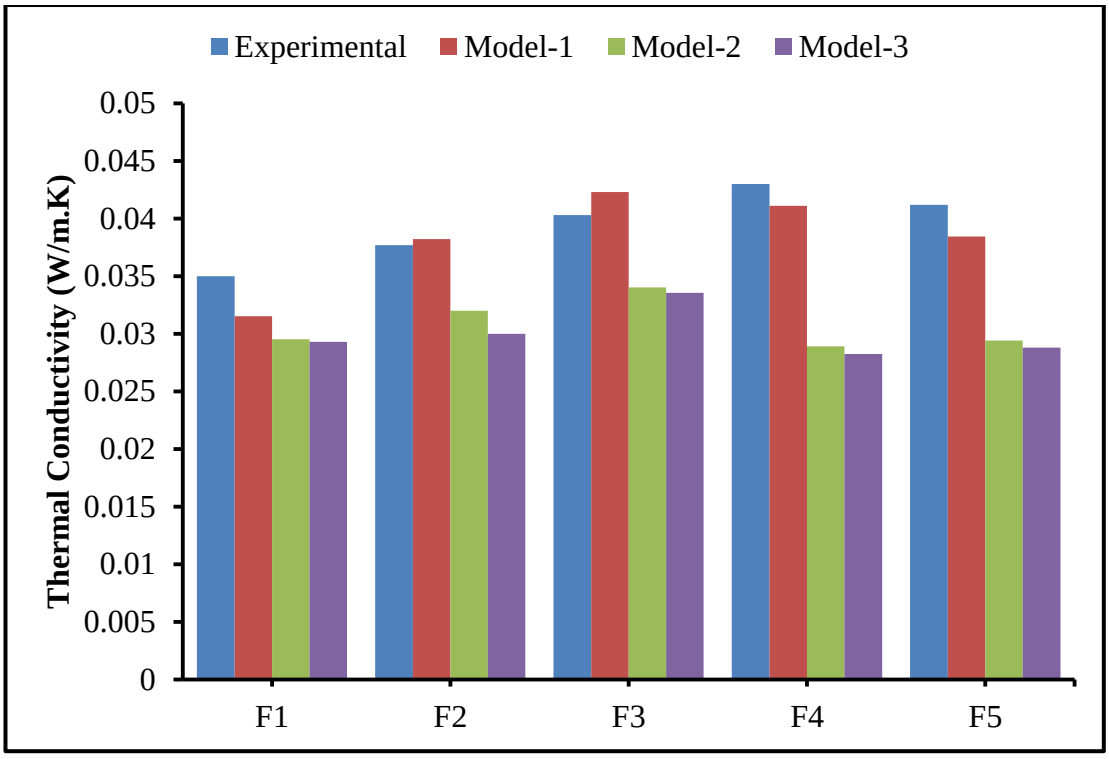

Figure 7.4: Effect of fibre orientation on effective thermal conductivity

Table 7.5: Comparison thermal resistance and mean absolute error (MAE)

Fabric Code	Thermal Resistance (m^2.K/W)			
	Model-1	Model-2	Model-3	Experimental
F1	0.015546	0.016605	0.016718	0.014
F2	0.0123	0.014692	0.015667	0.012467
F3	0.011584	0.014403	0.014601	0.012159
F4	0.019465	0.027682	0.028319	0.018605
F5	0.016853	0.022041	0.0225	0.015728
MAE (%)	5.78	28.77	32.087	-

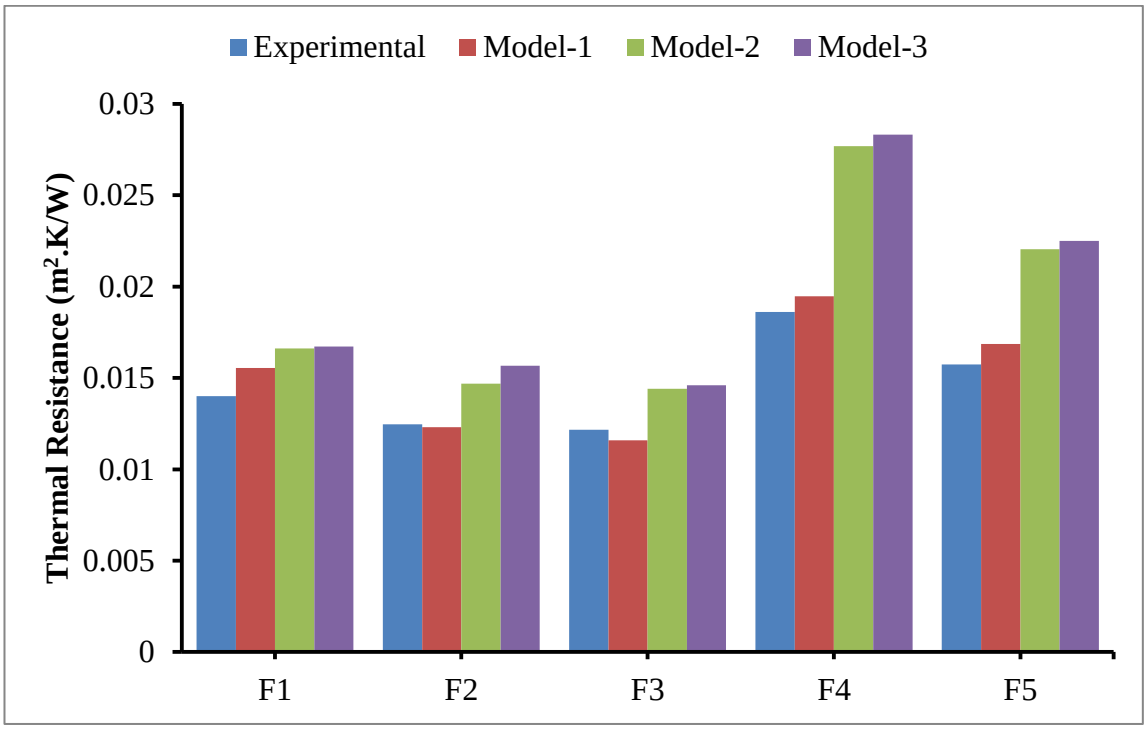

Figure 7.5: Effect of fibre orientation on thermal resistance

7.3.3 Temperature Dependent Thermal Conductivity of Fibre

Figure 7.6 shows the relationship between temperature and thermal conductivity of fibre and air. In this section temperature dependent heat transfer analysis was performed by using temperature dependent thermal conductivity of Nomex® III fibre [152] and air [180] as shown in the following relationships:

$$K_f(T) = \begin{cases} 0.13 + 0.0018(T - 300K) & \text{T} \le 700\ \text{K} \\ 1 & \text{T} > 700\ \text{K} \end{cases} \qquad 7.2$$

$$K_{air}(T) = \begin{cases} 0.026 + 0.000068\,(T - 300K) & \text{T} \le 700\ \text{K} \\ 0.053 + 0.000054\,(T - 700K) & \text{T} > 700\ \text{K} \end{cases} \qquad 7.3$$

This equation shows that the thermal conductivity of Nomex® III fibres appears to remain approximately constant after about 700 K; this temperature is close to the temperature range at which thermochemical reactions begins to occur [23].

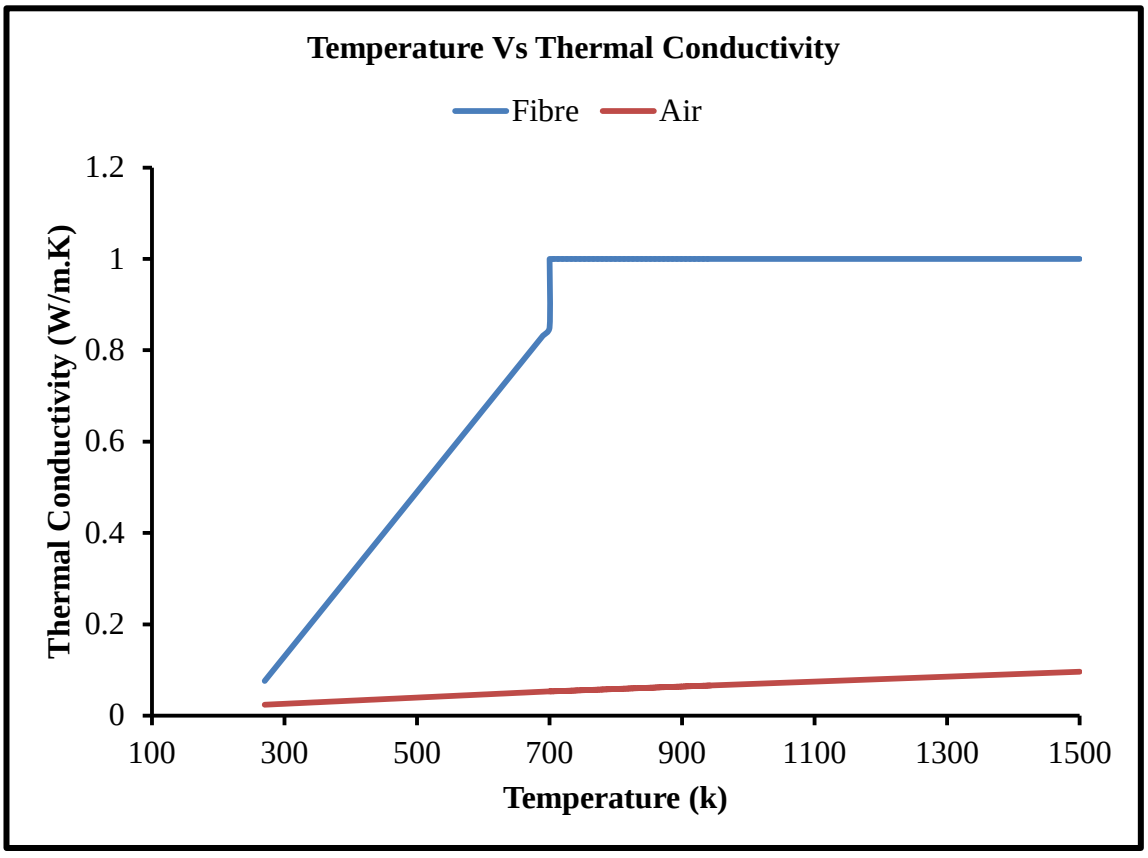

Figure 7.6: Thermal conductivity vs temperature

Nomex®III fibre has been mostly used in the heat protective clothing, for high temperature environment. Heat is transferred by means of radiation and convection outside the protective clothing and within the fabric and air gap heat is transferred by conduction and radiation.

The thermal conductivity value of fibre varies with temperature so that temperature dependent thermal conductivity of fibre was utilized to calculate the yarn axial and transverse thermal conductivity between the temperature ranges from 270K to 700K.

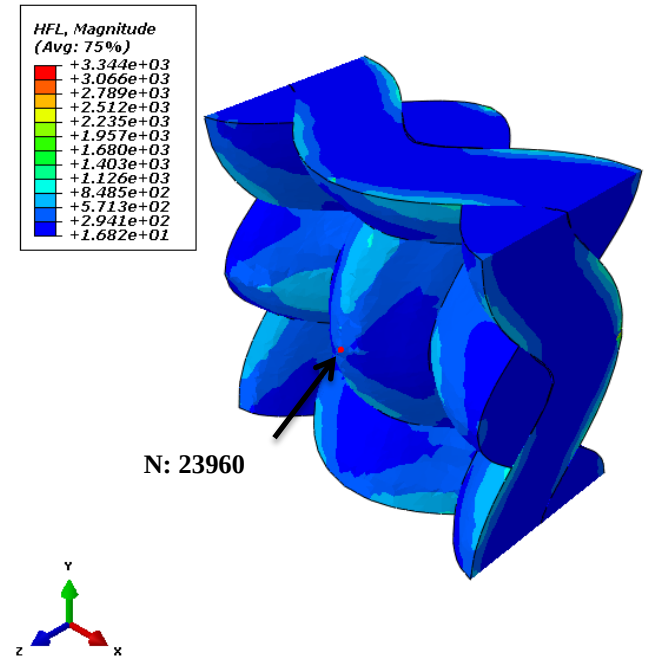

(a)

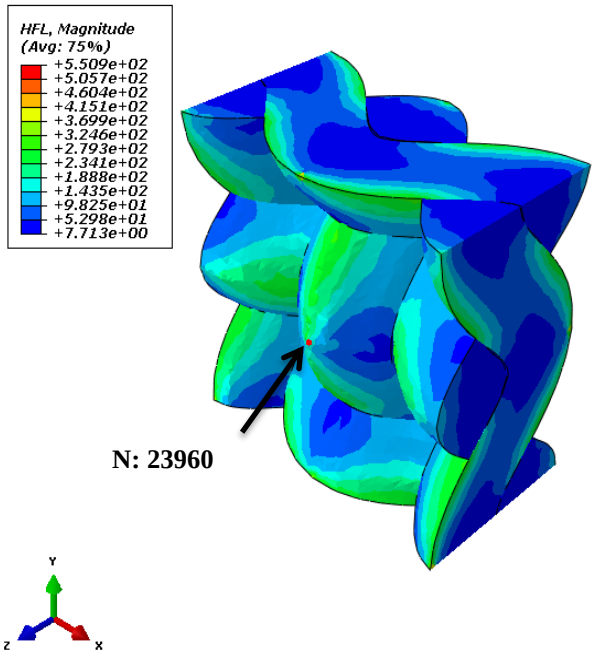

(b)

Figure 7.7: Heat flux distribution of unit cell: (a) Nomex®III with temperature dependent thermal conductivity (b) Nomex®III without temperature dependent thermal conductivity

Air properties were also considered as temperature dependent to achieve the realistic approach. Temperature specified boundary conditions were used for transient analysis. The temperatures applied on face and back of the fabric are 270K and 700K

respectively and run the analysis with and without temperature dependent thermal property. Figure 7.7 shows the heat flux distribution in both cases. Further investigation of the model to calculate the heat flux value across the thickness of the fabric is shown in Figure 7.8. Fabric analysed with temperature dependent thermal properties allows more heat to flow because fibre and air thermal conductivity both increase with the increase of temperature.

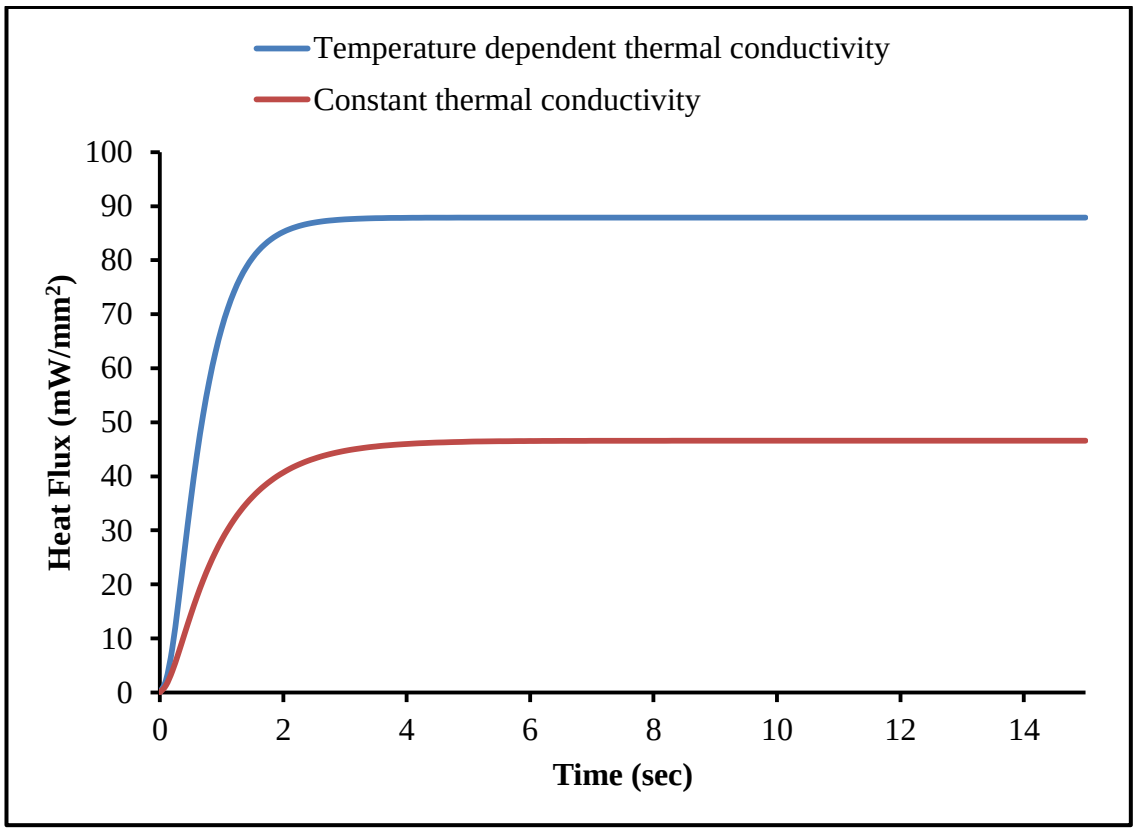

Figure 7.8: Heat flux with and without temperature dependent thermal conductivity

Figure 7.9 shows the dynamic temperature change with respect to time taking an example node 23960 specified in Figure 7.7. The node temperature in temperature dependent thermal conductivity model analysis achieved the equilibrium at 6.7 sec. while in constant thermal conductivity model it 9.4 sec. is needed to reach the equilibrium temperature. Similarly Figure 7.10 shows that the total heat flow equilibrium of fabric achieved more frequently with temperature dependent thermal conductivity. This type of analysis is more significant in heat protective clothing because multilayer fabric is exposed in high temperature environment for a long time. Therefore it is important to take temperature dependent thermal properties to create the realistic environment for simulation of heat transfer of textiles.

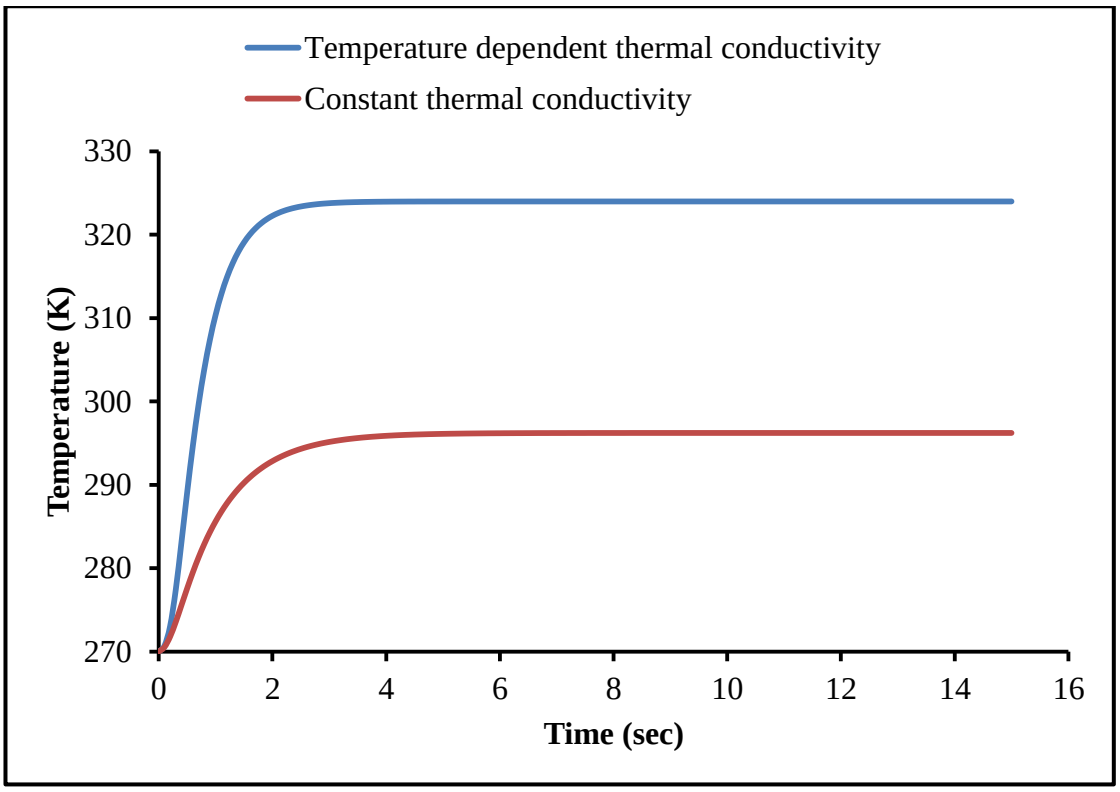

Figure 7.9: Temperature of Node: 23960 with and without temperature dependent thermal conductivity

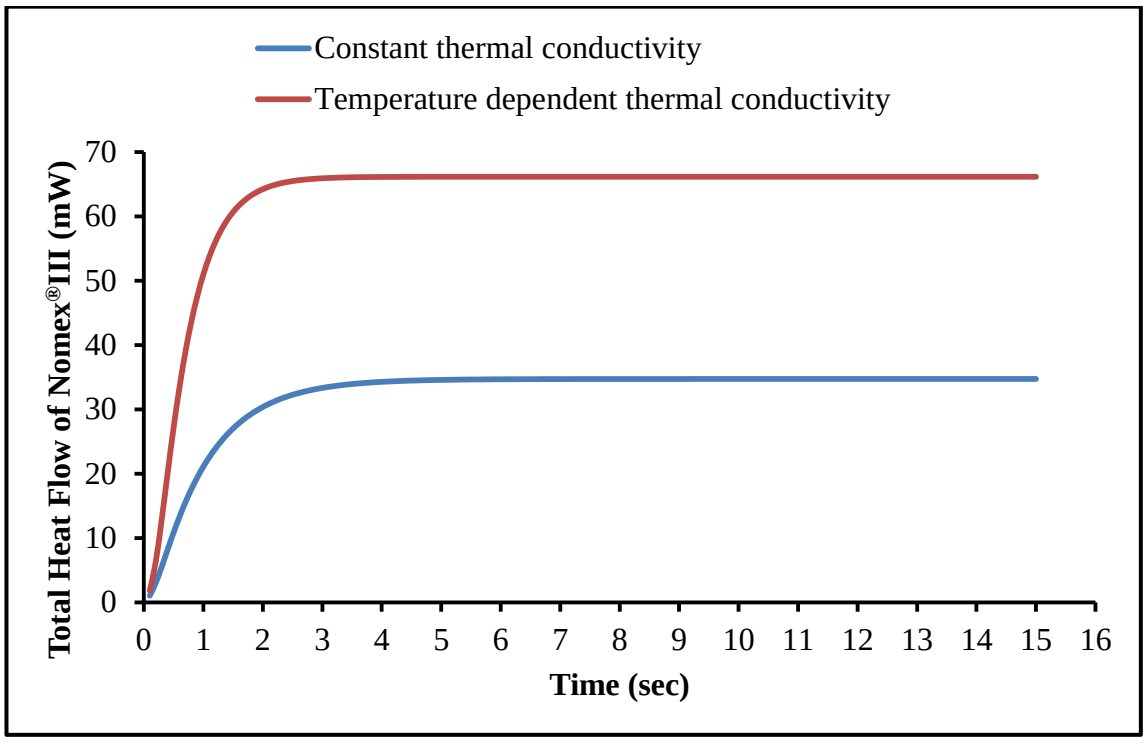

Figure 7.10: Total heat flux of fabric with and without temperature dependent thermal conductivity

7.3.4 Effect of Fibre Volume Fraction on Effective Thermal Conductivity

In this section further analysis of the validated models to evaluate some of the properties which cannot be experimentally tested have been carried out. The effect of fibre volume fraction and fibre thermal conductivity on the effective thermal conductivity and thermal resistance of fabric have been analysed.

Fabric insulation mainly depends on fibre volume fraction and thermal conductivity of fibre at constant fibre orientation. For this purpose the validated models were chosen to analyse the effect of fibre volume fraction and thermal conductivity of fibre on the overall heat transfer.

7.3.4.1 Woven Fabric

Table 7.6 and Figure 7.11 show the relationship of effective thermal conductivity with fibre volume fraction of the Twaron® fabric. It is obvious from the figure that effective thermal conductivity increases with the increase of fibre volume fraction. This can be explained by the fact that with the increase of fibre volume fraction, the content of air deceases resulting in increased thermal conductivity as compared to that with less fibre volume in the fabric.

Table 7.6: Effective thermal conductivity of Twaron® with different fibre volume fractions

V_{fy} (%)	K_{ya} (W/m.K)	K_{yt} (W/m.K)	K_{eff} (W/m.K)
10	0.3284	0.028461	0.03062
20	0.6308	0.031436	0.03471
30	0.9332	0.035105	0.03856
40	1.2356	0.039745	0.04233
50	1.538	0.045798	0.04618
60	1.8404	0.054026	0.05025
70	2.1428	0.065858	0.05473
80	2.4452	0.084324	0.06000

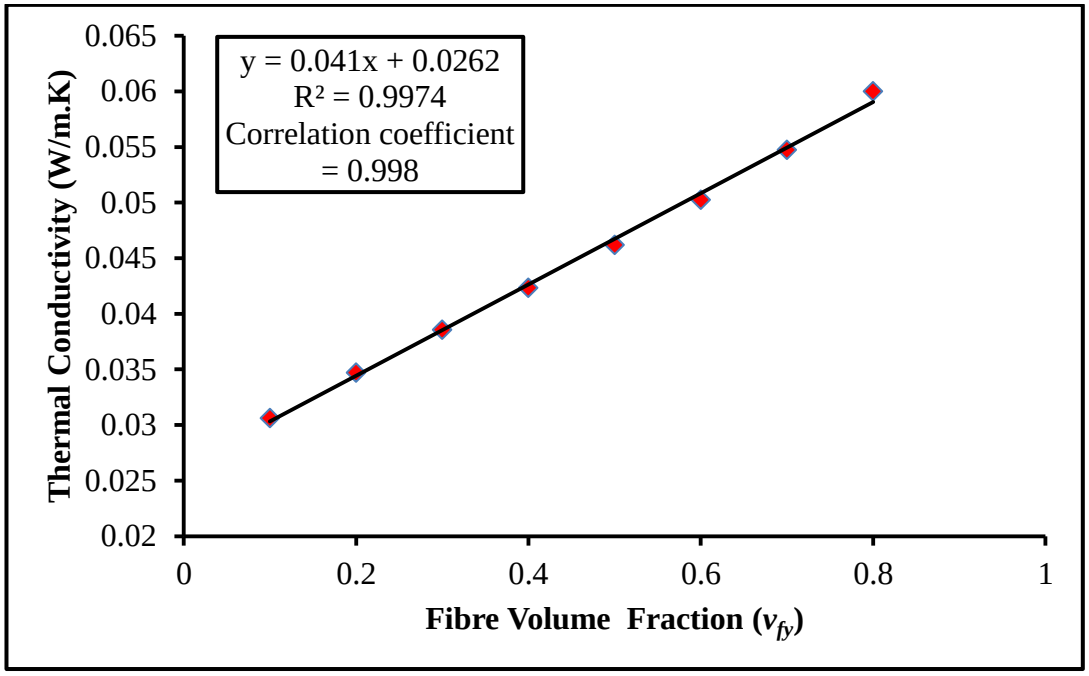

Figure 7.11: Relationship between fibre volume fraction and thermal conductivity of Twaron® fabric

7.3.4.2 Plain Weft Knitted Fabric Composites

A method is developed to determine the effective thermal conductivity of plain weft knitted composite fabric, by considering the same fabric construction specification of F3 with the amendment of fibre and matrix material. E-Glass fibres with FR-4 epoxy resin material were used for the analysis. Yarn is considered as porous material and the fibre volume/packing fraction of yarn (V_{fy}) can be calculated by:

$$V_{fy} = \frac{V_f \times V_{uc}}{V_y} \qquad 7.4$$

where V_f , V_{uc} and V_y are the fibre volume fraction unit cell, volume of unit cell and volume of yarn respectively.

Table 7.7 shows the thermal conductivities of epoxy resin and E-glass fibre.

Table 7.7. Thermal conductivity of epoxy resin and E-glass fibre

Material	Thermal conductivity (W/m.K)
FR-4 epoxy resin	0.190
E-Glass	2.25 (Longitudinal K_{fl}) [153] 0.509 (Transverse K_{ft}) [153]

Thermal conductivity of the impregnated yarn along the fibre axis (K_{ya}) can be calculated by the rule of mixture as shown in Equation 5.13.

Thermal conductivity of impregnated yarn along the transverse direction (K_{yt}) can be calculated by series models. Models made by Clayton [150] and Pilling [151] as shown in Equations 5.14-5.16.

Table 7.8 shows the effective thermal conductivity of E-glass/epoxy unit cell at different fibre volume fraction calculated by the same technique used for Model 1.

Table 7.8. Effective thermal conductivity at different fibre volume fraction

Fibre Volume Fraction of Yarn V_{fy} (%)	Fibre Volume Fraction of Unit Cell V_f (%)	Yarn thermal Conductivity in axial direction K_{ya} (W/m.K)	Yarn thermal Conductivity in transverse direction K_{yt} (W/m.K)	Effective Thermal Conductivity K_{eff} (W/m.K)
10	1.29	0.396	0.203	0.1933
20	2.59	0.602	0.217	0.1967
30	3.89	0.808	0.234	0.2002
40	5.19	1.014	0.254	0.2038
50	6.49	1.220	0.277	0.2076
60	7.79	1.426	0.305	0.2116
70	9.09	1.632	0.338	0.2160
80	10.39	1.838	0.381	0.2200

Note: K_{yt} was calculated by series model.

Figure 7.12 shows the effective thermal conductivity of plain E-glass/epoxy weft knitted composites. The thermal conductivity increases with the increase of fibre volume fraction. The fact is that in order to improve strength and thermal insulation property of composite structures the lower thermal conductivity of matrix material should be used with high fibre volume fraction.

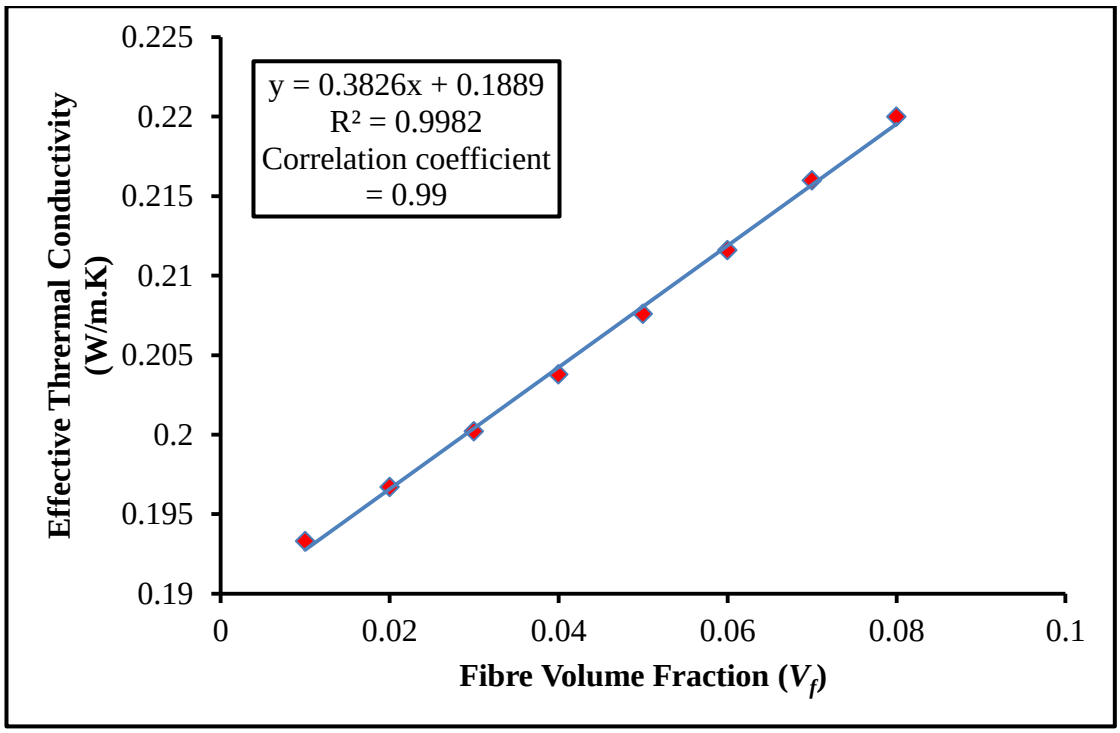

Figure 7.12: Effective thermal conductivity at different V_f

7.3.4.3 Nonwoven Fabric

Table 7.9 and Figure 7.13 show the effective thermal conductivity and thermal resistance of thermally bonded nonwoven at different levels of fibre volume fraction. It can be clearly observed that the effective thermal conductivity increases with the increase of fibre volume fraction and it reverses in case of thermal resistance.

Table 7.9: Effective thermal conductivity and thermal resistance of nonwoven fabric at different fibre volume fraction

Fibre volume fraction of fibrous portion, V_{fp} (%)	Fibre Volume Fraction of unit cell, V_f (%)	Thermal Conductivity of fibrous portion, K_{fp}* (W/m.K)	Predicted effective thermal conductivity K_{eff} (W/m.K)	Predicted thermal resistance R (m^2.K/W)
5.000	5.17	0.027035	0.02716	0.019882
10.00	7.85	0.028156	0.02775	0.019459
15.00	10.52	0.029374	0.02837	0.019034
20.00	13.20	0.030702	0.02905	0.018589
25.112	15.95	0.03219	0.02981	0.018115

* K_{fp} calculated on the bases of transverse thermal conductivity of fibre

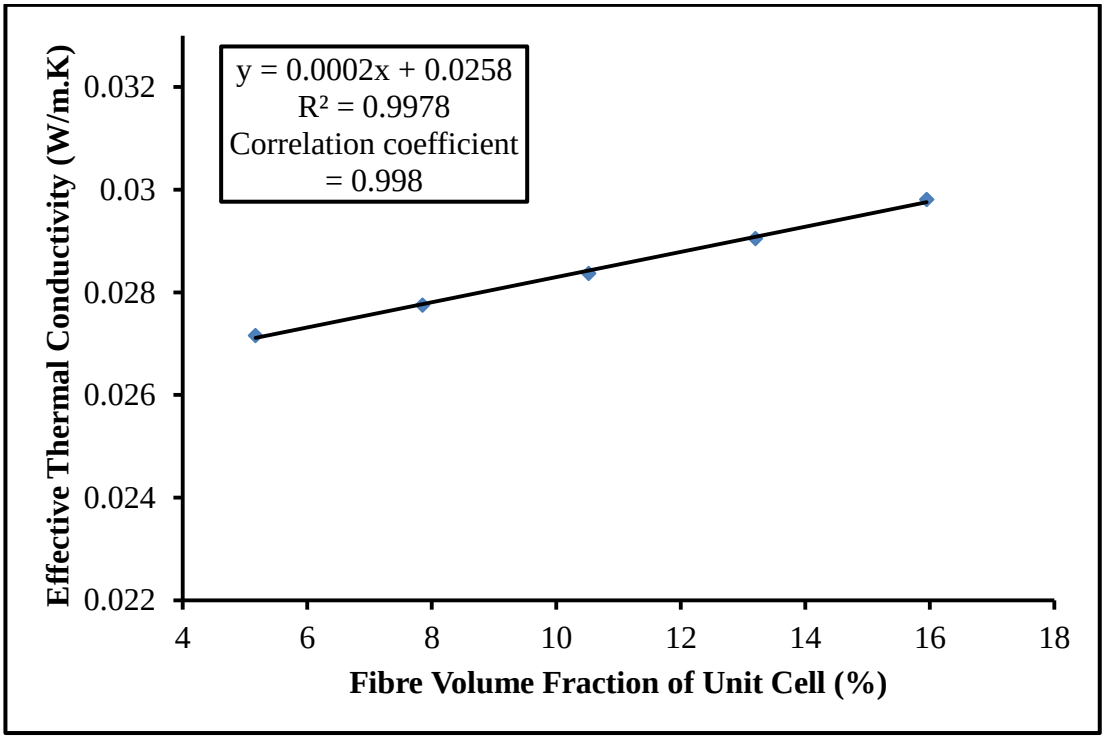

(a)

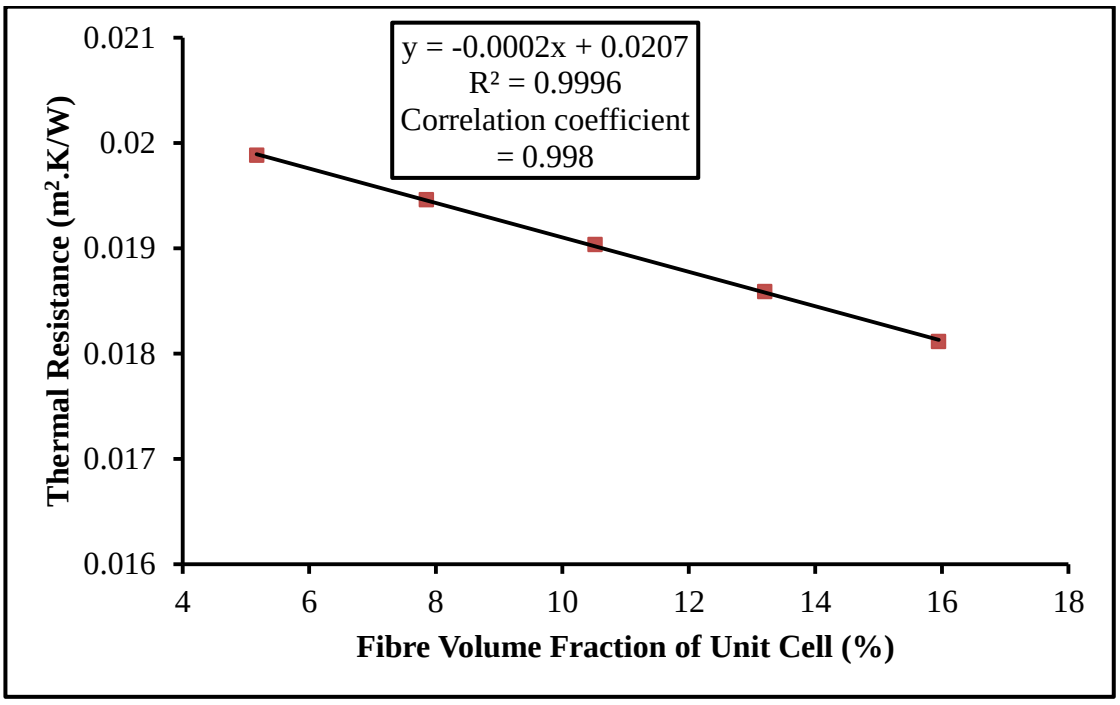

(b)

Figure 7.13: Relationship between: (a) Fibre volume fraction and thermal conductivity of sample-1 nonwoven fabric and (b) Fibre volume fraction and thermal resistance of sample-1 nonwoven fabric

7.3.4.4 MicroPCMs Composites

Furthermore the effect of core content on effective thermal conductivity of MicroPCMs composites has been investigated by keeping the volume fraction of MicroPCMs in matrix constant (10%). For that purpose the volume fraction of core within the microcapsules has been decreased and it was found that the effective thermal conductivity increases with the decrease of core content. This is caused by the higher thermal conductivity of shell material (melamine formaldehyde) compared to core material (n-octadecane) as shown in Figure 7.14. The results from FEA were agreed well with the results obtained from Maxwell's model as shown in Figure 7.14. The fact is that the shell thickness or core content has effect on effective thermal conductivity; it will increase or decrease depending on the thermal conductivity values of both materials.

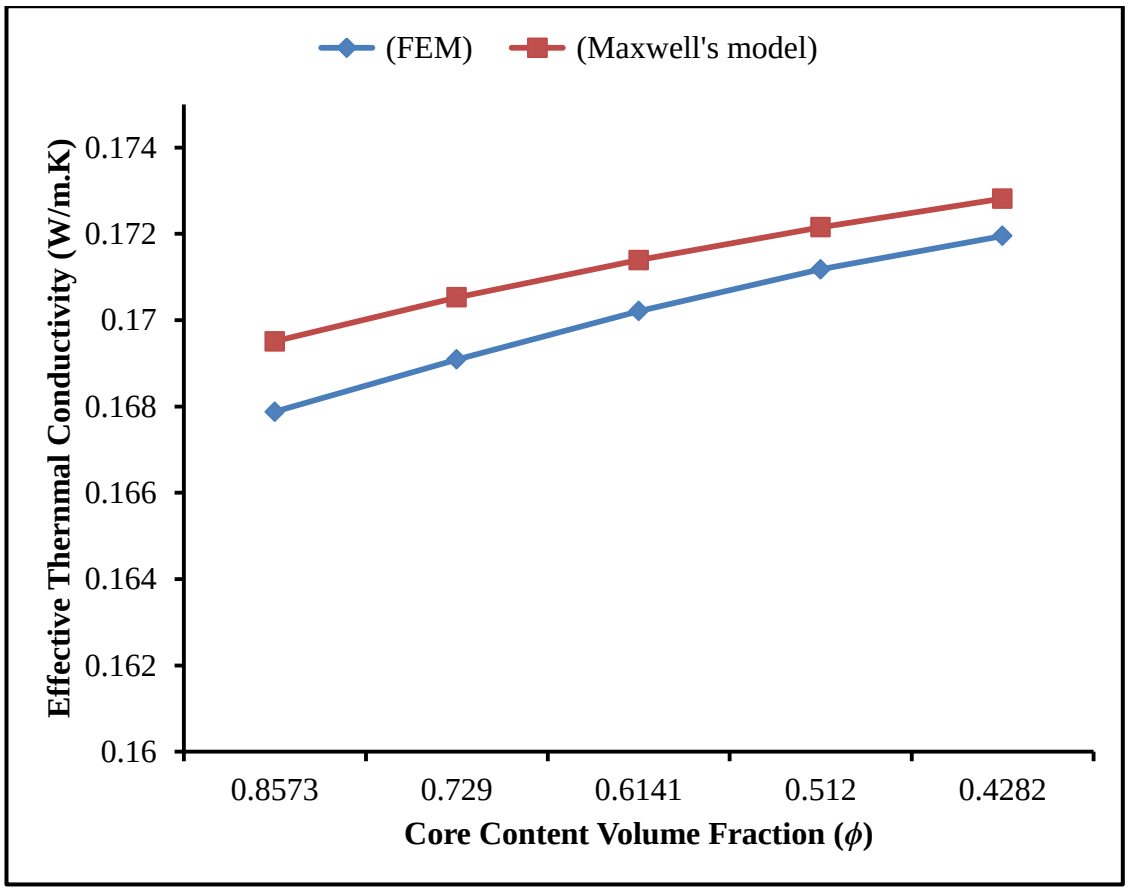

Figure 7.14: Effect of core content on effective thermal conductivity

7.4 Effect of PCM on Temperature Change vs Time

Figure 7.15 shows the unit cell model of MicroPCMs composite of acrylic binder and microcapsules which contain 20 percent volume fraction of Micro capsules. In order to

evaluate the effect of PCM on temperature change with respect to time, a transient heat transfer analysis was carried on unit cell by applying temperature specified boundary condition as shown in Figure 7.15. The initial temperature (273.15K) was applied on wall A, B, C, D and E at time zero second and a constant temperature (308.15K) was applied on wall E throughout the analysis.

A node was selected shown in Figure 7.15 to analyse the effect of PCM (latent heat) on temperature. Figure 7.16 (a) shows the heating curve of the selected node of MicroPCMs composite with PCM and without latent heat (during the analysis latent heat property of core material was removed). It shows clearly that during the analysis temperature of the node with PCM is increased slowly as compared to that of without latent heat. The highlighted portion in the graph of Figure 7.16 (a) shows that the PCM absorbs energy and changes its phase from solid to liquid while in the without latent heat its temperature increment uniformly. This phase change phenomena delayed the temperature change for the PCM composite.

Figure 7.16 (b) shows the cooling phenomena in which the initial temperature of 308.15K was used and 273.15K was applied on wall E. The effect is reverse to the heating phenomena. Without latent heat property of composite cooled and loses energy rapidly as compared to PCM composite.

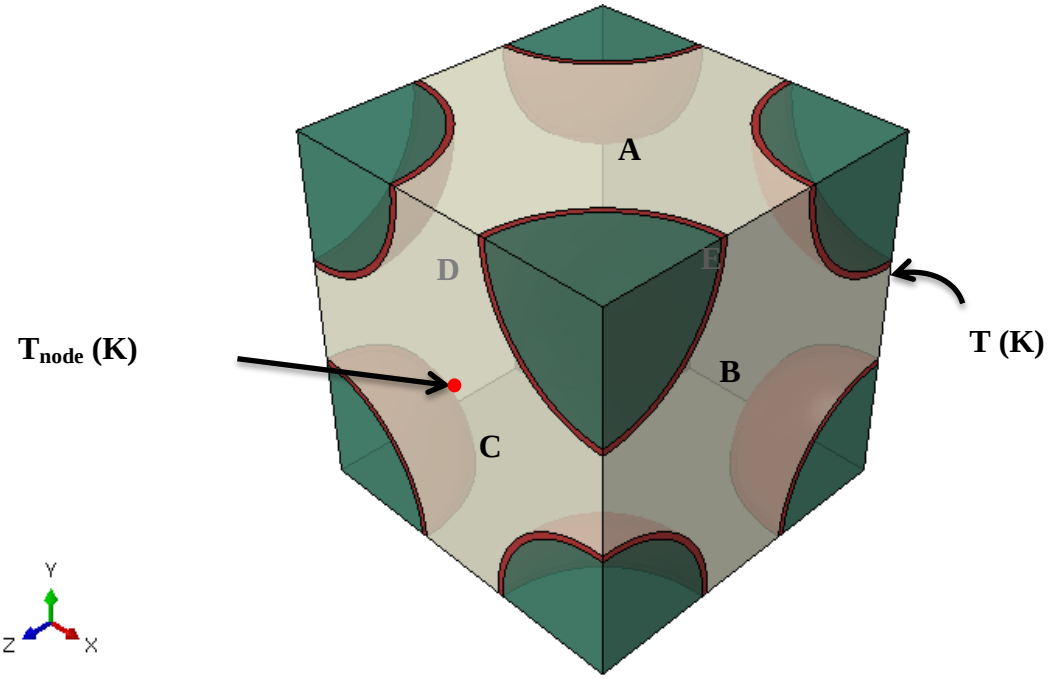

Figure 7.15: Unit cell model with boundary conditions

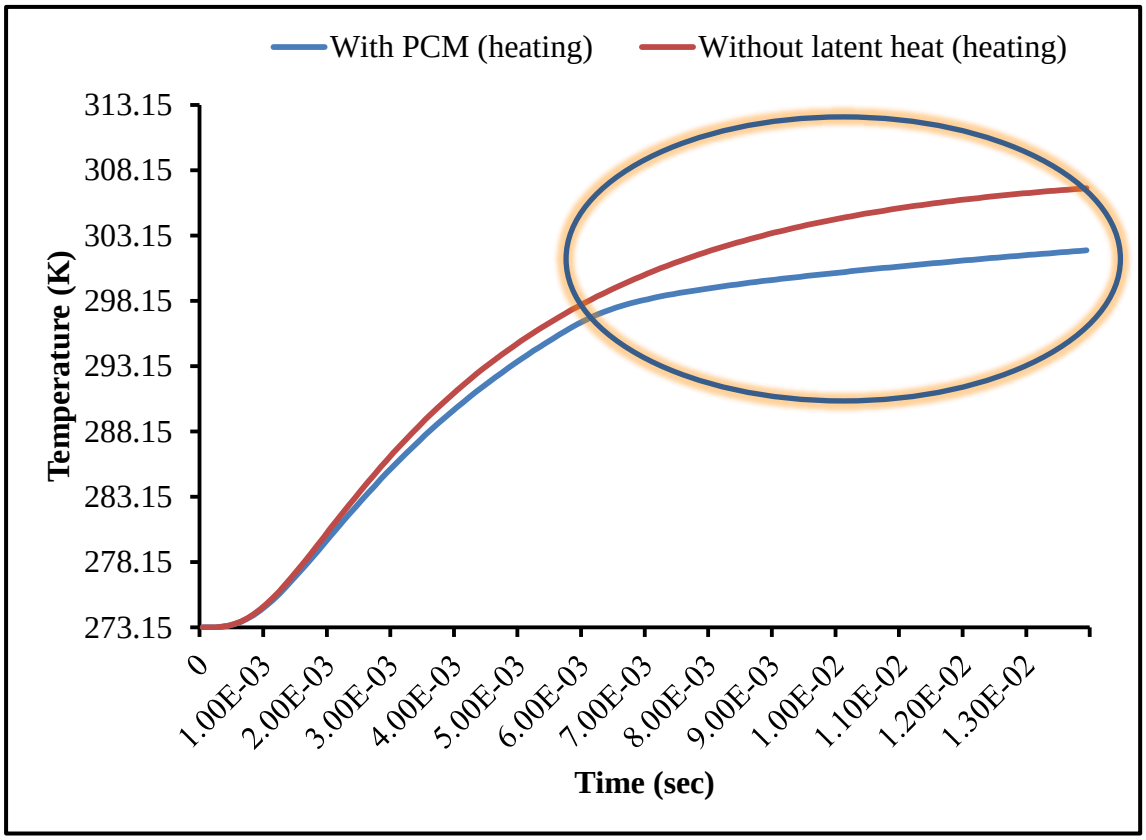

(a)

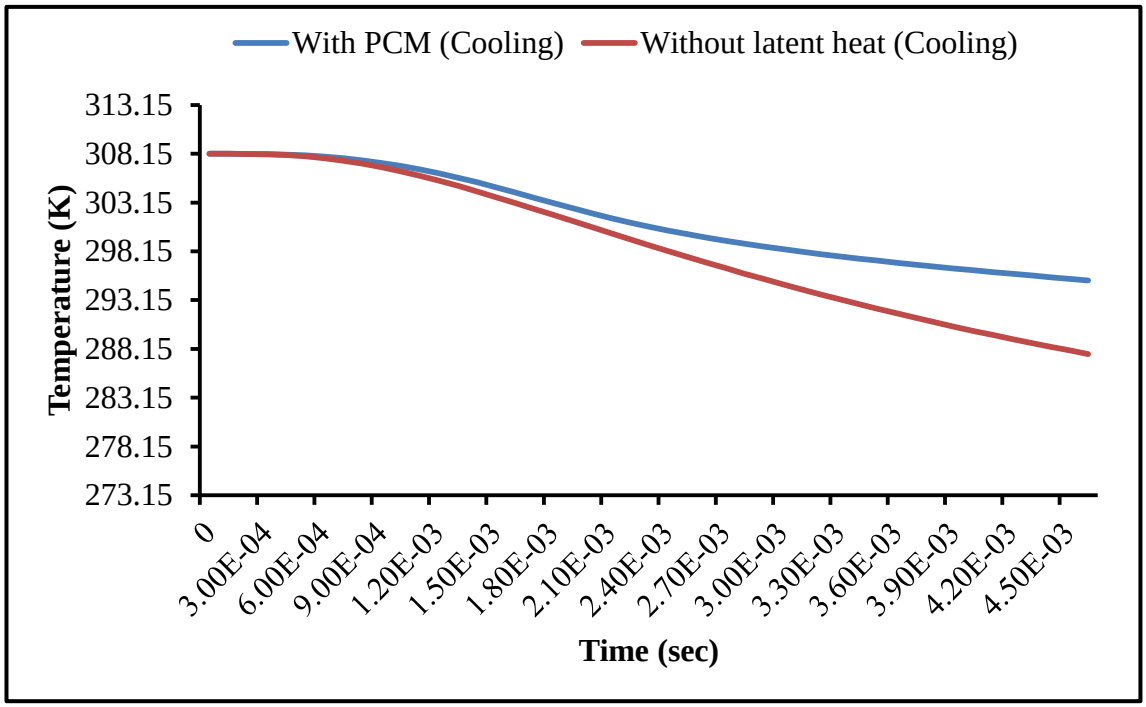

(b)

Figure 7.16: Heat and cooling curve at node of composites: (a) With PCM and (b) Without latent heat

Figure 7.17 shows that heating and cooling curve of the node in composites with and without MicroPCMs. Figure 7.17 (a) shows the heating phenomena in which initial temperature of MicoPCMs composite rises more rapidly. Due to the fact that the thermal conductivity of microcapsules is high as compared to matrix material, when the simulation process reaches to the stage that phase change phenomena starts and the temperature of MciroPCMs composite drops down, or vice versa for the cooling case.

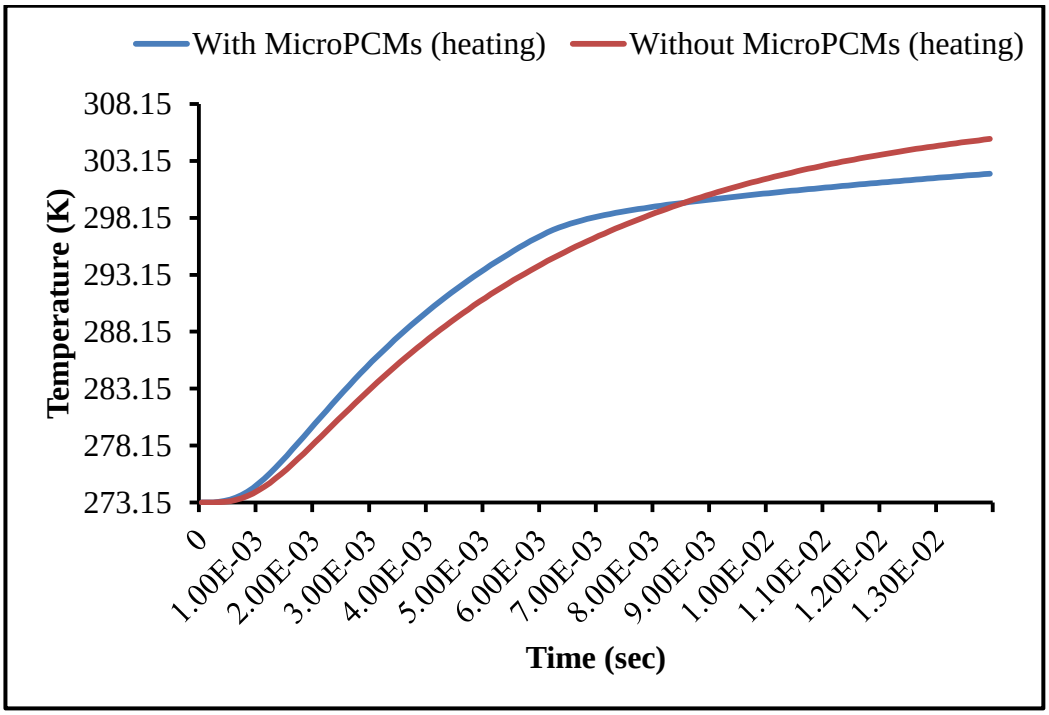

(a)

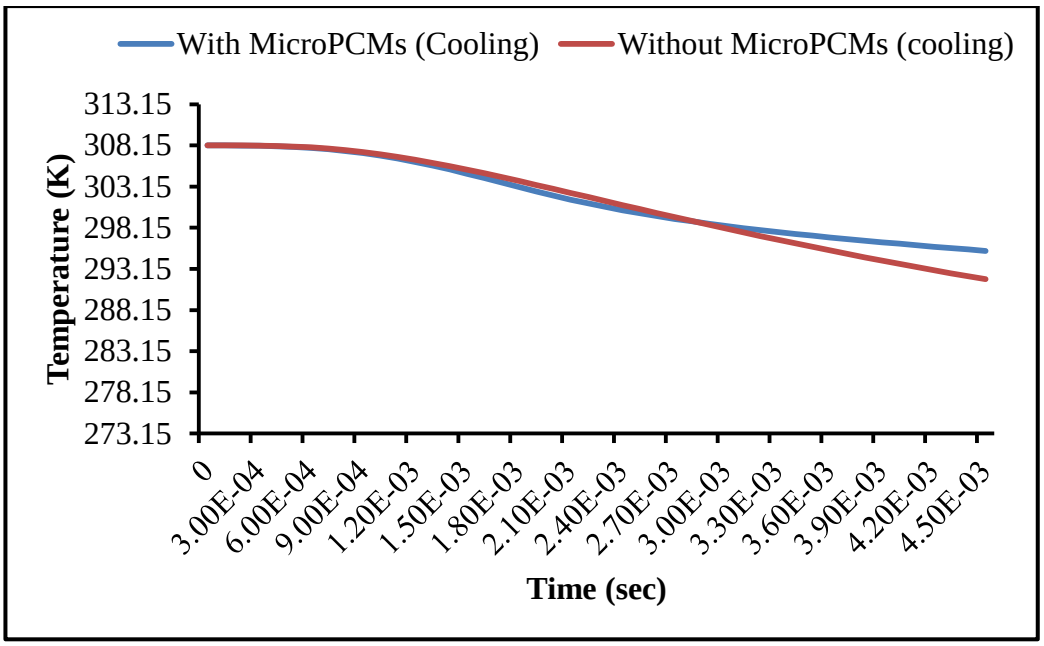

(b)

Figure 7.17: Heat and cooling curve at node of composites (a) With PCM and (b) Without PCM

Figure 7.18 shows the heating and cooling curve of the node of composites with different configurations within the solidus and liquidus temperature range of the core content (phase change material). The method described above is to predict the effective thermal conductivity of MicroPCMs composite and can be used for any kind of polymeric materials which contain microencapsulated phase change material.

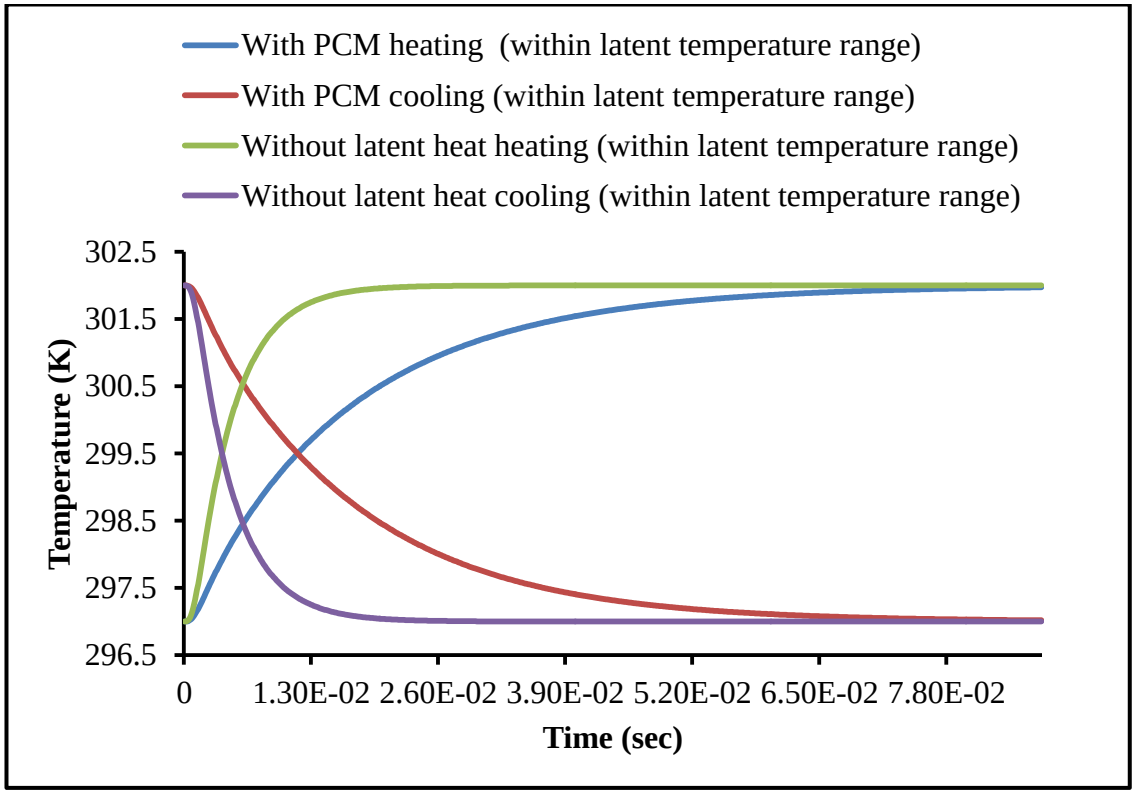

Figure 7.18: Heating and cooling curves of Composite with different configuration

7.5 Effect of Fibre Thermal Conductivity on Effective Thermal Conductivity

The validated model of sample-1 was also chosen to analyse the effect of fibre thermal conductivity on heat transfer phenomena. For this purpose a transient heat transfer analysis has been conducted by considering two different fibres polyester and polypropylene. Temperature specified boundary conditions were applied. At wall "A" 308.15 K was applied and the rest of the walls were considered at 298.15 K as shown in Figure 7.19. It clearly shows that the temperature of highlighted node of fabric made of polyester fibre achieved temperature equilibrium faster than sample-1(polypropylene fibre). The reason is that polyester fibre has higher thermal conductivity than polypropylene fibre.

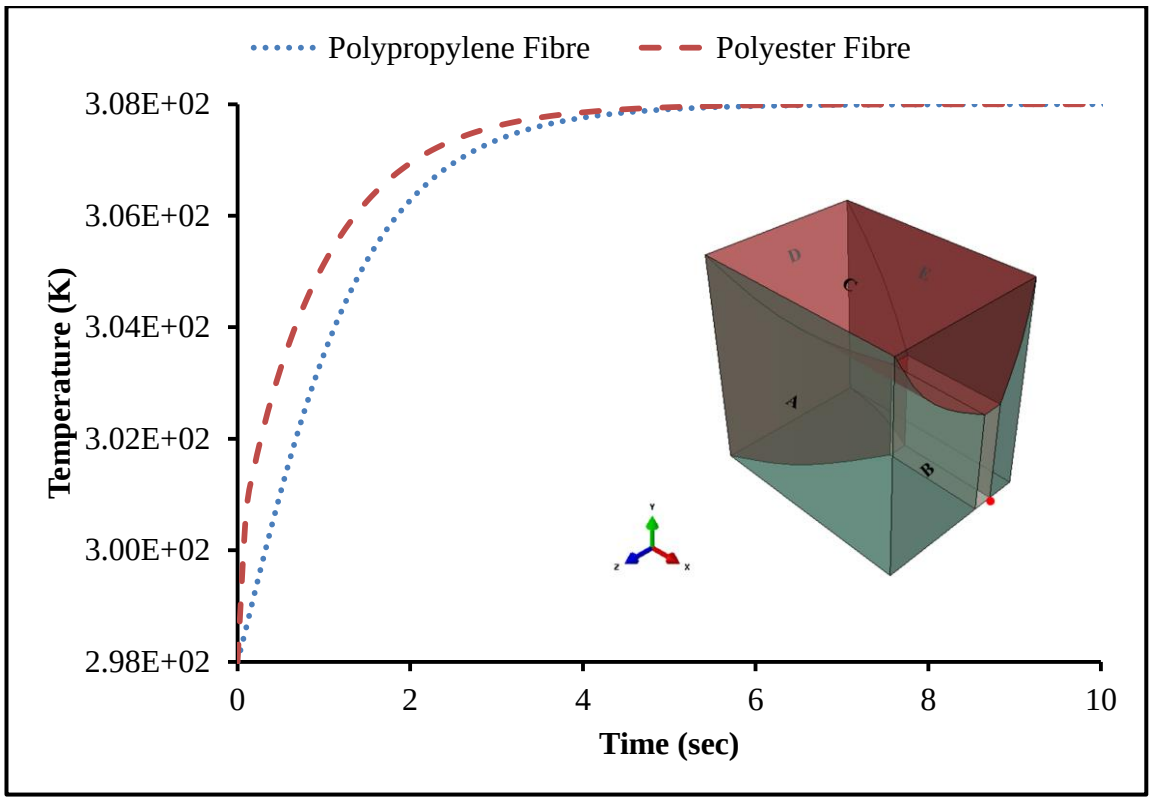

Figure 7.19: Temperature profile of highlighted node of polypropylene and polyester sample-1

7.6 Summary

In this chapter the developed finite element fabric models were successfully validated and analysed by the commercial finite element software Abaqus/CAE. The conclusion was based on the strong correlation in effective thermal conductivity of fabrics between experimental results and the predicted results from finite element models.

Statistical results such as mean absolute error, correlation coefficient and time dependent analysis from validated models revealed that the thermal anisotropy of fibres, fibres material orientation and temperature dependent thermal conductivity of fibre have significant impact on the effective thermal conductivity of fabrics.

Chapter 8 Conclusions and Future Work

8.1 Conclusions

The aim of this research was to develop finite element models to predict the effective thermal conductivity and thermal resistance of textile structures by using finite element method. In addition to the finite element modelling, this research work also covers the design and development of an experimental setup for measurement of fabric thermal property and plug-ins to generate different textile structures. This chapter gives conclusions and future recommendations of this research project.

The following objectives set for completing this PhD research include: (1) to develop an experimental setup for evaluation of the thermal conductivity and thermal resistance of textile structures; (2) to develop finite element models of textile structures by using the actual geometrical parameters and material thermal properties; (3) to develop a user friendly Graphical interface (GUI) plug-ins in Abaqus/CAE environment by using python scripting, to enable automatically generate geometrical models and calculate the effective thermal conductivity of textile structures; (4) to validate the finite element models by comparing results from model calculation and obtained from experimental setup and (5) to analyse and investigate the effect of thermal anisotropy, temperature dependent thermal conductivity, fibre volume fraction and fibre orientation on the effective thermal conductivity of textile structures based on the validated finite element models.

The following conclusions have been achieved from this research work:

(a) Prediction of effective thermal conductivity and thermal resistance

In this research the finite element geometric models of fabrics were successfully developed and analysed by the commercial finite element software Abaqus/CAE. Good correlation coefficients and coefficient determinations show the success of the developed finite element models for the prediction of effective thermal conductivity and thermal resistance of fabrics. The following findings have been established from the validated finite element models from parametric studies:

1) Material orientation has significant effect on the effective thermal conductivity of fabrics due to the effective thermal conductivity obtained from the models.
2) The effective thermal conductivity of fabrics was also affected by anisotropy of thermal conductivity of fibres because fibres have higher thermal conductivity in longitudinal direction as compared to the transverse direction. This explains the fact that heat also travels along the fibre direction in the yarn when determining the thermal conductivity across the thickness of fabric.
3) Temperature dependent thermal properties have significant impact on heat flow phenomena. It concludes that when simulating fabrics for protective clothing where fabrics are exposed to extreme temperature environment for a long time, it is important to take temperature dependent thermal properties to create a realistic simulation.
4) An advanced modelling technique was successfully established to develop a two scale finite element model of woven fabrics coated by microencapsulated PCM. At the microscopic level of analysis it has been found that the temperature increment of composites containing microencapsulated PCM was slow compared to non-PCM composites as a result of phase change phenomena.

(b) Design and development of experimental setup for testing thermal conductivity

1) Another achievement of this research was successful design and establishment experimental setup using two plates method. A good correlation coefficient and coefficient of determination between results obtained from the developed device and commercial instruments show the reliability of the developed setup in determining the thermal conductivity and thermal resistance of fabrics.
2) The setup can also be used for transient heat transfer analysis by using software to evaluate the heat flow rate with respect to time, and the cooling rate of a fabric by utilising the hot plate only.

(c) Development of user friendly GUI Plug-ins

1) One more achievement of the present work is the development of GUI-plugins in Abaqus/CAE environment, which can be used to automatically create geometrical models of monofilament plain weft knitted fabric, multifilament plain weft knitted fabric, plain weave composite and micro-scale unit cell model of Microencapsulated PCM composites respectively in order to avoid meshing

and analysis problems occur when importing geometrical models and parts created from other software packages.

2) A strong correlation coefficient and low absolute mean error confirm that the models created from the developed plug-ins are capable of predicting the effective thermal conductivity.
3) Furthermore comprehensive scripts have been established as an extended application tool for the determination of the porosity of plain weft knitted fabric and the effective thermal conductivity of plain weave and PCM coated fabric composites.

8.2 Recommendations for Future Research Work

In terms of the experimental setup the following areas may be explored further.

1) The experiment setup can have a significant development enabling it to visualise and analyse the heat flow rate and temperature with respect to time for transient heat transfer analysis. For that purpose, customised software will need to be developed by using any programming language which acquires data from temperature and heat flux sensors.

In terms of finite element simulation the following points may be considered for future research.

1) Finite element models developed in this research work is restricted to the 2D woven, knitted and nonwoven fabrics; they can be further extended to 3D and multi-layered textile structures.
2) In case of nonwoven fabrics, the exact material orientation can be obtained by image analysis of 2D reconstructed stack sliced image of nonwoven fabric for higher accuracy.

In terms of GUI plug-ins the following points may be considered for future research.

1) Further studies are required to develop new scripts for new GUI plug-ins which are capable of generating different structures of woven and knitted fabric.
2) Microencapsulated PCM plug-in can further be improved to analyse the transient heat transfer.

REFERENCES

[1]. Yoon, H.N., Sawyer, L.C., and Buckley, A., *Improved Comfort Polyester: Part II: Mechanical and Surface Properties.* Textile Research Journal, 1984. **54**(6): p. 357-365.

[2]. Ghali, K., Ghaddar, N., and Jones, B., *Phase change in fabrics*, in *Thermal and moisture transport in fibrous materials*, Pan, N. and Gibson, P., Editors. 2006, Woodhead Publishing Ltd: North America. p. 402-423.

[3]. Siddiqui, M.O.R. and Sun, D., *Automated model generation of knitted fabric for thermal conductivity prediction using finite element analysis and its applications in composites.* Journal of Industrial Textiles, 2014.

[4]. Yamashita, Y., Yamada, H., and Miyake, H., *Effective thermal conductivity of plain weave fabric and its composite material made from high strength fibers.* Journal of Textile Engineering, 2008. **54**(4): p. 111-119.

[5]. Li, Y., *The science of clothing comfort.* Textile Progress, 2001. **31**(1-2): p. 1-135.

[6]. Matusiak, M. and Kowalczyk, S., *Thermal-insulation properties of multilayer textile packages.* Autex Research Journal, 2014. **14**(4): p. 299-307.

[7]. Huang, J., *Sweating guarded hot plate test method.* Polymer Testing, 2006. **25**(5): p. 709-716.

[8]. Mondal, S., *Phase change materials for smart textiles–an overview*. Applied Thermal Engineering, 2008. **28**(11): p. 1536-1550.

[9]. Siddiqui, M.O.R. and Sun, D., *Computational analysis of effective thermal conductivity of microencapsulated phase change material coated composite fabrics.* Journal of Composite Materials, 2014.

[10]. Fengzhi, L. and Ren, P. *Influences of the PCM microcapsules on thermal properties of the garment*. in *First International Conference on Information Sciences, Machinery, Materials and Energy*. 2015. Atlantis Press.

[11]. Bühler, M., et al., *Heat protection by different phase change materials.* Applied Thermal Engineering, 2013. **54**(2): p. 359-364.

[12]. Xu, J.Y., et al. *Influence of Layer Configuration on Protecting Effect of Thermal Protective Clothing Containing PCM*. in *Advanced Materials Research*. 2013. Trans Tech Publ.

[13]. Wang, Y., et al., *Effects of inner and outer clothing combinations on firefighter ensembles' thermal-and moisture-related comfort levels.* Journal of the Textile Institute, 2013. **104**(5): p. 530-540.

[14]. Chen, C., Wang, L., and Huang, Y., *Electrospinning of thermo-regulating ultrafine fibers based on polyethylene glycol/cellulose acetate composite.* Polymer, 2007. **48**(18): p. 5202-5207.

[15]. Shin, Y., Yoo, D.-I., and Son, K., *Development of thermoregulating textile materials with microencapsulated phase change materials (PCM). II. Preparation and application of PCM microcapsules.* Journal of Applied Polymer Science, 2005. **96**(6): p. 2005-2010.

[16]. Nelson, G., *Microencapsulation in textile finishing.* Review of progress in coloration and related topics, 2001. **31**(1): p. 57-64.

[17]. Sánchez, P., et al., *Development of thermo-regulating textiles using paraffin wax microcapsules.* Thermochimica Acta, 2010. **498**(1): p. 16-21.

[18]. Ukponmwan, J.O., *The thermal-insulation properties of fabrics.* Textile Progress, 1993. **24**(4): p. 1-57.

[19]. Peirce, F.T. and Rees, W.H., *The transmission of heat through textile fabrics-part II.* Journal of the Textile Institute (Transactions), 1946. **37**(9): p. T181.

[20]. Farnworth, B., *Mechanism of heat flow through clothing insulation.* Textile Research Journal, 1983. **53**(12): p. 717-725.

[21]. Çengel, Y.A., *Basics of heat tranfer*, in *Heat transfer : a practical approach*. 2003, McGraw-Hill. p. 1-60.

[22]. Saville, B.P., *Comfort*, in *Physical testing of textiles*. 2002, Woodhead Publishing Limited: Cambridge, England. p. 209-243.

[23]. Torvi, D.A., *Heat transfer in thin fibrous materials under high heat flux conditions, PhD Thesis*, in *Department of Mechanical Engineering*. 1997, University of Alberta: Alberta.

[24]. Song , G., et al., *Modeling the thermal protective performance of heat resistant garments in flash fire exposures.* Textile Research Journal, 2004. **74**(12): p. 1033-1040.

[25]. Zhou, Y., *Development of lightweight soft body armour for ballistic protection, PhD Thesis*, in *School of Materials*. 2013, The University of Manchester.

[26]. Carr, D., *Ballistic-protective clothing and body armour*. Protective Clothing: Managing Thermal Stress, 2014: p. 146.

[27]. Starr, C.L., et al., *Thermal effects of design and materials on QuadGard™ body armor systems.* Clothing and Textiles Research Journal, 2015. **33**(1): p. 51-63.

[28]. El Aidani, R., et al., *Photochemical aging of an e-PTFE/NOMEX® membrane used in firefighter protective clothing.* Polymer Degradation and Stability, 2013. **98**(7): p. 1300-1310.

[29]. Fu, M., Yuan, M., and Weng, W., *Modeling of heat and moisture transfer within firefighter protective clothing with the moisture absorption of thermal radiation.* International Journal of Thermal Sciences, 2015. **96**: p. 201-210.

[30]. Kawabata, S., *Measurement of anisotropic thermal conductivity of single fiber.* Journal of the Textile Machinery Society of Japan 1986. **39**(12): p. T184-T186.

[31]. Woo, S.S., Shalev, I., and Barker, R.L., *Heat and moisture transfer through nonwoven fabrics: Part I: Heat transfer.* Textile Research Journal, 1994. **64**(3): p. 149-162.

[32]. Saldaeva, E., *Through thickness air permeability and thermal conductivity analysis for textile materials*. 2010, University of Nottingham.

[33]. Bhattacharjee, D. and Kothari, V.K., *Heat transfer through woven textiles.* International Journal of Heat and Mass Transfer, 2009. **52**(7–8): p. 2155-2160.

[34]. Baxter, S., *The thermal conductivity of textiles.* Proceedings of the Physical Society, 1946. **58**: p. 105-118.

[35]. Bogaty, H., Hollies, N.R.S., and Harris, M., *Some Thermal properties of fabrics: part I: The effect of fiber arrangement.* Textile Research Journal, 1957. **27**(6): p. 445-449.

[36]. Naka, S. and Kamata, Y., *Thermal conductivity of wet fabrics* Journal of the Textile Machinery Society of Japan 1976. **29**(7): p. T114-T119.

[37]. Schuhmeister, J., Ber. K. Akad. Wien (Math.-Naturw. Klasse), 1987. **76**: p. 283.

[38]. Ismail, M., Ammar, A., and El-Okeily, M., *Heat transfer through textile fabrics: mathematical model.* Appl.Math.Modeling, 1988. **12**: p. 434-440.

[39]. Imakoma, H., et al., *Effective thermal conductivity of fibrous insulations.* Heat Transfer - Japanese Research, 1990. **19**(7): p. 689-696.

[40]. Imakoma, H., Sang, H., and Okazaki, M., *Effective thermal conductivity of fibrous insulations.* International chemical Engineering, 1990. **30**(4): p. 738-746.

[41]. Stark, C. and Fricke, J., *Improved heat-transfer models for fibrous insulations.* International Journal of Heat and Mass Transfer, 1993. **36**(3): p. 617-625.

[42]. Sun, G., et al., *Radiant protective and transport properties of fabric used by wildland fighters.* Textile Research Journal, 2000. **70**(7): p. 567-573.

[43]. Li, Y., Zhu, Q., and Yeung, K., *Influence of thickness and porosity on coupled heat and liquid moisture transfer in porous textiles.* Textile Research Journal, 2002. **72**(5): p. 435-446.

[44]. Sun, Z. and Pan, N., *Thermal conduction and moisture diffusion in fibrous materials*, in *Thermal and moisture transport in fibrous materials*, Pan, N. and P.Gibson, Editors. 2006, Woodhead Publishing Ltd: North America. p. 439-466.

[45]. Dias, T. and Delkumburewatte, G., *The influence of moisture content on the thermal conductivity of a knitted structure.* Measurement Science and Technology, 2007. **18**(5): p. 1304-1314.

[46]. Oglakcioglu, N. and Marmarali, A., *Thermal comfort properties of some knitted structures.* Fibres & Textiles in Eastern Europe, 2007. **15**(5-6 (64-65)): p. 94-96.

[47]. Wang, M., et al., *Lattice Boltzmann modeling of the effective thermal conductivity for fibrous materials.* International Journal of Thermal Sciences, 2007. **46**(9): p. 848-855.

[48]. Cimilli, S., Nergis, F.B.U., and Candan, C., *Modeling of heat transfer measurement unit for cotton plain knitted fabric using a finite element method.* Textile Research Journal, 2008. **78**(1): p. 53-59.

[49]. Fayala, F., et al., *Neural network for predicting thermal conductivity of knit materials* Journal of Engineered Fibres and Fabrics, 2008. **3**(4): p. 53-60.

[50]. Stankovic, S.B., Popovic, D., and Poparic, G.B., *Thermal properties of textile fabrics made of natural and regenerated cellulose fibers.* Polymer Testing, 2008. **27**(1): p. 41-48.

[51]. Kothari, V.K. and Bhattacharjee, D., *Prediction of thermal resistance of woven fabrics. Part I: mathematical model.* Journal of The Textile Institute, 2009. **99**(5): p. 421-432.

[52]. Rengasamy, R., Das, B., and Patil, Y., *Thermo-physiological comfort characteristics of polyester air-jet-textured and cotton-yarn fabrics.* Journal of The Textile Institute, 2009. **100**(6): p. 507-511.

[53]. Zhu, F. and Li, K., *Determining effective thermal conductivity of fabrics by using fractal method.* International Journal of Thermophysics, 2010. **31**(3): p. 612-619.

[54]. Das, A., Alagirusamy, R., and Kumar, P., *Study of heat transfer through multilayer clothing assemblies: a theoretical prediction.* AUTEX Research Journal, 2011. **11**(2): p. 54-60.

[55]. Majumdar, A., *Modelling of thermal conductivity of knitted fabrics made of cotton–bamboo yarns using artificial neural network.* Journal of The Textile Institute, 2011. **102**(9): p. 752-762.

[56]. Ran, X., Zhu, Q., and Li, Y., *Investigation on heat and mass transfer in 3D woven fibrous material.* International Journal of Heat and Mass Transfer, 2011. **54**(15-16): p. 3575-3586.

[57]. Matusiak, M., *Modelling the thermal resistance of woven fabrics.* Journal of The Textile Institute, 2012: p. 1-12.

[58]. Hasani, H., Ajeli, S., and Nouri, N., *Modeling of heat transfer for interlock knitted fabric using finite element method.* Indian Journal of Fibre & Textile Research, 2013. **38**(4): p. 415-419.

[59]. Prakash, C. and Ramakrishnan, G., *Effect of blend ratio, loop length, and yarn linear density on thermal comfort properties of single jersey knitted fabrics.* International Journal of Thermophysics, 2013. **34**(1): p. 113-121.

[60]. Stefan, J., *Mathematische-Naturwissenschaftliche Classe Abteilung 2.* 1872. **65**: p. 45-69.

[61]. Bhattacharyya, R.K., *Heat-transfer model for fibrous insulations*, in *Thermal Insulation Performance (ASTM STP 718)*, McElrdy, D.L. and Tye, R.P., Editors. 1980, American Society for Testing and Materials. p. 272–286.

[62]. Ucar, N. and Yılmaz, T., *Thermal properties of 1×1, 2×2, 3×3 rib knit fabrics.* Fibres & Textiles in Eastern Europe, 2004. **12**(34-38).

[63]. Standard, B., *BS 4745: Determination of the thermal resistance of textiles-Two plate method: Fixed pressure procedure*. 2005, British Standard Institution.

[64]. *KES-F7 Thermo-Lab-II B, precise and fast Thermal-property measuring instrument*. Katotech Ltd: Japan.

[65]. Mahanta, N.K. and Abramson, A.R., *The dual-mode heat flow meter technique: A versatile method for characterizing thermal conductivity.* International Journal of Heat and Mass Transfer, 2010. **53**(23–24): p. 5581-5586.

[66]. *DTC-25. Thermal conductivity meter* 2014, TA Instruments: USA.

[67]. *ASTM E1530: Standard test method for evaluating the resistance of thermal transmission of materials by the guarded heat flow meter technique*. American Society for Testing and Materials.

[68]. Hes, L. and Ivan, D., *New method and equipment for measuring thermal properties of textiles.* Journal of the Textile Machinery Society of Japan, 1989. **42**: p. T124–T128.

[69]. Kothari, V.K. and Bhattacharjee, D., *Prediction of thermal resistance of woven fabrics. Part I: Mathematical model.* The Journal of The Textile Institute, 2008. **99**(5): p. 421-432.

[70]. *ASTM D 1518-85: Standard test method for thermal transmittance of textile materials*. 2003, American Society for Testing and Materials.

[71]. Cabeza, L.F., et al., *Use of microencapsulated PCM in concrete walls for energy savings.* Energy and Buildings, 2007. **39**(2): p. 113-119.

[72]. Brown, R.C., Rasberry, J.D., and Overmann, S.P., *Microencapsulated phase-change materials as heat transfer media in gas-fluidized beds.* Powder Technology, 1998. **98**(3): p. 217–222.

[73]. Hawlader, M., Uddin, M., and Khin, M.M., *Microencapsulated PCM thermal-energy storage system.* Applied Energy, 2003. **74**(1-2): p. 195–202.

[74]. Huang, M., et al., *Microencapsulated phase change slurries for thermal energy storage in a residential solar energy system.* Renewable Energy, 2011. **36**(11): p. 2932–2939.

[75]. Salaün, F., et al., *Thermoregulating response of cotton fabric containing microencapsulated phase change materials.* Thermochimica Acta, 2010. **506**(1-2): p. 82–93.

[76]. Sarier, N. and Onder, E., *Thermal characteristics of polyurethane foams incorporated with phase change materials.* Thermochimica Acta, 2007. **454**(2): p. 90-98.

[77]. Zhang, X.-X., et al., *Structures and properties of wet spun thermo-regulated polyacrylonitrile vinylidene chloride fibers.* Textile Research Journal, 2006. **76**(5): p. 351-359

[78]. Jiang, M., et al., *Preparation of PVA/paraffin thermal regulating fiber by in situ microencapsulation.* Composites Science and Technology, 2008. **68**(10-11): p. 2231–2237.

[79]. Bryant, Y. and Colvin, D., *Fibers with enhanced, reversible thermal energy storage properties*, in *Techtextil-Symposium*. 1992. p. 1-8.

[80]. Lamb, G.E. and Duffy-Morris, K., *Heat loss through fabrics under ventilation with and without a phase transition additive.* Textile Research Journal, 1990. **60**(5): p. 261-265

[81]. Pause, B., *Development of heat and cold insulating membrane structures with phase change material.* Journal of Industrial Textiles, 1995. **25**(1): p. 59-68.

[82]. Nuckols, M.L., *Analytical modeling of a diver dry suit enhanced with micro-encapsulated phase change materials.* Ocean Engineering, 1999. **26**(6): p. 547–564.

[83]. Kim, J. and Cho, G., *Thermal storage/release, durability, and temperature sensing properties Of thermostatic fabrics treated with octadecane-containing microcapsules.* Textile Research Journal, 2002. **72**(12): p. 1093-1098.

[84]. Ghali, K., et al., *Experimental and numerical investigation of the effect of phase change materials on clothing during periodic ventilation* Textile Research Journal, 2004. **74**(3): p. 205-214.

[85]. Li, Y. and Qingyong, Z., *A model of heat and moisture transfer in porous textiles with phase change materials.* Textile Research Journal, 2004. **74**(5): p. 447-457.

[86]. Fengzhi, L. and Li, Y., *A computational analysis for effects of fibre hygroscopicity on heat and moisture transfer in textiles with PCM microcapsules.* Modelling and Simulation in Materials Science and Engineering, 2007. **15**(3): p. 223.

[87]. Fengzhi, L., *Numerical simulation for effects of microcapsuled phase Change material (mpcm) distribution on heat and moisture transfer in porous textiles.* Modern Physics Letters B, 2009. **23**(3): p. 501−504.

[88]. Ying, B.-a., et al. *Mathematical modeling heat and moisture transfer in multi-layer phase change materials textile assemblies*. in *Information Engineering and Computer Science, 2009. ICIECS 2009. International Conference on*. 2009.

[89]. Bendkowska, W. and Wrzosek, H., *Experimental study of the thermoregulating properties of nonwovens treated with microencapsulated PCM.* FIBRES & TEXTILES in Eastern Europe, 2009. **17**(5): p. 87-91.

[90]. Sennur, A., Cemil, A., and Fethiye, G., *Steady-state thermal comfort properties of fabrics incorporated with microencapsulated phase change materials.* Journal of The Textile Institute, 2011. **103**(7): p. 757-765.

[91]. Yoo, H., Lim, J., and Kim, E., *Effects of the number and position of phase-change material-treated fabrics on the thermo-regulating properties of phase-change material garments.* Textile Research Journal, 2013. **83**(7): p. 671-682.

[92]. Hu, Y., et al., *Modeling thermal insulation of firefighting protective clothing embedded with phase change material.* Heat and Mass Transfer, 2013. **49**(4): p. 567-573.

[93]. Peirce, F.T., *The geometry of cloth structure.* Journal of the Textile Institute (Transactions), 1937. **28**(3): p. T45.

[94]. Behera, B.K. and Hari, P.K., *Geometrical modeling of woven fabric structure*, in *Woven Textile Structure*, Behera, B.K. and Hari, P.K., Editors. 2010, Woodhead Publishing. p. 9-29.

[95]. Hu, J., *Structural properties of fabric*, in *Structure and mechanics of woven fabrics*, Hu, J., Editor. 2004, Woodhead. p. 61-90.

[96]. Chen, X. and Hearle, J.W.S., *1 - Structural hierarchy in textile materials: an overview*, in *Modelling and Predicting Textile Behaviour*, Chen, X., Editor. 2010, Woodhead Publishing. p. 3-40.

[97]. Kemp, A., *An Extension of peirce's cloth geometry to the treatment of non-circular threads.* Journal of the Textile Institute Transactions, 1958. **49**(1): p. T44-T48.

[98]. Olofsson, B., *The setting of wool fabrics—A theoretical study.* Journal of the Textile Institute Transactions, 1961. **52**(6): p. T272-T290.

[99]. Shanahan, W.J. and Hearle, J.W.S., *An energy method for calculations in fabric mechanics part ii: examples of application of the method to woven fabrics.* Journal of the Textile Institute, 1978. **69**(4): p. 92.

[100]. Searles, K., Odegard, G., and Kumosa, M., *Micro- and mesomechanics of 8-harness satin woven fabric composites: I — evaluation of elastic behavior.* Composites Part A: Applied Science and Manufacturing, 2001. **32**(11): p. 1627-1655.

[101]. Lin, H.Y. and Newton, A., *Computer representation of woven fabric by using B-splines.* The Journal of The Textile Institute, 1999. **90**(1): p. 59-72.

[102]. Hofstee, J. and van Keulen, F., *3-D geometric modeling of a draped woven fabric*. Composite Structures, 2001. **54**(2–3): p. 179-195.

[103]. Gong, R.H., Ozgen, B., and Soleimani, M., *Modeling of yarn cross-Section in plain woven fabric.* Textile Research Journal, 2009. **79**(11): p. 1014-1020.

[104]. Backer, S., *1- An engineering approach to textile structures*, in *Structural mechanics of fibers : yarns and fabrics. Vol. 1*, Hearle, Grosberg, and Backer, Editors. 1969, Wiley-Interscience. p. 1-59.

[105]. Sherburn, M. *TexGen software*. [cited 2012 March]; Available from: http://texgen.sourceforge.net/index.php/Main_Page.

[106]. Sherburn, M., *Geometric and mechanical modelling of textiles*. 2007, University of Nottingham.

[107]. *TexEng Software Ltd.* [cited 2012 March]; Available from: http://www.texeng.co.uk/.

[108]. Hearle, J.W.S. *TechText CAD.* [cited 2012 March]; Available from: http://www.tensiontech.com/software/techtext_cad.html.

[109]. *WiseTex Software*. [cited 2013 April]; Available from: https://www.mtm.kuleuven.be/Onderzoek/Composites/software/wisetex.

[110]. *British Standard, BS : EN 1049-2:1994,Textiles. Woven fabrics. Construction. Methods of analysis. Determination of number of threads per unit length, British Standard Institution*.

[111]. *British Standard, BS EN ISO 139:2005, Textiles. Standard atmospheres for conditioning and testing, British Standard Institution*.

[112]. Hu, J., *Objective measurement technology of woven fabrics*, in *Structure and mechanics of woven fabrics*, Hu, J., Editor. 2004, Woodhead. p. 21-60.

[113]. Rasband, W. *ImageJ*. Available from: http://imagej.nih.gov/ij/.

[114]. Huwaldt, J.A. *Plot Digitizer*. [cited 2013 January]; Available from: http://plotdigitizer.sourceforge.net/.

[115]. Gao, C., Kuklane, K., and Holmér, I., *Cooling vests with phase change materials: the effects of melting temperature on heat strain alleviation in an extremely hot environment.* European journal of applied physiology, 2011. **111**(6): p. 1207-1216.

[116]. Chou, C., Tochihara, Y., and Kim, T., *Physiological and subjective responses to cooling devices on firefighting protective clothing.* European journal of applied physiology, 2008. **104**(2): p. 369-374.

[117]. Zhang, X.X., et al., *Fabrication and properties of microcapsules and nanocapsules containing n-octadecane.* Materials Chemistry and Physics, 2004. **88**(2–3): p. 300-307.

[118]. Li, W., et al., *Effects of ammonium chloride and heat treatment on residual formaldehyde contents of melamine-formaldehyde microcapsules.* Colloid and Polymer Science, 2007. **285**(15): p. 1691-1697.

[119]. Chen, Z. and Fang, G., *Preparation and heat transfer characteristics of microencapsulated phase change material slurry: A review.* Renewable and Sustainable Energy Reviews, 2011. **15**(9): p. 4624-4632.

[120]. COOKE, B., *The physical properties of weft knitted structures*, in *Advances in knitting technology*, Au, K.F., Editor. 2011, Woodhead Publishing Ltd. p. 34-47.

[121]. Chamberlain, J., *Hosiery yarns and fabrics : prepared for the textile trades advisory committee of the city of Leicester colleges of technology and art*. 1926: Leicester : J. W. Hemmings & Capey.

[122]. Peirce, F.T., *Geometrical principles applicable to the design of functional fabrics.* Textile Research Journal, 1947. **17**(3): p. 123-147.

[123]. Shinn, W.E., *An engineering approach to jersey fabric construction.* Textile Research Journal, 1955. **25**(3): p. 270-277.

[124]. Tompkins, E., *The science of knitting*. 1914, New York: Wiley. 330 p.

[125]. Leaf, G.A.V. and Glaskin, A., *The geometry of a plain knitted loop.* Journal of the Textile Institute Transactions, 1955. **46**(9): p. T587-T605.

[126]. Munden, D.L., *The geometry and dimensional properties of plain-knit fabrics.* Journal of the Textile Institute Transactions, 1959. **50**(7): p. T448-T471.

[127]. Hurd, J.C.H. and Doyle, P.J., *Fundamental aspects of the design of knitted fabrics.* Journal of the Textile Institute Proceedings, 1953. **44**(8): p. 561-578.

[128]. Postle, R., *Dimensional stability of plain-knitted fabrics.* The Journal of The Textile Institute, 1968. **59**(2): p. 65-77.

[129]. Kurbak, A., *Plain knitted fabric dimensions (Part II).* Textile Asia, 1998. **29**(4): p. 36-44.

[130]. Demiroz, A. and Dias, T., *A study of the graphical representation of plain-knitted structures part I: stitch model for the graphical representation of plain-knitted structures.* The Journal of The Textile Institute, 2000. **91**(4): p. 463-480.

[131]. Choi, K.F. and Lo, T.Y., *An energy model of plain knitted fabric.* Textile Research Journal, 2003. **73**(8): p. 739-748.

[132]. Kyosev, Y., Angelova, Y., and Kovar, R., *3D modelling of plain weft knitted structures of compressible yarn.* Research Journal of Textile and Apparel 2005. **9**(1): p. 88-97.

[133]. Ying-lin, L., et al., *3D modelling and simulation of fancy fabrics in weft knitting* Journal of Donghua University(English Edition), 2012. **29**(4): p. 351-358

[134]. EDANA. *What are nonwovens?* [cited 28 February 2015]; Available from: http://www.edana.org/discover-nonwovens/what-are-nonwovens-.

[135]. *BS EN ISO 9092:2011 Textiles. Nonwovens. Definition*. Textiles. Nontissés. Définition. 2011: BSI Standards Limited.

[136]. *ASTM Standard D 123-87.Standard terminology relating to textiles*. 1987, American Society for Testing Materials.

[137]. INDA. *About nonwovens* [cited 28 February 2015]; Available from: http://www.inda.org/about-nonwovens/.

[138]. *EDANA (2012), "EDANA 2012 nonwoven production statistics"*. [cited 2015 July]; Available from: http://www.edana.org/newsroom/news-announcements/news-article/2013/04/19/edana-2012-nonwoven-production-statistics.

[139]. Smith, P.A., *Technical fabric structures – 3. Nonwoven fabrics*, in *Handbook of technical textiles*, Horrocks, A.R. and Anand, S.C., Editors. 2000, Woodhead Publishing Limited: North and South America. p. 130-151.

[140]. Ostadi-Valiabad, H., *Micro and nano scale three-dimensional reconstruction of polymer electrolyte fuel cell porous layers*, in *School of Mechanical Engineering*. 2012, University of Birmingham.

[141]. *ImageVis3D 3.0.0*. NIH/NIGMS Center for Integrative Biomedical Computing (CIBC).

[142]. Rasband, W., *ImageJ*. 2013, National Institute of Helath: USA.

[143]. Otsu, N., *A threshold selection method from gray-level histograms.* Systems, Man and Cybernetics, IEEE Transactions on, 1979. **9**(1): p. 62-66.

[144]. Schmid, B., et al., *A high-level 3D visualization API for Java and ImageJ.* BMC Bioinformatics, 2010. **11**(1): p. 274.

[145]. Cignoni, P., *MesLab*. 2012, Visual Computing Lab-ISTI-CNR.

[146]. S.Baxter, *The thermal conductivity of textiles.* Proceedings of the Physical Society, 1946. **58**: p. 105-118.

[147]. Turan, R.B., et al., *Predicting the intra-yarn porosity by image analysis method.* Textile Research Journal, 2012. **82**(16): p. 1720-1728.

[148]. Barker, R.L. and Heniford, R.C., *Factors affecting the thermal insulation and abrasion resistance of heat resistant hydro-entangled nonwoven batting materials for use in firefighter turnout suit thermal liner systems.* JEFF, 2011. **6**: p. 1-10.

[149]. Kaviany, M., *Principles of heat transfer in porous media*. 2nd ed. 1995, New York: Springer.

[150]. Clayton, W.A. *Constituent and composite thermal conductivities of phenolic-carbon and phenolic-graphite ablators*. in *12th Structures, Structural Dynamics, and Materials Conference Proceedings*. 1971. California.

[151]. Pilling, M.W., et al., *The thermal conductivity of carbon fibre-reinforced composites.* Journal of Materials Science, 1979. **14**(6): p. 1326-1338.

[152]. Futschik, M.W. and Witte, L.C., *"Effective thermal conductivity of fibrous materials", General papers in heat and mass transfer, insulation, and turbonmachinery.* American Society of Mechanical Engineers, 1994. **271**: p. 123-134.

[153]. Hearle, J.W. and Morton, W.E., *Physical properties of textile fibres* 4th ed. Woodhead publishing in textiles: 68. 2008: Woodhead.

[154]. *Abaqus 6.12. User's Manual. 2012: ABAQUS Inc.*

[155]. Ayres, C.E., et al., *Measuring fiber alignment in electrospun scaffolds: a user's guide to the 2D fast Fourier transform approach.* Journal of Biomaterials Science, Polymer Edition, 2008. **19**(5): p. 603-621.

[156]. Siddiqui, M.O.R. and Sun, D., *Finite element analysis of thermal conductivity and thermal resistance behaviour of woven fabric.* Computational Materials Science, 2013. **75**: p. 45-51.

[157]. LI, Y. and ZHU, Q., *A model of heat and moisture transfer in porous textiles with phase change materials.* Textile Research Journal, 2004. **74**(5): p. 447-457

[158]. Martienssen, W. and Warlimont, H., *Handbook of condensed matter and materials data*. 2005: Springer Berlin Heidelberg.

[159]. Drin, A.P., Efanova, V.V., and Shut, N.I., *Thermal conductivity and kinetics of polymerization of an acrylate polymer coating.* Journal of Engineering Physics and Thermophysics, 1994. **66**(2): p. 164.

[160]. Ure, J.M., *An advanced lower and upper bound shakedown analysis method to enhance the R5 high temperature assessment procedure, PhD thesis*. 2013, University of Strathclyde.

[161]. Fong, J., et al. *A Design-of-Experiments plug-In for estimating uncertainties in finite element simulations*. in *Proceedings of International SIMULIA Conference*. 2009, p. 828 - 842.

[162]. Zhao, R., *Development tools for context aware and secure pervasive computing in embedded systems middleware.* 2013.

[163]. Nesládek, M., *Fatigue Prediction Utility for Abaqus/CAE.* Analysis. **6**: p. 5.

[164]. Mayer, J., Melzer, I., and Schweiggert, F., *Lightweight Plug-In-Based Application Development*, in *Objects, Components, Architectures, Services, and Applications for a Networked World*, Aksit, M., Mezini, M., and Unland, R., Editors. 2003, Springer Berlin Heidelberg. p. 87-102.

[165]. Prodanov, D. and Verstreken, K., *Automated Segmentation and Morphometry of Cell and Tissue Structures. Selected Algorithms in ImageJ*. 2012: INTECH Open Access Publisher.

[166]. Haji-Omar, M.S., *A novel workflow management system for handling dynamic process adaptation and compliance*. 2014, © Saiful Omar.

[167]. Schwarz, E.R., *Certain aspects of yarn structure.* Textile Research Journal, 1951. **21**(3): p. 125-136.

[168]. Hearle, J.W., *One-dimensional structures: Yarn geometry,* in *Structural mechanics of fibers, yarns, and fabrics*. 1969. p. 61-100.

[169]. Guidoin, R., et al., *Textile arterial prostheses: is water permeability equivalent to porosity?* Journal Of Biomedical Materials Research, 1987. **21**(1): p. 65-87.

[170]. Benltoufa, S., et al., *Porosity determination of jersey structure.* AUTEX Research Journal,, 2007. **7**(1): p. 63-69.

[171]. Ogulata, R.T. and Mavruz, S., *Investigation of porosity and air permeability values of plain knitted fabrics.* FIBRES & TEXTILES in Eastern Europe, 2010. **18**(5 (82)): p. 71-75.

[172]. Angelova, R.A., *Determination of the pore size of woven structures through image analysis.* Central European Journal of Engineering, 2012. **2**(1): p. 129-135.

[173]. Karaguzel, B., *Characterization and role of pororsity in knitted fabrics* in *Department of Textile Engineering, Chemistry, and Science*. 2004, North Carolina State University.

[174]. Dias, T. and Delkumburewatte, G.B., *The influence of moisture content on the thermal conductivity of a knitted structure.* Measurement Science and Technology, 2007. **18**(5): p. 1304-1314.

[175]. Abdolmaleki, S., Jeddi, A.A.A., and Amani, M., *Estimation on the 3D porosity of plain knitted fabric under uniaxial extension.* Fibers and Polymers, 2012. **13**(4): p. 535-541.

[176]. Delkumburewatte, G. and Dias, T., *Porosity and capillarity of weft knitted spacer structures.* Fibers and Polymers, 2009. **10**(2): p. 226-230.

[177]. Dasgupta, A. and Agarwal, R.K., *Orthotropic Thermal Conductivity of Plain-Weave Fabric Composites Using a Homogenization Technique.* Journal of Composite Materials, 1992. **26**(18): p. 2736-2758.

[178]. Park, Y.K., Kim, J.-G., and Lee, J.-K., *Prediction of thermal conductivity of composites with spherical microballoons.* Materials transactions, 2008. **49**(12): p. 2781-2785.

[179]. Maxwell, J.C., *A treatise on electricity and magnetism,* . 3rd ed. Vol. 1. 1954, New York: Dover.

[180]. Holman, J.P., *Heat transfer*. 1986, New York: McGraw-Hill Book Company.

APPENDIX

##

Plug-in Script of Plain Weft Knitted Fabric

##

AFXForm Script

```
from abaqusGui import *
from abaqusConstants import ALL
import osutils, os
import gUI_Plain_weft_knitted_DB

##########################################################################
####
# Class definition
##########################################################################
####

class GUIPlain_weft_KnittedForm(AFXForm):

#~~~~~~~~~~~~~~~~~~~~~~~~~~~~~~~~~~~~~~~~~~~~~~~~~~~~~~~~~~~~~~~~~~~~~~~~
~~~
def __init__(self, owner):

# Construct the base class.
#
AFXForm.__init__(self, owner)
self.radioButtonGroups = {}

self.cmd = AFXGuiCommand(mode=self, method='Plain_weft_Knitted_fabric',
objectName='Plain_weft_Knitted', registerQuery=False)
pickedDefault = ''
self.typeKw = AFXStringKeyword(self.cmd, 'type', True, 'Ideal Stitch loop Peirce
Model')
self.dKw = AFXFloatKeyword(self.cmd, 'Yarn_Diameter', True, 0.0)
self.wKw = AFXFloatKeyword(self.cmd, 'Wales_per_Centimeter', True, 0.0)
self.cKw = AFXFloatKeyword(self.cmd, 'Courses_per_Centimeter', True, 0.0)
self.lyKw = AFXFloatKeyword(self.cmd, 'e', True, 0.0)
self.tKw = AFXFloatKeyword(self.cmd, 'Thickness_of_Fabric', True, 0.0)
self.nKw = AFXFloatKeyword(self.cmd, 'No_of_wales', True, 1)
self.zKw = AFXFloatKeyword(self.cmd, 'No_of_courses', True, 1)

#~~~~~~~~~~~~~~~~~~~~~~~~~~~~~~~~~~~~~~~~~~~~~~~~~~~~~~~~~~~~~~~~~~~~~~~~
~~~~
def getFirstDialog(self):
```

```
import gUI_Plain_weft_KnittedDB
return gUI_Plain_weft_KnittedDB.GUI_Plain_weft_KnittedDB(self)



#~~~~~~~~~~~~~~~~~~~~~~~~~~~~~~~~~~~~~~~~~~~~~~~~~~~~~~~~~~~~~~~~~~~~~~~~
~~~~
def doCustomChecks(self):
for kw1,kw2,d in self.radioButtonGroups.values():
try:
value = d[ kw1.getValue() ]
kw2.setValue(value)
except:
pass
return True
#~~~~~~~~~~~~~~~~~~~~~~~~~~~~~~~~~~~~~~~~~~~~~~~~~~~~~~~~~~~~~~~~~~~~~~~~
~~~~
def okToCancel(self):
return False
```

AFXDATADIALOG Script

```
from abaqusConstants import *
from abaqusGui import *
from kernelAccess import mdb, session
import os

thisPath = os.path.abspath(__file__)
thisDir = os.path.dirname(thisPath)


##########################################################################
# Class definition
##########################################################################

class GUI_Plain_weft_KnittedDB(AFXDataDialog):

#~~~~~~~~~~~~~~~~~~~~~~~~~~~~~~~~~~~~~~~~~~~~~~~~~~~~~~~~~~~~~~~~~~~~~~~~~
def __init__(self, form):

# Construct the base class.
#

AFXDataDialog.__init__(self, form, 'PLUG-IN FOR PLAIN WEFT KNITTED
FABRIC',
self.OK|self.CANCEL, DIALOG_ACTIONS_SEPARATOR)

okBtn = self.getActionButton(self.ID_CLICKED_OK)
okBtn.setText('OK')
```

```
TabBook_1 = FXTabBook(p=self, tgt=None, sel=0,
opts=TABBOOK_NORMAL,
x=0, y=0, w=0, h=0, pl=DEFAULT_SPACING, pr=DEFAULT_SPACING,
pt=DEFAULT_SPACING, pb=DEFAULT_SPACING)

tabItem = FXTabItem(p=TabBook_1, text='About Plug-in', ic=None,
opts=TAB_TOP_NORMAL,
x=0, y=0, w=0, h=0, pl=6, pr=6, pt=DEFAULT_PAD, pb=DEFAULT_PAD)
TabItem_1 = FXVerticalFrame(p=TabBook_1,
opts=FRAME_RAISED|FRAME_THICK|LAYOUT_FILL_X,
x=0, y=0, w=0, h=0, pl=DEFAULT_SPACING, pr=DEFAULT_SPACING,
pt=DEFAULT_SPACING, pb=DEFAULT_SPACING, hs=DEFAULT_SPACING,
vs=DEFAULT_SPACING)

fileName = os.path.join(thisDir, 'Front_page_1.png')
icon = afxCreatePNGIcon(fileName)
FXLabel(p=TabItem_1, text='', ic=icon)

tabItem = FXTabItem(p=TabBook_1, text='3D Model Parametrs', ic=None,
opts=TAB_TOP_NORMAL,
x=0, y=0, w=0, h=0, pl=6, pr=6, pt=DEFAULT_PAD, pb=DEFAULT_PAD)

TabItem_2 = FXVerticalFrame(p=TabBook_1,
opts=FRAME_RAISED|FRAME_THICK|LAYOUT_FILL_X,
x=0, y=0, w=0, h=0, pl=DEFAULT_SPACING, pr=DEFAULT_SPACING,
pt=DEFAULT_SPACING, pb=DEFAULT_SPACING, hs=DEFAULT_SPACING,
vs=DEFAULT_SPACING)

if isinstance(TabItem_2, FXHorizontalFrame):
FXVerticalSeparator(p=TabItem_2, x=0, y=0, w=0, h=0, pl=2, pr=2, pt=2, pb=2)

else:
FXHorizontalSeparator(p=TabItem_2, x=0, y=0, w=0, h=0, pl=2, pr=2, pt=2, pb=2)

fileName = os.path.join(thisDir, '2ns page.png')
icon = afxCreatePNGIcon(fileName)
FXLabel(p=TabItem_2, text='', ic=icon)

if isinstance(TabItem_2, FXHorizontalFrame):
FXVerticalSeparator(p=TabItem_2, x=0, y=0, w=0, h=0, pl=2, pr=2, pt=2, pb=2)

else:
FXHorizontalSeparator(p=TabItem_2, x=0, y=0, w=0, h=0, pl=2, pr=2, pt=2, pb=2)

ComboBox_2 = AFXComboBox(p=TabItem_2, ncols=0, nvis=1, text='Select the type
of Loop Model', tgt=form.typeKw, sel=0)
ComboBox_2.setMaxVisible(10)
ComboBox_2.appendItem(text='Ideal Stitch loop Peirce Model')
ComboBox_2.appendItem(text='Parametric Model')

AFXTextField(p=TabItem_2, ncols=12, labelText='Diameter of Yarn (mm) ',
tgt=form.Yarn_DiameterKw, sel=0)
```

```
AFXTextField(p=TabItem_2, ncols=12, labelText='Wales per centimeter ',
tgt=form.wales_per_CentimeterKw, sel=0)
AFXTextField(p=TabItem_2, ncols=12, labelText='Course per centimeter',
tgt=form.Courses_per_CentimeterKw, sel=0)
AFXTextField(p=TabItem_2, ncols=12, labelText='Enter value of e (mm)',
tgt=form.eKw, sel=0)
AFXTextField(p=TabItem_2, ncols=12, labelText='Thickness of Fabric (mm)',
tgt=form.Thickness_of_FabricKw, sel=0)
spinner = AFXFloatSpinner(TabItem_2, 10, 'No. of Wales', form.No_of_walesKw, 0)
spinner.setRange(1, 1000)
spinner.setIncrement(1.0)
spinner = AFXFloatSpinner(TabItem_2, 10, 'No. of Courses ',  form.No_of_coursesKw,
0)
spinner.setRange(1, 1000)
spinner.setIncrement(1.0)
```

Kernel Script

```
from abaqus import *
from abaqusConstants import *
import regionToolset
import part
import Assembly
import __main__

def
Plain_weft_Knitted_fabric(type,wales_per_Centimeter,Courses_per_Centimeter,Thickn
ess_of_Fabric,Yarn_Diameter,e,No_of_wales,No_of_courses):

if type == "Ideal Stitch loop Peirce Model":

########################################################################
# Defining some parameters
########################################################################

t = 2*Yarn_Diameter
radius = Yarn_Diameter/2
Quarter_of_Wales_width = 2*radius
Course_width = 3.4643*2*r
e = 1.5*2*r
H = 2*e+Course_width

########################################################################
# Construct first half of the loop
########################################################################

p = mdb.models['Model-1'].Part(name='Part-1', dimensionality=THREE_D,
type=DEFORMABLE_BODY)
```

```
p.ReferencePoint(point=((3*Quarter_of_Wales_width)-r, e,0.0))
p = mdb.models['Model-1'].parts['Part-1']
session.viewports['Viewport: 1'].setValues(displayedObject=p)
p = mdb.models['Model-1'].parts['Part-1']
p.DatumPlaneByPrincipalPlane(principalPlane=XYPLANE, offset=0.0)
p = mdb.models['Model-1'].parts['Part-1']
p.DatumPlaneByPrincipalPlane(principalPlane=YZPLANE, offset=0.0)
p = mdb.models['Model-1'].parts['Part-1']
p.DatumPlaneByPrincipalPlane(principalPlane=XZPLANE, offset=0.0)
p = mdb.models['Model-1'].parts['Part-1']

p.WireSpline(points=(((3*Quarter_of_Wales_width-r), e,0.0),
((4*Quarter_of_Wales_width), 0.0, 0.25*t),((5*Quarter_of_Wales_width+r), e, 0.0),
((5*Quarter_of_Wales_width), e+.5*Course_width,-
0.25*t),(5*Quarter_of_Wales_width-r, e+Course_width, 0.0),
(6*Quarter_of_Wales_width, 2*e+Course_width, 0.25*t),
(7*Quarter_of_Wales_width+r, e+Course_width, 0.0), ((7*Quarter_of_Wales_width),
(e+0.5*Course_width), -0.25*t)), mergeWire=ON, meshable=OFF,
smoothClosedSpline=ON)

p = mdb.models['Model-1'].parts['Part-1']
e = p.edges
edges = e.findAt((((3*Quarter_of_Wales_width-r), e, 0.0), ))
p.Set(edges=edges, name='Wire-1-Set-1')
p = mdb.models['Model-1'].parts['Part-1']
p.DatumPointByCoordinate(coords=((3*Quarter_of_Wales_width-r), e,0.0))
p = mdb.models['Model-1'].parts['Part-1']
p.DatumCsysByThreePoints(name='Datum csys-1', coordSysType=CARTESIAN,
origin=(0.0, 0.0, 0.25*t), line1=(1.0, 0.0, 0.0), line2=(0.0, 1.0, 0.0))
p = mdb.models['Model-1'].parts['Part-1']
s = mdb.models['Model-1'].ConstrainedSketch(name='__profile__', sheetSize=3.17)
p.projectReferencesOntoSketch(sketch=s, filter=COPLANAR_EDGES)
s.Spot(point=(radius, 0.0))
s.CircleByCenterPerimeter(center=(0.0, 0.0), point1=(radius, 0.0))
s.unsetPrimaryObject()
p = mdb.models['Model-1'].parts['Part-1']
p = mdb.models['Model-1'].parts['Part-1']
e = p.edges
edges = e.findAt((((3*Quarter_of_Wales_width-r), e, 0.0), ))
pathEdges=edges
d2 = p.datums
p.SolidSweep(path=pathEdges, sketchUpEdge=d2[8].axis3, sketchOrientation=RIGHT,
profile=s)
del mdb.models['Model-1'].sketches['__profile__']
p1 = mdb.models['Model-1'].parts['Part-1']
session.viewports['Viewport: 1'].setValues(displayedObject=p1)

##########################################################################
# Cutting Box
##########################################################################

p = mdb.models['Model-1'].Part(name='Cutting Box',
```

```
objectToCopy=mdb.models['Model-1'].parts['Part-1'])
p = mdb.models['Model-1'].parts['Cutting Box']
p = mdb.models['Model-1'].parts['Cutting Box']
p = mdb.models['Model-1'].parts['Cutting Box']
del p.features['Solid sweep-1']
p = mdb.models['Model-1'].parts['Cutting Box']
del p.features['Wire-1']
p = mdb.models['Model-1'].parts['Cutting Box']
d2 = p.datums
tt = p.MakeSketchTransform(sketchPlane=d2[3], sketchUpEdge=d2[8].axis3,
sketchPlaneSide=SIDE1, sketchOrientation=RIGHT, origin=(0.0, e, 0.0))
s = mdb.models['Model-1'].ConstrainedSketch(name='__profile__', sheetSize=762.1,
gridSpacing=19.05, transform=tt)
p = mdb.models['Model-1'].parts['Cutting Box']
s.rectangle(point1=(-H,2*t ), point2=(H, -2*t))
p = mdb.models['Model-1'].parts['Cutting Box']
d1 = p.datums
p.SolidExtrude(sketchPlane=d1[3], sketchUpEdge=d1[8].axis3,
sketchPlaneSide=SIDE1, sketchOrientation=RIGHT, sketch=s,
depth=(Quarter_of_Wales_width*4),flipExtrudeDirection=OFF)
del mdb.models['Model-1'].sketches['__profile__']


##############################################################################
# Construct second half of the loop
##############################################################################

p = mdb.models['Model-1'].Part(name='Part-2',
dimensionality=THREE_D,type=DEFORMABLE_BODY)
p.ReferencePoint(point=((5*Quarter_of_Wales_width), (e+.5*Course_width), -0.25*t))
p = mdb.models['Model-1'].parts['Part-2']
p = mdb.models['Model-1'].parts['Part-2']
p.DatumPlaneByPrincipalPlane(principalPlane=XYPLANE, offset=0.0)
p = mdb.models['Model-1'].parts['Part-2']
p.DatumPlaneByPrincipalPlane(principalPlane=YZPLANE, offset=0.0)
p = mdb.models['Model-1'].parts['Part-2']
p.DatumPlaneByPrincipalPlane(principalPlane=XZPLANE, offset=0.0)
p = mdb.models['Model-1'].parts['Part-2']

p.WireSpline(points=(((5*Quarter_of_Wales_width), (e+.5*Course_width), -0.25*t),
((5*Quarter_of_Wales_width-r), (e+Course_width), 0.0),
((6*Quarter_of_Wales_width),(2*e+Course_width), 0.25*t),
((7*Quarter_of_Wales_width+r),(e+Course_width), 0.0),
((7*Quarter_of_Wales_width), (e+0.5*Course_width, -
0.25*t)),((7*Quarter_of_Wales_width-r), e, 0.0), ( (8*Quarter_of_Wales_width), 0.0,
0.25*t), ((9*Quarter_of_Wales_width+r), e, 0.0)), mergeWire=ON,
meshable=OFF,smoothClosedSpline=ON)

p = mdb.models['Model-1'].parts['Part-2']
e = p.edges
edges = e.findAt((((5*Quarter_of_Wales_width), (e+.5*Course_width),-0.25*t), ))
p.Set(edges=edges, name='Wire-1-Set-1')
```

```
p = mdb.models['Model-1'].parts['Part-2']
p.DatumPointByCoordinate(coords=((5*Quarter_of_Wales_width),
(e+.5*Course_width,-0.25*t)))
p = mdb.models['Model-1'].parts['Part-2']
p.DatumCsysByThreePoints(name='Datum csys-1', coordSysType=CARTESIAN,
origin=(0.0, 0.0, 0.25*t), line1=(1.0, 0.0, 0.0), line2=(0.0, 1.0, 0.0))
p = mdb.models['Model-1'].parts['Part-2']
s = mdb.models['Model-1'].ConstrainedSketch(name='__profile__', sheetSize=3.17)
p.projectReferencesOntoSketch(sketch=s, filter=COPLANAR_EDGES)
s.Spot(point=(radius, 0.0))
s.CircleByCenterPerimeter(center=(0.0, 0.0), point1=(radius, 0.0))
s.unsetPrimaryObject()
p = mdb.models['Model-1'].parts['Part-2']
p = mdb.models['Model-1'].parts['Part-2']
e = p.edges
edges = e.findAt((((5*Quarter_of_Wales_width), (e+.5*Course_width),-0.25*t), ))
pathEdges=edges
d2 = p.datums
p.SolidSweep(path=pathEdges, sketchUpEdge=d2[8].axis3, sketchOrientation=RIGHT,
profile=s)
del mdb.models['Model-1'].sketches['__profile__']
p = mdb.models['Model-1'].parts['Part-2']

##########################################################################
# Full loop formation
##########################################################################

a = mdb.models['Model-1'].rootAssembly
a = mdb.models['Model-1'].rootAssembly
p = mdb.models['Model-1'].parts['Cutting Box']
a.Instance(name='Cutting Box-1', part=p, dependent=ON)
p = mdb.models['Model-1'].parts['Part-1']
a.Instance(name='Part-1-1', part=p, dependent=ON)
p = mdb.models['Model-1'].parts['Part-2']
a.Instance(name='Part-2-1', part=p, dependent=ON)
a = mdb.models['Model-1'].rootAssembly
a = mdb.models['Model-1'].rootAssembly
a.InstanceFromBooleanCut(name='Part-3', instanceToBeCut=mdb.models['Model-
1'].rootAssembly.instances['Part-1-1'],  cuttingInstances=(a.instances['Cutting Box-1'],
),  originalInstances=SUPPRESS)
a = mdb.models['Model-1'].rootAssembly
a.features['Cutting Box-1'].resume()

a = mdb.models['Model-1'].rootAssembly
a.LinearInstancePattern(instanceList=('Cutting Box-1', ), direction1=(1.0,0.0, 0.0),
direction2=(0.0, 1.0, 0.0), number1=2, number2=1,
            spacing1=(Quarter_of_Wales_width*6), spacing2=0)

a = mdb.models['Model-1'].rootAssembly
a.InstanceFromBooleanCut(name='Part-4',
instanceToBeCut=mdb.models['Model-1'].rootAssembly.instances['Part-3-1'],
cuttingInstances=(a.instances['Cutting Box-1-lin-2-1'], ),
```

```
originalInstances=SUPPRESS)

a = mdb.models['Model-1'].rootAssembly
a.LinearInstancePattern(instanceList=('Cutting Box-1', ), direction1=(1.0,0.0, 0.0),
direction2=(0.0, 1.0, 0.0), number1=2, number2=1,
        spacing1=(Quarter_of_Wales_width*2), spacing2=0)


a = mdb.models['Model-1'].rootAssembly
a.InstanceFromBooleanCut(name='Part-5',
instanceToBeCut=mdb.models['Model-1'].rootAssembly.instances['Part-2-1'],
cuttingInstances=(a.instances['Cutting Box-1-lin-2-1-1'], ),
originalInstances=SUPPRESS)

a = mdb.models['Model-1'].rootAssembly
a.LinearInstancePattern(instanceList=('Cutting Box-1', ), direction1=(1.0, 0.0, 0.0),
direction2=(0.0, 1.0, 0.0), number1=2, number2=1,
        spacing1=(Quarter_of_Wales_width*8), spacing2=0)

a = mdb.models['Model-1'].rootAssembly
a.InstanceFromBooleanCut(name='Part-6',
instanceToBeCut=mdb.models['Model-1'].rootAssembly.instances['Part-5-1'],
cuttingInstances=(a.instances['Cutting Box-1-lin-2-1-2'], ),
originalInstances=SUPPRESS)

a = mdb.models['Model-1'].rootAssembly
a.features['Cutting Box-1'].suppress()
a = mdb.models['Model-1'].rootAssembly
a.InstanceFromBooleanMerge(name='Part-single loop', instances=(a.instances['Part-4-
1'], a.instances['Part-6-1'], ), originalInstances=SUPPRESS,
domain=GEOMETRY)


##########################################################################
# Defining no of wales
##########################################################################

a = mdb.models['Model-1'].rootAssembly
a.LinearInstancePattern(instanceList=('Part-single loop-1', ), direction1=(1.0, 0.0, 0.0),
direction2=(0.0, 1.0, 0.0), number1=No_of_wales, number2=1,
spacing1=(Quarter_of_Wales_width*4), spacing2=0)

a=mdb.models['Model-1'].rootAssembly
mylist= []
mylist=tuple(a.instances["Part-single loop-1-lin-" +str(2+i)+"-1"] for i in
range(No_of_wales-1))
a.InstanceFromBooleanMerge(name='Part-1', instances=(mylist),)

a = mdb.models['Model-1'].rootAssembly
a.InstanceFromBooleanMerge(name='one wale', instances=(
a.instances['Part-single loop-1'], a.instances['Part-1-2'], ),
originalInstances=SUPPRESS, domain=GEOMETRY)
```

```
#######################################################################
# Defining no of courses
#######################################################################

a = mdb.models['Model-1'].rootAssembly
a.LinearInstancePattern(instanceList=('one wale-1', ), direction1=(1.0, 0.0,
0.0), direction2=(0.0, 1.0, 0.0), number1=1, number2=No_of_courses,
spacing1=0, spacing2=(Yarn_Diameter*3.364))
a = mdb.models['Model-1'].rootAssembly

a.deleteFeatures(('Cutting Box-1', 'Part-1-1', 'Part-2-1', 'Part-3-1', 'Cutting Box-1-lin-2-
1', 'Part-4-1', 'Cutting Box-1-lin-2-1-1', 'Part-5-1', 'Cutting Box-1-lin-2-1-2', 'Part-6-1',
Part-single loop-1', 'Part-single loop-1-lin-2-1', 'Part-single loop-1-lin-3-1', 'Part-single
loop-1-lin-4-1', 'Part-1-2', ))

p = mdb.models['Model-1'].parts['Cutting Box']
session.viewports['Viewport: 1'].setValues(displayedObject=p)
del mdb.models['Model-1'].parts['Cutting Box']
del mdb.models['Model-1'].parts['Part-1']
del mdb.models['Model-1'].parts['Part-2']
del mdb.models['Model-1'].parts['Part-3']
del mdb.models['Model-1'].parts['Part-4']
del mdb.models['Model-1'].parts['Part-5']
del mdb.models['Model-1'].parts['Part-6']
del mdb.models['Model-1'].parts['Part-single loop']
p = mdb.models['Model-1'].parts['one wale']
a = mdb.models['Model-1'].rootAssembly
session.viewports['Viewport: 1'].setValues(displayedObject=a)
session.viewports['Viewport: 1'].view.setValues(session.views['Back'])
```

Plug-in Registration Script

```
from abaqusGui import getAFXApp
from gUIPlain_weft_KnittedForm import GUIPlain_weft_KnittedForm

toolset = getAFXApp().getAFXMainWindow().getPluginToolset()
toolset.registerGuiMenuButton(
buttonText='Plug-in for Plain Weft Knitted Fabric',
object= GUIPlain_weft_KnittedForm (toolset),
kernelInitString='Plain_weft_Knitted_fabric')
```